universität wien

DISSERTATION / DOCTORAL THESIS

Titel der Dissertation /Title of the Doctoral Thesis

Clock entrainment by sun- and moonlight in *Platynereis dumerilii*

verfasst von / submitted by

Martin Zurl, BSc M.Sc.

angestrebter akademischer Grad / in partial fulfilment of the requirements for the degree of

Doctor of Philosophy (PhD)

Wien, 2021 / Vienna 2021

Studienkennzahl lt. Studienblatt / degree programme code as it appears on the student record sheet:	UA 794 685 490
Dissertationsgebiet lt. Studienblatt / field of study as it appears on the student record sheet:	Molekulare Biologie
Betreut von / Supervisor:	Assoz. Prof. Dr. Florian Raible

Table of contents

1. Acknowledgements

I want to thank Florian Raible for being a very supportive and enthusiastic supervisor, who allowed me to freely explore different research directions throughout my PhD, and at the same time was always there to discuss and guide me along these projects. A special thanks also goes to Kristin Tessmar-Raible for stimulating scientific discussions and her continuous support and supervision for the “swarming onset” and the “peripheral clock” project.

I want to thank all past and present members of the Raible and Tessmar-Raible group for the friendly and supportive lab atmosphere that made my time here really enjoyable. A special thanks goes to my colleague Birgit for her support and advice with many experiments throughout my PhD. I also want to thank our lab managers Monika, Lukas and Dunja for their excellent technical support, as well as Andrji and Rita from the marine facility for the excellent worm care.

I want to thank Charlotte Helfrich-Förster, Dirk Rieger and the other members of the Helfrich-Förster lab for warmly welcoming me in their lab in Würzburg and introducing me to *Drosophila´s* chronobiology. I also want to thank Eva Wolf and Shruthi Krishnan for the fruitful collaboration on the L-Cry project.

I want to thank the former VBC PhD programme coordinator Inês Crisóstomo and my thesis advisory committee members Manuel Zimmer, Christopher Gerner and Andrew Straw for their valuable advice across different stages of my PhD.

Finally, thanks to my parents, my sister, and friends for always being there for me. Merci Irène.

2. Summary

2.1. Abstract

Animals possess endogenous clocks to anticipate cyclic environmental changes driven by astronomical cycles to optimally adjust their physiology and behaviour. Ambient light is one of the most important cues used by animals to synchronize their internal clock(s) with these environmental cycles. While moonlight is typically thought to entrain monthly circalunar clocks, which are well known to exist in many marine species that use them to synchronize reproduction across a population to certain lunar phases, sunlight is considered as the main entrainment cue for the daily circadian clock. However, there is growing evidence that moonlight also affects daily timing in various species, ranging from invertebrates to humans. Nevertheless, how moonlight is perceived and is discriminated from sunlight on a molecular level and how it affects the circadian clock remains largely elusive, also due to a lack of suitable model species.

In this thesis, I use the marine bristle worm *Platynereis dumerilii* as a genetically accessible model system to assess how moonlight affects circadian timing. By establishing a novel behavioural paradigm, I show that circadian timing of reproductive behaviour is governed by a moonlight-sensitive plastic circadian clock that times reproductive behaviour to the respective portion of the night where no moonlight is present. By testing *Platynereis* mutant lines that are deficient in candidate photoreceptors, I identify two photoreceptors, L-Cry and r-Opsin1, that mediate the effects of moonlight on the circadian clock in a non-redundant manner. While *r-opsin1* is genetically required to advance swarming onset in response to a waning moonlight regime, I find a dual function of L-Cry in adjusting the plastic circadian clock to light: it entrains the circadian clock to naturalistic sunlight, and also mediates a shortening of circadian period under prolonged moonlight exposure. Furthermore, we provide biophysical, biochemical and behavioural evidence that L-Cry engages in two distinct signaling pathways that encode sun and moonlight valence. We extend this finding to *Drosophila*, were we show that *Drosophila* Cry is also required to correctly interpret ambient moonlight in order to prevent a disturbance of the circadian clock by moonlight. Together with a companion study that investigated the function of L-Cry in the context of the worms' monthly circalunar clock, we provide molecular insights into the decoding of moonlight versus sunlight for circadian and circalunar timing.

Finally, to better understand how circadian time is communicated within the organism, I also participated in a study that provides new insights into the entrainment of peripheral circadian oscillators by local light input as well as by input from the central oscillator in the worm brain.

2.2. Zusammenfassung

Tiere verfügen über endogene Uhren um zyklische Umweltveränderungen, die von astronomische Zyklen bestimmt werden, zu antizipieren und so ihre Physiologie und ihr Verhalten optimal anzupassen. Dabei nutzen Tiere das Umgebungslicht als Signal um ihre innere(n) Uhr(en) mit diesen Umgebungszyklen zu synchronisieren. Während bekannt ist das einige marine Tierarten Mondlicht nutzen um monatliche, sogenannte zirkalunare Uhren einzustellen, die es ihnen erlauben den Zeitpunkt ihrer Fortpflanzung mit bestimmten Mondphasen zu synchronisieren, gilt Sonnenlicht als Hauptreiz um die tägliche zirkadiane Uhr einzustellen. Es gibt jedoch immer mehr Hinweise darauf, dass auch Mondlicht die zirkadiane Zeitmessung bei verschiedenen Spezies, von Wirbellosen bis hin zum Menschen, beeinflusst. Wie Mondlicht wahrgenommen und auf molekularer Ebene von Sonnenlicht unterschieden wird und wie es die zirkadiane Uhr beeinflusst, ist jedoch noch weitgehend ungeklärt, auch weil geeignete Tiermodelle fehlen.

In dieser Arbeit verwende ich den marinen Borstenwurm *Platynereis dumerilii* als genetisch zugängliches Modellsystem, um zu untersuchen, wie Mondlicht die zirkadiane Uhr beeinflusst. Mit Hilfe eines neuartigen Verhaltensparadigmas zeige ich, dass das zirkadiane Timing des Fortpflanzungsverhaltens von einer mondlichtempfindlichen, plastischen zirkadianen Uhr gesteuert wird, die das Fortpflanzungsverhalten auf den jeweiligen dunklen Teil der Nacht legt, in dem kein Mondlicht vorhanden ist. Weiters zeige ich mit Hilfe von zwei gentechnisch veränderte *Platynereis* Linien, denen jeweils ein bestimmter Lichtrezeptor fehlt, dass die beiden Lichtrezeptoren L-Cry und r-Opsin1 auf nicht-redundante Weise die Auswirkungen von Mondlicht auf die zirkadiane Uhr vermitteln. Während r-Opsin1 genetisch erforderlich ist, um den Beginn des Schwärmverhaltnes an ein abnehmendes Mondlichtregime anzupassen, hat L-Cry eine Doppelfunktion bei der Anpassung der plastischen zirkadianen Uhr an Licht: Es stimmt die zirkadiane Uhr auf natürliches Sonnenlicht ab, und vermittelt zusätzlich eine Verkürzung der zirkadianen Periodenlänge unter längerer Mondlichtexposition. Darüber hinaus liefern wir biophysikalische, biochemische und verhaltensbiologische Hinweise

dafür, dass L-Cry über zwei unterschiedliche Signalwege die Valenz von Sonnen- und Mondlicht kodiert. Wir weiten diesen Befund auf *Drosophila* aus und zeigen, dass *Drosophila* Cry ebenfalls benötigt wird, um Mondlicht richtig zu interpretieren und so eine Störung der zirkadianen Uhr durch Mondlicht zu verhindern. Zusammen mit einer begleitenden Studie, die die Funktion von L-Cry im Zusammenhang mit der monatlichen zirkalunaren Uhr der Würmer untersucht, liefern wir molekulare Einblicke in die Dekodierung von Mond- und Sonnenlicht für die zirkadiane und zirkalunare Zeitmessung. Um besser zu verstehen wie zirkadiane Zeit innerhalb des Organismuses kommuniziert wird, habe ich schließlich an einer Studie mitgewirkt, die neue Einblicke in das Entrainment von peripheren zirkadianen Oszillatoren durch lokalen Lichteinfluss sowie durch Einfluss vom zentralen Oszillator im Gehirn der Würmer liefert.

3. Introduction

3.1. Biological clocks enhance adaptation to a periodically changing environment

Life on earth evolved in an environment that is subjected to periodic changes. These periodic changes span different timescales and are caused by the periodic rotation of the earth around its axis (24h), the rotation of the moon around the earth (29,5 days) and the rotation of the earth around the sun (1 year). Besides these three periodicities the gravitational pull of the moon and the sun together with the centrifugal force generated by the rotation of the earth give rise to the tidal cycles (12,4h and 14,5 days) to which life in coastal waters has to adapt.

Most living organisms have evolved endogenous clocks that run in synchrony with at least one of these astronomically defined periods in order to anticipate and therefore better adapt to the environmental changes that are associated with these cycles such as light availability, temperature or food availability. A biological clock is characterized by three main features: (i) it is self-sustained, i.e. it continuous to oscillate under the absence of any external cues; (ii) it is entrainable, i.e. external cues called "Zeitgebers" such as light and temperature synchronize the phase of the endogenous oscillation with the external environment; and (iii) it is temperature compensated, i.e. its period length stays constant over various physiological temperatures. This thesis will focus on the entrainment of the clock that tracks time across a solar day (circadian clock) and the clock that tracks time across a lunar month (circalunar clock).

3.2. Sun and moonlight temporally structure the environment in a periodic manner

Biological clocks can be entrained by several environmental stimuli that oscillate with the respective astronomically defined cycle. These include temperature, food intake and mechanosensory stimulation. However, in most cases the most prominent cue for clock entrainment is ambient light. As sun and moonlight conditions change predictably with the respective daily and monthly astronomical defined period, they pose a reliable cue to synchronize circadian and circalunar clocks with the environment. While the sun reaches its highest point above the horizon every 24h, the time between two culminations of the moon takes 24.8h. This means that the moon rises on average approx. 49min later each day in relation to the solar cycle, and therefore moonlight is present during different

portions of the night across a lunar month: during a full moon night the moon rises during night onset and sets during night offset; during the waning moon phase moonlight is present during later portions of the night; and during the waxing moon phase moonlight is present during earlier portions of the night (see article #1 Fig.1D´). In addition to these temporal changes in the availability of nocturnal moonlight across the month, moonlight intensity also changes drastically across a lunar month in a non-linear fashion, with moonlight intensity at quarter moon reaching only ~10% of the light intensity at full moon (Brown, 1952; Krisciunas, 1991; Longcore et al., 2017).

As moonlight is reflected sunlight, their spectral compositions are very similar, only that moonlight is slightly red-shifted, as the moon surface reflects light at the red end of the spectrum slightly better than blue light (Boch et al., 2011; Ciocca & Wang, 2013). The far more prominent difference is its intensity: while sunlight intensity lies in a range between 1000-100000 lux dependent on weather conditions (Longcore et al., 2017), the light intensity of a full moon during the middle of a clear night is estimated to lie in the range of 0.1-0.3 lux (~50-150nW/cm2) (Kyba et al., 2017).

3.3. Entrainment and maintenance of the molecular circadian clock

The mechanistically best understood clock is the circadian clock, which – as the name implies - runs with a period length close ("circa") to 24h ("dian") in constant conditions and tracks time across a solar day. It exists in almost all animals, as well as in plants, fungi and bacteria. At the core of the animal circadian clock lies a transcriptional translational feedback loop (TTFL), which generates sustained oscillations in gene expression of about 24h. This mechanism and the genes involved in the TTFL have been first discovered in the fruit fly *Drosophila melanogaster*, starting with the isolation of the arrhythmic *period* (*per*) mutant in a forward genetic screen (Konopka & Benzer, 1971). Subsequent studies showed that Per is a transcriptional inhibitor that forms a dimer with another transcriptional inhibitor - Timeless (Tim). Together they translocate to the nucleus where they inhibit their own expression by inhibiting transcription of the two transcriptional activators Clock (Clk) and Cycle (Cyc). The lack of Clk and Cyc expression leads to a lack of Per and Tim expression, thereby disinhibiting the repressive action on Clk and Cyc. Newly expressed Clk and Cyc form a heterodimer and activate Per and Tim again and thereby start a new cycle (reviewed in Patke et al., 2020). The biochemical processes of this TTFL,

which involve several posttranslational modifications of Tim and Per that regulate their accumulation, nuclear translocation and degradation, together with a second interlocked feedback loop, generate the endogenous about 24h rhythm in the expression of core clock transcription factors. Clk and Cyc then pass on this temporal signal from the core molecular clock by activating downstream genes that harbor an E-box motif in their promoter.

Circadian clock genes are typically expressed in different tissues throughout the body. However, animals usually possess a central clock neuron network located in the brain, that functions as a master circadian regulator and typically synchronizes circadian clock gene oscillations in other tissues of the body. In *Drosophila*, this central pacemaker cells compromise ~150 brain neurons, which are subdivided into 5 clusters per brain hemisphere based on anatomical location. This network is required and sufficient to generate circadian locomotor behaviour even when flies are kept over many days in constant darkness without any entrainment cues (reviewed in King & Sehgal, 2020).

Although several Zeitgebers can synchronize circadian clock gene oscillations of the central oscillator to the environment, in most animals ambient sunlight is the dominant entrainment cue. In *Drosophila*, and also other insects, the main circadian photoreceptor is a light-responsive cryptochrome. *Drosophila* Cryptochrome (dCry) is expressed directly in a subset of the central master circadian pacemaker neurons as well as in the compound eyes (Benito et al., 2008; Yoshii et al., 2008). Under blue-light illumination, photon absorbance of dCry leads to a reduction of flavin adenine dinucleotide (FAD) bound cofactor (Berndt et al., 2007; Hoang et al., 2008). This leads to a conformational change of dCry that allows it to interact with the core clock protein Tim and the E3-ligase JETLAG (Ozturk et al., 2011), which eventually leads to a light dependend degradation of both Tim and dCry (Peschel et al., 2009), thereby resetting the TTFL.
In addition to dCry, rhodopsin's expressed in the compound eyes and the Hofbauer-Buchner eyelets contribute to the light entrainment of the circadian clock neurons (reviewed in Schlichting, 2020). Entrainment of circadian clock gene oscillations through the visual system is believed to rely on monosynaptic (from the Hofbauer-Buchner cells) and polysynaptic (from the compound eyes) signal transmission to a subgroup of circadian clock neurons, namely the s-LNvs and l-LNvs, which release the neuropeptide

pigment dispersing factor (PDF) (Ogueta et al., 2018; Schlichting et al., 2019). PDF released by these neurons affects circadian clock gene oscillations in other circadian clock neuron clusters. Flies where the PDF mediated light input from the visual system to the circadian clock is impaired, cannot adjust their evening activity to long photoperiods, suggesting that under natural light regimes visual input to the circadian clock is important to adapt circadian activity to photoperiod (reviewed in Schlichting, 2020).

Extending from the identification of the core clock genes in *Drosophila*, subsequent studies in mice showed that the principal mechanism of the molecular clock is conserved across insects and mammals. One notable difference between the mammalian and *Drosophila* clock is the role of Cryptochrome. Mammals possess two Cry proteins (Cry1 and Cry2), which in contrast to dCry are not light receptive and act together with Per homologs as transcriptional repressors within the core TTFL (repressing transcription of the activators CLOCK and BMAL1) (Fullston et al., 2012). Hence, within the mammalian TTFL Crys have taken over the function of *Drosophila* Tim.
To entrain clock gene oscillations to the light-dark cycle, mammals possess a specialized photoreceptive cell in the retina, the so-called intrinsically photoreceptive retinal ganglion cells (ipRGC) (reviewed in Foster et al., 2020). These cells express the blue light-sensitive opsin melanopsin and additionally receive input via inner retinal neurons from rod and cone cells, which express rhodopsin and cone opsins, respectively. Ambient light, therefore, elicits firing of ipRGCs, which project via the hypothalamic tract to specialized clock neurons of the suprachiasmatic nucleus (SCN) and thereby synchronizes circadian clock gene oscillations in these neurons with the light/dark cycle. The SCN is regarded as the mammalian master circadian control unit and synchronizes the peripheral oscillators of the body.

3.4. Central and peripheral clocks form a hierarchical multi-oscillatory system

Circadian clock gene oscillations exist also in peripheral tissues, where they adapt the local physiology to meet the specific requirement associated with the time of day. This multi-oscillatory network is organized in a hierarchical fashion, where the central pacemaker in the brain transmits temporal information to downstream peripheral oscillators. However, peripheral clocks are not exclusively entrained by the central

oscillator but can also be locally entrained. The dependence of peripheral clocks on the central clock varies between tissues and species. For example, in mice, non-photic cues such as the timing of food intake reset the phase of the hepatic clock, without affecting the central clock in the SCN (Damiola et al., 2000; Stokkan et al., 2001). Whereas in mice photic entrainment of peripheral clocks happens exclusively via the central clock, this is different in non-mammalian species such as zebrafish (Whitmore et al., 1998, 2000) or *Drosophila* (Giebultowicz et al., 2000; Giebultowicz & Hege, 1997), where peripheral tissues also express photoreceptors that can locally entrain the tissue to photic cues. In *Drosophila*, circadian rhythms in some tissues, such as the prothoracic gland which times the circadian eclosion rhythm, depend on the input from the central clock (Selcho et al., 2017), while other tissues including the antennae or the malpighian tubules, which serve as the fly´s kidney, are directly light entrainable and are capable of functioning independently of the central clock (Giebultowicz et al., 2000; Giebultowicz & Hege, 1997; Ivanchenko et al., 2001; Plautz et al., 1997).

Therefore, to fully understand how a specific circadian rhythm in physiology or behaviour is entrained and maintained in an animal, it is important to assess if the concerned rhythm is controlled by a peripheral oscillator, and if so, to which degree this oscillator is controlled by the central clock.

3.5. Circalunar rhythms and clocks

In addition to the intensely studied circadian rhythms, a rich body of literature describes rhythmic monthly phenomena controlled by the lunar cycle (reviewed in Tessmar-Raible et al., 2011). Especially among marine species that reproduce via broadcast spawning where many individuals release gametes synchronously into the sea, reproduction is often synchronized to a certain phase of the lunar cycle. A famous example are the broadcast spawning events of corals at the Great Barrier Reef, where dozens of coral species release their gametes during the nights following a full moon (Babcock et al., 1986; Harrison et al., 1984). The phenomenon of moon phase dependent timing of reproduction has been described for many marine species, including several fish species, annelids, mollusks, crustaceans, and even extends to algae species (reviewed in Tessmar-Raible et al., 2011).

In most cases, moonlight is the critical cue to entrain these monthly rhythms, as it has been shown that dim nocturnal light given under controlled conditions is sufficient to set

a monthly reproductive rhythm in several marine species including fishes (Fukunaga et al., 2020), corals (Kaniewska et al., 2015), annelids (Franke, 1985; Hauenschild, 1960) crustaceans (Saigusa, 1980) and insects (Neumann, 1988). In addition to moonlight, hydrostatic pressure and/or mechanical stimuli associated with spring tides (reoccurs every 14,8 days) can serve as cues in some species to entrain circasemilunar (~15 days) reproductive rhythms (reviewed in Naylor, 2010).

Interestingly, it has been demonstrated in several species that circalunar rhythms are not necessarily a direct response to moonlight or tidal cycles, but that these lunar cues rather entrain an endogenous monthly oscillator (circalunar clock) that in turn times reproduction (Franke, 1985; Hauenschild, 1960; Hsiao, 1996; Neumann, 1988; Saigusa, 1980). In analogy to the circadian clock, this means that these animals must possess some type of endogenous oscillator that is able to run with a period length of several weeks. Despite the widespread occurrence and fundamental importance of these circalunar clocks, their molecular mechanisms as well as the photoreceptive pathways required to entrain these clocks to moonlight remain elusive.

In corals one candidate photoreceptor that has been proposed to play a role in moonlight sensation is Cry2 (Levy et al., 2007). This has been based on the observation that its expression is upregulated during full moon nights compared to new moon nights. Similarly, certain lunar-synchronized fish species show a lunar regulation of cryptochrome expression, however not in the same direction as discovered in corals: cryptochrome mRNA levels in the golden-lined spinefoot (Cry1b and Cry2) and in the tropical grouper (Cry1 and Cry2) are upregulated during new moon compared to full moon (Fukunaga et al., 2020; Fukushiro et al., 2011; Takeuchi et al., 2018). Therefore, in fish it was hypothesized that Cry might not act as a moonlight sensor itself but rather as a state-variable of the lunar cycle that is itself regulated by a moonlight responsive molecule (Fukushiro et al., 2011). As these studies are only of correlative nature, functional studies including biochemical assessment of light sensitivity as well as genetic manipulations of these *cryptochrome* genes are needed to clarify their potential role in lunar timing.

3.6. Circadian effects of moonlight under natural conditions

While it is well established that sunlight entrains circadian clocks through specialized photoreceptors to allow animals to optimally adapt to the 24h solar cycle, the contribution of moonlight in regulating circadian timing remains less clear.

Moonlight improves nocturnal vision and is therefore thought to play a central role in the temporal structuring of predator-prey interactions in nocturnal animals (Prugh & Golden, 2014). One of the first observations that implicated moonlight as a cue for predation risk came from nocturnal kangaroo rats, which were shown to avoid foraging during the moonlit portions of the night (Lockard & Owings, 1974). Many more field studies mainly with terrestrial nocturnal species followed that found a strong influence of moon phase on circadian activity cycles (reviewed in Kronfeld-Schor et al., 2013). If an animal increases or decreases activity under moonlight is a complex decision that balances the benefits and risks of foraging under moonlight: if predation risk under moonlight outweighs foraging success, prey species are expected to be lunarphobic; conversely, lunarphilic behaviour is expected if foraging success under moonlight outweighs predation risk (Kronfeld-Schor et al., 2013). The influence of moonlight on foraging activity has been extensively studied in terrestrial mammalian carnivores and their nocturnal prey, with several of these species showing pronounced effects of moonlight on their circadian activity profiles (Botts et al., 2020; Huck et al., 2017; John et al., 2012; Prugh & Golden, 2014).

Although in aquatic species biologists have mainly focused on the effects of moonlight on monthly timing phenomena, especially the monthly lunar synchronization of reproduction, there are also several reports that document effects of moonlight on structuring the daily timing of predator-prey interaction in aquatic ecosystems. For example, it has been shown that reef sharks hunt groupers during full moon nights (Mourier et al., 2016) and moonlight influences zooplankton capture success of both freshwater and marine predatory fish (Gliwicz, 1986; Hernández-León et al., 2002). Furthermore, it has been shown that during the arctic winter, when sunlight is very limited, moonlight drives diel vertical migration of zooplankton (Last et al., 2016). During this time vertical migration is synchronized with the ~24.8h lunar day, with zooplankton staying at deeper layers of the ocean during the time moon is up, likely to avoid predators that hunt during moonlight.

An example of a marine species where moonlight has been reported to strongly impact on daily behaviour is the bioluminescent crustacean *Vargula annecohenae.* Reproductive and feeding behaviour of this species during the adult stage is restricted to the portions of the night where moonlight is absent or is below a critical light intensity threshold (Gerrish et al., 2009).

Effects of moonlight on daily behaviour also extend to several primate species. Owl monkeys *(A. azarai boliviensis)*, one of the rare examples of nocturnal primates, restrict activity almost exclusively to the moonlit portions of the night, which leads to activity profiles that perfectly track the ~24.8h lunar periodicity (Fernández-Duque et al., 2010). During a lunar eclipse, where the full moon temporarily moves into the earth's shadow, activity was negatively masked by the absence of moonlight, letting the authors suggest that lunarphilic behaviour is likely not driven by an endogenous clock, but rather by direct masking effects of moonlight. The importance of light masking for the increased activity of owl monkeys under moonlight has also been shown under controlled laboratory conditions (Erkert & Gröber, 1986). However, LD cycles with light of 0.1 lux have been proven to entrain the endogenous circadian clock in owl monkeys (Erkert & Thiemann, 1983) and mouse lemurs (Erkert, 2008), indicating that the circadian system of these primates is in principle sensitive to light with moonlight intensity.

Recently, evidence accumulates that also in humans circadian activity, specifically the onset and duration of sleep, is influenced by lunar phase (Cajochen et al., 2013; Casiraghi et al., 2021; Smith et al., 2014). In the most recent study of Casiraghi et al. they used wrist bands to monitor sleep over several weeks in three indigenous Argentinian communities that had either no, limited or full access to electricity. They found that during the evenings that lead up to a full moon, where the moon is already up in the sky during night onset, sleep onset was delayed on average by 22 min in the group without and with limited access to electricity and by 9 min in the group with full access to electricity (overall sleep across the night was reduced by 25min, 19min and 11min, respectively). Interestingly, they then discovered the same moon phase dependent sleep oscillation in a fourth study group that consisted of colleague students living in a highly urbanized postindustrial environment in the United States. This suggests that the availability of moonlight during the beginning of the night extends human activity into the moonlit portion of the night,

likely representing a modulation of circadian activity by moonlight that was of even higher relevance before the invention of electricity.

3.7. Circadian effects of artificial moonlight under laboratory conditions

To investigate if moonlight is affecting daily activity via the endogenous circadian clock or merely by direct light effects referred to as light masking, requires to study these effects under controlled laboratory conditions. Furthermore, to identify the proteins involved in moonlight signaling and how these potentially interact with the molecular circadian clock requires genetically accessible model organisms with annotated clock genes.

Although for the conventional chronobiologic model species, such as mice, hamsters and *Drosophila*, circadian effects of moonlight under natural or semi-natural light and temperature conditions are not reported, it is well established that their circadian system is sensitive to light levels that lie in the range of full moon light intensity and even far below that (subsequently referred to as "dim light" or "artificial moonlight", defined by an intensity of <0.15 lux if not otherwise specified). For example, the circadian clock of mice can be entrained by LD cycles with white light of 0.1 lux (~full moon intensity) (Altimus et al., 2010), while *Drosophila´*s circadian clock is entrainable to LD cycles with light intensities that are even far below full moon light intensity (Hirsh et al., 2010). Furthermore, if mice (Lall et al., 2010), hamsters (J. A. Evans et al., 2007) or *Drosophila* (Konopka et al., 1989) are held under constant dim light their circadian period length (determined based on locomotor activity) is longer compared to when held in constant darkness, indicating that light with moonlight intensity can alter circadian period length.

However, under combined bright light/dim light conditions (i.e. dim light during the night), bright light dominates in entrainment of the circadian clock, and dim nocturnal light has only subtle effects on circadian timing in the conventional laboratory model systems studied so far. For example, in hamsters circadian locomotor activity is similar under completely dark and dimly lit (<0.2 lux) nights. However, when subjected to a phase shift of the light cycle, adjustment is accelerated in hamsters subjected to dimly lit nights (J. Evans et al., 2009).

In *Drosophila*, artificial moonlight during the night has been shown to shift its crepuscular locomotor activity towards the night (Bachleitner et al., 2007). This is partly caused by light masking effects that bypass the endogenous clock, as this effect has been shown to also occur in *Drosophila* clock mutants that lack a functional circadian clock (Kempinger et al., 2009). Nevertheless, it has been shown that under dimly lit nights clock gene oscillations in the two circadian cell clusters that control morning and evening activity are slightly phase advances and phase delayed, respectively (Bachleitner et al., 2007). This indicates that artificial moonlight is indeed capable of modulating circadian clock gene oscillations even under a combined sun/moonlight regime in *Drosophila*. However, behavioural monitoring under semi-natural conditions revealed no increased locomotor activity during full moon nights compared to new moon nights nor were circadian clock gene oscillations in circadian clock neurons affected during full moon nights (Vanin et al., 2012). The discrepancies probably lie in the colder nighttime temperature under semi-natural conditions. However, *Drosophila melanogaster* likely originated in the tropics (Lachaise & Silvain, 2004) where nighttime temperatures are mild and it might therefore still be possible that moonlight affects nocturnal activity in populations living in more tropical areas.

To reveal which photoreceptors are involved in the entrainment of the circadian system of *Drosophila* and mouse to dim light, behavioural responses to dim light have been assessed in mutant lines deficient in candidate dim light receptors. In mice, rod photoreceptors that impinge on ipRGC are required to photoentrain the circadian clock to LD cycles of 0.1 lux (Altimus et al., 2010; Lucas et al., 2012). However, a recent study suggests that also melanopsin in a subset of ipRGC, namely the M1 ipRGC, can signal at very low light intensities and is involved in entraining the clock to dim light (Lee et al., 2019).
In *Drosophila* entrainment to dim LD cycles (<0.12 lux) involves PLC-β mediated rhodopsin signaling from the visual system (Stanewsky et al., 1998). Furthermore, it has been shown that the delay of evening locomotor activity into the night under artificial moonlight conditions (i.e. 0.01 lux during the night) depends on rhodopsin1 and rhodopsin6, which are expressed in the compound eyes (Schlichting et al., 2014). However, there is evidence that also dCry is involved in circadian responses to dim light in *Drosophila*. Vinayak and colleagues showed that behavioural phase advances in response to a very dim blue light pulse (3nw/cm^2 for 6 hours) during the late subjective night

depend primarily on dCry and not on PLC-β mediated canonical rhodopsin signaling (Vinayak et al., 2013). Furthermore, it has been shown that circadian period lengthening of fly activity under constant dim light (0.1 lux) is dependent on dCry (Yoshii et al., 2004).

Although the above studies in *Drosophila* and mice are useful to understand which photoreceptors are involved in circadian responses to dim light, they only give limited insights on how the circadian system of these species would respond to moonlight under natural conditions. This is partly because the aforementioned studies, at least those performed in mice, do not provide artificial moonlight in combination with an artificial sunlight cycle, as it would happen in nature. However, rodent studies that assessed locomotor rhythms of mice and rats subjected to dim light only at night, found no effect on locomotor rhythms, even though the light intensities in these studies (2-5lux) by far exceed full moon light intensity (reviewed in Rumanova et al., 2020). Similarly, and as mentioned previously, in *Drosophila* no effect of moonlight on circadian timing could so far be found under semi-natural conditions (Vanin et al., 2012).
Therefore, to understand the molecular pathways on how moonlight affects circadian or circalunar timing in species under natural conditions, studies on model organisms that are both genetically accessible and at the same time exhibit potent effects of moonlight under naturalistic conditions are needed. While no laboratory model system has been established that exhibits pronounced effects of moonlight on circadian timing under naturalistic conditions, there are a few marine model species for which an effect of moonlight on synchronizing monthly reproductive timing under natural conditions has been well established (reviewed in Tessmar-Raible et al., 2011).

3.8. *Platynereis* as model species for lunar chronobiology

Among the many marine species that exhibit influences of the lunar cycle on the timing of reproduction, the marine bristle worm *Platynereis dumerilii* has been established as a particularly useful model system to address the involved molecular mechanisms, due to its well established genetic toolkit and because it can easily be maintained in the lab. These animals were first reported in coastal waters of the Mediterranean sea and later were found to live also in many other coastal waters around the world (reviewed in Hartmann-Schroeder, 1996). Before these worms reach sexual maturity, they live a

benthic lifestyle and are commonly found at depths between 0-5 m (Giangrande, 1988; Giangrande et al., 2003), where they live in silk tubes attached on substrates like algae covered hard bottoms (Giangrande et al., 2003) or seagrass (Jacobs & Pierson, 1979). However, when they reach sexual maturity they emerge from their tubes and swarm in high numbers to the water surface. As soon as a male and female worm encounter, pheromones are exchanged and elicit a stereotypical nuptial dance that results in sperm and egg release after which both males and females die within one day. Oocytes are then fertilized outside the body in the open water. To increase the probability to encounter individuals of the opposite sex, sexual maturation is synchronized among a population to certain phases in the lunar month. Field experiments conducted already in the first half of the last century in the Bay of Naples concluded that the vast majority of worms reproduce 2-7 days after full moon (Ranzi, 1931). However, differences in lunar timing seem to exist among geographically distinct populations, as another field study conducted at the coast of Brittany (France) documented a second peak in reproducing worms during the waxing full moon phase (Fage & Legendre, 1923; reviewed in Korringa, 1947).

A first lab culture based on worms collected from the Bay of Naples (Italy) was established by Carl Hauenschild in the early 1950s. By synchronizing the monthly reproductive timing of a *Platynereis* culture by monthly stimuli of nocturnal dim light, he could show that moonlight is indeed the critical stimulus to synchronize sexual maturation to specific phases of the lunar month (Hauenschild, 1960). Interestingly, he also found that once this monthly reproductive rhythm is established in a population, *Platynereis* worms still show a monthly synchronization of sexual maturation even if the monthly nocturnal light stimuli are omitted, indicating that moonlight entrains an endogenous monthly oscillator that keeps running for several cycles even without the initial entrainment stimulus. While this initial experiment was only performed with limited numbers of animals, a more recent publication could validate the existence of an endogenous circalunar timekeeper (Zantke et al., 2013). Biological clocks with a period length of one month have been described also in other marine invertebrates (as discussed in section 3.5), but the components and the molecular mechanism of such a monthly biological oscillator remain elusive.

Among the species which are used to study circalunar timing, *Platynereis* is the one with the most advanced genetic toolkit (reviewed in Zantke et al., 2014), which opens the possibility to functionally assess which genes are required for the perception of moonlight and its downstream pathways.

3.9. Aims of the study

Although the circadian clock of many animals is sensitive to light levels that equal moonlight intensity and several species, including humans, have been shown to adapt circadian behaviour according to moon phase under natural conditions (reviewed in section 3.6), little is known on how moonlight affects circadian timing. The only insights about photoreceptor signaling pathways that are involved in circadian clock entrainment to dim light in the range of moonlight intensity come from studies in *Drosophila* and mice (reviewed in section 3.7) - two species for which any effect of moonlight on circadian timing under naturalistic conditions has not been established.

Therefore, I aimed to explore if the marine annelid *Platynereis dumerilii* would be a suitable model species to study the effects of naturalistic moonlight on circadian timing. Specifically, I aimed to address 4 fundamental questions concerning the entrainment of the circadian clock by naturalistic moon and sunlight:

1. Is there any effect of naturalistic moonlight on circadian timing in *Platynereis*?
2. How does the circadian clock in these animals distinguish naturalistic moonlight from sunlight?
3. Are any of the implied mechanisms evolutionary conserved in *Drosophila*, which represents a different clade of Protostomes?
4. How is circadian time communicated within the organism *Platynereis*?

4. Article 1: Two light sensors decode moonlight versus sunlight to adjust a plastic circadian/circalunidian clock to moon phase

Status: submitted to *Proceedings of the National Academy of Sciences* on 31.08.2021 and posted on bioRxiv: https://doi.org/10.1101/2021.04.16.440114

Authors:

Martin Zurl, Birgit Poehn, Dirk Rieger, Shruthi Krishnan, Dunja Rokvic, Vinoth Babu Veedin Rajan, Elliot Gerrard, Matthias Schlichting, Lukas Orel, Robert J. Lucas, Eva Wolf, Charlotte Helfrich-Förster, Florian Raible, and Kristin Tessmar-Raible

Outline:

In this article, I established a novel behavioural paradigm that assesses the exact time when *Platynereis* initiates its swarming behaviour under naturalistic sun- and moonlight conditions. By using this assay, I found that swarming onset is regulated by a plastic circadian clock, that is sensitive to naturalistic moonlight and that times swarming onset to the portion of the night, where no moonlight is present. To test which photoreceptors are involved in the entrainment of the circadian clock to light, I tested mutant lines that were deficient in candidate photoreceptors. By this approach, I identified L-Cry as a photoreceptor that entrains the clock to sunlight, while both L-Cry and r-opsin1 are involved to adjust the clock to moonlight conditions. Furthermore, we provide biochemical and behavioural evidence that suggests that L-Cry signals differently under moonlight and sunlight conditions, and that L-Cry is required to discriminate these two light valences for circadian timing. Finally, we found that the function of light receptive Cryptochrome to distinguish moonlight from sunlight seems also to be conserved in *Drosophila*, as we show that *Drosophila* Cry prevents the fly circadian system to be disturbed by moonlight. These results address aims 1-3 of my thesis.

Contributions:

I provided major contributions in the conceptualization and experimental design of the project. Furthermore, I established the swarming assay and performed all swarming

onset experiments (Fig. 1b-g, 2, 6b-e, Fig S1, S4b), contributed to analyzing and planning of L-Cry immunostainings (Fig. 3 and S3), performed and analyzed immunohistochemistry experiment on *Drosophila* together with D. R. and C.H.F. (Fig. 4 D-H), statistically analyzed *Drosophila* locomotor activity (Fig. 4C), calculated moonlight spectra from primary data and contributed to the development of naturalistic sun and moonlight LEDs. I provided major contributions to the summary model in Fig. 7, in preparing figures and writing the manuscript.

Two light sensors decode moonlight versus sunlight to adjust a plastic circadian/circalunidian clock to moon phase

Short title: Moonlight sets a plastic circadian/-lunidian clock

Martin Zurl[1,2], Birgit Poehn[1,2], Dirk Rieger[3], Shruthi Krishnan[4,5], Dunja Rokvic[1,2], Vinoth Babu Veedin Rajan[1,2], Elliot Gerrard[6], Matthias Schlichting[7], Lukas Orel[1,2], Robert J. Lucas[6], Eva Wolf[4,5], Charlotte Helfrich-Förster[3], Florian Raible[1,2,@] and Kristin Tessmar-Raible[1,2,@]

[1] Max Perutz Labs, University of Vienna, Vienna BioCenter, Dr. Bohr-Gasse 9/4, 1030 Vienna, Austria

[2] Research Platform "Rhythms of Life", University of Vienna, Vienna BioCenter, Dr. Bohr-Gasse 9/4, 1030 Vienna, Austria

[3] Department for Neurobiology and Genetics, Theodor-Boveri Institute, Biocentre, University of Würzburg, Am Hubland, 97074 Würzburg, Germany

[4] Institute of Molecular Biology (IMB), 55128 Mainz, Germany

[5] Institute of Molecular Physiology, Hanns-Dieter-Hüsch Weg 17, Johannes Gutenberg-University of Mainz, 55128 Mainz, Germany

[6] Division of Neuroscience & Experimental Psychology, University of Manchester, Oxford Road, Manchester M13 9PT, UK

[7] Brandeis University, Waltham, USA

[@] correspondence: florian.raible@univie.ac.at, kristin.tessmar@maxperutzlabs.ac.at

Abstract

Many species synchronize their physiology and behavior to specific hours. It is commonly assumed that sunlight acts as the main entrainment signal for ~24h clocks. However, the moon provides similarly regular time information. Consistently, a growing number of studies have reported correlations between diel behavior and lunidian cycles. Yet, mechanistic insight into the possible influences of the moon on ~24hr timers remains scarce.

We have explored the marine bristleworm *Platynereis dumerilii* to investigate the role of moonlight in the timing of daily behavior. We uncover that moonlight, besides its role in monthly timing, also schedules the exact hour of nocturnal swarming onset to the nights' darkest times. Our work reveals that naturalistic moonlight adjusts a plastic clock that exhibits <24h (moonlit) or >24h (no moon) periodicity. Abundance, light sensitivity, and genetic requirement indicate that the *Platynereis* light receptor molecule r-Opsin1 serves as a receptor that senses moonrise, whereas the cryptochrome protein L-Cry is required to discriminate the proper valence of nocturnal light as either moon- or sunlight. Comparative experiments in *Drosophila* suggest that cryptochrome's principle requirement for light valence interpretation is conserved. Its exact biochemical properties differ, however, between species with dissimilar timing ecology.

Our work advances the molecular understanding of lunar impact on fundamental rhythmic processes, including those of marine mass spawners endangered by anthropogenic change.

Main text

A moonlight-sensitive clock times swarming behavior

Platynereis dumerilii reproduces by nocturnal mass spawning, with sexually mature males and females synchronously raising from seagrass to the water surface (Fig. 1a) during the night (*1*). Whereas it is well established that this spawning is synchronized to specific nights of the month by a circalunar oscillator (*2–4*), we reasoned that it should further increase reproductive success if worms synchronized the onset of swarming behavior also to specific hours during those nights. In fact, such an interconnection of different timing systems is well established for polychaete relatives like the palolo worms (*5*) and fireworms (*Odontosyllis*) (*6*).

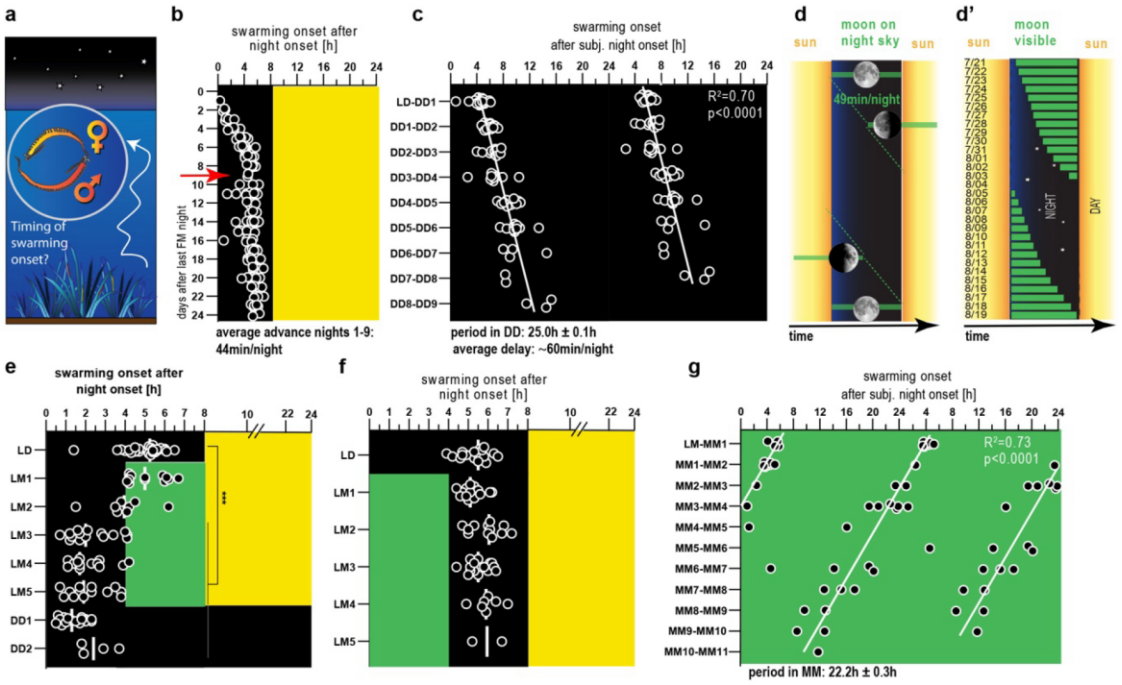

Fig. 1 | A moonlight sensitive plastic circadian/circalunidian (PCC) clock times swarming onset to darkness. (a) Schematized swarming behavior of *Platynereis dumerilii*. **(b)** Swarming onset of individual, separated worms across different days of an artificial lunar month, where worms receive 8 nights of continuous nocturnal light (=full moon: FM) every month in addition to a 16h:8h LD cycle (for details see *4, 7*). Red arrow indicates from which day of the circalunar cycle onwards worms were used for all subsequent experiments (except Fig. 2f and g). **(c,g)** Swarming onset of worms released into constant darkness (DD; (c) or constant moonlight (MM; g). Data are double-plotted for better visualization. White lines are linear regression lines. Period lengths were calculated based on the slope of the regression line ± the 95% CI of the slope. **(d,d')** Schemes illustrating moonrise and -set times in a simplified averaged model (d) and a natural habitat (Bay of Naples, July/August 1929) (d'). See: https://www.timeanddate.com/moon/italy/naples and ref. *(1)* **(e,f)** Swarming onset of worms subjected to naturalistic moonlight during the second (e) or first (f) half of the night. black: no light, yellow: naturalistic sunlight, green: naturalistic moonlight.

This prompted us to investigate if *Platynereis dumerilii* also exhibits preferred hours of spawning. We placed maturing, monthly (circalunar) entrained *Platynereis dumerilii* adults (*3*, *8*) in individual wells of our automated behavioral recording device (*9*). As swarming is accompanied by a burst of swimming activity ("nuptial dance"), analysis by automated video tracking allowed us to systematically deduce

the time of swarming onset with respect to the daylight/darkness (LD:16:8h) cycle (Fig. S1a,b, Movie S1). Analyses of 139 individuals revealed that swarming onset across the culture was indeed synchronized to a ~1-2hr window during the night (Fig. 1b). (Note that we selected about equal numbers of spawning worms/night. Therefore, the monthly spawning synchronization is invisible.) The precise time point depended on the time since the last artificial "full moon" (FM) night (Fig. 1b), which is provided to entrain the worms' monthly oscillator (*2*, *3*). In nights directly following the last "full moon" night, animals started the characteristic swarming behavior directly following night onset. This onset of swarming gradually shifted by app. 44min/night within the first 8 nights (Fig.1b: days preceding the red arrow). For the remaining lunar month, the time of swarming onset remained unaltered at ~5 h after night onset (Fig. 1, Fig. S1b). To assess whether this synchronization was driven by an endogenous oscillator, we next monitored swarming onset in worms that were kept in constant darkness for several days. Under these dark-dark (DD) conditions, swarming was still synchronously initiated, with an average delay of ~1h ± 0,1h per day (Fig. 1c). This established that the specific hour of nocturnal swarming onset is controlled by an endogenous clock.

The time delay of about 44min within the first 8 nights after full moon is reminiscent of the average delay of the rise of the waning moon (~ 49min/night, Fig. 1d). This apparent delay of moon rise time relative to sunset is caused by the period difference of the daily solar cycle (24h) and the lunidian cycle (24.8h; the average timespan between two successive moon rises) (Fig. 1d). The latter matches the period length of the endogenous clock (~25h) controlling swarming onset under DD conditions (compare Fig. 1c,d). The combination of these facts let us speculate that the worm's ~24hr timing system could help to synchronize *Platynereis* swarming onset to the darkest hours of the night, but would require the moon for entrainment. Furthermore, the exact change of moon rise relative to sunset is not always exactly ~49min/night, but varies under natural conditions (Fig. 1d'), making an additional adjustment by moonlight likely advantageous. We thus next studied if the endogenous clock was sensitive to moonlight for its exact entrainment. To mimic moonlight and sunlight under laboratory conditions, we complemented available surface measurements (*10*) by analyzing systematic light measurements at a natural habitat of *Platynereis* (Fig. S2a), which guided the design of "naturalistic sunlight" and "naturalistic moonlight" illumination devices (Fig. S2b, see also ref. *4*, *9*).

We next exposed animals (>= 9 days after the end of the monthly nocturnal light stimulus, see red arrow Fig. 1b) to "naturalistic moonlight" (Fig. S2b) provided during the second half of the night for 5 consecutive nights (Fig. 1e, LM1-5). In response to this light regime mimicking "waning moon", worms shifted their swarming onset gradually into the dark portion of these "moonlit" nights (Fig. 1e). The advanced swarming onset caused by the "waning moonlight regime" persisted when worms were subsequently released into constant darkness (Fig. 1e: DD1), arguing that this shift was caused by an impact of moonlight on the endogenous clock, rather than being an acute masking effect (i.e. direct

response to light). Consistent with timing the dark portion of the night, the same "naturalistic moonlight" provided during the first half of the night (mimicking times of waxing moon) did not impact on the worms' hourly timing (Fig. 1f). Finally, under a constant "naturalistic moonlight" (MM) regime, spawning onset remained synchronized, but occurred with a markedly decreased period length of ~22.2h ± 0.4h, compared to DD conditions (Fig. 1c vs. g).

Taken together, these results suggest the existence of a plastic oscillator system that regulates nocturnal swarming onset, whose period is modulated by naturalistic moonlight. This results in a swarming preference during the dark portion of the night, consistent with natural observations. We refer to this clock as plastic circadian/circalunidian clock (PCC clock).

L-Cry is required to correctly interpret sun– and moonlight to set the swarming hour

In order to understand how (naturalistic) sun– and moonlight are sensed and distinguished by this system, we next sought to identify photoreceptor(s) relevant for the light impact on the PCC clock. One candidate receptor of particular interest was *Platynereis* L-Cryptochrome (L-Cry), whose distant homolog Cry2 in the coral *Acropora* has been speculated to mediate moonlight sensation based on expression changes (*11*). We also uncovered that *Pdu*-L-Cry has the biochemical and cellular properties to discriminate between sun- and moonlight and is required to correctly detect the full moon phase for monthly oscillator entrainment (*4*).

To assess if *Platynereis* L-Cry is also relevant for the light input into an oscillator with the period length of ~24hrs, the PCC clock, we analyzed a *Platynereis l-cry* loss-of-function strain generated by TALEN-technology (for details on mutants see ref: *4*). When exposed to constant darkness, *l-cry*$^{-/-}$ individuals still exhibited rhythmic initiation of swarming onset, with a period length (24.6h ± 0.3h) indistinguishable from wildtypes (Fig. 2a). This indicates that L-Cry is not required for the endogenous oscillation of the PCC clock.

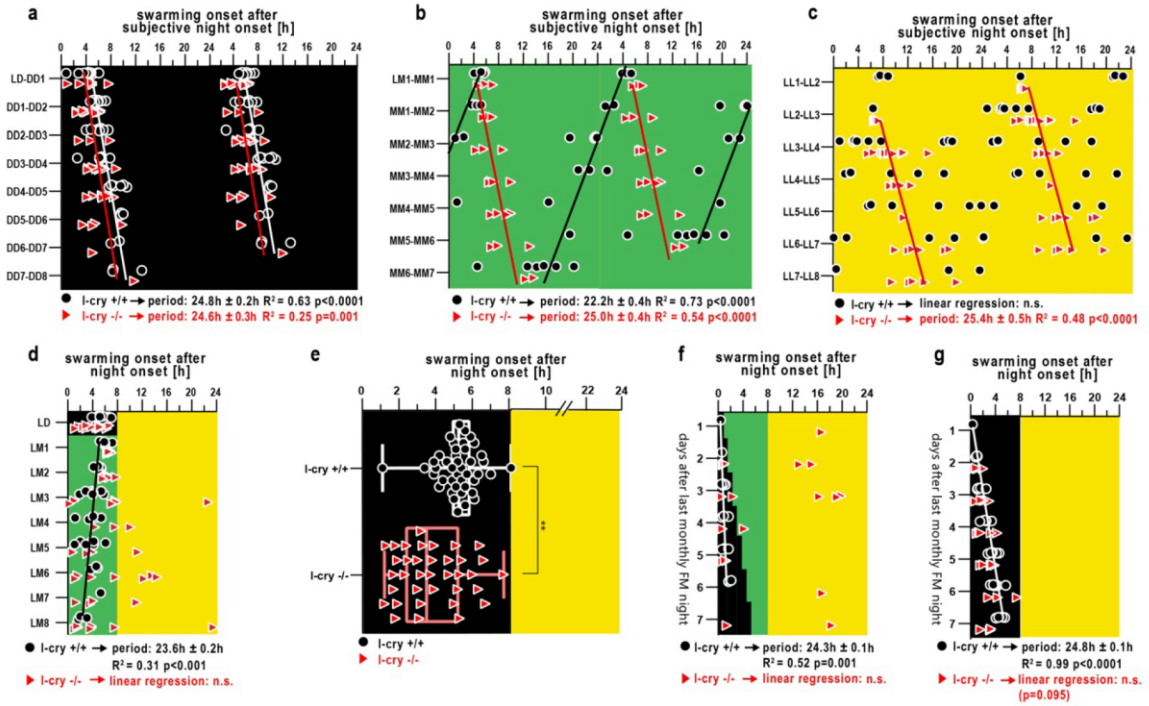

Fig. 2.| *Platynereis* L-Cry enables the PCC, a clock with ~24hr period, to distinguish sun- versus moonlight. (a-e) Swarming onset of *l-cry* mutants (red triangles) and wildtypes (black circles) entrained to 16:8h LD cycles subsequently released into **(a)** constant darkness (DD), **(b)** constant naturalistic moonlight (MM), or **(c)** constant naturalistic sunlight (LL), or **(d)** subjected to alternations of naturalistic sunlight during the day and moonlight during the night (LM) or **(e)** maintained under 16:8h LD cycles (**p=0.004, F-test to test if the variances in the two groups are significantly different). Data in a-c are double-plotted. Black and red lines indicate linear regression lines of wildtype and *l-cry*$^{-/-}$ mutants, respectively. The period length was calculated based on the slope of the regression line ± the 95% CI of the slope. **(f)** Swarming onset of *l-cry* mutants and wildtypes assessed directly after the monthly nocturnal full moon (FM) light stimulus with either an additional waning moonlight regime (f) or kept under LD cycles (g).

To probe for roles of L-Cry in mediating light input into the PCC clock, we next investigated spawning rhythmicity in *l-cry* mutants exposed to constant "naturalistic moonlight" (MM) or "naturalistic sun light" (LL). Under both conditions, *l-cry* mutants exhibited a synchronized swarming onset, with period lengths (MM: 25h ± 0.4h; Fig. 2b; LL: 25.4h ± 0.5h. Fig. 2c) highly reminiscent of the period of wildtype in DD conditions (Fig. 2a). In contrast, wildtype siblings shortened their period (MM) or became arrhythmic (LL), respectively (Fig. 2b,c). These clear differences between wildtype and mutants let us conclude that L-Cry is relevant for the conveying naturalistic sun- and moonlight information to the PCC clock.

The absent adjustment of the PCC clock in *l-cry*$^{-/-}$ individuals to respond to light could be explained by a general reduction in light sensitivity. Alternatively, these findings are compatible with a role of L-Cry in distinguishing moon– and sunlight, as L-Cry enables the PCC clock to respond differently to the two light conditions and as it also possesses this property in the context of worm's monthly oscillator (for monthly oscillator see ref: *4*). To discriminate between the two possibilities, we exposed *l-cry* mutants to a combined naturalistic day/night light regime of 16h:8h, where they were exposed to "naturalistic

sunlight" during the day, and "naturalistic moonlight" during the night (LM) (Fig 2d). If *l-cry-/-* animals were simply blind to light they should continue to exhibit the spawning timing seen in Fig.2b,c. However, if *l-cry-/-* rather provides interpretation of the nature of the light stimulus to other photoreceptors, the prediction is that this will cause an increased behavioral variability between individual worms, as critical light valence information is missing in a mixed naturalistic sun-/moonlight regime. Indeed, unlike wildtype animals, that restricted swarming onset strictly to nocturnal hours (Fig.2d), and different to the timing observed under constant moonlight (Fig.2b) or constant sunlight (Fig.2c), *l-cry* mutants exhibited aberrant, much more variable swarming onset timing under the complex naturalistic sun- and moonlight regime (Fig.2d). Starting with 3 days of the LM regime, around a quarter of the recorded animals initiated swarming during the day and no significant regression line was present in the data (Fig. 2d). Furthermore and again consistent with L-Cry's valence function, all *l-cry* mutants restricted swarming onset to the night when no moonlight was present, albeit slightly less synchronized than wildtype, (Fig. 2d: see LD before LM, Fig.2e), further supporting that the shifted timing into the day was caused by the naturalistic moonlight stimulus, which got misinterpreted by the *l-cry-/-* animals.

The abnormal ("confused") swarming onset of *l-cry*$^{-/-}$ animals was also observed in a light regime in which a staggered, artificial waning moonlight regime (Fig. S2c) was provided directly after the end of the standard monthly culture FM stimulus, more closely mimicking the natural timing under which swarming is observed (Fig. 2f, compare Fig. 1d,d´) compared to the identical time and light regime lacking the waning moon stimulus (Fig. 2g). Overall, this suggests that the *l-cry* mutation does not simply render worms less sensitive to moonlight, but that L-Cry is required to provide the correct light valence information to the PCC clock.

Subcellular localization and stability of L-Cry supports distinct signaling under moonlight and sunlight conditions

In the common view based on the work in *Drosophila melanogaster*, the fly homolog of L-Cry – dCry – undergoes light dependent binding to Timeless, which leads to the degradation of both Timeless and dCry, by this resetting the flies' circadian clock upon light input (reviewed in ref. *12*). This binary signaling model is difficult to reconcile with our finding that *Platynereis* L-Cry is relevant for distinguishing between different light valences in the context of circadian/circalunidian timing. Furthermore, we observed that under conditions relevant for monthly oscillator entrainment, L-Cry's subcellular localization markedly differs between naturalistic sun- versus moonlight conditions (*4*). However, as the conditions relevant for the PCC clock entrainment are different from those relevant for the monthly oscillator entrainment, we therefore tested if L-Cry protein in the worm exhibited any differences when animals were exposed to naturalistic sun–or moonlight under conditions relevant for

the behavioral paradigms shown in Fig. 1 and 2. We made use of a *Pdu*-L-Cry-specific antibody (for antibody generation and validation see (*4*). We first assessed L-Cry abundance in head extracts of animals sampled at the midpoint of the subjective night (at new moon: NM), after 4h of darkness or exposure to either naturalistic sun- or moonlight (Fig. 3a, CT20, red arrows). As expected by the canonical *Drosophila* model and consistent with our previous analyses in S2 cells (*3*), naturalistic sunlight led to a significant reduction of L-Cry compared to heads sampled from animals maintained in darkness (Fig. 3b,c). In contrast, the levels of L-Cry protein in the heads of naturalistic moonlight-exposed animals was indistinguishable from dark levels (Fig. 3b,c).

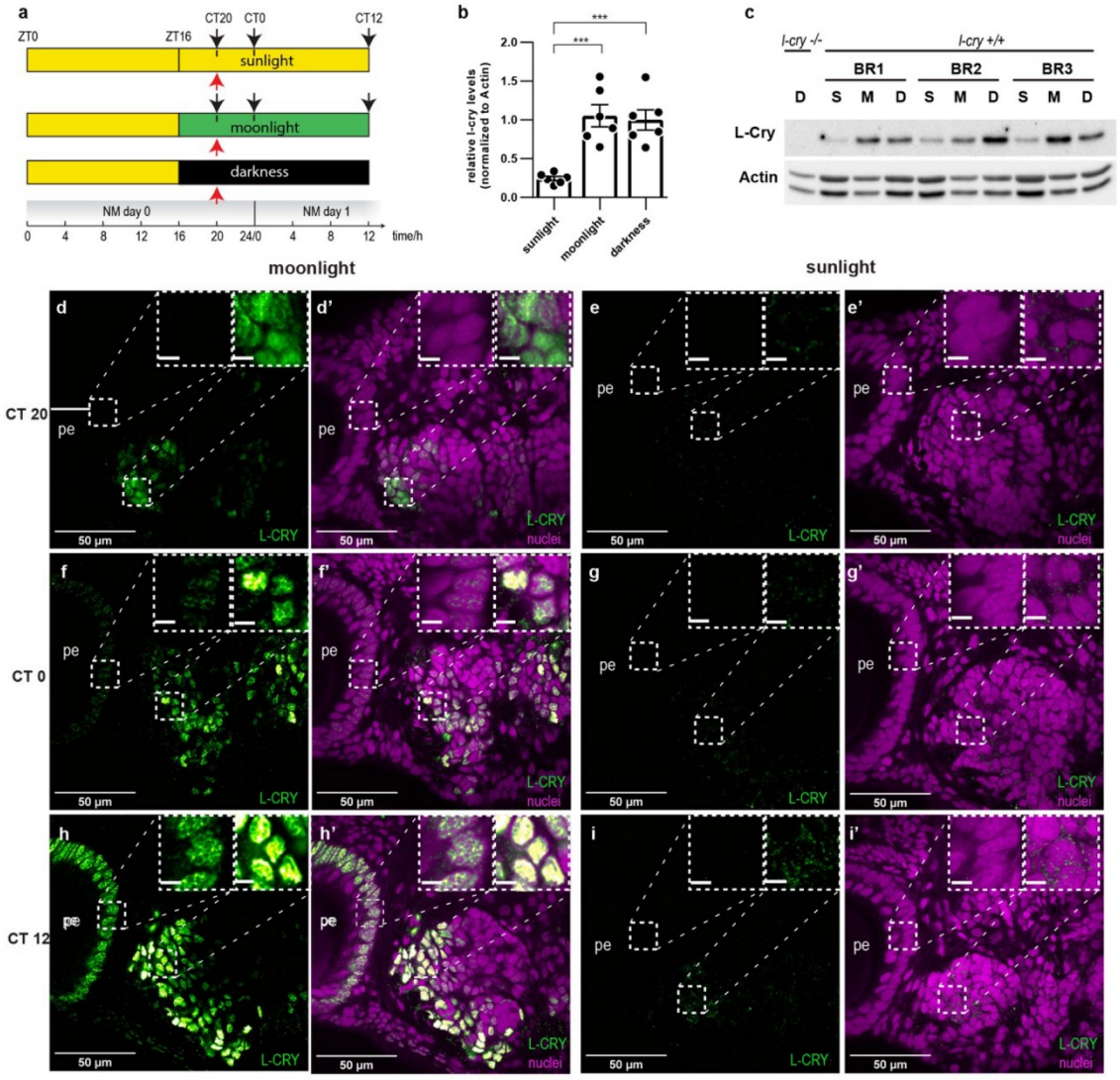

Fig. 3 | *Pdu*- L-Cry abundance and localization under darkness, naturalistic sun- and moonlight. (a) Sampling scheme of *Platynereis* heads for Western blot and immunohistochemistry. Red arrows: Western blots. Black arrows: immunohistochemistry. **(b)** Naturalistic sun- but not moonlight reduces L-Cry abundance. Head extracts sampled under naturalistic sunlight (S), moonlight (M) and darkness (D) were analyzed by Western blot and normalized against beta-actin, n=6 BRs. Bar graph: mean ± s.e.m. **(c)** Representative Western blot of 3 biological replicates (BR1-3). **(d-i)** Wildtype worm heads sampled under indicated naturalistic moon- or sunlight conditions, stained with an antibody against *Pdu*-L-Cry (green). **(d'-i')** and including nuclei stained with HOECHST (violet). Scale bar: 5µm. For comparison to dark night conditions see Fig. S3 and (*4*)

Immunohistochemical analyses at two distinct time points during the first subjective night of the respective light regime (CT20; CT0, black arrows Fig. 3a), and the following mid-day point (CT12, black arrows Fig. 3a) revealed that in naturalistic moonlight, L-Cry was predominantly localized in the nuclei of the eye photoreceptors and of cells in the posterior oval-shaped brain domain (Fig. 3d-h' and insets, for comparison to light/dark conditions: Fig. S3). By contrast, residual immunoreactivity of L-Cry under naturalistic sunlight appeared to be predominantly localized to the cytosol (insets Fig. 3e-i'), in line with a sunlight-dependent degradation pathway.

These results indicate that L-Cry has the potential to signal in distinct cellular compartments to discriminate between sun and moonlight valence under conditions relevant for impacting on the PCC clock, and in combination with the behavioral phenotypes suggests that L-Cry is required for the correct interpretation of sun- versus moonlight for the PCC clock.

Pharmaceutical disruption of canonical core circadian clock oscillations affects the PCC clock

We next wondered whether the PCC clock required the activity of the conventional core circadian clock. We previously showed that an inhibitor of the casein kinases 1δ/ε, PF670462, disrupts the worms' core circadian clock gene oscillations (*3*). The effect of this drug on the core circadian clock has also been shown in several other aquatic animals, as diverse as cnidarian, crustacean and teleost fish species (*13*–*15*).

After validating that an incubation in 160nM of PF670462 abolished molecular oscillations of core circadian clock transcripts (Fig. S4a), we assessed the effects of the drug on the timing of swarming onset. In contrast to mock-treated controls, the swarming onset in constant darkness was disrupted upon drug treatment (Fig. S4b). This finding is consistent with the notion that at least a subset of canonical circadian clock genes is required for the PCC clock, although we can at present not rule out that this effect could be caused by other targets of casein kinases 1δ/ε.

dCry prevents the fly's circadian clock from misinterpreting moonlight

As a regular nocturnal stimulus, moonlight reaches aquatic and terrestrial habitats. The ability to properly discriminate between moon– and sunlight is therefore likely important for any species that uses light-sensitive clocks. In many species, the conventional circadian clock should likely run with a constant period, irrespective of lunar phase. Thus, moonlight would need to be "blocked" from interfering with circadian rhythmicity in those organisms. Indeed, whereas fruit fly circadian behaviour can be experimentally entrained to LD cycles with light below full moon light intensity (*16*, *17*), and constant light at moonlight intensity can extend the period length of wildtype flies (*18*, *19*), moonlight

does not cause major effects on the circadian clock when combined with a LD cycle in this species (*20–23*).

Given our results about the importance of *Platynereis* L-Cry in discriminating between naturalistic sun- versus moonlight, and *Drosophila* dCry being its direct 1:1 ortholog, we hypothesized that this principal functionality of the d/L-Cry family might also be present in *Drosophila melanogaster*. Specifically, we wondered if nocturnal light mimicking moonlight would cause an increased shift of the circadian clock in *dCry* mutant flies compared to controls.

We monitored locomotor behaviour of both "cantonized" *cry*^{01} (*24*) and CantonS wildtype flies under LM conditions, adapting an existing locomotor paradigm (*25*), and using an artificial moonlight source matching full moon light intensities measured on land (Fig. S2d,e). In wildtype flies, moonlight delayed the evening peak to 2.2h± 0.13h (mean ± s.e.m.) after night onset (Fig. 4a,c), in line with previous observations (*21*), whereas *cry*^{01} mutants exhibited a significantly stronger delay, with the evening activity peak shifting to 4.4h ± 0.11h (mean ± s.e.m.) after night onset (Fig. 4b, c).

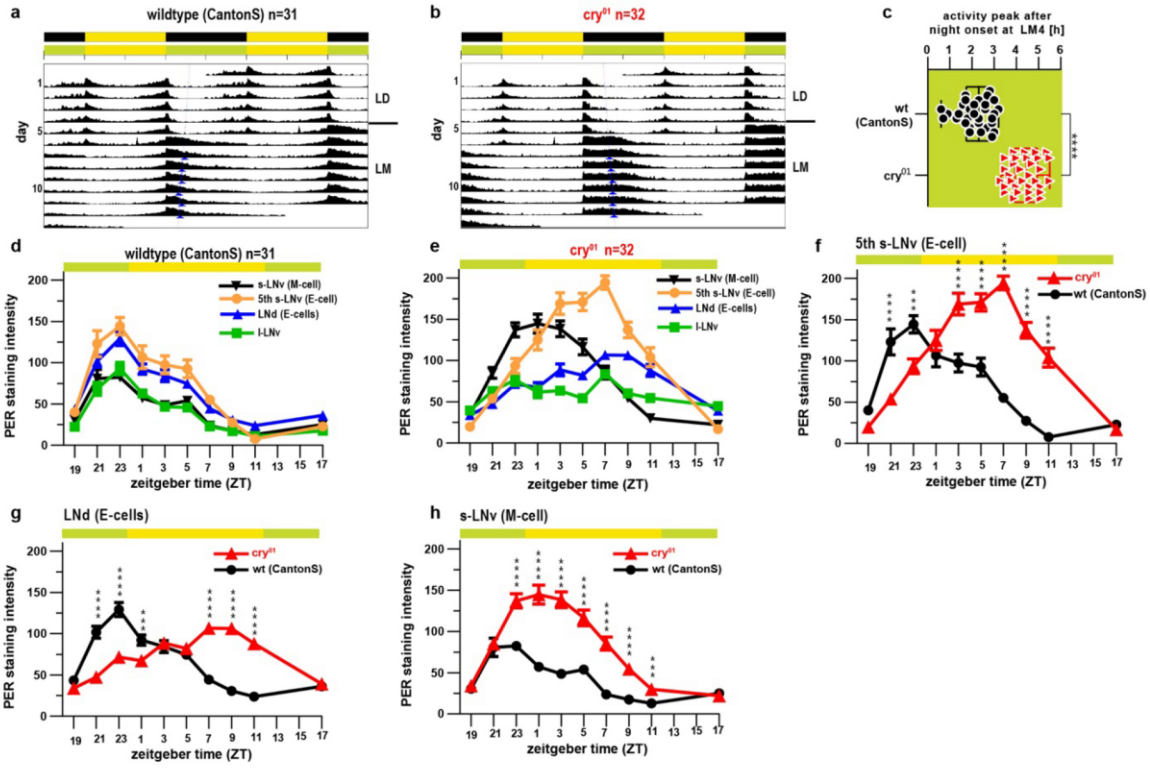

Fig. 4 | Drosophila cry protects circadian oscillator synchrony against moonlight. (a,b) Double-plotted actograms depicting average activity of wildtype (a) and *cry*^{01} (b) flies subjected to 12:12h light:dark (LD) cycles followed by light:moonlight (LM) cycles. Blue arrowheads indicate acrophases of the respective activity rhythms. **(c)** Timing of the E-peak during LM4, calculated from the data shown in (a) and (b). The value 0 represents the time of lights off **(d,e)** Quantified anti-PER immunolabeling intensity in different groups of lateral circadian clock neurons under LM conditions (LM4) in wild-type (c) and *cry*^{01} (d) individuals. **(f,g)** Detailed comparison of PER oscillations for neurons controlling evening activity, reveal a pronounced phase delay of about ~8h in cry^{01} mutants; **(h)** whereas neurons controlling morning activity show a more modest phase delay (2h-4h). Data in (f-h) are replotted from (d,e). *** : p<0.001; **** : p<0.001 ANOVA followed by Sidak´s multiple comparison test.

The increased delay of the evening activity peak in *cry*^{01} mutants could either be caused by acute effects of artificial moonlight on behaviour or by a shift in the fly's circadian clock. In order to discriminate between these possibilities, we subjected flies to artificial LM conditions and used an established immunolabeling strategy to systematically assess, over 10 distinct time points, changes in the abundance of the core circadian clock protein Period (PER) in the lateral neurons harboring the fly's circadian pacemaker. Anatomical location and the presence or absence of immunoreactivity against the neuropeptide PDF allowed us to quantify Period abundance in l-LN$_v$s, s-LN$_v$s (below also referred to as morning/M-cells), as well as 5th s-LN$_v$s and LN$_d$s (clusters harboring the evening/E-cells) (Fig. 4d-h).

Quantification across 132 CantonS wildtype individuals exposed to LM conditions revealed that oscillations of Period protein levels in the different sub-clusters were in synchrony with each other (Fig. 4d). In contrast, the corresponding *cry*^{01} mutants exhibited pronounced desynchronization of Period protein oscillations between cell groups, with E-cells differing from M-cells by ~ 6h (Fig. 4e). Similar analyses of *cry*^{01}-mutant flies raised in various LD cycles have not revealed such desynchronization (*26*), indicating that the effects we observed were specifically caused by exposure to artificial moonlight. When comparing Period protein abundances for the different cell classes between *cry*^{01} mutants and wildtypes, Period levels in E-cells exhibited a stronger peak delay (~8h; Fig. 4f,g) than M-cells (~2h; Fig. 4h). This correlates with the fact that the peak of evening activity is significantly delayed in our behavioural analyses of *cry*^{01} mutants compared to wildtypes under LM (Fig. 4a,b). Taken together, these results indicate that the increased delay of the evening activity peak in cry^{01} mutants under a LM light regime is the result of a desynchronization of the circadian clock rather than an acute light effect. This suggests that *Drosophila* dCry is naturally required to reduce the effects of moonlight on circadian clock oscillations, in particular in the cell clusters harboring the evening oscillator.

L-Cry, but not dCry is highly sensitive to moonlight

Given the genetic requirement of both L-Cry and dCry to correctly interpret moonlight under a combined moonlight/sunlight regime, we next wondered if the biochemical light sensitivity of both orthologs was also comparable. For this we purified both proteins in the presence of their co-factor flavine adenine dinucleotide (FAD) and tested for changes in absorbance after illumination. When light is sensed by dCry (*27*) or L-Cry (*4*), it changes the oxidized FAD to the reduced anionic radical FAD°$^-$ form, visible in the proteins' absorbance spectrum (*27*). Extending our work on L-Cry's biochemical features, we find that *Platynereis* L-Cry does not only respond to naturalistic full moon light (*4*), but does this even at intensities corresponding to 30% of full moon intensity at 4-5m seawater depths (Fig. 5a).

In contrast, dCry completely failed to respond to naturalistic moonlight levels equivalent to – and exceeding – those eliciting responses in *Platynereis* L-Cry (compare Fig. 5a with b,c). However, dCry was activated by naturalistic sunlight, reaching complete FAD reduction within 20min (Fig. 5b) as observed for L-Cry (*4*), underscoring the integrity of the purified dCry protein and the functionality of the assay.

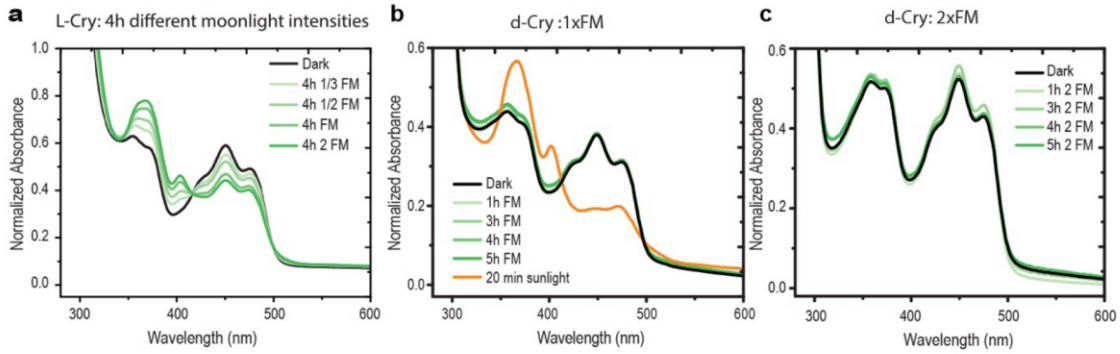

Fig. 5 | Comparison of L-Cry and dCry light detection. (a) Illumination of purified L-Cry protein with different moonlight intensities (green) for 4h results in photoreduction ($FAD^{\circ-}$ formation). FM= full moon: naturalistic full moon intensity ($9.7x10^{10}$ photons/cm^2/s), 1/3 FM: one third, 1/2 FM: one half, 2 FM: double of FM intensity. **(b,c)** dCry stimulation by moonlight (green) with naturalistic FM intensity (b) or double FM intensity (c) does not result in photoreduction, whereas naturalistic sunlight (orange) does. For detailed analyses on *Pdu*-L-Cry responses to naturalistic sun and moonlight see (*4*).

Even though dCry's sensitivity to dim light might be higher in its cellular context (*28*), this result clearly points at differences in the molecular mechanisms between dCry and L-Cry functions, possibly due to difference in the ability for dimer formation. On the ecophysiological level, this might be connected to the different meanings that moonlight has as an environmental cue for the daily behavior of flies versus swarming worms: Whereas fly circadian biology is likely optimized to buffer against the effect of moonlight, *Platynereis* worms, as shown above, use moonlight to precisely adjust their nocturnal swarming time to a favorable dark time window.

R-opsin1 detects moonrise to optimize the time of swarming onset

The retention of moonlight sensitivity in *Platynereis l-cry* mutants (as evidenced by the different mutant responses under the combined moon-and sunlight regimes versus no-moonlight regimes, Fig 2d-g) indicated the existence of one or more additional light receptors required for moonlight sensation. We reasoned that the spectral sensitivity of these photoreceptors likely includes the blue-green range, given the relatively high levels of blue-green light in our moonlight measurements (Fig. S2a).

The gene encoding r-Opsin1 is expressed in the adult *Platynereis* eyes both during early development (*29*, *30*) and later stages (*31*). In a heterologous expression assay established for assessing photoreceptor action spectra (*32*), *Platynereis* r-Opsin1 exhibits an irradiance response peak in the

blue range (λ_{max}= app. 470nm) (*33*), similar to the peak of its human melanopsin homolog. When we assessed the respective sensitivities of both receptors in side-by-side comparisons, the half-maximal effective irradiation (EI_{50}) of *Platynereis* r-Opsin1 ($2{,}3x10^{10}$ photons $cm^{-2}s^{-1}$) was ~100 times lower than that of melanopsin ($2{,}5x10^{12}$ photons cm^{-2} s^{-1}; Fig 6a), indicating a remarkably high sensitivity of *Pdu*-r-Opsin1.

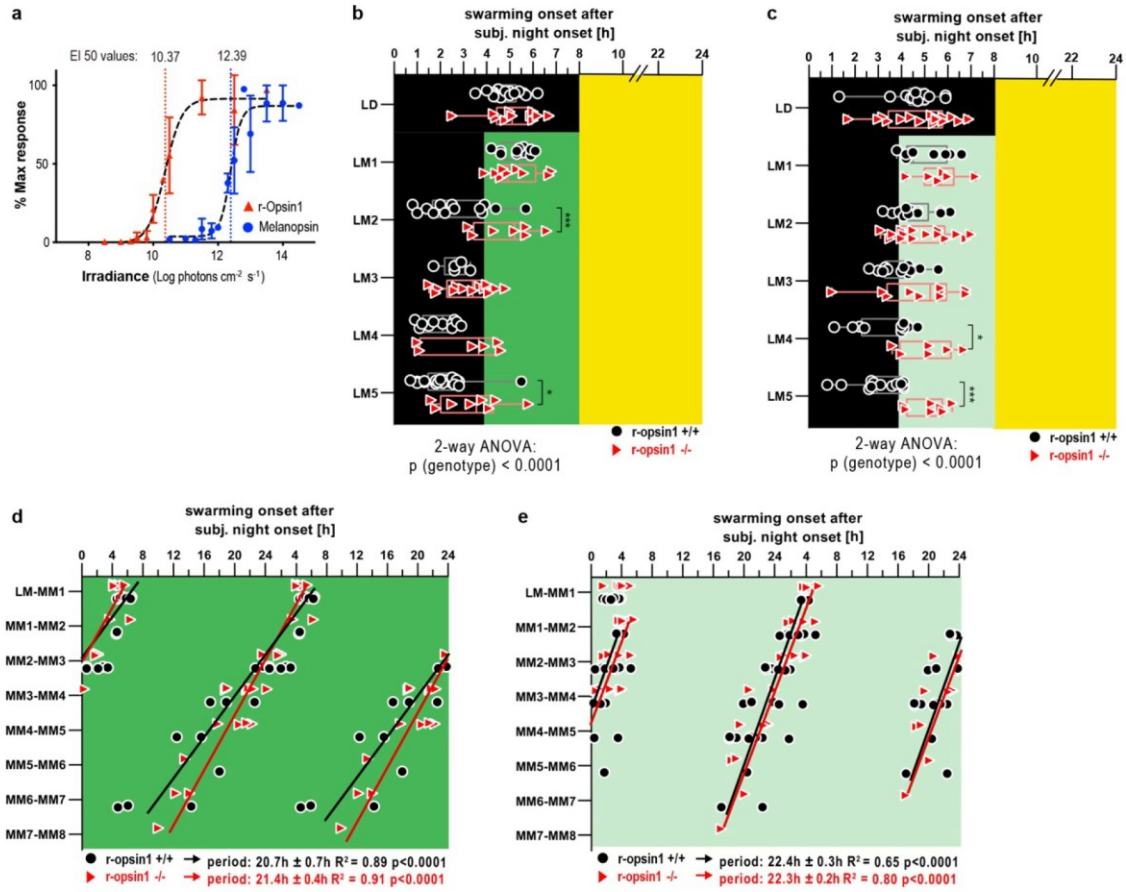

Fig. 6 | *Pdu*-r-Opsin1 functions as highly light-sensitive photoreceptor to adjust swarming onset under a waning moon light timing. (a) Responses of *Pdu-r-Opsin1* (red) and human Melanopsin (blue) to different blue light intensities (480nm ± 10nm) as quantified by a cell-based bioluminescent assay, reveal an ~100-fold higher sensitivity of Pdu-r-Opsin1. **(b-e)** Swarming onset of *r-opsin1*$^{-/-}$ and *r-opsin1*$^{+/+}$ worms entrained to 16:8h LD cycles and then subjected to a moon light regime typical for waning moon, i.e. moonlight during the second half of the night (LM) **(b,c)** or to constant moonlight **(d,e)** either with full moon light intensity (dark green) **(b,d)** or waning moon light intensity (light green = 20 % of full moon light intensity) **(c,e)**. * : p<0.05; ** : p<0.001; *** : p<0.0001 2-way ANOVA followed by Sidak´s multiple comparison test. Black and red lines in (d,e) indicate linear regression lines of wildtype and *r-opsin1*$^{-/-}$ mutants, respectively. The period length was calculated based on the slope of the regression line (from MM1-MM8) ± the 95% CI of the slope.

In the animal, this molecular sensitivity is combined with a high abundance of r-Opsin1: On the transcript level, a cellular profiling analysis revealed that *r-opsin1* is one of the topmost expressed genes in *Platynereis* adult eye photoreceptors, outnumbering a distinct co-expressed opsin – *r-opsin3* – by nearly three orders of magnitude (*33*). Moreover, in the course of the metamorphic changes that occurs during the days immediately prior to swarming, the outer segments of the eye photoreceptors –

where Opsin molecules are concentrated in tightly packed membrane stacks – extend to around twice their length, suggesting an even increased sensitivity (*34*). All these facts infer that r-Opsin1 acts as a particularly high-sensitive light detector at the time of swarming.

To test whether r-Opsin1 was indeed required to mediate the impact of moonlight on the timing of swarming onset, we capitalized on an existing *r-opsin1*$^{-17/-17}$ loss-of-function allele (*33*). Following the experimental design of Fig. 1e, we subjected homozygous *r-opsin1*$^{-17/-17}$ mutants and related wildtype individuals for 5 days to naturalistic moonlight during the second half of the night (Fig. 6b). *r-opsin1*$^{-/-}$ animals exhibited a significantly reduced ability to shift their swarming onset to the dark portion of the night compared to wildtypes (Fig. 6b). This difference became even stronger with naturalistic moonlight at lower intensities (as this would be the case for the natural waning moon) (Fig. 6c). Finally, we wondered if *r-opsin1* mutants would also exhibit a reduced ability to reset the PCC clock under constant moonlight. Under constant moonlight at naturalistic full moon (Fig. 6d) or waning moon (Fig. 6e) light intensities, *r-opsin1* mutants were indistinguishable from wildtype. This let us conclude that *r-opsin1* specifically enables the worms to detect moon rise to align the PCC clock accordingly, .

Taken together, our data argue for two distinct roles of L-Cry and r-Opsin1 in decoding naturalistic moonlight and adjusting the PCC clock (Fig. 7): L-Cry, with its biochemically distinct “moonlight-state”, yet slow activation kinetics *in vitro* (*4*), is able to shorten the period of the PCC clock under sustained moonlight conditions, as they occur around natural “full moon” phases (Fig.7a). In turn, r-Opsin1’s sensitivity, response kinetics and abundance in the eye photoreceptors make it suited to detect even weak, acute dim light, as caused by the rising moon in a “waning moon” phase, and advance the PCC clock under conditions of the waning moon which cannot be appropriately detected by L-Cry alone due to its properties (Fig. 7b). We hypothesize that – like in the case of the monthly oscillator – the distinct nuclear localization of L-Cry during night and day (Fig.7a-c) provides key information on the valence of light. Whereas *r-opsin1* has no involvement in the entrainment of the monthly oscillator (unpublished data), our data indicate that in case of the PCC clock, it is relevant for mediating dim light information. The combination of L-Cry’s and r-Opsin1’s properties therefore allow the PCC clock to distinguish not only between sunlight, full and new moon, but also the progressive phases of the waning moon, which are particularly relevant to set the right spawning hour (Fig. 7).

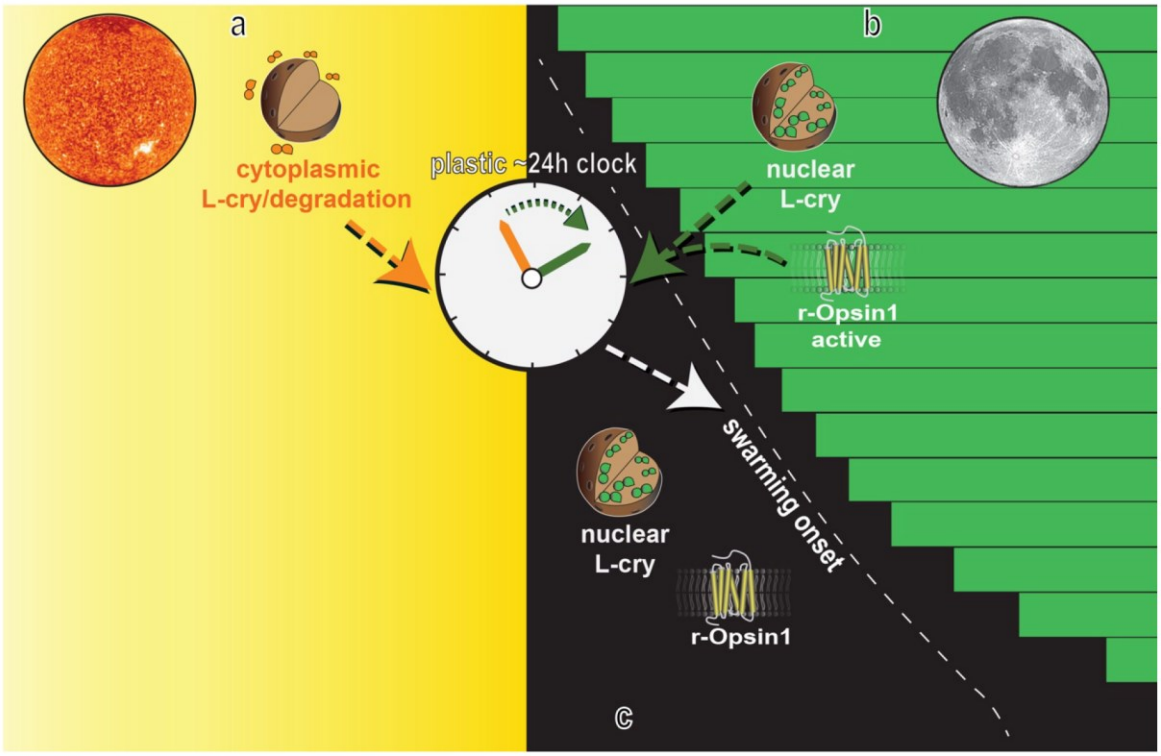

Fig. 7. Model of how the combinatorial responses of L-Cry and r-Opsin1 might encode sunlight, moonlight and darkness to adjust the plastic circadian/circalunidian clock to control the hour of swarming onset. (a) Sunlight fully photoreduces L-Cry (*4*), triggers its degradation (Fig. 3b and *4*) and likely synchronizes the PCC clock to the 24h solar day. **(b)** Prolonged moonlight likely activates nuclear L-Cry in a non-canonical fashion, as L-Cry is required to shorten circadian period length under prolonged moonlight conditions (Fig. 2b). r-Opsin1 with its rapid activation and high light sensitivity is critical to correctly adjust the PCC clock to the dim light of the waning moon (Fig. 6 b,c) in order to optimize swarming onset time prior to naturally occurring moonrise. **(c)** Under darkness, L-Cry is also abundantly present in the nucleus (Fig. S3 and ref. (*4*)), but neither r-opsin1 or L-Cry are photoactivated.

Discussion

Here we uncover a ~24hr endogenous oscillator in marine broadcast-spawning worms that exhibits marked, moonlight-dependent plasticity in its period length. Its modulation by naturalistic moonlight provides a plausible model for how worms synchronize their nuptial dance, targeting a specific hour during the dark portion of moonlit nights. Restricting swarming behaviour to the dark portion of the night might be advantageous to avoid predators that hunt during moonlight. On a mechanistic level, we suggest that this PCC clock shares elements with the conventional core circadian oscillator, and reveal two highly sensitive light receptors, r-Opsin1 and L-Cry, that are critical to sense and interpret naturalistic moonlight.

Sensitivity to moonlight is directly relevant for a broad panel of marine broadcast spawners. The challenge of “tagging” nocturnal light information with the correct valence, however, likely extends beyond this specific ecological context. The classical categorization of organisms into nocturnal versus diurnal species (*35*, *36*) typically neglects the aspect of moonlight. Any animal entraining its ~24hr clock

to light will need to correctly interpret the occurrence of nocturnal light. Even though it has been shown that the circadian system of many species is sensitive to light levels as low as moonlight intensity, such as in flies (*16*, *17*) and mice (*37*), chronobiological studies have so far spent relatively little effort in dissecting how animal clocks prevent potential disturbance of moonlight, and interpret naturalistic light regimes that combine both sun– and moonlight.

The data presented here provide possible mechanistic explanations for the ability of the PCC clock to decode a combined sun– and moonlight regime. A first tier is connected to the specific properties of cryptochrome: Whereas under naturalistic moonlight, *Platynereis* L-Cry protein levels remain elevated, comparable to dark conditions, and are predominantly localized to the nucleus, the onset of sunlight causes a rapid degradation, with residual L-Cry protein found in the cytoplasm. On the biochemical level, L-Cry is highly sensitive to naturalistic moonlight. Moonlight evokes a different state in L-Cry than sunlight (see extensive comparison of sunlight vs. moonlight in reference *4*). Taken together, these data are consistent with the idea that – besides the canonical strong-light induced degradation-based signaling pathway for cytoplasmic Cryptochrome – L-Cry possesses a second, dim-light induced, nuclear mode of signaling. A second lead is provided by our identification of r-Opsin1 as a second moonlight sensor. It remains to be uncovered, however, how the r-Opsin1-dependent signals tie in with the different signaling states of L-Cry.

Evidence for plasticity of the conventional circadian clock has started to emerge from other marine systems: Work on the circatidal oscillators of oysters maintained under controlled lab conditions revealed that core circadian clock genes exhibit ~12.4hr cycles under constant darkness, whereas the transcripts of the same genes cycle with a ~24hr oscillation under light/dark conditions (*38*). This provides evidence for the ability of the canonical clock to alternate between circadian (~24h) and (semi)circalunidian (~12.4h/~24.8h) periodicities. Of note, switches between circadian and circalunidian cycles might also occur in humans. For instance, mood switches of bipolar patients correlate with a period lengthening of their body temperature cycles that looks as if the circadian timing system can be intermittently entrained to a 24.8h rhythm (*39*). Moreover, already classical chronobiological studies documented changes of the ~24h clock periodicity under dim light in various organisms, including birds, mice, hamsters and humans *(40, 41)*, as well as the fruit fly *Drosophila melanogaster (42)*. Whereas the meaning of these results had remained enigmatic, they could well be explained by the conceptual framework of combined solar and lunar light cues that we present in our study. We anticipate that research on organisms for which lunar impact is of known biological relevance will be key to disentangle the interplay of solar and lunar timing cues.

Material and Methods

Worm culture

Worms were grown as described previously (*8*). In short: worms were kept in plastic boxes filled with a 1:1 mixture of natural sea water and artificial sea water (30% Tropic Marine) and exposed to a 16h : 8h light:dark light regime. To entrain their circalunar clock, worms receive 8 nights of continuous nocturnal light each month to mimic full moon (FM).

Strains: *l-cry*$^{-/-}$*:* homozygous Δ34, generated in the VIO-strain background (see (*4*)). Wildtype worms used for comparison to *l-cry*$^{-/-}$ worms are cousin relatives to *l-cry*$^{-/-}$ worms.

r-opsin1$^{-/-}$*:* homozygous Δ17, generated in the *r-ops1::GFP* transgenic strain (*33*). Wildtype worms used for comparison are from the *r-ops1::GFP* transgenic strain from which the mutant was generated.

Natural light measurements

Under water measurements of natural sun- and moonlight at the habitat of *Platynereis* were acquired using a RAMSES-ACC-VIS hyperspectral radiometer (TriOS GmbH) for UV to IR spectral range (see (*9*) for details). Radiometers were placed at 4m and 5m water depth close to *Posidonia oceanica* meadows, which are a natural habitat for *P. dumerilii*. Measurements were recorded automatically every 15min across several weeks in the winter 2011/2012 (at 5m depth) and during spring 2011 (at a 4m depth). To obtain an exemplary sunlight spectrum, the sunlight measurements taken at 5m depth between 10 am-4 pm on 25.11.2011 we averaged. To obtain a full moon spectrum for the 5m depth location measurements taken from 10pm to 1am on a clear full moon night (10-11.11.2011) were averaged. To control for technical noise caused by the measurement device at these low light intensities, a NM spectrum was obtained by averaging measurements between 7:15pm to 5am on a NM night on 24.11.2011, and subtracted from the FM spectrum. The resulting spectrum is plotted in Fig. S2a. To validate that this spectrum is representative of a typical full moon spectrum at the habitat of *Platynereis*, we averaged moonlight measured between 10:15 pm to 2am during a full moon night (17.-18.04.2012) and subtracted a NM spectrum measured two weeks earlier from 4m depth (Fig. S2a). To benchmark these moonlight spectra measured under water with moonlight measured on land, we compared the underwater spectra to a publicly available full moon spectrum measured on land on 14.04.2014 in the Netherlands (Fig. S2a, http://www.olino.org/blog/us/articles/2015/10/05/spectrum-of-moon-light). As expected, light with longer wavelengths was strongly reduced in the underwater measurements compared to the surface spectrum, since light with longer wavelengths penetrates water less efficiently.

461 **Behavioural setup and analyses of swarming onset**

462 All behavioural experiments, except Fig. 1b and Fig. 2f,g were performed with worms that received LD
463 conditions without any nocturnal light (FM) for at least 9 days. Since most *l-cry* mutants spawn during
464 the first 9 nights after the FM stimulus under standard worm culture conditions (*4*) , the monthly FM
465 stimulus was omitted for *l-cry* mutants and wildtypes in order to test swarming worms without
466 confounding effect of a recent nocturnal (highly artificial) light stimulus on swarming onset.
467 Sexually maturing worms were placed in seawater filled individual hemispherical concave wells
468 (diameter = 35mm, depth = 15mm) of a custom-made 36-well clear plastic plate. Video recording of
469 worm's behavior over several days was accomplished as described previously (*3*), using an infrared (λ
470 = 990 nm) LED array (Roschwege GmbH) illuminating the behavioral chamber and an infrared high-
471 pass filter restricting the video camera. Worms were recorded at least until initiation of swarming
472 (fig.S1A). Naturalistic sun- and moonlight were generated by custom made LEDs (Marine Breeding
473 Systems, St. Gallen, Switzerland) (for spectra and intensity see Fig. S2b,e). Naturalistic sun- and
474 moonlight were used in all worm experiments, except for data obtained in Fig. 1b and Fig. 2e-g were
475 we used prototype artificial sun- and moonlight LEDs (Fig. S2c).
476 Spectra were measured with a calibrated ILT950 spectrometer (International Light Technologies Inc.,
477 Peabody, USA). To reliable measure the artificial moonlight, the detector was placed 12cm away from
478 the moonlight source, and based on this measurement moonlight intensity was calculated using the
479 inverse square law for worm position, which was ~51 cm away from the moonlight source.
480 After video recording, an automated tracking software was used to deduce locomotor activity of
481 individual worms across the time of the recording (*9*). The exported locomotor activity trajectories,
482 which reflect the distance moved of each worm's center point across 6 min time bins, were analyzed
483 in ActogramJ to manually identify the swarming onset moment. In ambiguous cases (e.g. only little
484 movement detected) we manually analyzed the video recordings to identify the moment when a
485 sexually mature worm left its tube, which was regarded as swarming onset. Swarming onset data were
486 plotted and analyzed using GraphPad Prism 8.0 (La Jolla, USA). ANOVA was used to test if swarming
487 onset was statistically different across the different days of an experiment. This was followed by
488 Dunnetts multiple comparison test, comparing each day of the experiment with swarming onset during
489 LD conditions. To test differences in swarming onset between mutants and wildtypes across different
490 days of an experiment with varying light conditions, 2-way ANOVA was used followed by Sidak´s
491 multiple comparison test. To identify the free-running periodicity under constant light conditions linear
492 regression analysis was performed. The period length was calculated based on the slope of the
493 regression line ± the 95% CI of the slope. Swarming onset data are presented including the individual
494 data points and a box plot. The whiskers of the box blot represent minimal and maximal values.
495

Recording of locomotor activity in *Drosophila melanogaster*

Locomotor activity was recorded under constant temperature (20°C) from 0-1 day old male Canton-S and cry^{01} (CantonS background) flies using the *Drosophila* Activity Monitors from Trikinetics Incorporation (Waltham, MA, USA)(*25*). Flies were first recorded for 5 days under 12h light - 12h dark cycles (=LD with ~100 lx standard white light LED), and then under for 7 days under 12h light – 12h artificial moonlight cycles (=LM cycles; for spectrum and intensity of artificial moonlight see fig.S2C). The average actograms and the centers of maximal activity were calculated and plotted with ActogramJ (*43*). The phases of evening activity maxima under LM conditions were determined using the ActogramJ tool "acrophase". To test for differences in the acrophase of wildtype and cry^{01} flies at LM4, an unpaired student-test was performed.

Western blots

Four anaesthetized worms were decapitated and heads transferred to a 1.5ml tube containing 150 µl RIPA lysis buffer (R0278 Sigma-Aldrich) supplemented with 10% Triton X100 and protease inhibitor (cOmplete Tablets, EDTA-free, EASYpack, Roche) per biological replicate. The tissue was homogenized by grinding using a tightly fitting pestle. All steps on ice. Cell debris was pelleted by centrifugation. Protein concentration of lysates was determined using Bradford reagent (BIORAD). Proteins were separated by SDS-gel electrophoresis (10% Acrylamide) and transferred to nitrocellulose membrane (Amersham™ Protran™ 0,45µm NC, GE Healthcare Lifescience). Quality of transfer was confirmed by staining with Ponceau-S solution (Sigma Aldrich). After 1h of blocking with 5% slim milk powder (Fixmilch Instant, MARESI) in 1xPTW (1xPBS/0.1% TWEEN 20) at room temperature, the membrane was incubated with the appropriate primary antibody, diluted in 2.5% milk/PTW at 4°C O/N. [anti-L-Cry 5E3-3E6-E8 (1:100) and anti-L-Cry 4D4-3E12-E7 (1:100); anti-beta-Actin (Sigma, A-2066, 1: 20.000)]. After 3 rinses with 1xPTW the membrane was incubated with the species specific secondary antibody [anti-Mouse IgG-Peroxidase antibody, (Sigma, A4416, 1:7500); Anti-rabbit IgG-HRP-linked antibody (Cell Signaling Technology, #7074, 1:7.500] diluted in 1xPTW/1% slim milk powder for 1 hour. After washing, SuperSignal™ West Femto Maximum Sensitivity Substrate kit (Thermo Fisher Scientific) was used for HRP-signal detection and finally signals were visualized by ChemiDoc Imaging System (BIORAD). Bands were quantified in "Image Lab 6.1" (BIORAD)

Immunohistochemistry

Portions of *Platynereis dumerilii* bodies containing head and jaw were dissected and fixed in 4% PFA at 4° C for 24 h. Afterwards, methanol washes at room temperature (r.t., shaking) and a 5-minutes long digestion using Proteinase K (r.t., not shaking) were employed as means of permeabilization. The worm heads and jaws were then post-fixed with 4% PFA for 20 min at r.t. and washed using 1x PTW (PBS-

0.1% Tween 20® (Sigma Aldrich)) 5 times for 5 min. This was followed by over-night incubation in a hybridization mixture (*42*), commonly used for in situ hybridization (at 65° C in water bath; the solution exchanged once, after the first hour of incubation). Several washing steps were performed the following day, at 65° C in a thermo-block, not shaking (washing sequence, solutions and durations: a. 2 times 20 min with 50% formamide/2X standard saline citrate - 0.1% Tween 20® (Sigma Aldrich), SSCT; b. 2 times 10 min with 2X SSCT; c. 2 times 20 min with 0.2X SSCT). Samples were subsequently blocked using 5% sheep serum (Sigma-Aldrich) (r.t., 90 min, shaking) and incubated for at least 36 h (4° C, shaking) in a mixture of two monoclonal antibodies against L-Cry, 5E3-3E6-E8 and 4D4-3E12-E7 (1:100 and 1:50, correspondingly, in 5% sheep serum (Sigma-Aldrich)) (see accompanying manuscript for further details). Next, samples were washed with 1x PTW 3 times for 15 min (r.t., shaking) and a 1 time over night (4° C, shaking). A Cy3 goat anti-mouse IgG secondary antibody (A10521, Thermo Fisher Scientific) was added in dilution 1:400 in 2.5% sheep serum to specifically detect the bound primary antibody (incubation time and conditions, as well as the following washing steps, were the same as those of the primary antibody). To label nuclei, samples were incubated for 30 min in Höchst 33342 (H3570, Thermo Fisher Scientific), diluted 1:2000 (r.t., shaking), washed 3 times for 15 min using 1x PTW and mounted in 87% glycerol (Sigma-Aldrich)/ddH_2O containing 25 mg/ml DABCO (Roth/Lactan). All solutions were made using 1x PTW unless stated otherwise.

Imaging of the worm heads was done using a Zeiss LSM 700 laser scanning confocal microscope and LD LCI Plan-Apochromat 25X and Plan-Apochromat 40X by CHD objectives, T-PMT detection system and Zeiss ZEN 2012 software (lasers used: DAPI 405 nm and Cy3 555 nm). Image analysis was performed using the software Fiji/ImageJ (*45*).

Period oscillations in Drosophila clock neurons

To compare the effect of moonlight between cry mutants and wildtypes on the Period oscillations in the different clock neuron clusters we entrained 0-1 day old male Canton-S and *cry01* (CantonS background) flies first under 12h light - 12h dark cycles (~100 lx standard white light LED), and then subjected them to artificial moonlight during the night (=LM cycles; for spectrum fig.S2C) for another 4 days. At LM4 whole flies were fixed at the indicated ZTs (for 3h) with 4% PFA + 0.1% TritonX100. Flies were then washed 3x10min in PBT 0.5% and their brains were dissected. Subsequently, brains were blocked with 5% NGS in PBT 0.5% for 3 hours. Brains were incubated for 48h at 4°C with the following primary antibodies diluted in PBT 0.5% + 5% NGS: rabbit anti-PER (1:1000), mouse anti-Pdf (1:1000). The secondary antibodies were goat anti-rabbit Alexa™ fluor 488 (1:200) and goat anti-mouse Alexa™ 635 (1:200) incubated at 4°C overnight. Before mounting, brains were washed 6x with PBT 0.5% (last wash with PBT 0.1%) and then mounted in Vectashield H-1000. Images were acquired with TCS SPE Leica confocal microscope using a 20-fold glycerol immersion objective (Leica Mikrosystems, Wetzlar, Germany) and analyzed with ImageJ as described in ref. (*46*). PER staining intensity in the different

pacemaker cell groups was examined in 12-15 brains (one hemisphere per brain) per timepoint and genotype. To obtain PER staining intensity above background for of each cell group, the PER signal of all cells of a cell group in one hemisphere was averaged and background signal measured near this cell group was subtracted. In case not all cells of a specific cell group could be identified, these missing cells were ignored for analysis.

Finally, to obtain an average staining intensity per cell group, the corresponding staining intensities of all 12-15 brain hemispheres sampled during one timepoints were averaged.

Opsin spectral sensitivity comparison

To investigate the spectral sensitivity comparison of Pdu r-opsin1 to human melanopsin, mammalian expression vectors for both opsins were independently co-transfected into HEK293 cells along with an expression vector containing the luminescent calcium sensitive protein, Aeuqorin (pcDNA5/FRT/TO mtAeq) using Lipofectamine 2000 to access the activation of Gαq signaling as shown in previously published work (Roger publication, Bailes et al). After 6hrs incubation, the medium was changed to DMEM containing 10% FBS and 10uM 9-cis retinal, after which point the cells were protected from light. The following day, medium was changed to L-15 without phenol red, containing 10uM Coelentrazine-h and 10uM 9-cis retinal. Individual wells were briefly exposed to a 2s flash of near monochromatic light (480nm +/- 10nm) produced from an Xenon arc lamp and delivered via a fiber-optic cable fixed ~10cm above the relevant well and accessed for increase in calcium level by measuring the raw luminescence (RLU) signal with a resolution of 0.5s and cycle of 2s. Luminescence was read using a Clariostar (BMG labtech). Light intensity was modified using combinations of 0.9, 0.2 and 0.1 Neutral density filters. RLU measured during dark incubation preceding the light pulse were used as baseline. Maximum response was determined by the peak luminescence value post light flash, normalised to the maximum luminescence value recorded, per opsin, for that experiment. The resultant maximal response value acquired from each replicate were plotted against the irradiance measured for tested wavelength. This irradiance response curve was then fitted with a sigmoidal dose response function to understand the maximum sensitivity of both opsins.

Casein kinase inhibitor treatment and qPCRs

Worms were treated with indicated concentrations of PF-670462 for 3 days under LD conditions during new moon. For sampling, worms were first anaesthetized for ca. 10min with a 1:1 mixture of seawater and 7.5% (w/v) MgCl2 solution. The head was then cut behind the posterior eyes with a scalpel at the indicated timepoints. Five heads were pooled per biological replicate, immediately frozen in liquid nitrogen and stored at -80°C until RNA extraction.

For RNA extraction, 350µl of RNAzol RT (Sigma-Aldrich) were added to the samples and lysis was performed with TissueLyser II (Qiagen) at 30Hz for 2min. Afterwards, RNA was extracted using Direct-zol RNA Miniprep kit (Zymo Research) following the manufacturer's instructions with additional on-column DNaseI digest. RNA was eluted in 34µl of nuclease-free water.

Total RNA (300ng per sample) was reverse transcribed using QuantiTect Reverse Transcription Kit (Qiagen). The resulting cDNA was diluted to a volume of 60µl. qPCR reactions were performed in 20µl total volume with Luna Universal qPCR Master Mix (New England Biolabs). Target genes and reference controls were analysed in duplicate reactions for all samples. Plate control cDNA and -RT controls were included on each plate. cdc5 was used as reference gene(*3*). Expression levels were calculated using the Δct method. Relative expression values were calculated with the formula: relative expression = 2 - Δct.

Recombinant expression and purification of L-Cry and dCry proteins

L-Cry was expressed and purified from insect cells as described in (*4*). N-terminally His6-tagged dCry was expressed in *Spodoptera frugiperda* (*Sf9*) insect cells using a pFastBac HTb expression vector (Berndt et al, 2007). 1 L of 1 * 10^6 *Sf9* cells/ml in sf900II media were transfected with P1 virus stock and incubated at 27°C for 72 h. Harvested cell pellets were resuspended in lysis buffer (25 mM Tris pH 8.0, 300 mM NaCl, 20 mM imidazole, 5% glycerol, 5 mM β-mercaptoethanol) and lysed by sonication. The lysate was centrifuged and the clarified supernatant loaded onto a 5ml HisTrap HP nickel affinity column (GE Healthcare). dCry protein was eluted with 100 mM imidazole, diluted with low salt buffer (50 mM Tris pH 8.0, 5% glycerol, 1mM DTT) and loaded onto a 5 ml DEAE sepharose anion exchange column (GE Healthcare). After gradient elution (0 to 500 mM NaCl), dCry containing fractions were concentrated and loaded onto a HiLoad S200 16/60 size exclusion chromatography (SEC) column (buffer 25 mM Tris pH 8.0, 150 mM NaCl, 5% glycerol, 1 mM TCEP). SEC fractions containing pure dCry protein were pooled, concentrated and stored at -80°C until further use. All purification steps were carried out in dark- or dim red light conditions.

UV/VIS spectroscopy of L-Cry and dCry

UV/VIS absorption spectra of purified L-Cry and dCry proteins were recorded on a Tecan Spark 20M plate reader. An intensity calibrated naturalistic moonlight source (Fig. S2b) was used for moonlight UV/VIS spectroscopy on L-Cry and dCry. Naturalistic full moon (FM) intensity was set to 9.67 x 10^{10} photons $cm^{-2}s^{-1}$. To analyze moonlight dose-dependent FAD photoreduction of L-Cry, dark-adapted L-Cry was illuminated with different moonlight intensities (1/3 FM, 1/2 FM, FM and 2 FM intensity) continuously for 4 h on ice and UV-VIS spectra (300 – 700 nm) were collected after 4 h. To analyze sunlight- and moonlight dependent FAD photoreduction of dCry, dark-adapted dCry (kept on ice) was

continuously illuminated with naturalistic sunlight (1.55 x 10^{15} photons cm^{-2} s^{-1} at the sample) or naturalistic moonlight (9.67 x 10^{10} photons cm^{-2} s^{-1} at the sample) and UV-VIS spectra (300 – 700 nm) were collected at different time points.

Statistical analyses

We used one-way ANOVA followed by Dunnett´s test to test if the timing of swarming onset during LD conditions differs compared to conditions were worms are subjected to moonlight conditions on top of a LD cycle. We used two-way ANOVA followed by Sidak´s test to test if and during which days the timing of swarming onset differs between mutant and wildtypes across different days of a behavioural experiment. To compare if two sets of data had different variances, a F-test as part of t-test statistics was performed. Swarming onset data are shown as individual data points, and additionally represented as box plots with whiskers reaching to the maximal and minimal value.

Western blot data, which assessed head L-Cry levels during sunlight, moonlight and darkness conditions were analyzed with one-way ANOVA followed by Tukey´s multiple comparison test to test for significant differences in L-Cry abundance between the different light conditions.

To compare period oscillation in the different cell groups between *cry01* mutants and wildtype flies over different ZTs we used two-way ANOVA followed by Sidak´s test.

Acknowledgements

We thank the members of the Tessmar-Raible, Raible, Helfrich-Förster and Wolf groups for discussions. Andrej Belokurov and Margaryta Borysova for excellent worm care at the MFPL aquatic facility. We are grateful for support by the IMB Protein Production and Proteomics Core Facilities (instrument funded by DFG INST 247/766-1 FUGG).

Funding: K.T-R. received funding for this research from the European Research Council under the European Community‘s Seventh Framework Programme (FP7/2007–2013) ERC Grant Agreement 337011 and the Horizon 2020 Programme ERC Grant Agreement 819952, the research platform ‘Rhythms of Life’ of the University of Vienna, the Austrian Science Fund (FWF, http://www.fwf.ac.at/en/): SFB F78 and the HFSP (http://www.hfsp.org/) research grant (#RGY0082/2010). S.K. is a recipient of a DFG fellowship through the Excellence Initiative by the Graduate School Materials Science in Mainz (GSC 266). C.H-F. was funded by Deutsche Forschungsgemeinschaft (DFG), collaborative research center SFB 1047 “Insect timing,” Project A1 and A2. None of the funding bodies was involved in the design of the study, the collection, analysis, and interpretation of data or in writing the manuscript. RJL received support from the HFSP (project grant RGP0034/2014).

669
670
671 # References

672 1. S. Ranzi, *Pubbl. del Stn. Zool. Napoli*. **11**, 271–292 (1931).

673 2. C. Hauenschild, *Cold Spring Harb. Symp. Quant. Biol.* **25**, 491–497 (1960).

674 3. J. Zantke *et al.*, *Cell Rep.* **5**, 99–113 (2013).

675 4. B. Poehn *et al.*, *bioRxiv* (2021), doi:10.1101/2021.04.16.439809.

676 5. H. Caspers, *Mar. Biol.* **79**, 229–236 (1984).

677 6. G. R. Gaston, J. Hall, *Gulf Caribb. Res.* **12**, 47–51 (2000).

678 7. J. Zantke, S. Bannister, V. B. V. Rajan, F. Raible, K. Tessmar-Raible, *Genetics*. **197**, 19–31 (2014).

679 8. S. Schenk *et al.*, *Elife*. **8**, 1–39 (2019).

680 9. V. B. Veedin Rajan *et al.*, *Nat. Ecol. Evol.* **5**, 204–218 (2021).

681 10. M. van der Steen, Spectrum of moon light, (available at
682 http://www.olino.org/blog/us/articles/2015/10/05/spectrum-of-moon-light).

683 11. O. Levy *et al.*, *Science*. **318**, 467–470 (2007).

684 12. L. E. Foley, P. Emery, *J. Biol. Rhythms*. **35** (2020), pp. 16–27.

685 13. L. Zhang *et al.*, *Curr. Biol.* **23**, 1863–1873 (2013).

686 14. S. S. Storz *et al.*, *PLoS One*. **8** (2013), doi:10.1371/journal.pone.0054189.

687 15. M. Oren, A. M. Tarrant, S. Alon, N. Simon-blecher, I. Elbaz, *Sci. Rep.* **5**, 1–15 (2015).

688 16. A. Klarsfeld *et al.*, *J. Neurosci.* **24**, 1468–1477 (2004).

689 17. J. Hirsh *et al.*, *Curr. Biol.* **20**, 209–214 (2010).

690 18. T. Yoshii *et al.*, *J. Insect Physiol.* **50**, 479–488 (2004).

691 19. R. J. Konopka, C. Pittendrigh, D. Orr, *J. Neurogenet.* **6**, 1–10 (1989).

692 20. L. Kempinger, R. Dittmann, D. Rieger, C. Helfrich-Förster, *Chronobiol. Int.* **26**, 151–166 (2009).

693 21. W. Bachleitner, L. Kempinger, C. Wülbeck, D. Rieger, C. Helfrich-Förster, *Proc. Natl. Acad. Sci.*
694 **104**, 3538–3543 (2007).

695 22. S. Vanin *et al.*, *Nature*. **484**, 371–375 (2012).

696 23. M. Schlichting, R. Grebler, P. Menegazzi, C. Helfrich-Förster, *J. Biol. Rhythms*. **30**, 117–128
697 (2015).

698 24. E. Dolezelova, D. Dolezel, J. C. Hall, *Genetics*. **177**, 329–345 (2007).

699 25. M. Schlichting, C. Helfrich-Förster, *Methods Enzymol.* **552**, 105–123 (2015).

700 26. C. Kistenpfennig *et al.*, *J. Biol. Rhythms*. **33**, 24–34 (2018).

701 27. A. Berndt *et al.*, *J. Biol. Chem.* **282**, 13011–13021 (2007).

702 28. N. Hoang *et al.*, *PLoS Biol.* **6**, 1559–1569 (2008).

703 29. D. Arendt, K. Tessmar, M.-I. M. de Campos-Baptista, A. Dorresteijn, J. Wittbrodt, *Development*.

129, 1143–54 (2002).

30. N. Randel, L. A. Bezares-Calderón, M. Gühmann, R. Shahidi, G. Jékely, *Integr. Comp. Biol.* **53**, 7–16 (2013).

31. B. Backfisch *et al.*, *Proc. Natl. Acad. Sci. U. S. A.* **110**, 193–8 (2013).

32. H. J. Bailes, R. J. Lucas, *Proc. R. Soc. B Biol. Sci.* **280** (2013), doi:10.1098/rspb.2012.2987.

33. R. Revilla-i-Domingo *et al.*, *Elife*. **10** (2021), doi:10.7554/eLife.66144.

34. A. Fischer, J. Brökelmann, *Zeitschrift für Zellforsch.* **71**, 217–244 (1966).

35. C. S. Pittendrigh, *Cold Spring Harb. Symp. Quant. Biol.* **25**, 159–184 (1960).

36. J. Aschoff, *Z. Tierpsychol.* **49**, 225–249 (1979).

37. C. M. Altimus *et al.*, *Nat. Neurosci.* **13**, 1107–1112 (2010).

38. D. Tran, M. Perrigault, P. Ciret, L. Payton, *Proc. R. Soc. B*. **287**, 1–9 (2020).

39. T. A. Wehr, *Nat. Publ. Gr.* **23**, 923–931 (2018).

40. Aschoff, J. *Cold Spring Harb Sym* 25, 11–28 (1960).

41. Aschoff, J. *Science* 148, 1427–1432 (1965).

42. Konopka, R. J., Pittendrigh, C. & Orr, D. *J Neurogenet* 6, 1–10 (2009).

43. B. Schmid, C. Helfrich-Förster, T. Yoshii, *J. Biol. Rhythms*. **26**, 464–467 (2011).

44. K. Tessmar-Raible, P. R. H. Steinmetz, H. Snyman, M. Hassel, D. Arendt, *Biotechniques*. **39**, 460–462 (2005).

45. J. Schindelin *et al.*, *Nat. Methods*. **9** (2009), doi:10.1038/nmeth.2019.

46. T. Yoshii, S. Vanin, R. Costa, C. Helfrich-Förster, **24**, 452–464 (2009).

PNAS
www.pnas.org

Supplementary Information for

Two light sensors decode moonlight versus sunlight to adjust a plastic circadian/circalunidian clock to moon phase

Martin Zurl, Birgit Poehn, Dirk Rieger, Shruthi Krishnan, Dunja Rokvic, Vinoth Babu Veedin Rajan, Elliot Gerrard, Matthias Schlichting, Lukas Orel, Robert J. Lucas, Eva Wolf, Charlotte Helfrich-Förster, Florian Raible and Kristin Tessmar-Raible

Correspondence:

Florian Raible; Email: florian.raible@univie.ac.at

Kristin Tessmar-Raible; Email: Kristin.tessmar@maxperutzlabs.ac.at

This PDF file includes:

Figures S1 to S4

Legend for Movie S1

Other supplementary materials for this manuscript include the following:

Movie S1

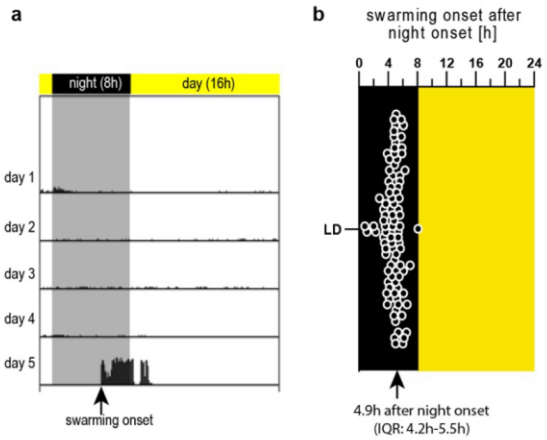

Fig. S1. Determination of the timing of swarming onset by tracking locomotor activity.

(a) Exemplary actogram showing locomotor activity of a sexually maturing worm during the days prior to swarming and in the night of swarming. Swarming onset is correlated with a striking increase in locomotor activity. See Video S1. **(b)** Coordinated swarming onset of separated worms that were kept under a 16h:8h LD cycle for at least 9 days prior to swarming (n=92). Median swarming onset was 4.9h after night onset (IQR: 4.2h-5.5h)

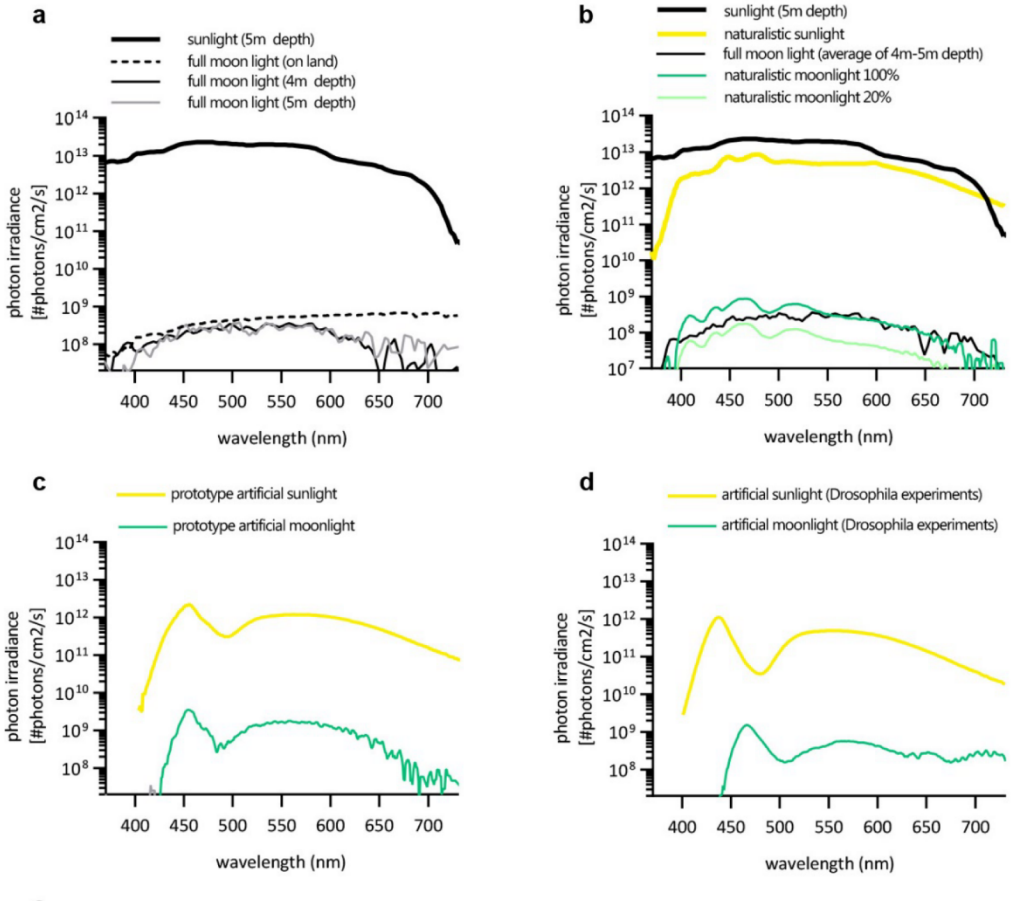

e

light source	photons/cm^2/s [380nm-750nm]
sunlight (5m depth)	**4.4x10^{15} photons/cm^2/s**
naturalistic sunlight	1.3x10^{15} photons/cm^2/s
prototype artificial sunlight	2.3x10^{14} photons/cm^2/s
artificial sunlight (Drosophila exp)	3.5x10^{13} photons/cm^2/s
full moon light under water (average 4m and 5m depth)	**5.9x10^{10} photons/cm^2/s**
naturalistic moonlight 100%	9.7x10^{10} **photons/cm^2/s**
naturalistic moonlight 20%	1.9x10^{10} **photons/cm^2/s**
prototype artificial moonlight	6.2x10^{10} **photons/cm^2/s**
full moon light on land	**1.8x10^{11} photons/cm^2/s**
artificial moonlight (Drosophila exp)	1.2x10^{11} **photons/cm^2/s**

Fig. S2. Sun- and moonlight spectra.

(a) Exemplary natural sunlight and full moon spectra measured under water at the natural *Platynereis* habitat in the coastal waters of Ischia/Italy. Sunlight spectrum was measured at 5m water depth on November 25, 2011 (9.7x10^{10} photons/cm2/s [380nm-750nm], average 10am-4pm), and the two full moon spectra were measured at 4m and 5m water depth on April 17-18, 2012 (average 10:15pm-2am) and 10-11, 2011 (average 10pm-1am), respectively. To benchmark the underwater moonlight measurements a publicly available full moon light spectrum measured on land is included (http://www.olino.org/blog/us/articles/2015/10/05/spectrum-of-moon-light). **(b)** Spectra of custom-designed naturalistic sun- (yellow) and moonlight (dark and light green) used for all *Platynereis* experiments (except for Fig.2e-g and Fig. S1) compared to natural sun- and moonlight spectra. **(c)** Prototype artificial sun- and moonlight spectra used for experiments shown in Fig. 1b and Fig. 2e-g. **(d)** Artificial sun and moonlight experiments used for Drosophila experiments. **(e)** Total light intensities of the spectra shown in (a-d). All spectra reflect light intensities at the distance relevant for experiments.

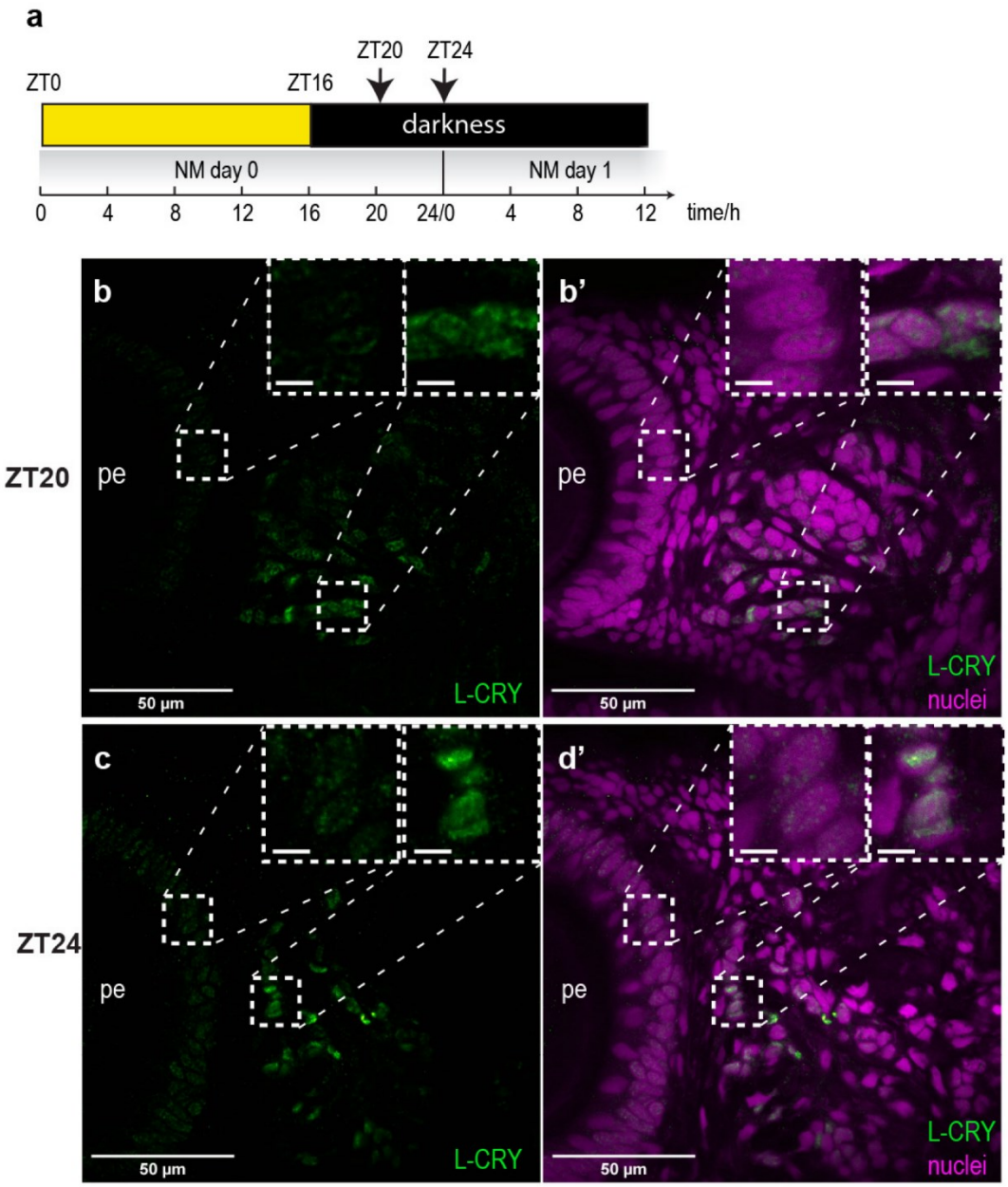

774

775 **Fig. S3. L-Cry localizes to the nucleus during dark nights.**

776 **(a)** Sampling scheme of *Platynereis* heads for immunohistochemistry. **(b,c)** *Platynereis* L-Cry protein
777 (green); **(b'c')** additional visualization of nuclei stained with HOECHST (violet). For further details see
778 **Fig.3**.
779

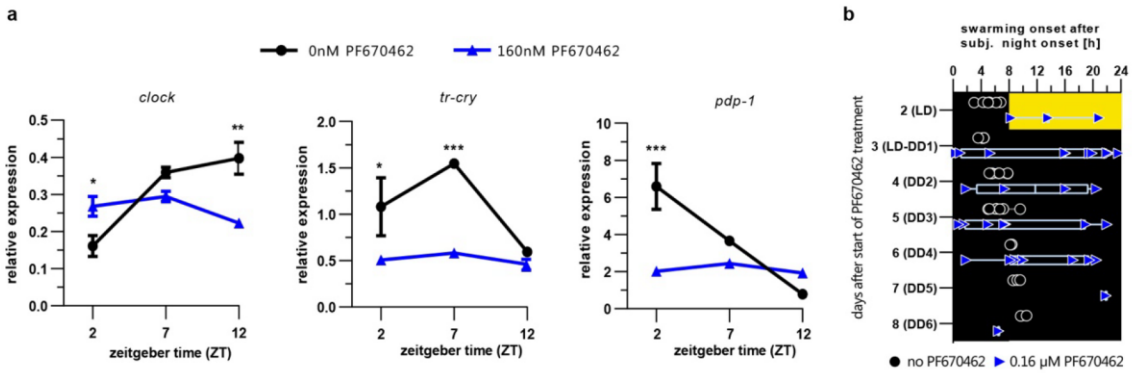

Fig. S4. Treatment with a casein kinase 1δ/ε inhibitor disrupts circadian clock oscillations and synchronizes swarming onset.

(a) Treatment of 160nM of casein kinase 1δ/ε inhibitor PF670462 results in severely disrupted circadian clock gene transcriptional oscillations in head extracts of premature worms. Expression levels are normalized to *cdc5* transcript levels. **(b)** Swarming onset of worms after at least 9 days after last FM stimulus under LD followed by DD conditions treated with the casein kinase 1δ/ε inhibitor PF670462 (blue triangles); untreated references (black dots) include individuals also shown in **Fig. 1c**. Values are means ± SEM; n = 3BRs with 4-5 heads/BR. * : p<0.05; ** : p<0.001; *** : p<0.0001 2-way ANOVA followed by Sidak´s multiple comparison test.

Movie S1 (separate file). Exemplary video showing mature swarming worms, as well as worms just before swarming

5. Article 2: A Cryptochrome adopts distinct moon- and sunlight states and functions as sun- versus moonlight interpreter in monthly oscillator entrainment

Status: submitted to *Nature Ecology & Evolution* and posted on bioRxiv: https://doi.org/10.1101/2021.04.16.440114

Authors:

Birgit Poehn*, Shruthi Krishnan*, **Martin Zurl**, Aida Coric, Dunja Rokvic, Enrique Arboleda, Lukas Orel, Florian Raible, Eva Wolf, Kristin Tessmar-Raible

*Co-first authors

Outline:

Despite the wide occurrence of moonlight entrained monthly (circalunar) rhythms in marine species, the photoreceptors that mediate circalunar entrainment remain elusive. Here, we assess the role of the light-receptive cryptochrome L-Cry for entrainment of the circalunar clock of *Platynereis dumerilii*. We find that *l-cry* mutants re-entrain their circalunar phase slower in response to a shifted naturalistic moonlight regime, suggesting that L-Cry contributes to circalunar entrainment. However, paradoxically *l-cry* mutants re-entrain circalunar phase faster than wildtypes if the nocturnal light pulse has a light intensity considerably higher than natural moonlight. This indicates that L-Cry blocks strong light to interfere with circalunar entrainment. Consistent with a function of L-Cry in discriminating sunlight from moonlight we find that photoreduction and recovery kinetics of L-Cry´s chromophore flavin adenine dinucleotide are distinct under naturalistic moon- and sunlight, and also abundance and subcellular localization of L-Cry differs under moon- and sunlight conditions. This indicates that the role of L-Cry in correctly distinguishing sun- versus moonlight valence extends from circadian timing (see article #1) to circalunar timing. Furthermore, this work constitutes the first functional data on a photoreceptor involved in circalunar clock entrainment.

These results contribute to address aim 3 of my thesis.

Contributions:

I contributed to the development and implementation of naturalistic sun and moonlight LED setups used in this publication. Furthermore, I provided conceptual input.

A Cryptochrome adopts distinct moon- and sunlight states and functions as sun- versus moonlight interpreter in monthly oscillator entrainment

Birgit Poehn[*1,2], *Shruthi Krishnan*[*3], *Martin Zurl*[1,2], *Aida Coric*[#1,2], *Dunja Rokvic*[#1,2], *Enrique Arboleda*[1,2,4], *Lukas Orel*[1,2], *Florian Raible*[1,2], *Eva Wolf*[@3] *and Kristin Tessmar-Raible*[@1,2]

[1]Max Perutz Labs, University of Vienna, Vienna BioCenter, Dr. Bohr-Gasse 9/4, 1030 Vienna

[2]Research Platform "Rhythms of Life", University of Vienna, Vienna BioCenter, Dr. Bohr-Gasse 9/4, A-1030 Vienna

[3] Structural Chronobiology, Institute of Molecular Physiology (IMP) and Institute of Molecular Biology (IMB) Mainz, Hanns-Dieter-Hüsch-Weg 17, 55128 Mainz, Germany.

[4] present address: Institut de Génomique Fonctionnelle de Lyon (IGFL), École Normale Supérieure de Lyon, 32 avenue Tony Garnier, 69007 Lyon, France

[*,#] *equal contribution*

[@] *correspondence:*

Eva Wolf: evawolf1@uni-mainz.de

Kristin Tessmar-Raible: kristin.tessmar@mfpl.ac.at

Abstract

Measuring time by the moon's monthly cycles is a wide-spread phenomenon and crucial for successful reproduction in countless marine organisms. In several species, such as the mass-spawning bristle worm *Platynereis dumerilii*, an endogenous monthly oscillator synchronizes reproduction to specific days. Classical work showed that this oscillator is set by full moon. But how do organisms recognize this specific moon phase?

We uncover L-Cry's involvement: photoreduction and recovery kinetics of its co-factor FAD differ strongly when purified L-Cry is exposed to naturalistic moonlight, naturalistic sunlight, or their different successions. L-Cry's sun- versus moonlight states correlate with distinct sub-cellular localizations, indicating differential signalling. These properties enable a discrimination between sun- and moonlight, as well as moonlight duration as a moon phase indicator.

Consistent with L-Cry's function as natural light interpreter, its loss leads to a faster re-entrainment under artificially strong nocturnal light, suggesting that L-Cry blocks "wrong" light from impacting on this oscillator. Our work provides a new level of functional and mechanistic understanding of moon-regulated biological processes.

Main text

The moon fascinates biologists and non-biologists alike. An impact of lunar light on the nervous system, and ultimately on the behavior and metabolism of animals, may at first seem eccentric to modern scientists. But as a matter of fact, lunar influences on animals are especially well documented in the marine environment [1-3]. Starting with the early 20th century, numerous scientific studies have shown that the reproductive behavior and sexual maturation of animals as diverse as corals, polychaetes, echinoderms, fishes or turtles are synchronized by the lunar cycle [1,3-7]. A recent study suggests that the lunar cycle coordinates the behaviour of a nocturnal migratory bird [8], and recently uncovered clear correlations of human sleep and menstrual cycle properties with moon phases have re-initiated the discussion of an impact of the moon even on human biology [9,10]. In animals, these synchronizations are not only impressive, but typically also important to ensure successful reproduction [11]. In turn, desynchronization of these reproductively critical rhythms due to anthropogenic disturbances, as documented for corals, poses a threat to species survival [11].

Despite the importance and widespread occurrence of lunar rhythms, any functional mechanistic insight is lacking. Importantly, this synchronization among conspecifics is in many cases not simply a direct reaction to a stimulus, but instead governed by endogenous monthly oscillators: circalunar clocks [3,12-16]. The marine bristle worm *Platynereis dumerilii* is well-documented to possess such a circalunar clock, which controls its reproductive timing and can be entrained by nocturnal light in the lab [5,14,17]. Several reports have linked the expression of cryptochromes (CRYs) with moon phase, suggesting that these genes could be involved in circalunar time-keeping [18], possibly- as proposed for corals- as lunar light receptors [2,19,20]. However, no functional molecular support for such an involvement exists. In order to move from expression correlation to a mechanistic understanding, we investigated the biochemical properties and functional role of the light-receptive cryptochrome L-Cry in the annelid *Platynereis dumerilii* [14].

L-Cry discriminates between naturalistic sun- and moonlight by forming differently photoreduced states

While we have previously shown that *Pdu*-L-Cry is degraded upon light exposure in S2 cell culture [14], it has remained unclear if L-Cry has the spectral properties and sensitivity to sense moonlight and whether this would differ from sunlight sensation. To test this, we purified full-length L-Cry from insect cells (Extended Data Fig.1a-c). Multiangle light scattering (SEC-MALS) analyses of purified dark-state L-Cry revealed a molecular weight of 133 kDa, consistent with the predicted molecular homodimer weight of 135 kDa (Fig. 1a). Purified L-Cry binds Flavin Adenine Dinucleotide (FAD) as its chromophore (Extended Data Fig.1d,e). We then used UV/Vis absorption spectroscopy to analyze the

FAD photoreaction of L-Cry. The absorption spectrum of dark-state L-Cry showed maxima at 450nm and 475nm, consistent with the presence of oxidized FAD (Extended Data Fig.1f, black line).

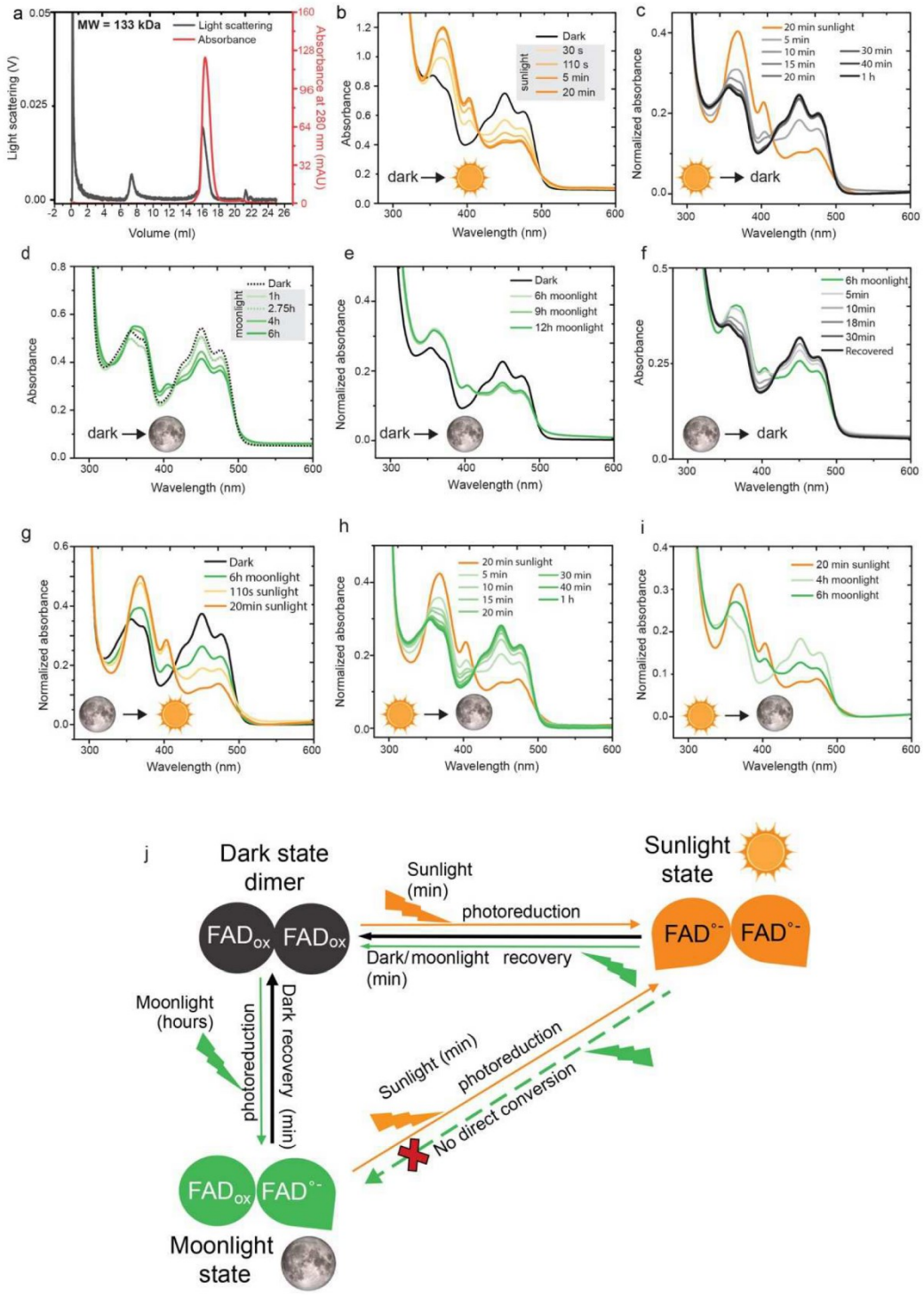

Figure 1: L-Cry forms differently photoreduced sunlight- and moonlight states.
(a) Multi-Angle Light Scattering (MALS) analyses of dark-state L-Cry supports L-Cry homodimer formation (theoretical MW 135 kDa). **(b)** Absorption spectrum of L-Cry in darkness (black) and after sunlight exposure (orange). Additional timepoints: S2A. **(c)** Dark recovery of L-Cry after 20min sunlight on ice. Absorbance at 450nm in EDF 2b. **(d,e)** Absorption spectra of L-Cry after exposure to naturalistic moonlight for different durations. **(f)** Full spectra of dark recovery after 6h moonlight. Absorbance at 450nm: EDF 2d. **(g)** Absorption spectrum of L-Cry after 6h of moonlight followed by 20min of sunlight. **(h)**

Absorption spectrum of L-Cry after 20min sunlight followed by moonlight first results in dark-state recovery. Absorbance at 450nm: EDF 2e. **(i)** Absorption spectrum of L-Cry after 20min sunlight followed by 4h and 6h moonlight builds up the moonlight state. **(j)** Schematic model of *Pdu* L-Cry responses to sun- and moonlight. MALS data (a) and SEC (EDF.1a) suggest that L-Cry forms homodimers. Also see discussion and EDF 2i.

As basic starting point to analyze its photocycle, L-Cry was photoreduced with a 445nm emitting strong blue light LED (Extended Data Fig.3d) for 110s [21]. The light-activated spectrum showed that blue-light irradiation of L-Cry leads to the complete conversion of FAD_{ox} into an anionic FAD radical (FAD^{o-}) with characteristic FAD^{o-} absorption maxima at 370 nm and 404 nm and reduced absorbance at 450 nm (Extended Data Fig.1f, blue spectrum, black arrows). In darkness, L-Cry reverted back to the dark state with time constants of 2 min (18°C), 4 min (6°C) and 4.7 min (ice) (Extended Data Fig.1g-k).

We then investigated the response of L-Cry to ecologically relevant light, i.e. sun- and moonlight using naturalistic sun- and moonlight devices we designed based on light measurements at the natural habitat of *Platynereis dumerilii* [22] (Extended Data Fig.3a,c,e). Upon naturalistic sunlight illumination, FAD was photoreduced to $FAD^{\circ-}$, but with slower kinetics than under the blue light source, likely due to the intensity differences between the two lights (Extended Data Fig.3c-e). While blue-light illumination led to a complete photoreduction within 110s (Extended Data Fig.1f), sunlight-induced photoreduction to $FAD^{\circ-}$ was completed after 20 min (Fig. 1b) and did not further increase upon continued illumation for up to 2h (Extended Data Fig.2a). Dark recovery kinetics had time constants of 3.2min (18°C) and 5min (ice) (Fig.1c, Extended Data Fig.2b,c).

As the absorbance spectrum of L-Cry in principle overlaps with that of moonlight at the *Platynereis* natural habitat (Extended Data Fig. 3a), L-Cry has the principle spectral prerequisite to sense moonlight. However, the most striking characteristic of moonlight is its very low intensity (1.79×10^{10} photons/cm^2/s at -5m, Extended Data Fig. 3a,e). To test if *Pdu*-L-Cry is sensitive enough for moonlight, we illuminated purified L-Cry with our custom-built naturalistic moonlight, closely resembling full moon light intensity and spectrum at the *Platynereis* natural habitat (Extended Data Fig. 3a,c,e). Naturalistic moonlight exposure up to 2.75 hours did not markedly photoreduce FAD, notably there was no difference between 1 hours and 2.75 hours (Fig. 1d). However, further continuous naturalistic moonlight illumination of 4h and longer resulted in significant changes (Fig. 1d), whereby the spectrum transitioned towards the light activated state of FAD^{o-} (note peak changes at 404nm and at 450nm). This photoreduction progressed further until 6 h naturalistic moonlight exposure (Fig. 1d). No additional photoreduction could be observed after 9 h and 12 h of naturalistic moonlight exposure (Fig.1e), indicating a distinct state induced by naturalistic moonlight that reaches its maximum after ~6hrs, when about half of the L-Cry molecules are photoreduced. This time of ~6hrs is remarkably consistent with classical work showing that a minimum of ~6hrs of continuous nocturnal light is important for circalunar clock entrainment, irrespective of the preceding

photoperiod[5]. The dark recovery of L-Cry after 6 h moonlight exposure occurred with a time constant of 6.7 min at 18°C (Fig. 1f, Extended Data Fig.2d). Given that both sunlight and moonlight cause FAD photoreduction, but with different kinetics and different final $FAD^{\circ-}$product/FAD_{ox} adduct ratios, we wondered how purified L-Cry would react to transitions between naturalistic sun- and moonlight (i.e. during "sunrise" and "sunset").

Mimicking the sunrise scenario, L-Cry was first illuminated with naturalistic moonlight for 6 h followed by 20 min of sunlight exposure. This resulted in an immediate enrichment of the $FAD^{\circ-}$ state (Fig. 1g). Hence, naturalistic sunlight immediately photoreduces remaining oxidized flavin molecules, that are characteristic of moonlight activated L-CRY, to $FAD^{\circ-}$, to reach a distinct fully reduced sunlight state.

In contrast, when we next mimicked the day-night transition ("sunset") by first photoreducing with naturalistic sunlight (or strong blue light) and subsequently exposed L-Cry to moonlight, L-Cry first returned to its full dark state within about 30 min (naturalistic sunlight: τ=7min (ice): Fig.1h, Extended Data Fig.2e; blue light: τ=9 min (ice): Extended Data Fig.2f-h), despite the continuous naturalistic moonlight illumination. Prolonged moonlight illumination then led to the conversion of dark-state L-Cry to the "moonlight state" (Fig. 1i, Extended Data Fig.2f), i.e. fully photoreduced "sunlight-state" L-Cry first has to return into the dark state before entering the "moonlight-state" characterized by the stable presence of the partial $FAD^{\circ-}$product/FAD_{ox} adduct. In contrast to "sunlight-state" L-Cry, "moonlight-state" L-Cry does not return to the oxidized ("dark") state under naturalistic moonlight. Taken together, these results indicate the existance of kinetically and structurally distinct "sunlight" and "moonlight" states of L-Cry (Fig.1j, Extended Data Fig.2i).

Naturalistic sun- and moonlight differently affect L-Cry subcellular localization

To further study the function of L-Cry in *Platynereis*, we generated two *l-cry* mutant alleles (Δ34 and Δ11bp) (Fig.2a) using TALENS [23], as well as a monoclonal antibody against *Pdu*-L-Cry. Using the mutant worms, we first verified the specificity of the anti-L-Cry antibody in Western blot (Fig. 2b) and immunohistochemistry (Fig. 2e-j). Furthermore, we verified that the staining of the antibody in wildtype worms (Fig. 2e-h) matches the regions where *l-cry* mRNA is expressed (Fig. 2d). These tests confirmed the absence of L-Cry protein in mutants and the specificity of the anti-L-Cry antibody.

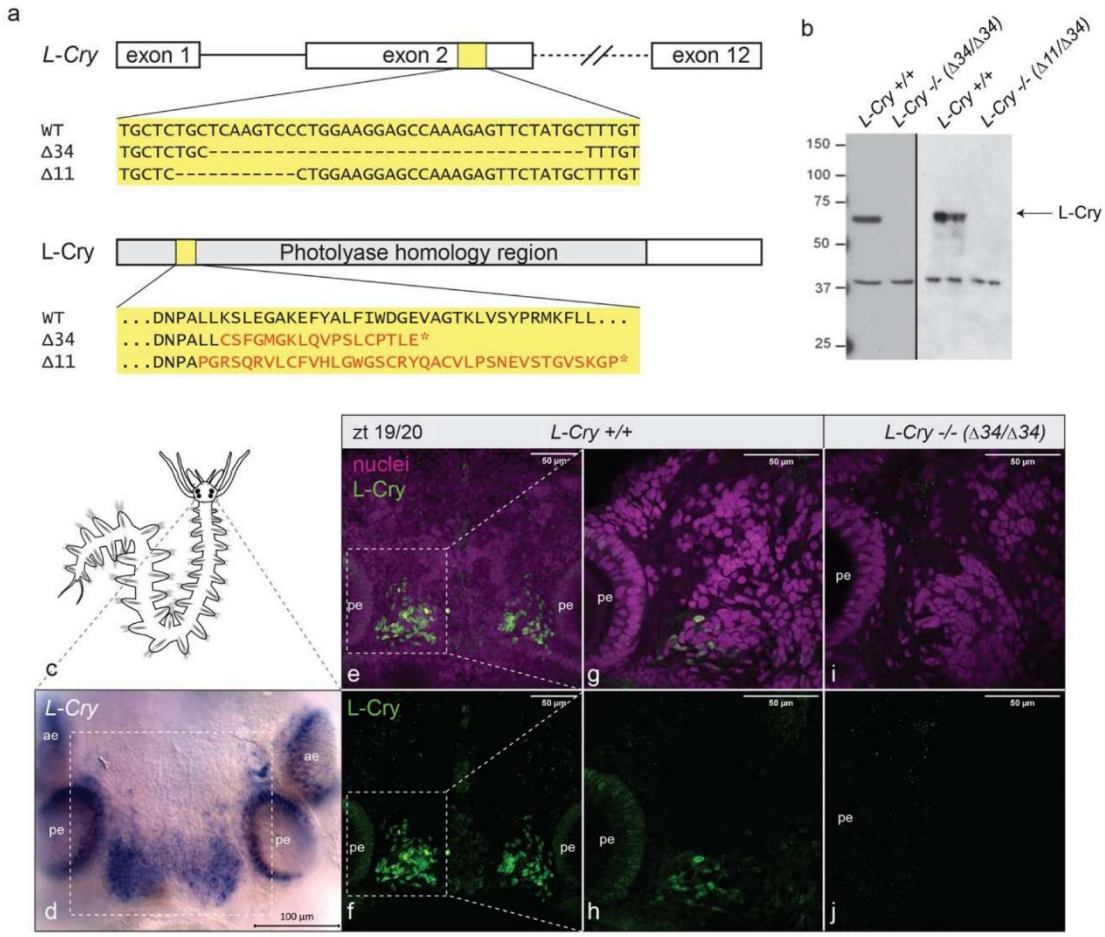

Figure 2. *l-cry -/-* mutants are loss-of-function alleles
(a) Scheme of the *L-Cry* genomic locus for wt and mutants. Both mutant alleles result in an early frameshift and premature stop codon. The Δ34 allele has an additional 9bp deletion in exon 3. **(b)** Western Blots of *P. dumerilii* heads probed with anti-L-Cry antibody. **(c)** scheme of *P. dumerilii.* **(d)** whole mount *in situ* hybridization against *l-cry* mRNA on worm head. ae, anterior eye; pe, posterior eye. **(e-j)** Immunohistochemistry of premature wildtype (e-h) and mutant (i,j) worm heads sampled at zt19/20 using anti-L-Cry antibody (green) and Hoechst staining (magenta), dorsal views, anterior up. e,f: z-stack images (maximal projections of 50 layers, 1.28µm each) in the area highlighted by the rectangle in (d), whereas (g-j) are single layer images of the area highlighted by the white rectangles in (e) and (f).

In order to further investigate the response of L-Cry to naturalistic sun- and moonlight, we conducted Western blots and immunohistochemistry at different lunar and daily timepoints (Figs. 3a-a''). For the analyses of total protein levels via Western blots, we compared equal lengths of sun- versus moonlight illumination versus darkness, each having 8hrs duration during their naturally occurring time (Fig.3a-a''). L-Cry levels after 8h of naturalistic sunlight (day before full moon = FM-1, diel time: zeitgeber time 8 = zt8, Figs. 3a,a') were significantly reduced compared to 8h under darkness at the same moon phase (FM-1, zt 0-10mins, Figs. 3b,c), in line with (canonical) L-Cry degradation in response to naturalistic sunlight.

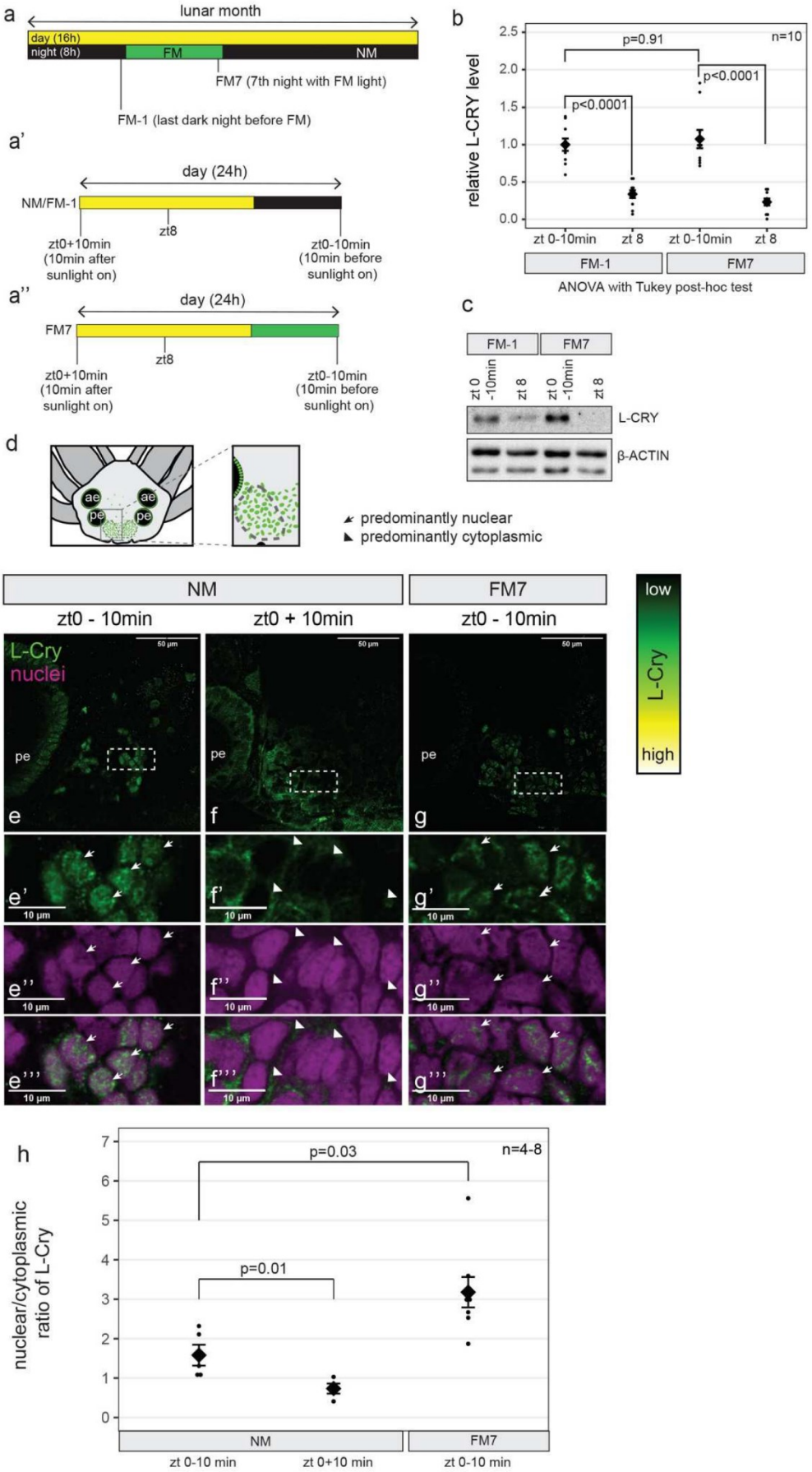
a
lunar month
day (16h)
night (8h)
FM
NM
FM7 (7th night with FM light)
FM-1 (last dark night before FM)
a'
day (24h)
NM/FM-1
zt8
zt0+10min (10min after sunlight on)
zt0-10min (10min before sunlight on)
a''
day (24h)
FM7
zt8
zt0+10min (10min after sunlight on)
zt0-10min (10min before sunlight on)
b
relative L-CRY level
p=0.91
n=10
p<0.0001
p<0.0001
zt 0-10min
zt 8
zt 0-10min
zt 8
FM-1
FM7
ANOVA with Tukey post-hoc test
c
FM-1
FM7
zt 0 -10min
zt 8
zt 0 -10min
zt 8
L-CRY
β-ACTIN
d
ae
pe
predominantly nuclear
predominantly cytoplasmic
NM
FM7
zt0 - 10min
zt0 + 10min
zt0 - 10min
low
L-Cry
high
L-Cry
nuclei
50 µm
pe
e
f
g
e'
f'
g'
e''
f''
g''
e'''
f'''
g'''
10 µm
h
nuclear/cytoplasmic ratio of L-Cry
p=0.03
n=4-8
p=0.01
NM
FM7
zt 0-10 min
zt 0+10 min
zt 0-10 min

160

8

Figure 3: Naturalistic moon- and sunlight impact differently on L-Cry localization and levels.
(a,a',a'') Scheme of sampling timepoints. 16hrs day (light) and 8 hrs night (dark or moonlight) per 24hrs, with 8 nights of moonlight per month. **(b)** relative L-Cry levels at indicated timepoints, as determined by Western Blot. Individual data points as well as mean ± SEM are shown. **(c)** Representative Western Blot used for quantification in (b), see Extended Data Fig 8 for all other. **(d)** *P.dumerilii* head scheme. Dashed ovals designate the oval-shaped posterior domains between the posterior eyes. Green dots: L-Cry+ cells. ae, anterior eye; pe, posterior eye. **(e-g)** Maximal projections of confocal images of worm heads stained with anti-L-Cry antibody (green) and HOECHST (magenta: nuclei). White rectangles: areas of the zoom-ins presented below. **(e'-g''')** zoomed, single layer (1.28µm) pictures of the areas depicted in e-g. Arrows: predominant nuclear L-Cry, arrowheads: predominant cytoplasmic L-Cry. Scale bars: 10um. Overview images with nuclear stain: Extended Data Fig 4 a-c. **(h)** quantification of subcellular localization of L-Cry as nuclear/cytoplasmic ratio at indicated timepoints. Individual data points as well as mean ± SEM are shown. p-values: two-tailed t-test. For quantification as categorical data, see Extended Data Fig 4a'-f.

In contrast to sunlight, exposure to an equal length (8hrs) of naturalistic moonlight did not cause a reduction in L-Cry levels compared to an equivalent time (8hrs) in darkness (FM-1, zt0-10min versus FM7, zt0-10min: Figs.3b,c, Extended Data Fig.8). Thus, any potential moonlight signalling via L-Cry occurs via a mechanism independent of L-Cry degradation.

We next examined the spatial distribution of L-Cry in worm heads (scheme Fig. 3d) at lunar and diel timepoints (Fig. 3a-a''). After 8hrs of a dark night (i.e. NM, zt0-10min), L-Cry is found predominantly in the nucleus of individual cells, (Fig. 3e-e''', quantification as numerical data, i.e. nuclear/cytoplasmic ratio: Fig. 3h, for quantification as categorical data [24]: Extended Data Fig. 4a'-c'', d-f). Given that an equivalent time of 8hrs of sunlight exposure results in strong degradation of L-Cry and hence loss of staining signal (see Western blots above), we analyzed L-Cry's localization after a short exposure. Already after 10mins of exposure to naturalistic sunlight (NM zt0+10mins, Fig. 3a,a'), the L-Cry nuclear localization strongly diminished, becoming predominantly cytoplasmic (Fig. 3f-f''', numerical quantification Fig. 3h, categorical quantification Extended Data Fig. 4a'-c'', d-f). This suggests that naturalistic sunlight causes a shift of the protein to the cytoplasm, followed by degradation.

Given the degradation of L-Cry by naturalistic sunlight, we next asked the question if L-Cry is present at night timepoints, allowing for sufficient exposure to naturalistic moonlight to reach the moonlight state. We tested two diel timepoints of the first night lit by the naturalistic moonlight for circalunar entrainment (FM1): at zt16 (just after the naturalistic sunlight is off and moonlight is on) and at zt20 (after 4hrs of naturalistic moonlight exposure) (Extended Data Fig. 5a,a'). We observe that low levels of L-Cry can already be detected at FM1 zt16 (Extended Data Fig. 5b-b'''), and increase within the next hours (see FM1 zt20, Extended Data Fig. 5c-c'''), a timepoint after which still 4hours remain for the protein to biochemically reach the full moonlight state. Based on these data we conclude that in the organism L-Cry has sufficient time to reach its moonlight state (by changing from sunlight to dark to moonlight state and/or by *de novo* synthesis of dark adapted L-Cry that reaches the moonlight state within 4hrs- see biochemical kinetics, Fig.1d-j, Extended Data Figures 2f,g).

Upon further naturalistic moonlight exposure for seven continuous nights (FM7, zt0-10min) L-Cry remained clearly nuclear (Fig. 3g-g''', numerical quantification Fig. 3h, categorical quantification:

Extended Data Fig. 4f). Thus, the sunlight and moonlight-states of L-Cry correlate with distinct subcellular distribution patterns. In fact, we observed that L-Cry at FM7, zt0-10min is even more nuclear restricted than at zt0-10min under NM, both in the numerical analysis of the nuclear/cytoplasmic ratio (Fig. 3h), as well as in the blind categorical scoring (Extended Data Fig 4f). This suggests that also the dark and moonlight states of L-Cry have distinct subcellular distribution patterns.

Taken together, these findings show that moonlight and sunlight impact differentially on L-Cry quantity and localization. Thus, both on biochemical and on cellular signalling level L-Cry possesses properties that allow it to discriminate between (naturalistic) sun- and moonlight.

l-cry mutants show higher spawning synchrony than wild-type animals under non-natural light conditions

Given L-Cry's molecular ability to sense and discriminate between naturalistic sun- and moonlight, we wondered if it is functionally required for the entrainment of the worms' circalunar oscillator. In order to address this question, we first assessed the circalunar maturation timing of wildtypes and *l-cry* mutant populations in conventional culture conditions, i.e. worms grown under typical indoor room lighting (named here artificial sun- and moonlight, Extended Data Figure 3b). We analysed the maturation data using two statistical approaches (linear and circular statistics). We used the classical linear plots and statistics to compare the monthly spawning data distribution (Fig4a-c,i). This revealed a clear difference between mutant animals, which exhibited a stronger spawning peak at the beginning of the NM phase, compared to their wildtype and heterozygous counterparts (Fig. 4a-c, Kolmogorov-Smirnov-Test on overall data distribution, Fig. 4i).

We analysed the same data using circular statistics (as the monthly cycle is repeating, see details in Methods section), which allowed us to describe the data with the mean vector (defined by the direction angle μ and its length r, shown as arrows in Fig. 4e-g). The phase coherence r (ranging from 0 to 1) serves as a measure for synchrony of the population data. As expected for circalunarly entrained populations, all genotypes distributed their spawning across a lunar month significantly different from random (Fig. 4e-g, p-values in circles, Rayleigh's Uniformity test [25]. Consistent with the observed higher spawning peak of the *l-cry-/-* mutants in the linear plots, the circular analysis revealed a significant difference in spawning distribution (Mardia-Watson-Wheeler test, for details see Methods section) and higher spawning synchrony of mutants (r=0.614) than in wildtypes and heterozygotes (r=0.295 and r=0.222) (Fig. 4i). The specificity of this phenotype of higher spawning precision for *l-cry* homozygous mutants was confirmed by analyses on trans-heterozygous *l-cry* $^{(\Delta 34/\Delta 11)}$ mutants (Extended Data Figure 6a-e), and by the fact that such a phenotype is not detectable in any other light receptor mutant available in *Platynereis* (*r-opsin1*: Extended Data Figure 7a,b,e,f,i; *c-opsin1:* Extended Data Figure 7c,d,g,h,i, *Go-opsin*: refs. [26,27]).

This finding was initially counterintuitive, as we had expected either no phenotype (if L-Cry was not involved in circalunar clock entrainment) or a decreased spawning precision (if L-Cry was functioning as moonlight receptor in circalunar clock entrainment). Upon an investigation of very detailed spawning data over multiple months from the worms' natural habitat published prior to environmental/light pollution, we noticed that the higher spawning synchrony in *l-cry*$^{-/-}$ worms mimics the actual spawning synchrony of *Platynereis dumerillii* populations in their natural habitat. For better accessibility and comparability we combined all months and replotted the data published in 1929 [28] (Fig. 4d,h,I; see details in Methods section; r=0.631). Given that recent, non-inbred isolates from the same habitat as our lab inbred strains (which is the same habitat as the data collected from in ref. [28]) exhibit a broad spawning distribution under standard worm culture light conditions (which includes the bright artificial moon light) [29], we reasoned that the difference in spawning synchrony between the wildtype in culture versus at its natural habitat is caused by the rather crude and bright nocturnal light stimulus typically used for the standard laboratory culture (Extended Data Figure 3).

Lunar spawning precision of wild-type animals depends on naturalistic moonlight conditions

We thus next reasoned that the high population synchrony of *l-cry-/-* animals (close to wildtype under natural conditions) is a result of the absence of *l-cry*. We predicted that in wildtype animals L-Cry would reduce the impact of the artificially bright moonlight on the worms' circalunar oscillator. Based on this logic we hypothesized that L-Cry identifies the artificial nocturnal light from the normal culture conditions to be not proper moonlight. This predicts that naturalistic moonlight should increase the spawning precision of the wildtype population. To test this prediction, we assessed the impact of the naturalistic sun- and moonlight (Extended Data Fig. 3c) on wildtype animals, maintaining the default temporal regime (8 nights of "full moon"). Indeed, merely adjusting the light increased the precision and phase coherence of population-wide reproduction: After several months under naturalistic sun- and moonlight, wildtype worms spawned with a major peak highly comparable to the wildtype at the natural habitat (Fig. 4d,h vs. j,k), and also exhibited an increased population synchrony (r=0.398 compared to r=0.295 under standard worm room light conditions). This increased similarity to the spawning distribution at the natural habitat ("Sea") is confirmed by statistical analyses (Fig. 4l): The phase difference (angle between the two mean vectors) is only one day (corresponding to 12°). In contrast, the spawning distribution of wildtypes under standard worm room light versus naturalistic light conditions is highly significantly different in linear and circular statistical tests and has a phase difference of 7.7 days (Fig. 4l).

These findings evidence that L-Cry blocks artificial, but not naturalistic moonlight from efficiently synchronizing the circalunar clock of wildtype animals. This block is removed in *l-cry-/-* animals,

leading to a better synchronization of the *l-cry-/-* population. This suggests that L-Cry's major role could be that of a signal gate-keeper.

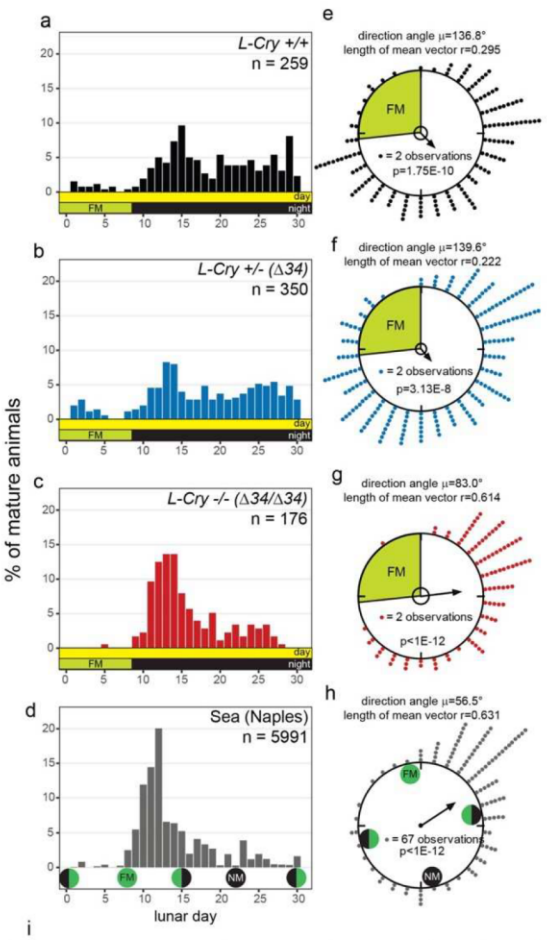

Comparison	Kolmogorov-Smirnov Test (p)	Mardia-Watson-Wheeler Test (p)	phase difference of vectors (days)
L-Cry +/+ vs. *L-Cry* -/- wormroom light	$4.45 \cdot 10^{-7}$	$6.29 \cdot 10^{-7}$	4.5
L-Cry +/+ vs. *L-Cry* +/- wormroom light	0.142	0.155	0.2
L-Cry +/- vs. *L-Cry* -/- wormroom light	$2.43 \cdot 10^{-6}$	$2.46 \cdot 10^{-9}$	4.7
wt sea vs. *L-Cry* +/+ wormroom light	$< 2.2 \cdot 10^{-16}$	$<10^{-12}$	6.7
wt sea vs. *L-Cry* +/- wormroom light	$< 2.2 \cdot 10^{-16}$	$<10^{-12}$	6.9
wt sea vs. *L-Cry* -/- wormroom light	$3.04 \cdot 10^{-13}$	$5.08 \cdot 10^{-4}$	2.2

Comparison	Kolmogorov-Smirnov Test (p)	Mardia-Watson-Wheeler Test (p)	phase difference of vectors (days)
L-Cry +/+ wormroom vs naturalistic light	$6.38 \cdot 10^{-10}$	$3.58 \cdot 10^{-6}$	7.7
wt sea vs *L-cry* +/+ naturalistic light	0.058	$5.99 \cdot 10^{-4}$	1.0

Figure 4: L-Cry shields the circalunar clock from light that is not naturalistic moonlight
(**a-d,j)** Spawning of *l-cry* +/+ (a), *l-cry* +/- (Δ34) (b) and *l-cry* -/-(Δ34/ Δ34) (c) animals over the lunar month in the lab with 8 nights of artificial moonlight (a-c), under natural conditions in the sea (d, replotted from ref. [28,30]) and in the lab using naturalistic sun- and moonlight (j, 8 nights moonlight). **(e-h,k)** Data as in (a-d,j) as circular plot. 360° correspond to 30 days of the lunar month. The arrow represents the mean vector, characterized by the direction angle μ and r (length of μ). r indicates phase coherence (measure of population synchrony). p-values inside the plots: result of Rayleigh Tests. Significance indicates non-random distribution of data points. The inner circle represents the Rayleigh critical value (p=0.05). **(i,l)** Results of multisample statistics on spawning data shown in (a-h,j,k). The phase differences in days can be calculated from the angle between the two mean vectors (i.e. 12°= 1 day).

l-cry functions as a light signal gate-keeper for circalunar clock entrainment

A prediction of the hypothesis that L-Cry can discriminate between naturalistic moon- and sunlight and functions as a gate-keeper to only allow the 'right' light signal to set the circalunar clock, is that

mutants should entrain better to an out-of-phase artificial moonlight stimulus than wildtypes, as in wildtypes L-Cry should block the "wrong" moonlight at least partially from re-entraining the circalunar oscillator.

We thus compared the spawning rhythms of *l-cry*$^{+/+}$ and *l-cry*$^{-/-}$ worms under a re-entrainment paradigm, where we provided our bright artificial culture moon at the new moon phase (Fig.5a). In order to compare the spawning data distribution relative to the initial full moon (FM) stimulus, as well as to the new full moon stimulus (i.e. new FM), we used two nomenclatures for the months: months with numbers are analyzed relative to the initial nocturnal light stimulus (i.e. FM), whereas months with letters are analyzed relative to the new (phase-shifted) nocturnal light stimulus (i.e. new FM) (scheme in Fig.5a). When the nocturnal light stimulus is omitted (to test for the oscillator function) we then refer to 'free-running FM' (FR-FM) or 'new free-running FM' (new FR-FM), respectively (Fig.5a).

When using the artificial nocturnal light conditions, the re-entrainment of *l-cry*$^{-/-}$ animals was both faster and more complete than for their wildtype relatives. This is evident from the linear data analysis and Kolmogorov-Smirnov tests when comparing the month before the entrainment (month 1) with two months that should be shifted after the entrainment (months C,D, Fig. 5b,c,f,g).

Most notably, while *l-cry-/-* worms are fully shifted in month D, wildtype animals are mostly still spawning according to the initial lunar phase (Fig.5b,c: compare boxes and spawning at dark blue arrowheads indicating the old FM, with spawning at the old NM indicated by light blue arrowheads, with the spawning at the initial FM and NM in months 1,2). The faster re-entrainment of *l-cry*$^{-/-}$, compared to *l-cry+/+* animals is also confirmed by the Mardia-Watson-Wheeler test (see Methods section for details), which shows less/no significance in the comparison of mutants before and after entrainment, but very highly significant differences in the distribution of the wildtype spawning data in the same comparison. Consistently, the phase differences in days calculated from the angle between the two mean vectors from the circular analysis is smaller in the mutants than in the wildtypes when comparing the phase of the month before the entrainment (month 1) with two months after the entrainment (months C,D) (Fig. 5d-g). The fact that there are still differences in the mutant population before and after entrainment is likely due to the fact that even the mutants are not fully re-entrained, however, from the perspective of multiple analyses they have shifted stronger in response to an artificial nocturnal light stimulus than the wildtypes.

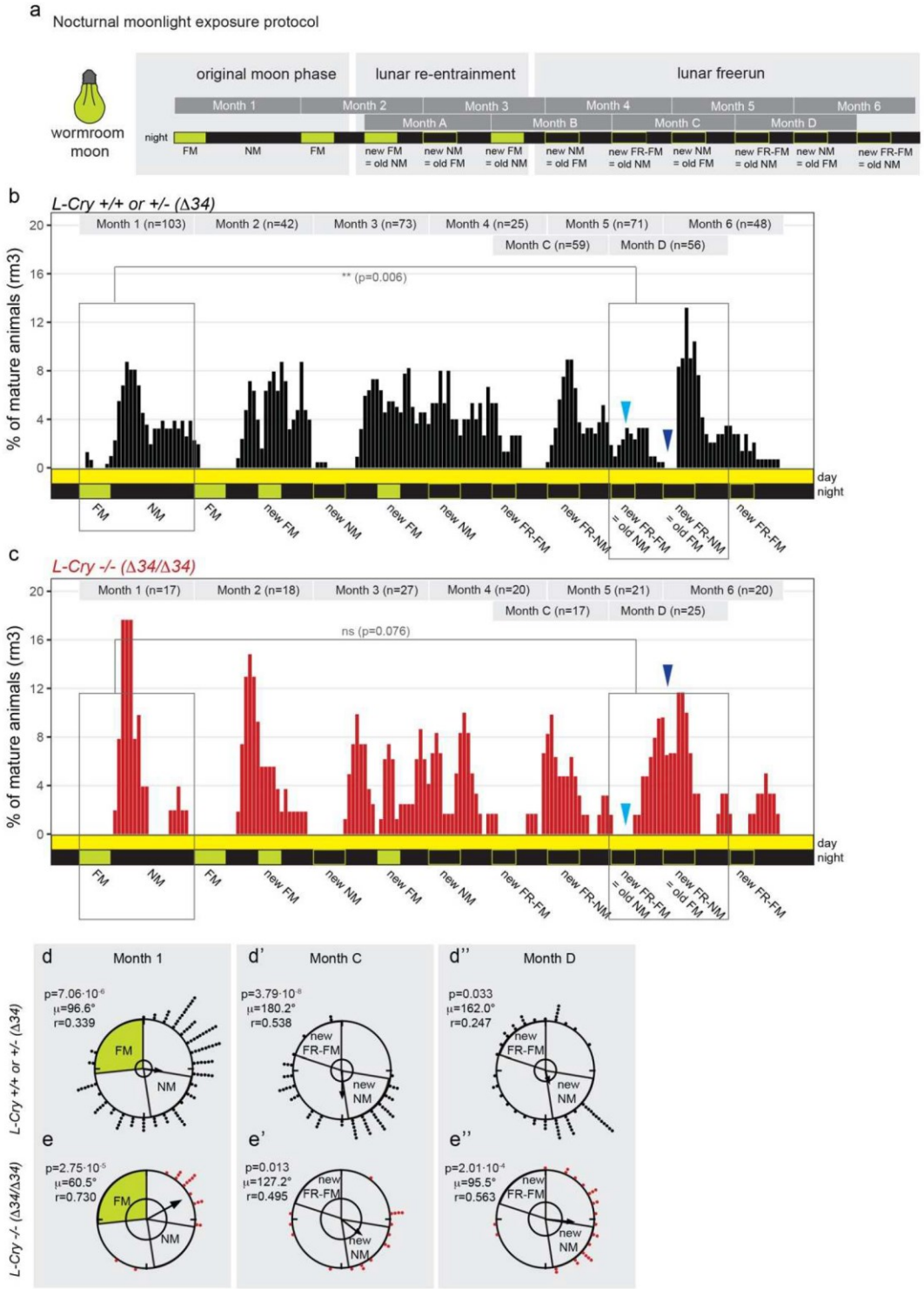

f *L-Cry +/+ or +/- (Δ34)*

Comparison	Kolmogorov-Smirnov Test (p)	Mardia-Watson-Wheeler Test (p)	phase difference of vectors (days)
Month 1 vs C	$1.2 \cdot 10^{-6}$	$7.5 \cdot 10^{-6}$	7.0
Month 1 vs D	0.006	0.002	5.5

g *L-Cry -/- (Δ34/Δ34)*

Comparison	Kolmogorov-Smirnov Test (p)	Mardia-Watson-Wheeler Test (p)	phase difference of vectors (days)
Month 1 vs C	0.002	0.002	5.6
Month 1 vs D	0.08	0.02	2.9

Figure 5: *l-cry-/-* mutants entrain the circalunar clock faster than wt to a high intensity artificial moonlight stimulus **(a)** Nocturnal moonlight exposure protocol of lunar phase shift (entrained by 8 nights, phased shifted by 6 nights of artificial culture moon, light green). **(b,c)** Number of mature animals (percent per month, rolling mean with a window of 3 days) of *l-cry* wildtype (b) and homozygous mutant (c) animals. p-values indicate results of Kolomogorov-Smirnov tests. Dark blue arrowheads- old FM phase: wt show a spawning minimum, indicative that the worms are not properly phase shifted.

Mutants spawn in high numbers, but don't spawn at the old NM indicated by light blue arrowhead. Also compare to initial FM and NM in months 1,2. **(d-e)** Circular plots of the data shown in (b) and (c). Each circle represents one lunar month. Each dot represents one mature worm. The arrow represents the mean vector characterized by the direction angle μ and r. r (length of μ) indicates phase coherence (measure of population synchrony). The inner circle represents the Rayleigh critical value (p=0.05). **(f,g)** Results of multisample statistics of data in (d,e). Phase differences in days can be calculated from the angle between the two mean vectors (i.e. 12°= 1 day).

This provides further evidence that L-Cry indeed blocks the "wrong" light from entering into the circalunar clock and thus functions as a light gate-keeper. But why would it be required to do this in nature? As we expand in more detail in the discussion, we speculate that this is necessary to entrain to a specific moon phase, which is the full moon phase for *Platynereis*. This moon phase is specifically characterized by the long duration of detectable moonlight, i.e. moonlight during the entire night [31] (Fig.7a). Interestingly, this matches the biochemical kinetics of at least 6hours of light exposure to acquire L-Cry's biochemical moonlight state. However in nature, where the setting of the full and waning moons is immediately followed by sunrise (i.e. no darkness window, Fig.7a, [31]), measuring the duration of light exposure alone would not allow the worms to detect a specific moonphase. Thus, under the natural conditions of waning/waxing moonphases and sunrise/sunsets, being able to detect the switch from moonlight to sunlight is essential. Furthermore, it likely also makes the entrainment system more stable against irregular illumination as it could arise from thunderstorms.

L-Cry functions mainly as light interpreter, while its contribution as direct moonlight entraining photoreceptor is minor

As we found that L-Cry functions as a sun- versus moon light interpreter on biochemical, cellular and physiological level and as a gate keeper for circalunar oscillator entrainment, we next wondered to which extent it would itself function as a sensor for re-entrainment signal.

In principle, signal gate keeping and oscillator re-entrainment could be mediated by the same or distinct photoreceptors. Based on the finding that *l-cry-/-* worms can still re-entrain the circalunar oscillator (see above), it is clear that even if L-Cry also directly contributed to the entrainment, it cannot be the only moonlight receptor mediating entrainment. With the experiments below, we aimed to test if L-Cry has any role as an entraining photoreceptor.

Thus, we tested how the circalunar clock is shifted in response to a re-entrainment with naturalistic moonlight in *Platynereis* wt versus *l-cry-/-* worms. For this, animals initially raised and entrained under standard worm room light conditions of artificial sun- and moonlight (Extended Data Figure 3b,e) were challenged by a deviating FM stimulus of 8 nights of naturalistic moonlight (Fig. 6a, Extended Data Figure 3c,e). This re-entraining stimulus was repeated for three consecutive months (Fig. 6a).

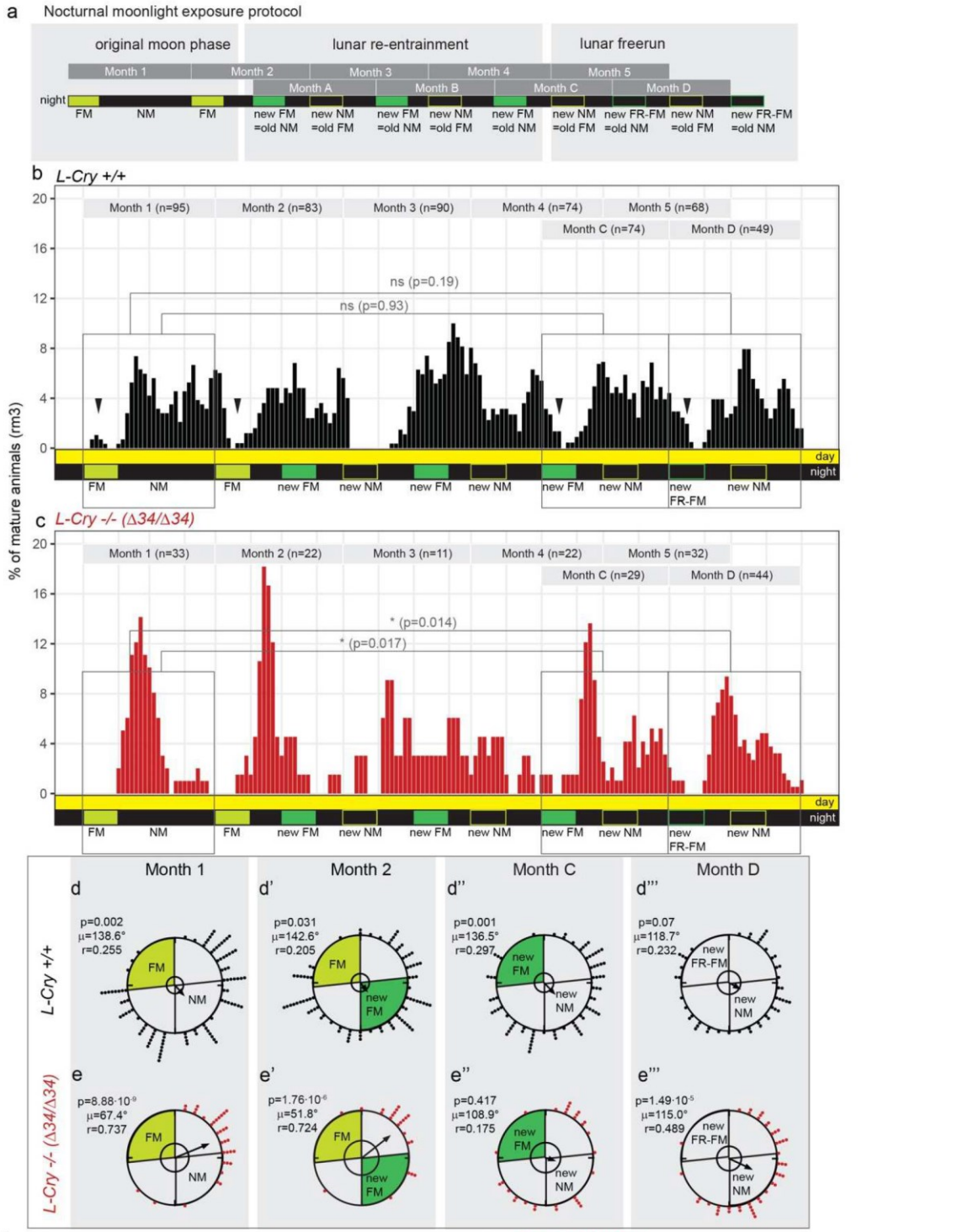

f *L-Cry +/+*

Comparison	Kolmogorov-Smirnov Test (p)	Mardia-Watson-Wheeler Test (p)	phase difference of vectors (days)
Month 1 vs 2	0.44	0.91	0.3
Month 1 vs C	0.93	0.82	0.2
Month 2 vs C	0.94	0.74	0.5
Month 1 vs D	0.19	0.91	1.7
Month 2 vs D	0.70	0.94	2.0

g *L-Cry -/- (Δ34/Δ34)*

Comparison	Kolmogorov-Smirnov Test (p)	Mardia-Watson-Wheeler Test (p)	phase difference of vectors (days)
Month 1 vs 2	0.42	0.08	1.3
Month 1 vs C	0.02	>0.001	3.5
Month 2 vs C	0.04	0.006	4.8
Month 1 vs D	0.01	0.006	4.0
Month 2 vs D	0.008	0.006	5.3

Figure 6: *l-cry* contributes to circalunar clock entrainment

(a) Nocturnal moonlight exposure protocol of lunar phase shift with 8 nights of naturalistic moonlight (dark green). **(b,c)** Number of mature animals (percent per month, rolling mean with a window of 3 days) of *l-cry* wildtype (b) and mutant (c) animals. p-values: Kolomogorov-Smirnov tests. Black arrowheads indicate spawning-free intervals of the wildtype, which shifted to the position of the new FM (under free-running conditions: FR-FM). **(d,e)** Data as in (b,c) plotted as circular data.

360° correspond to 30 days of the lunar month. The arrow represents the mean vector characterized by the direction angle μ and r. r (length of μ) indicates phase coherence (measure of population synchrony). p-values are results of Rayleigh Tests: Significance indicates non-random distribution of data points. The inner circle represents the Rayleigh critical value (p=0.05). **(f,g)** Results of multisample statistics on spawning data shown in (a-e). Phase differences in days can be calculated from the angle between the two mean vectors (i.e. 12°= 1 day).

The resulting spawning distribution was analysed for the efficacy of this "naturalistic moonlight" to phase-shift the circalunar oscillator. In order to test if the animals had shifted their spawning to the new phase, we again compared the spawning pattern before the exposure to the new fullmoon stimulus (months with numbers: data distribution analyzed relative to the initial/old FM, Fig. 6a) to the spawning pattern after the exposure to the new fullmoon stimulus (months with letters: data distribution analyzed relative to the new FM, Fig. 6a). The more similar the data distributions of months 1,2 are to the months C,D, the more the population has been shifted to the new phase.

Wildtype animals completely shifted their spawning pattern to the naturalistic moonlight stimulus, as supported by the following statistical analyses: When comparing the months 1 and 2 (relative to the old FM before the shift) to the months C and D (relative to the new FM after the shift), both the Kolmogorov-Smirnov test (Fig.6b: grey rectangles, 6f) and the Mardia-Watson-Wheeler test of the same data were non-significant (Fig.6f), indicative of the population shifting to the new phase.
Consistently, the direction angle (μ) of the mean vectors before and after the shift was highly similar, resulting in a phase difference of only 0.2 days between months 1 and C and 0.5 days between month 2 and month C (Fig. 6f, for details see methods).
Of note, wildtype worms would eventually reach the high spawning precision found under naturalistic moonlight only after several more months based on independent experiments (Fig. 4j,k and unpublished).
When we analyzed the spawning distribution of *l-cry* mutants in the same way as the wildtypes, we found that the data distribution exhibited significant differences in the linear Kolmogorov-Smirnov test when comparing months 1 and 2 before the shift to the months C and D after the shift (Fig. 6c: grey rectangles, Fig. 6g); as well as in the phase distribution in the circular analyses when comparing the months before the shift (months 1 and 2) with the last months of the shift (months C,D) (Fig. 6e,e' versus e'',e''',g). The populations also exhibited a noticeable phase difference of ≥3.5 days (Fig. 6g).

Based on the statistical significant difference in the re-entrainment of *l-cry-/-*, but not wild-type populations under a naturalistic sun- and moonlight regime, we conclude that L-Cry also contributes to circalunar entrainment as a photoreceptor. However, as these differences are rather minor, compared to the much stronger differences seen under artificial light regime, we conclude that its major role is the light gate keeping function (Fig7).

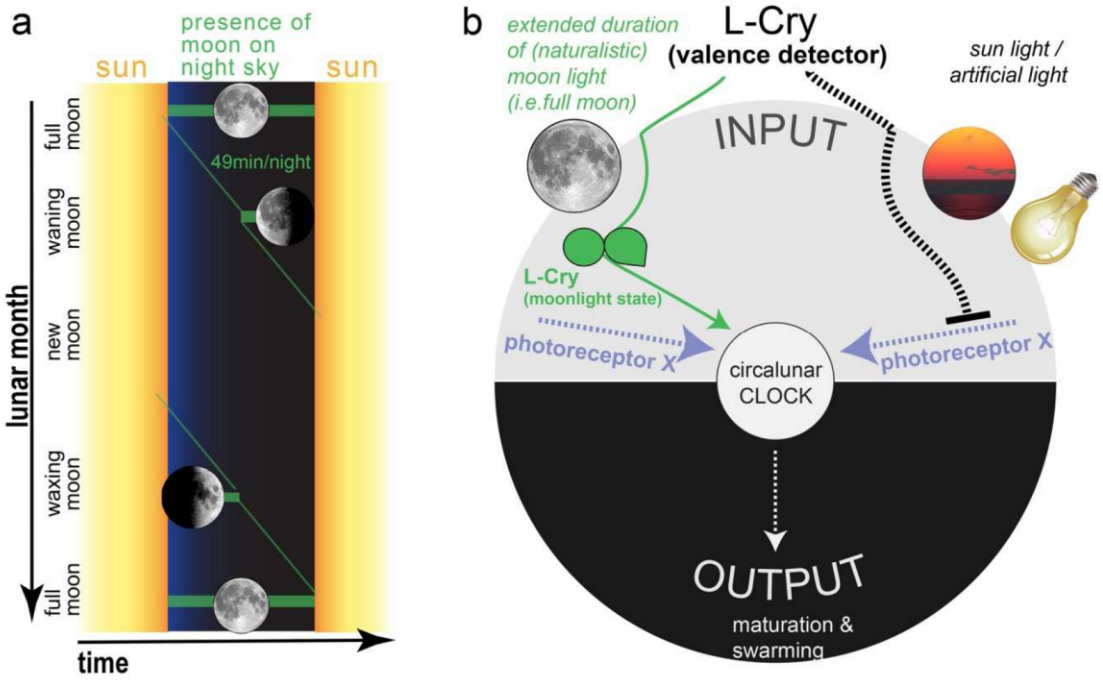

Figure 4. The entrainment of the monthly oscillator requires the detection of a specific moonphase. **a)** Schematic representation of the presence of the moon on the sky depending on moonphase. As a full cycle of the moon around the earth takes on average 24.8hrs, the presence of the moon relative to the sun shifts every night by ~49mins, indicated by the green diagonal. Worms need to specifically detect the full moon phase for circalunar oscillator entrainment, which requires that they can realize when a specific light (moonlight) starts and ends [31]. **b)** Scheme of L-Cry's function as moonlight duration and valence detector for circalunar clock entrainment. L-Cry's biochemical property of only reaching the full moonlight state after extended periods of (naturalistic) moonlight illumination allow for a discrimination of moonlight duration. As moon phases are characterized by the duration of the moon on the night sky, moonlight exposure duration translates into moon phase detection. L-Cry also discriminates the valence of light, strongly favoring (naturalistic) moonlight to entrain the circalunar clock.

Discussion

Our work delivers the first molecular entry point into the mechanisms underlying a moonlight-entrained monthly oscillator. It also provides the new concept that a light receptor does not just sense light, but by its intensity and duration can give light a valence that is relevant to discriminate between different naturally existing light sources (Fig. 7a,b). While we see the most apparent behavioral/physiological phenotype of the *l-cry-/-* worms under artificial lab light conditions, these conditions are nevertheless highly informative about *l-cry's* role as light valence detector. As briefly mentioned above, we interpret that this valence detection is under natural conditions necessary in order for the worms to synchronize to a specific moonphase: full moon. Full moon has the specific property that it is the moonphase during which the moon illuminates the entire night from sunset to sunrise (Fig.7a). In order for the organism to 'know' this specific moonphase under natural conditions with waning and waxing moons as well as sunrise/sunsets (Fig.7a), it needs to determine the duration not just of illumination, but specifically of the dim light illumination. This discrimination is made by L-Cry. Under the lab artificial light conditions, the moonlight stimulus is much more intense

and misses signals of the waning/waxing moon phases. We hypothesize that under these artificial situations, the circalunar clock is still somewhat entrained, because there is no other entrainment stimulus it otherwise can entrain to. However, L-Cry signals that it is not really the "right" nocturnal light, which results in the observable, rather low population synchronization. If L-Cry is not present (as in the *l-cry-/-* worms), the nocturnal artificial light signal of the lab condition fully impacts on the circalunar clock. As it is (artificially) highly precise without possibly confusing waning and waxing moon signals, the entrainment results in the observed higher synchrony of the *l-cry-/-* population. If the nocturnal light signal mimics more closely the naturalistic full moon light, L-Cry permits its full impact on the circalunar oscillator, which results in the observed high population synchrony of wildtype worms under naturalistic lab light conditions. Furthermore, L-Cry's function as a light valence detector also likely makes the entrainment system more stable against natural acute light disturbances, such as lightning.

At present, we can only speculate, how L-Cry can exert its valence function. We provide biochemical evidence that at dim light levels, corresponding to moonlight in nature, L-Cry can accumulate photons over time. L-Cry's photoreduction response to this accumulation is in its duration markedly different from its rapid, well-established response to strong light and non-linear, suggesting that a different "moonlight" signalling state might exist. Consistent with different L-Cry biochemical states under dim and strong light, L-Cry under naturalistic moonlight is not following the conventional cytoplasmic degradation pathway, but localizes at higher levels to the nucleus. This suggests that different cellular compartments convey the different light messages to different downstream pathways.

Upon exposure to naturalistic daylight, L-Cry rapidly moves to the cytoplasm, where its protein levels become reduced, fully consistent with our previous data in S2 cells [14]. In *Drosophila melanogaster* dCry is degraded via its light-induced interaction with the circadian clock protein Timeless and subsequent JETLAG (JET) ubiquitin-ligase–mediated proteolytic degradation [32]. Given that both Timeless and Jetlag exist in *Platynereis* (*Pdu*-Tim: [14], *Pdu*-Jet: reciprocal best blast hit in ESTs), it is possible that a similar mechanism exists in *Platynereis*. It is however noteworthy that *timeless* transcript levels are affected by room light in the bristle worm [14], indicative of additional levels of regulatory complexity.

In contrast to the suggested mechanism about L-Cry's fate in the cytoplasm based on existing knowledge from its *Drosophila* ortholog, the signalling downstream of nuclear L-Cry is at present completely enigmatic. It is clear from our data (and the accompanying manuscript Zurl et al) that neither darkness nor naturalistic moonlight causes degradation of nuclear L-Cry. This might indicate that ratios of cytoplasmic versus nuclear L-Cry could be important for circalunar clock moonlight

entrainment. To complicate matters even further- it is possible that different spatial expression domains, such as eye versus brain, need to be considered separately in their responses to extended naturalistic moonlight and subsequent downstream signalling cascades.

In its role as a light-signal gate keeper, only the accumulation of L-Cry molecules in the nuclear moonlight signalling state following prolonged moonlight exposure during full-moon, would enable lunar entrainment via an additional photoreceptor "X", which by itself is not able to discriminate between the correct full-moon signal and other "wrong" signals, such as sunlight or (in our lab experiment) the artificial/non-naturalistic nocturnal light source (Fig. 7b).

When L-Cry is photoreduced by light other than (naturalistic) moonlight, the light signalling of photoreceptor X towards the circalunar oscillator is inhibited (Fig.7b). *L-cry* mutant worms lack this inhibitory mechanism, resulting in the observed (unnatural) synchronisation to artificial moon light. On the other hand, the somewhat better response of wildtype worms to naturalistic moonlight under re-entraining conditions indicates that the accumulation of moon-light state L-Cry not only releases the inhibition, but might enhance the activity of the yet to be identified photoreceptor X or provide additional light signalling by itself to the monthly oscillator.

Connected to the question of the transmission of the moonlight signal to the circalunar oscillator is also a better understanding of L-Cry's "moonlight state". Is this state "just" a partial photoreduction of the state reached upon artificial sunlight exposure or perhaps also a conformationally different state with distinct formation and decay kinetics? And what is the role of the L-Cry dimers? An intriguing observation is, that in presence of moonlight the moonlight state can be stably maintained over several hours, whereas the sunlight state completely reverts to the fully-oxidized dark-state within minutes without accumulating the moonlight state while transitioning through partial photoreduction (Fig.1j). These different responses to moonlight illumination suggest that the moonlight- and sunlight states are conformationally and kinetically not equivalent (Extended Data Figure 2i). Based on its sequence homology and the similarity of its FAD photoreaction to *Drosophila* CRY (dCry), it is conceivable that L-Cry also displaces the regulatory C-terminal tail in the photoreduced state as observed for dCry [21,33]. However, as dCry is monomeric, L-Cry homodimer formation may impact these conformational changes, and these may further vary depending on whether moonlight or sunlight operates on the initial dark-state L-Cry homodimer. We propose, that partial FAD photoreduction in the moonlight state could be related to the formation of asymmetric L-Cry dimers, where one monomer retains oxidized FAD, while in the second monomer FAD is photoreduced to $FAD^{\bullet -}$ (Fig. 1j). This requires, that the flavins in the two L-Cry monomers have different redox potentials, likely resulting from different chemical environments due to conformational differences between the monomers (Extended Data Figure 2i). Hence different

amounts of energy (photon numbers) would be needed to photoreduce the flavins in the two L-CRY monomers. Moonlight, due to its very low intensity can only induce the lower energy transition, resulting in the partially photoreduced moonlight state. In presence of intense sunlight, however, the larger energy barrier to photoreduce the second flavin can also be overcome. Certainly, more extensive mechanistic studies are required to further support our model. However, this model is consistent with all our current *in vitro* data, and moreover, it plausibly illustrates how the very different intensities of moon- and sunlight can lead to the formation of conformationally distinct dark state (new moon), moonlight state (full moon) and sunlight state L-Cry proteins. Thereby L-Cry could translate different light qualities into different cellular signaling events, e.g. by changing L-Cry's subcellular localizations and cellular degradation rates (Fig. 3), to ultimately affect moonlight dependent physiology (Fig. 4-6).

Finally, an evolutionary consideration: Monthly synchronization by the moon has been documented for a wide range of organisms- including brown and green algae, corals, crustaceans, worms, but also vertebrates (reviewed in [6]). Furthermore, recent reports also provide increasing evidence that the lunar cycle influences human behaviour (reviewed in [31,34]). Are the lunar effects mediated by conserved or different mechanisms?

When considering monthly oscillators with period lengths in the range of weeks, our implication of L-Cry as a light receptor in the circalunar entrainment pathway at first glance rather suggests that such monthly oscillator might not be conserved, given that direct L-Cry orthologs are not present in all the groups that are affected by the lunar cycle [35]. However, taking further aspects into account, such a conclusion might be too quick. Could other members of the Cry/photolyase family take over similar functions? Furthermore, our entrainment data suggest the presence of additional moonlight entrainment photoreceptors, which might be conserved. Last, but not least the molecular mechanisms underlying the circalunar oscillator also await identification, and it is possible that conservation exists on this level. Examples are known from circadian biology and it will now require further work to reach a similar level of understanding for moon-controlled monthly rhythms and clocks.

Materials and Methods

Natural light measurements

Under water measurements of natural light at the habitat of *Platynereis dumerilii* were acquired using a RAMSES-ACC-VIS hyperspectral radiometer (TriOS GmbH) for UV to IR spectral range. In coastal waters of the Island of Ischia, in the Gulf of Naples, the two radiometers were placed on sand flat at 5m depth near to *Posidonia oceanica* meadows, which are a natural habitat for *P. dumerilii.* Measurements were recorded automatically every 15min across several weeks in the winter

2011/2012. To obtain a fullmoon spectrum, measurements taken from 10pm to 1am on a clear fullmoon night on the 10.11.2011 were averaged. To subtract baseline noise from this measurement, a NM spectrum was obtained by averaging measurements between 7:15pm to 5am on a NM night on 24.11.2011, and subtracted from the FM spectrum. Resulting spectrum: fig. S3A. To benchmark these moonlight spectra measured under water with moonlight measured on land, we compared the underwater spectra to a publicly available full moon spectrum measured on land on 14.04.2014 in the Netherlands (fig. S3G, spectrum available at http://www.olino.org/blog/us/articles/2015/10/05/spectrum-of-moon-light). As expected, light with longer wavelengths was strongly reduced in the underwater measurements compared to the surface spectrum, since longer wavelengths penetrate water less efficiently. For the sunlight spectrum, measurements taken from 8am to 4pm on a sunny day on 9.11.2011 were averaged.

Naturalistic Light Systems (NELIS devices)

To emulate naturalistic sunlight and moonlight conditions, we employed NELIS (Natural Environment Light Intensity System) (Marine Breeding Systems GmbH)[22]. The naturalistic moonlight device was composed of a combination of LEDs and an Ulbricht sphere for homogenous light mixing. For improved light distribution across the shelf, a naturalistic moonlight device was attached to each end of an acrylglass rod (two light sources and one rod per shelf). For details on the naturalistic sunlight source see ref. [22]. Light spectra were measured using ILT950 Spectroradiometer (International Light Technologies).

Cloning and recombinant virus generation for L-Cry

Full length N-terminally His_6-tagged *Platynereis dumerilii* L-Cry (1-567) was heterologously expressed in *Spodoptera frugiperda (Sf9)* insect cells using the Bac-to-Bac baculovirus expression system with the pCoofy27 expression vector. 1 * 10^6 *Sf9* cells were transfected with recombinant bacmid DNA using Cellfectin. The first generation P0 virus was harvested 3 days after bacmid transfection. A further virus amplification step was carried out and the P1 virus stock was used for protein expression. The volume of P1 virus stock to be added for sufficient protein expression was determined by test expression.

Protein expression and purification

Sf9 cells were grown as suspension cultures in sf900II media at 27°C, 80 RPM. 1 L of 1 * 10^6 *Sf9* cells/ml were transfected with P1 virus stock and incubated at 27°C for 72 h. Cells were harvested by centrifugation at 7000 rpm for 20 min and stored at -80°C until purification. All purification steps were carried out in dark or dim red light conditions. Columns were wrapped with aluminum foil to avoid light-activation of L-Cry. The cell pellets were resuspended in lysis buffer (20 mM Tris pH 7.5, 150 mM NaCl, 20 mM imidazole, 5% glycerol, 5 mM β-mercaptoethanol) and lysed using a

552 microfluidizer. The lysate was centrifuged at 27000 rpm for 45 min and the clarified supernatant
553 incubated with nickel beads for 1 h. The nickel beads were loaded onto a batch column, washed with
554 50-100 mM imidazol and the L-Cry protein was eluted with 250 mM imidazole. Elution fractions
555 containing L-Cry were concentrated, diluted with low salt buffer (50 mM Tris pH 7.5, 50 mM NaCl, 5%
556 glycerol, 1mM DTT) and loaded onto a 5 ml Hitrap Q sepharose anion exchange column (GE
557 Healthcare). A gradient from 0 % to 100 % high salt buffer (50 mM Tris pH 7.5, 1 M NaCl, 5% glycerol,
558 1mM DTT) was applied. L-Cry containing fractions were pooled, concentrated and loaded onto a
559 HiLoad S200 16/60 size exclusion chromatography (SEC) column (buffer 25 mM Bis-Tris propane pH
560 8.0, 150 mM NaCl, 5% glycerol, 1 mM TCEP). Fractions containing pure L-Cry were pooled,
561 concentrated to 10 mg/ml and snap frozen in liquid nitrogen for storage at -80°C. 2 mg of L-Cry was
562 obtained from 10 g of pellet. The identity of the L-Cry protein was confirmed by mass spectrometry.

563 **Reverse-phase HPLC analyses of the chromophore content of L-Cry**

564 Flavin Mononucleotide (FMN), Flavin Adenine Dinucleotide (FAD) and Methenyltetrahydrofolate
565 (MTHF) were dissolved in buffer (25 mM Bis-Tris propane pH 8.0, 150 mM NaCl, 5% glycerol) and run
566 at 1ml/min (20 °C) over a Macherey-Nagel C18 Gravity-SB (150/4/5 µm) column to separate the
567 chromophores by reverse phase (RP) HPLC analyses. A gradient from 20-100% of methanol against
568 water (+0.1% Trifluoroacetic acid) was used for optimal separation. To analyse the chromophore
569 content of L-Cry, purified L-Cry was heat-denatured for 5 min at 97°C and centrifuged at 14000 RPM
570 for 10 min at 4°C. The supernatant was subjected to RP-HPLC analysis. The chromophores were
571 monitored by absorption at 370 nm.

572 **Analytical Size Exclusion Chromatography (SEC) and SEC coupled with Multiangle**
573 **light scattering (SEC-MALS)**

574 Analytical SEC of dark-state L-Cry was carried out on a S200 10/300 size exclusion column (SEC buffer
575 25 mM Bis-Tris propane pH 8.0, 150 mM NaCl) under red light conditions. SEC-MALS was carried out
576 to determine the exact molecular weight and oligomeric state of purified L-Cry based on the SEC
577 elution volume and light scattering. For SEC-MALS, purified L-Cry was loaded onto a Superose 6
578 10/300 size exclusion column and run at a flowrate of 0.4 ml/min in SEC buffer. MALS data were
579 obtained from a DAWN DSP instrument (Wyatt Tech, Germany) and processed using ASTRA 4.90.07.
580 Elution volumes and corresponding molecular weight of calibration standards: 10.3 ml – 670 kDa
581 (Thyroglobulin), 13.67 ml – 158 kDa (γ-globulin), 15.71 ml – 44 kDa (ovalbumin), 17.42 ml – 17 kDa
582 (myoglobin) and 20.11 ml – 1350 Da (vitamin B12).

583 **UV/VIS spectroscopy on L-Cry: Blue light-, sunlight- and moonlight photoreduction**
584 **and dark recovery**

585 UV/Visible absorption spectra of the purified L-Cry protein were recorded on a Tecan Spark 20M
586 plate reader unless otherwise stated. A light-state spectrum of L-Cry with fully photoreduced $FAD^{\circ-}$

was collected after illuminating dark-adapted L-Cry for 110 sec with a 450 nm blue light emitting diode (fig S3D,E; 6.21 x 10^{16} photons/cm^2/sec at the sample). To analyze sunlight- and moonlight dependent FAD photoreduction, dark-adapted L-Cry (kept on ice) was continuously illuminated with naturalistic sunlight (fig. S3C,E; 1.55 x 10^{15} photons/cm^2/sec at the sample) or naturalistic moonlight (fig. S3C,E; 9.65 x 10^{10} photons/cm^2/sec at the sample) and UV-VIS spectra (300 – 700 nm) were collected at different time points.

Dark recovery kinetics (FAD reoxidation) of L-Cry at 18°C following illumination with blue-light (110 sec), sunlight (20 min on ice) or moonlight (6 h on ice) were measured by recording absorbance changes at 450 nm over time or by extracting 450 nm absorbance values from complete UV/VIS spectra. To measure dark recovery kinetics on ice, complete UV-VIS spectra (300 – 700 nm) were collected at different time points following 110 sec blue light- or 20 min sunlight illumination and absorbance values at 450 nm were extracted from the full spectra (sample was kept on ice and in darkness between measurements). Additionally, a temperature controlled Jasco V-550 UV-VIS spectrophotometer was used to determine dark recovery kinetics of L-Cry (after 110 sec blue-light) at 6°C based on absorbance changes at 450 nm. The time constants for dark recovery were calculated by fitting a single exponential curve to the experimental data. Spectra were analyzed using Origin (Version 7.5/10.5(trial); OriginLab Corporation, Northampton, MA, USA).

Recovery of L-Cry dark state in presence of moonlight

To assess if moonlight can maintain the light state, L-Cry was initially illuminated with sunlight for 20 min or with blue light for 110 sec, followed by continuous moonlight illumination up to 6 hours with the sample kept on ice. Complete UV-VIS spectra (300 – 700 nm) were collected at different time points. Absorbance values at 450 nm were taken from the complete spectra obtained between 5 min and 2h 30 min moonlight exposure and used to determine the time constant for recovery of oxidized FAD after blue-light or sunlight induced photoreduction in presence of moonlight.

Sunlight illumination of moonlight activated L-Cry

To assess if sunlight can further increase FAD photoreduction starting from the moonlight activated state, L-CRY was first illuminated with continuous moonlight for 6 hours, followed by 20 min of sunlight illumination (on ice). Complete UV-VIS spectra from 300 – 700 nm were measured in each case.

Worm Culture

Platynereis dumerilii were grown as previously described [14,36]. All animal work was conducted according to Austrian and European guidelines for animal research. Photoperiod 16:8 (L/D), circalunar entrainment: nocturnal light for 6-8 nights (see Figure legends for each experiment) every 29 to 30 days (centering around full moon (“inphase”) or new moon (“outphase”) in Vienna). Light

spectra and intensities of fig. S3 were measured with a recently calibrated ILT950 spectrometer (International Light Technologies Inc Peabody, USA) and converted to photons/cm^2/s.

Generation and Genotyping of *l-cry* KO worms

Design and construction of TALENs targeting *l-cry* is described in [23]. For genotyping, DNA extraction of immature and premature worms was conducted by cutting 5-10 tail segments with a scalpel and incubating them in 20µl 50mM NaOH at 95° for 20min. After adding 5µl of Tris/HCl pH 7.5, the supernatant was used as template for the PCR reaction. Mature worms were frozen as whole at -20°C and DNA was later extracted using NucleoSpin Tissue Mini kit for DNA from cells and tissue (Macherey-Nagel). PCR was performed with OneTaq Quick-Load 2x Master Mix with Standard Buffer (New England Biolabs). PCR product was run on an agarose gel and genotype was determined on size (168bp: wildtype, 134bp: Δ34+Δ9 mutant allele, 157bp: Δ11 mutant allele).

Primer	**Sequence 5'-3'**
l-cry_fwd	AAGAGAAGACTGACGATTGGGAC
l-cry_rev	CTGCAACTTCCCCATCCC

Primers used for l-cry genotyping

Full length *l-cry* cDNA- GenBank: MW161054

Monoclonal Antibody Production

A peptide consisting of amino acids 52 - 290 of L-Cry protein (GenBank ID: MT656570, predicted size 25kDa) was cloned and expressed in bacteria cells. Subsequently, this peptide was purified and used for mouse immunization, thereby acting as epitope in production of a monoclonal antibody against L-Cry. Upon screening of multiple clones, two clones (4D4-3E12-E7 and 5E3-3E6-E8) were selected and used in combination. Monoclonal antibodies were produced by and purchased from the Monoclonal Antibody Facility at Max Perutz Labs (Medical University of Vienna, Department of Medical Biochemistry).

Immunohistochemistry, microscopy and L-Cry localization determination

Worm heads were dissected with jaws and fixed in 4% PFA for 24h at 4°C. Samples were subsequently permeabilized using methanol, digested for 5 min with Proteinase K at room temperature without shaking and post-fixed with 4% PFA for 20 min at room temperature. Next, samples were washed 5 times for 5 min with 1x PTW and incubated in hybridization mixture[37] used in *in situ* hybridization protocol, at 65° C overnight. Worm heads were washed with 50% formamide/2X SSCT - standard saline citrate containing 0.1% Tween 20® (Sigma Aldrich) (2x, 20 min), then with 2X SSCT (2x, 10 min) and with 0.2X SSCT (2x, 20 min); all washing steps at 65° C. After blocking for 90 min with 5% sheep serum (Sigma-Aldrich) at room temperature, samples were incubated in L-Cry antibodies 5E3-3E6-E8 (1:100) and 4D4-3E12-E7 (1:50) in 5% sheep serum (Sigma-Aldrich). Secondary

antibody, Cy3 goat anti-mouse IgG (A10521, Thermo Fisher Scientific) was diluted 1:400 in 2.5% sheep serum (Sigma-Aldrich). Incubations were done for at least 36h at 4° C shaking and after each incubation time, samples were washed with 1x PTW three times for 15 min at room temperature and a fourth time over night at 4° C. After this, Höchst 33342 (H3570, Thermo Fisher Scientific), diluted 1:2000, was added for at least 30 min at room temperature. Samples were then washed three times for 15 min with 1x PTW at room temperature and mounted with 25 mg/ml DABCO (Roth/Lactan) in an 87% glycerol (Sigma-Aldrich) solution. All solutions were made with 1x PTW (PBS + 0.1% Tween 20®) (Sigma Aldrich). Heads were imaged on a Zeiss LSM 700 laser scanning confocal microscope using LD LCI Plan-Apochromat 25X, Plan-Apochromat 40X by CHD: T-PMT detection system and Zeiss ZEN 2012 software. Lasers: DAPI 405 nm and Cy3 555 nm.

Categorical scoring: Using Fiji/ImageJ [38], nuclear outlines were marked as Regions Of Interest (ROI) on the 405 nm channel images (Höchst staining). ROIs were then used for scoring of the signal localization (inside =nucleus versus outside= cytoplasm) on the 555nm channel of the same images (L-Cry).

Quantitative scoring: Using the deep learning-based image segmentation algorithm Cellpose [39] on the 405 nm channel images, the Hoechst-stained nuclei were identified and marked as Regions Of Interest (ROI). L-Cry signal was then determined for these nuclear ROIs using in Fiji/ImageJ [38]. Signal intensity was determined by calculating Corrected Total Cell Fluorescence (CTCF) using the formula CTCF=Area (ROI_1)*Mean (ROI_1)-Area (ROI_1)*Mean(ROI_(background ROIs)). A sum of CTCF values of all the nuclei was subtracted from the CTCF value of the whole brain area, to obtain the corresponding value for non-nuclear, i.e. cytoplasmic signal. Finally, the ratio between nuclear and non-nuclear (cytoplasmic) signal intensity was calculated for corresponding regions of different worm heads to compare between different ZTs.

Protein extraction and Western Blots

Per biological replicate four premature worms were anaesthetized (7.5% $MgCl_2$-/H_20, 1:1 diluted with sea water), decapitated and heads transferred to a 1.5ml tube containing 150 µl RIPA lysis buffer (R0278 Sigma-Aldrich), 10% Triton X100 and protease inhibitor (cOmplete Tablets, EDTA-free, *EASYpack*, Roche). The tissue was homogenized by grinding using a tight fitting pestle. All steps on ice. Cell debris was pelleted by centrifugation. Protein concentration of lysates was determined using Bradford reagent (BIORAD), subjected to SDS-gel electrophoresis (10% Acrylamide) and transferred (Transferbuffer: 39mM Gylcine, 48mM Tris, 0.04% SDS, 20% MetOH) to a nitrocellulose membrane (Amersham™ Protran™ 0,45µm NC, GE Healthcare Lifescience). Quality of transfer was checked by Ponceau-S (Sigma Aldrich) staining. After 1h of blocking with 5% slim milk powder (Fixmilch Instant, Maresi) in 1xPTW (1xPBS/0.1% TWEEN 20) at room temperature, the membrane was incubated with

the appropriate primary antibody diluted in 2.5% milk/PTW at 4°C overnight. [anti-L-Cry 5E3-3E6-E8 (1:100) and anti-L-Cry 4D4-3E12-E7 (1:100); anti-beta-Actin (Sigma, A-2066, 1: 20.000)]. After 3 rinses with 1xPTW the membrane was incubated with the species specific secondary antibody [anti-Mouse IgG-Peroxidase antibody, (Sigma, A4416, 1:7500); Anti-rabbit IgG-HRP-linked antibody (Cell Signaling Technology, #7074, 1:7.500] diluted in 1xPTW/1% slim milk powder for 1 hour, RT. After washing, SuperSignal™ West Femto Maximum Sensitivity Substrate kit (Thermo Fisher Scientific) was used for HRP-signal detection and finally signals were visualized by ChemiDoc Imaging System (BIORAD). Specific protein bands were quantified in "Image J" and L-Cry was normalized to beta-Actin.

Collection and analysis of spawning data

Worm boxes were checked daily for mature worms. Worms which had metamorphosed into their sexually mature male or female form and had left their tube to perform their nuptial dance were scored as mature animals.

The recordings of mature animals in nature (collected from June 1929 to June 1930 in Naples [28,30]) were digitalized and all months were aligned to relative to the same moonphase and combined. For comparisons of these data with our spawning data from the lab, we aligned the first day after full moon in nature with the last day of full moon stimulus in the lab, since *Platynereis dumerilii* synchronizes its circalunar clock to the end of the full moon stimulus[5].

For analysis, each day of the lunar month was assigned a number from 1 to 30. For linear plots, the percentage of mature worms per lunar day was then plotted as a histogram. The spawning distributions of two conditions were compared using the Kolmogorov-Smirnov Test. For the circular analysis [40-42] of spawning data, the lunar day of spawning was multiplied by 12 for each worm, so that the 30 lunar days regularly distributed on the 360° circle. Each dot represents one mature worm unless stated otherwise. Circular data can be described using the mean vector (displayed as an arrow), which is defined by its direction angle (μ) and its length (r). The direction angle μ is given relative to 0° (moon off). The value of length r (also called phase coherence) ranges from 0 to 1, where higher values indicate higher phase coherence (i.e synchrony). In order to test, if the observed data distribution is significantly different from random, we performed the Rayleigh's Uniformity Test and used $p<0.05$ as cutoff for significance. Non-uniform distribution is consistent with lunar rhythmicity. For comparing two circular datasets (e.g. of different genotypes or different months in the phase shift experiments), we used the non-parametric Mardia-Watson-Wheeler test. Circular analysis of these data was performed using Oriana (Version 4.02, Kovach Computing Services).

Phase-Shift Experiments

For Phase-Shift experiments, boxes with adult worms (at least 3 months old) were transferred from standard light conditions (see "worm culture") to the naturalistic light systems (sun- and moonlight)

mounted in light-tight black shelves. Number of mature worms was recorded daily and number of mature worms per day was used to calculate percentage of mature worms (one month: 100%). Data were smoothened using a rolling mean with a window size of 3 days. Data analysis was performed as described in "Collection and analysis of spawning data".

Whole mount *in situ* Hybridisation combined with immunohistochemistry for L-Cry

Probes were generated *de novo* using previously cloned plasmids as template. Genes of interest were amplified via PCR using Phusion Polymerase (NEB) and primers for pJET 1.2 with an overhang of Sp6 promoter. PCR product was purified following the protocol for "QIAquick PCR Purification Kit" (Qiagen). Agarose gel electrophoresis showed right amplicon sizes and single bands. For the in vitro transcription, 1µg of linearized template was used. Riboprobes were labelled with anti-Digoxigenin UTPs (Roche Diagnostics) and transcribed with Sp6 polymerase at 37°C for 4h. Probes were purified according to the "RNeasy Kit" (QIAGEN) and eluted in 40ul RNase-free water. 600-1000ng of the riboprobes were used.

Whole-mount *in situ* Hybridisation was carried out on premature worms of the RE strain, following published procedures [37,43] with adjustments made to combine it with L-Cry immunohistochemistry. Worm heads were fixed in 4% PFA for 2h at RT while shaking. Proteinase K digest: 5min, during which samples were very slightly rocked. After blocking in 5% sheep serum/1X PTW, worm heads were incubated with the monoclonal L-Cry antibodies (5E3-3E6-E8 diluted 1:100 and 4D4-3E12-E7 diluted 1:50), anti-Digoxigenin-AP coupled antibody (Roche Diagnostics) and sheep serum diluted to 2.5% with 1xPTW for 36-40h at 4°C, shaking. After detection using NBT/BCIP, samples were incubated in the secondary antibody Alexa Fluor-488 goat anti-mouse IgG (Thermo Fisher Scientific), 1:400 (36-40h at 4°C, shaking), washed in 1xPTW and mounted in DABCO/Glycerol. Imaging was done using Axioplan Z2 Microscope (Carl Zeiss) with AxioCam MRc5 colour CCD camera (Carl Zeiss) and captured using ZenPro Software (Carl Zeiss). The images were edited with either ImageJ or Photoshop CC.

Statistical Analysis

All data analysis was conducted using R 3.6.1[44], GraphPad Prism 8.4.2, Oriana 4.02 and Microsoft Excel 2010.

Acknowledgements

We thank the members of the Tessmar-Raible and Wolf groups for discussions. Andrej Belokurov and Margaryta Borysova for excellent worm care at the MFPL aquatic facility. We are grateful for support by the IMB Protein Production and Proteomics Core Facilities (mass spec instrument funded by DFG INST 247/766-1 FUGG). In particular, we wish to thank Dr. Mario Dejung of the Proteomics Core Facility for carrying out preliminary mass spec data analysis. We would like to thank Dr Svenja

753 Morsbach and Beate Müller from the Max Planck Institute for Polymer Research for helping with
754 HPLC experiment and Prof Dr Elmar Jaenicke from University of Mainz for help with SEC-MALS.

755 Funding

756 K.T-R. received funding for this research from the European Research Council under the European
757 Community's Seventh Framework Programme (FP7/2007–2013) ERC Grant Agreement 337011 and
758 the Horizon 2020 Programme ERC Grant Agreement 819952, the research platform 'Rhythms of Life'
759 of the University of Vienna, the Austrian Science Fund (FWF, http://www.fwf.ac.at/en/): SFB F78 and
760 the HFSP () research grant (#RGY0082/2010). S.K. is a recipient of a DFG fellowship through the
761 Excellence Initiative by the Graduate School Materials Science in Mainz (GSC 266). None of the
762 funding bodies was involved in the design of the study, the collection, analysis, and interpretation of
763 data or in writing the manuscript.

764 References:

765 1 Fox, H. M. Lunar periodicity in Reproduction. *Proceedings of the Royal Society of London*
766 **Series B 95**, 523-550 (1924).
767 2 Levy, O. *et al.* Light-responsive cryptochromes from a simple multicellular animal, the coral
768 *Acropora millepora*. *Science* **318**, 467-470 (2007).
769 3 Numata, H. & Helm, B. *Annual, lunar, and tidal clocks : patterns and mechanisms of nature's*
770 *enigmatic rhythms*. (Springer, 2014).
771 4 Korringa, P. Relations between the moon and periodicity in the breeding of marine animals.
772 *Ecological Monographs* **17**, 347-381 (1947).
773 5 Hauenschild, C. Lunar periodicity. *Cold Spring Harb. Symp. Quant. Biol.* **25**, 491-497 (1960).
774 6 Tessmar-Raible, K., Raible, F. & Arboleda, E. Another place, another timer: Marine species
775 and the rhythms of life. *Bioessays* **33**, 165-172, doi:10.1002/bies.201000096 (2011).
776 7 Bézy, V. S. *et al.* Mass-nesting events in olive ridley sea turtles: environmental predictors of
777 timing and size. *Anim. Behav.* **163**, 85-94, doi:https://doi.org/10.1016/j.anbehav.2020.03.002
778 (2020).
779 8 Norevik, G., Akesson, S., Andersson, A., Backman, J. & Hedenstrom, A. The lunar cycle drives
780 migration of a nocturnal bird. *PLoS Biol.* **17**, e3000456, doi:10.1371/journal.pbio.3000456
781 (2019).
782 9 Casiraghi, L. *et al.* Moonstruck sleep: Synchronization of human sleep with the moon cycle
783 under field conditions. *Sci Adv* **7**, doi:10.1126/sciadv.abe0465 (2021).
784 10 Helfrich-Forster, C. *et al.* Women temporarily synchronize their menstrual cycles with the
785 luminance and gravimetric cycles of the Moon. *Sci Adv* **7**, doi:10.1126/sciadv.abe1358 (2021).
786 11 Shlesinger, T. & Loya, Y. Breakdown in spawning synchrony: A silent threat to coral
787 persistence. *Science* **365**, 1002-1007, doi:10.1126/science.aax0110 (2019).
788 12 Neumann, D. Temperature compensation of circasemilunar timing in the intertidal insect
789 *Clunio*. *Journal of Comparative Physiology A - Sensory Neural and Behavioral Physiology* **163**,
790 671-676 (1988).
791 13 Franke, H.-D. The Role of Light and Endogenous Factors in the Timing of the Reproductive
792 Cycle of Typosyllis prolifera and Some Other Polychaetes. *Am. Zool.* **26**, 433-445 (1986).
793 14 Zantke, J. *et al.* Circadian and Circalunar Clock Interactions in a Marine Annelid. *Cell Reports*
794 **5**, 99-113, doi:10.1016/j.celrep.2013.08.031 (2013).

15 Franke, H. D. On a clocklike mechanism timing lunar-rhythmic reproduction inTyposyllis prolifera (Polychaeta). *Journal of Comparative Physiology A: Neuroethology, Sensory, Neural, and Behavioral Physiology* **156**, 553-561 (1985).
16 Raible, F., Takekata, H. & Tessmar-Raible, K. An Overview of Monthly Rhythms and Clocks. *Frontiers in Neurology* **8**, doi:ARTN 189 10.3389/fneur.2017.00189 (2017).
17 Hauenschild, C. Über das lunarperiodische Schwärmen von *Platynereis dumerilii* in Laboratoriumszuchten. *Naturwissenschaften* **41**, 556-557 (1954).
18 Fukunaga, K., Yamashina, F., Takeuchi, Y., Yamauchi, C. & Takemura, A. Moonlight is a key entrainer of lunar clock in the brain of the tropical grouper with full moon preference. *BMC Zoology* **5**, 11, doi:10.1186/s40850-020-00060-8 (2020).
19 Fukushiro, M. *et al.* Lunar phase-dependent expression of cryptochrome and a photoperiodic mechanism for lunar phase-recognition in a reef fish, goldlined spinefoot. *PLoS ONE* **6**, e28643, doi:10.1371/journal.pone.0028643 (2011).
20 Brady, A. K., Willis, B. L., Harder, L. D. & Vize, P. D. Lunar Phase Modulates Circadian Gene Expression Cycles in the Broadcast Spawning Coral Acropora millepora. *Biol. Bull.* **230**, 130-142, doi:10.1086/BBLv230n2p130 (2016).
21 Berndt, A. *et al.* A novel photoreaction mechanism for the circadian blue light photoreceptor *Drosophila* cryptochrome. *J. Biol. Chem.* **282**, 13011-13021, doi:M608872200 [pii] 10.1074/jbc.M608872200 [doi] (2007).
22 Veedin Rajan, V. B. *et al.* Seasonally relevant UVA light alters neurohormone amounts and behavior via a ciliary opsin in a marine mass spawning annelid. *Nature Ecology & Evolution*, doi:10.1038/s41559-020-01356-1 (2021).
23 Bannister, S. *et al.* TALE Nucleases mediate efficient, heritable genome modifications in the marine annelid *Platynereis dumerilii*. *Genetics* **197**, 19-31, doi:10.1534/genetics.112.148254 (2014).
24 Xu, B., Feng, X. & Burdine, R. D. Categorical data analysis in experimental biology. *Dev Biol* **348**, 3-11, doi:10.1016/j.ydbio.2010.08.018 (2010).
25 Fisher, N. I. *Statistical analysis of circular data*. (cambridge university press, 1995).
26 Ayers, T., Tsukamoto, H., Gühmann, M. & Tessmar-Raible, K. A Go-type Opsin mediates the Shadow Reflex in the annelid Platynereis dumerilii. *BMC Biol.* **16**, 41, doi:10.1186/s12915-018-0505-8 (2018).
27 Guehmann, M. *et al.* Spectral Tuning of Phototaxis by a Go-Opsin in the Rhabdomeric Eyes of Platynereis. *Curr. Biol.* **25**, 2265-2271, doi:10.1016/j.cub.2015.07.017 (2015).
28 Ranzi, S. Ricerche sulla biologia sessuale degli Anellidi. *Pubbl. Staz .Zool. Napoli* **11**, 271-292 (1931).
29 Zantke, J., Bannister, S., Veedin Rajan, V. B., Raible, F. & Tessmar-Raible, K. Genetic and Genomic Tools for the marine annelid *Platynereis dumerilii. Genetics* **197**, 9-31, doi:10.1534/genetics.112.148254 (2014).
30 Ranzi, S. Maturita sessuale degli Anellidi e fasi lunari. . *Boll. Soc. Ital. Biol. Sperim.* **6**, 18 (1931).
31 Andreatta, G. & Tessmar-Raible, K. The Still Dark Side of the Moon: Molecular Mechanisms of Lunar-Controlled Rhythms and Clocks. *J. Mol. Biol.*, doi:10.1016/j.jmb.2020.03.009 (2020).
32 Peschel, N., Chen, K. F., Szabo, G. & Stanewsky, R. Light-Dependent Interactions between the Drosophila Circadian Clock Factors Cryptochrome, Jetlag, and Timeless. *Curr. Biol.* **19**, 241-247, doi:10.1016/j.cub.2008.12.042 (2009).
33 Czarna, A. *et al.* Structures of Drosophila Cryptochrome and Mouse Cryptochrome1 Provide Insight into Circadian Function. *Cell* **153**, 1394-1405, doi:10.1016/j.cell.2013.05.011 (2013).
34 Häfker, N. S. & Tessmar-Raible, K. Rhythms of behavior: are the times changin'? *Curr. Opin. Neurobiol.* **60**, 55-66, doi:10.1016/j.conb.2019.10.005 (2020).

35 Oliveri, P. *et al.* The Cryptochrome/Photolyase Family in aquatic organisms. *Marine Genomics* **14**, 23-37, doi:10.1016/j.margen.2014.02.001 (2014).
36 Hauenschild, C. & Fischer, A. Platynereis dumerilii. Mikroskopische Anatomie, Fortpflanzung, Entwicklung. [Platynereis dumerilii. Microscopical anatomy, reproduction and development] 1-55 (Stuttgart, 1969).
37 Tessmar-Raible, K., Steinmetz, P. R., Snyman, H., Hassel, M. & Arendt, D. Fluorescent two-color whole mount in situ hybridization in Platynereis dumerilii (Polychaeta, Annelida), an emerging marine molecular model for evolution and development. *Biotechniques* **39**, 460, 462, 464 (2005).
38 Schindelin, J. *et al.* Fiji: an open-source platform for biological-image analysis. *Nat. Methods* **9**, 676-682, doi:10.1038/nmeth.2019 (2012).
39 Stringer, C., Wang, T., Michaelos, M. & Pachitariu, M. Cellpose: a generalist algorithm for cellular segmentation. *Nat. Methods* **18**, 100-106, doi:10.1038/s41592-020-01018-x (2021).
40 Huang, R. S., Chen, C. F. & Sereno, M. I. Mapping the complex topological organization of the human parietal face area. *Neuroimage* **163**, 459-470, doi:10.1016/j.neuroimage.2017.09.004 (2017).
41 Lee, A. Circular data. *WIREs Computational Statistics* **2**, 477-486, doi:https://doi.org/10.1002/wics.98 (2010).
42 Landler, L., Ruxton, G. D. & Malkemper, E. P. Circular data in biology: advice for effectively implementing statistical procedures. *Behav. Ecol. Sociobiol.* **72**, 128, doi:10.1007/s00265-018-2538-y (2018).
43 Backfisch, B. *et al.* Stable transgenesis in the marine annelid *Platynereis dumerilii* sheds new light on photoreceptor evolution. *Proc Natl Acad Sci USA* **110**, 193-198, doi:10.1073/pnas.1209657109 (2013).
44 R: A Language and Environment for Statistical Computing. (https://www.R-project.org/ Vienna, Austria, 2016).

Extended Data Figures

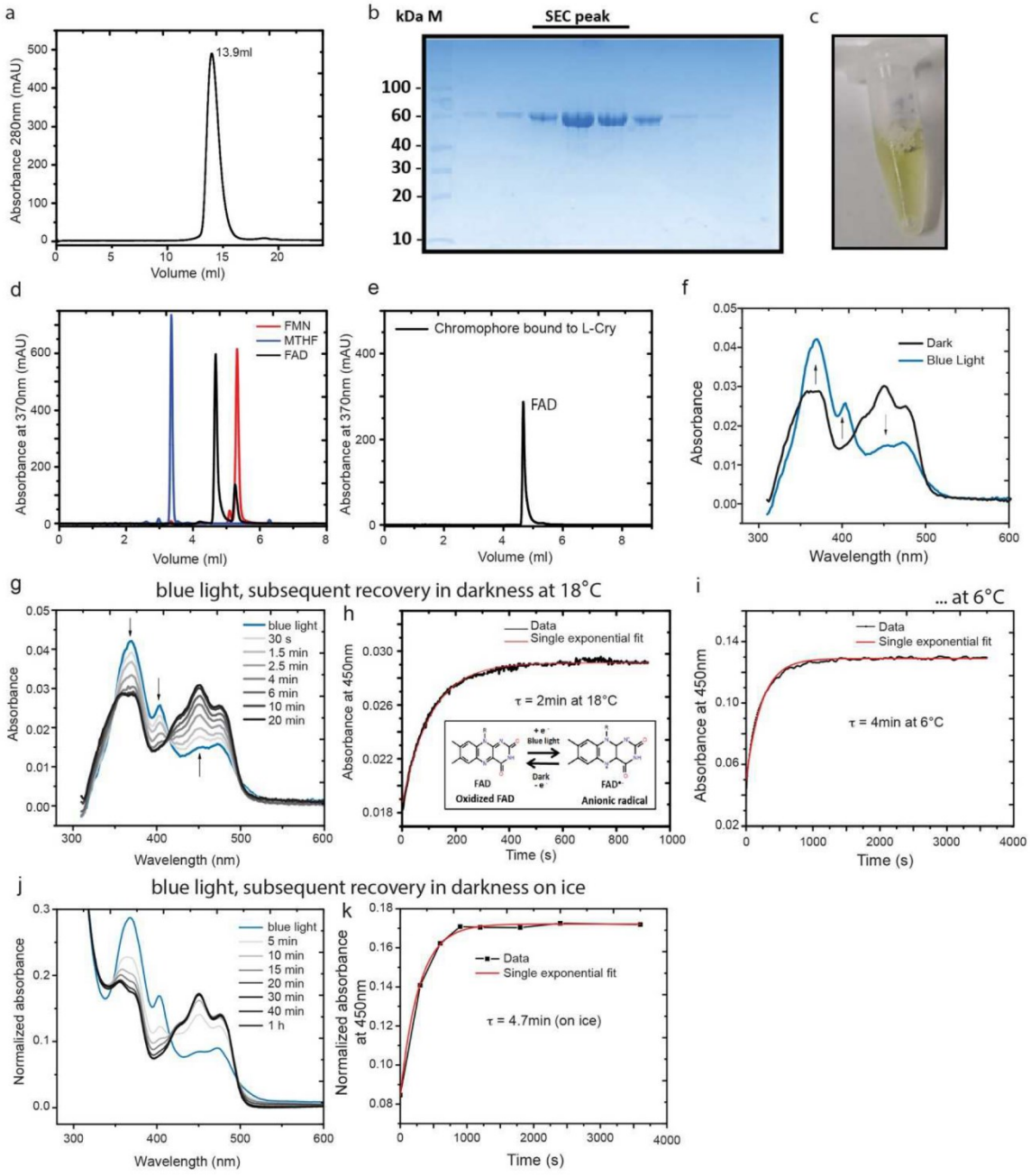

Extended Data Figure 1: Purification, biochemical and spectral characterization of L-Cry with blue light.

(a) Size-exclusion chromatography (SEC) of L-Cry on analytical S200 10/300 column. L-Cry elutes at 13.9 ml, suggesting a homodimer based on calibration standards. **(b)** 10% Bis-Tris gel loaded with fractions from the L-Cry SEC peak in (a). **(c)** L-Cry protein solution (5 mg/ml) with yellow color from bound oxidized FAD. **(d,e)** Reverse phase HPLC analysis identifies FAD as only L-Cry chromophore. Elution profile of standard chromophores FMN, MTHF and FAD (d) were compared with the L-Cry bound chromophore obtained after heat denaturation (e). **(f)** Absorption spectrum of L-Cry in dark (black) and after 110s blue light (blue). Arrows indicate the change in absorbance at 370nm, 404nm and 450nm between FAD (dark) and $FAD^{\bullet-}$ (after blue light). **(g,h)** L-Cry dark recovery after blue light activation at 18°C. Full Spectra in (g), 450nm absorbance in

(h). Inset in (h): Schematic of FAD photoreaction. **(i)** Dark recovery after blue light activation at 6°C (450 nm absorbance). **(j,k)** Dark recovery after blue light activation on ice. Full spectra in J, 450nm absorbance in k.

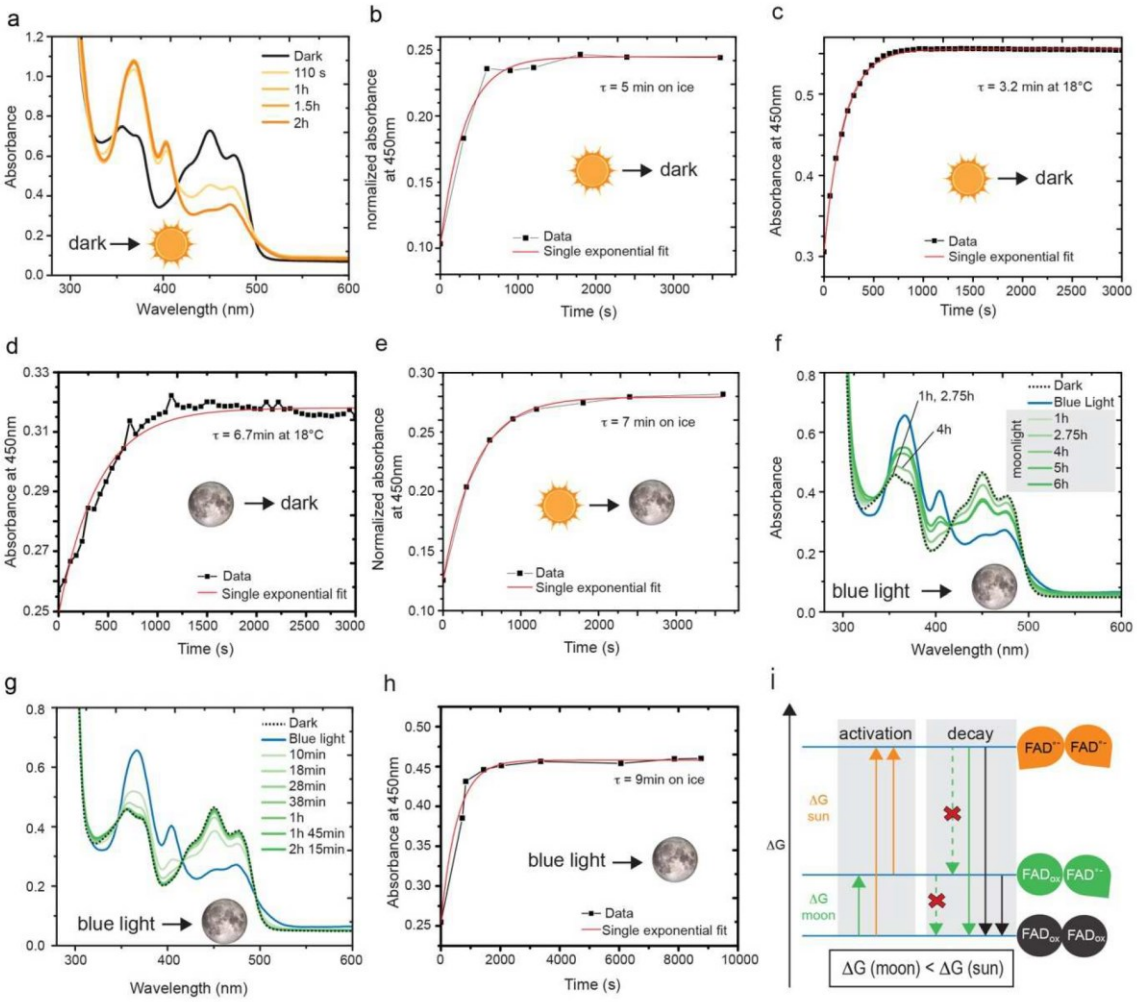

Extended Data Figure 2: Spectral characterization of L-Cry under naturalistic sun- and moonlight

(a) Absorption spectrum of L-Cry in dark (black) and after sunlight exposure (orange). Additional timepoints shown in Fig. 1b. **(b)** Dark recovery of L-Cry after 20min of sunlight on ice: absorbance at 450 nm, full spectra in Fig. 1c. **(c)** Dark recovery of L-Cry after 20min sunlight at 18°C: absorbance at 450 nm. **(d)** Dark recovery of L-Cry after 6h of naturalistic moonlight: absorbance at 450 nm. Full spectra in Fig. 1f. **(e)** Absorbance at 450nm after 20min sunlight followed by dark-state recovery in presence of moonlight. Full spectra in 1h. **(f)** Absorption spectra of L-Cry after 110s blue light illumination followed by an up to 6h exposure to naturalistic moonlight. L-Cry first returns to the dark state (1h, 2.45 h) and after 3h starts to build the moonlight state (4h, 5h, 6h). **(g)** Recovery of oxidized FAD from the blue light-induced anionic $FAD^{\circ -}$ radical under naturalistic moonlight shows that L-Cry first returns to the dark state. **(h)** Absorbance values at 450 nm from EDF2g. Note: strong blue light results in L-Cry's sunlight state.

(i) Schematic model of relative energy levels (ΔG) and transitions of dark-, moonlight- and sunlight states of L-Cry. MALS and SEC analyses of dark-sate L-Cry (Fig.1a, EDF 1a) show that L-Cry forms homodimers. The energy difference between the dark- and moonlight state (ΔG moon) is significantly smaller than the energy required to get from the dark state to the sunlight state or from the moonlight state to the sunlight state (ΔG sun) (ΔG moon and ΔG sun not drawn to scale). This can be explained by an asymmetric L-Cry dimer with different redox potentials of the flavin cofactors and hence different transition energies between FAD_{ox} and $FAD^{\circ -}$ in each monomer. *Activation:* Low intensity moonlight (green arrows) can only photoreduce the lower energy flavin within one monomer resulting in the moonlight state, but cannot overcome the larger energy barrier to photoreduce the second flavin molecule. This is, however, possible in presence of sunlight (orange

arrows) with much higher intensity, resulting in the fully photoreduced sunlight state. *Decay:* In darkness (black arrows) or in presence of moonlight, the sunlight state directly decays to the dark state, i.e. moonlight does not maintain the sunlight state. Furthermore, the moonlight state does not accumulate upon decay of the sunlight state in presence of moonlight (crossed-out dashed green arrow) or in darkness, likely due to the much faster decay kinetics of the sun- and moonlight states (within min) compared to repopulation of the moonlight state (6 hours). In contrast, moonlight is able to maintain existing moonlight-state L-Cry populations, that have accumulated after 6 h moonlight exposure, i.e. moonlight-state L-Cry does not decay to the dark-state in presence of moonlight (crossed-out dashed green arrow), but only in complete darkness (black arrow).

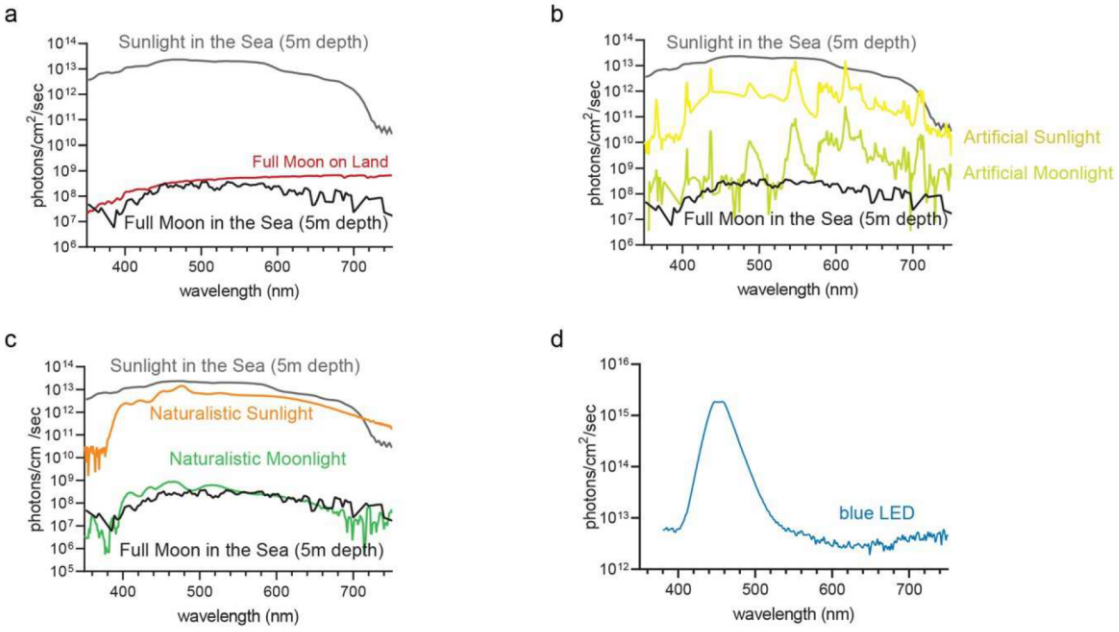

e

Light Source	photons/cm²/s[380-750nm]
Full Moon in the Sea (5m depth)	$1.79 \cdot 10^{10}$
Full Moon on Land	$1.77 \cdot 10^{11}$
Artificial Moonlight	$2.46 \cdot 10^{12}$
Naturalistic Moonlight	$9.65 \cdot 10^{10}$
Sunlight in the Sea (5m depth)	$1.30 \cdot 10^{15}$
Artificial Sunlight	$3.23 \cdot 10^{14}$
Naturalistic Sunlight	$1.55 \cdot 10^{15}$
blue LED	$6.21 \cdot 10^{16}$

Extended Data Figure 3: Spectra of light sources

(a) Light spectra in nature: sunlight (grey) and full moon in 5m depth in Ischia (black) as well as full moon light on land (red). **(b)** Spectra of the highly artificial sun- (yellow) and moonlight (light green) in the worm culture room. **(c)** Spectra of designed naturalistic sun- (orange) and moonlight (green). **(d)** Spectrum of blue light LED used for spectroscopic experiments. **(e)** number of photons/cm²/s of (a-d). Intensity and spectrum were always measured in the distance relevant for the experiments.

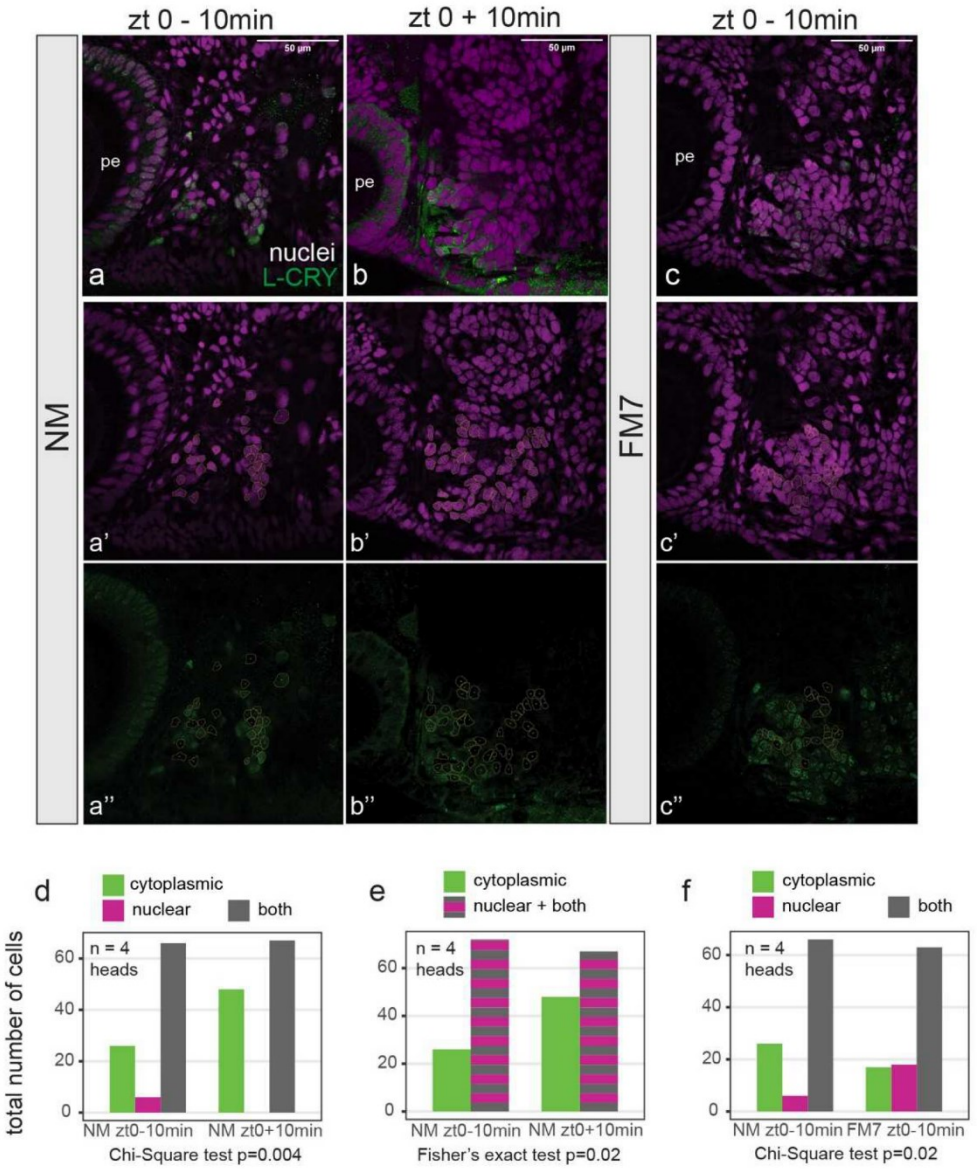

Extended Data Figure 4: L-Cry immunohistochemistry on *Pdu* heads

(a-c) Single layers of confocal images (1.28µm thick) of worm heads stained with anti-L-Cry antibody (green) and HOECHST (magenta) at indicated timepoints. Details of these pictures: Fig. 3e-g''. pe, posterior eye. **(a'-c'')** Examples for selection of Regions of Interest (ROI) used for the quantification of L-Cry protein localization in d-f. **(d-f)** Categorical quantification of L-Cry's subcellular localization at indicated timepoints. The statistical analysis was performed according to the requirements for categorical data (24).

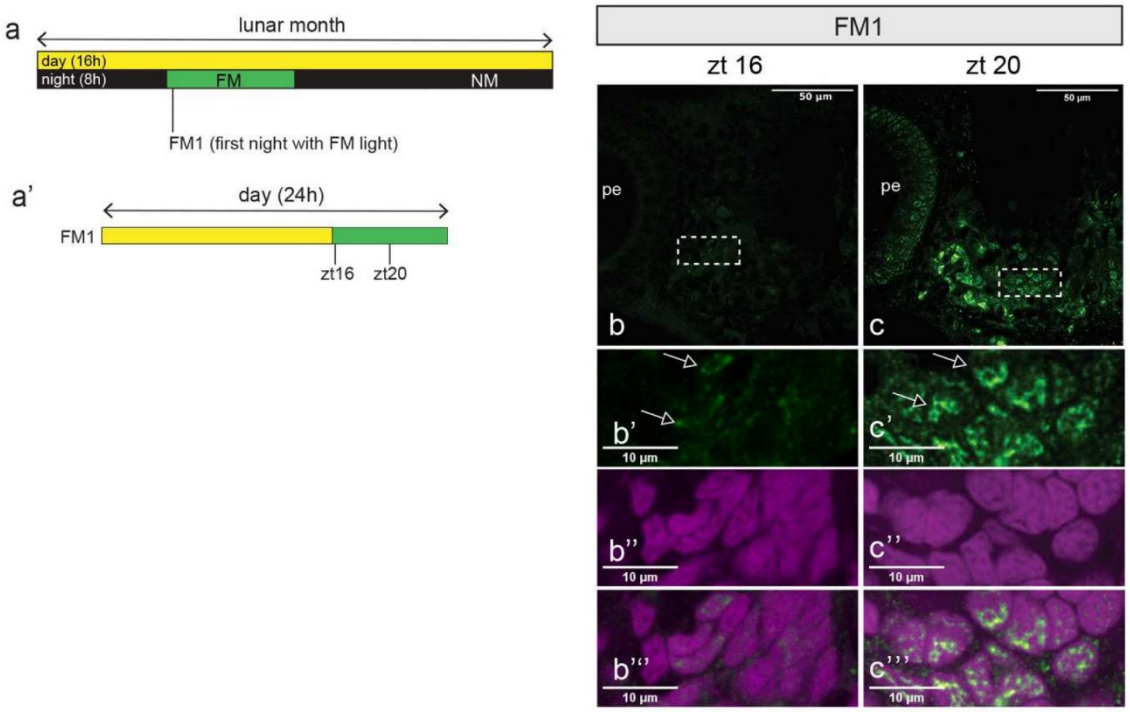

936

937 **Extended Data Figure 5: L-Cry protein is endogenously present at timepoints that allow for sufficient time to reach the**
938 **moonlight-state upon naturalistic moonlight exposure.**

939 **(a,a')** Scheme of sampling timepoints. 16hrs day (light) and 8 hrs night (dark or moonlight) per 24hrs, with 8 nights of
940 moonlight per month. **(b-c)** Maximal projections of confocal images of worm heads stained with anti-L-Cry antibody (green).
941 White rectangles: areas of the zoom-ins presented below. **(b'-c''')** zoomed, single layer (1.28µm) pictures of the areas
942 depicted in b-c. anti-L-Cry antibody (green), HOECHST (magenta: nuclei), Arrows indicate L-Cry staining. Scale bars: 10um.

943

944

945

946

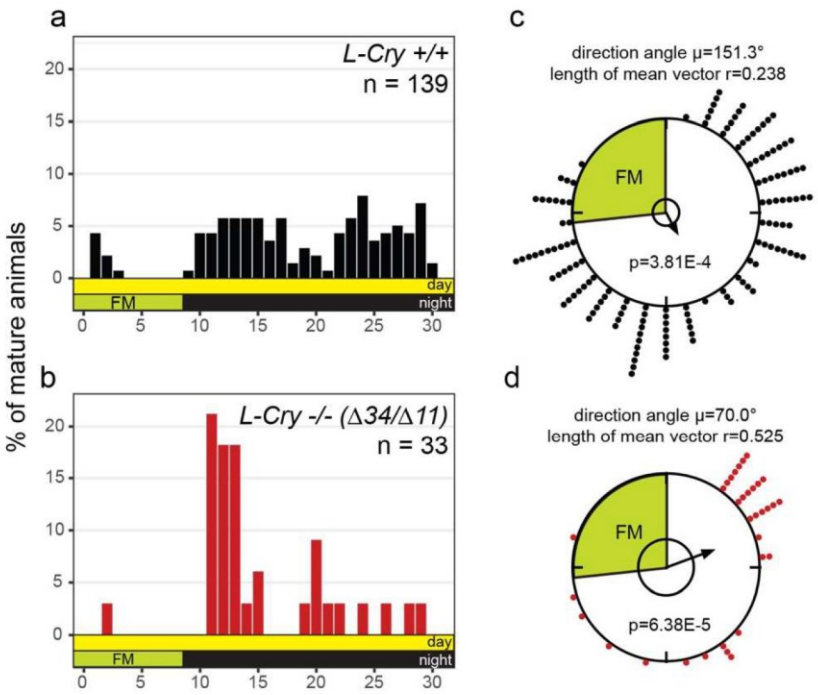

e

Comparison	Kolmogorov-Smirnov test (p)	Mardia-Watson-Wheeler test (p)	phase difference of μ (°)	phase difference of vectors (days)
L-Cry +/+ vs *L-Cry -/- (Δ11/Δ34)*	0.007	$8.24 \cdot 10^{-4}$	81.3	6.8
Sea vs *L-Cry -/- (Δ11/Δ34)*	0.207	0.635	13.5	1.1
Sea vs *L-Cry +/+*	$4 \cdot 10^{-15}$	$<10^{-12}$	94.8	7.9

Extended Data Figure 6: *l-cry* transheterozygous (Δ11/Δ34) mutants show increased spawning synchrony

(a-c) Spawning of *l-cry +/+* (a) and *l-cry -/-(Δ11/Δ34)* (b) animals over the lunar month under 8 nights of standard worm room culture full moon. **(c,d)** Same data as in (a,b) plotted as circular data. 360° correspond to 30 days of the lunar month. The arrow represents the mean vector characterized by the direction angle μ and r. r (length of μ) indicates phase coherence (measure of population synchrony). p-values inside the plots are results of Rayleigh Tests: Significance indicates non-random distribution of data points. The inner circle represents the Rayleigh critical value (p=0.05). **(e)** Results of multi-sample statistics on spawning data shown in (a-d). Phase differences in days can be calculated from the angle between the two mean vectors (i.e. 12° = 1 day).

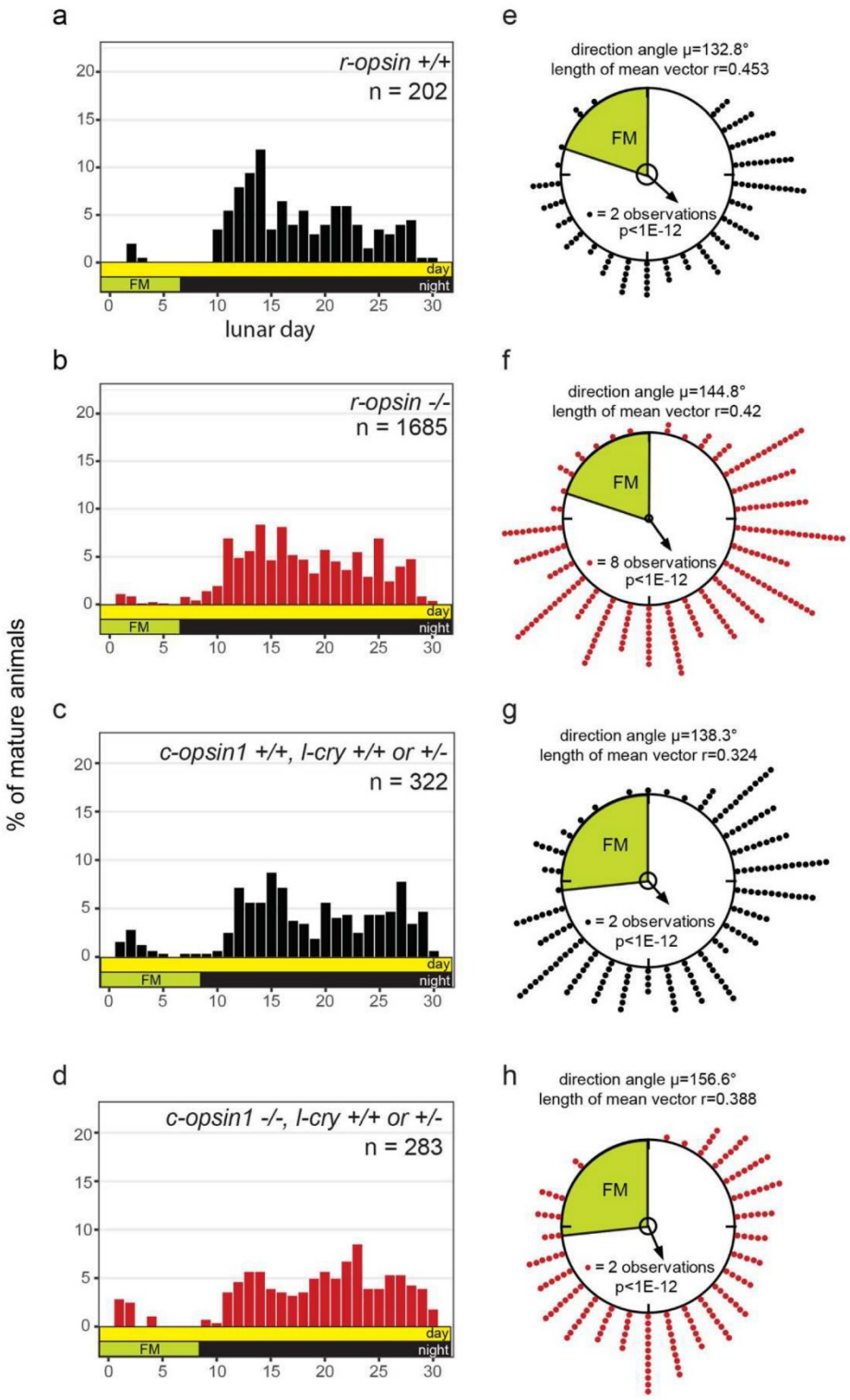

i

Comparison	Kolmogorov-Smirnov Test (p)	Mardia-Watson-Wheeler Test (p)	phase difference of μ (°)	phase difference of vectors (days)
r-opsin +/+ vs -/-	0.204	0.263	11.9	1.0
c-opsin1 +/+ vs -/-	0.053	0.069	18.3	1.5

Extended Data Figure 7: *r-opsin* and *c-opsin1* mutants show no alterations in spawning synchrony

(a-d) Spawning of indicated genotypes under standard laboratory conditions with 6 nights (*r-opsin*) or 8 nights (*c-opsin1*) of full moon. Animals in c and d are *l-cry +/+* or *+/-*. **(e-h)** Same data as in (a-d) plotted as circular data. 360° correspond to 30

days of the lunar month. The arrow represents the mean vector characterized by the direction angle μ and r. r (length of μ) indicates phase coherence (measure of population synchrony). p-values inside the plots are results of Rayleigh Tests: Significance indicates non-random distribution of data points. The inner circle represents the Rayleigh critical value (p=0.05). **(i)** Results of multi-sample statistics on spawning data shown in (a-h). Phase differences in days can be calculated from the angle between the two mean vectors (i.e. 12° = 1 day).

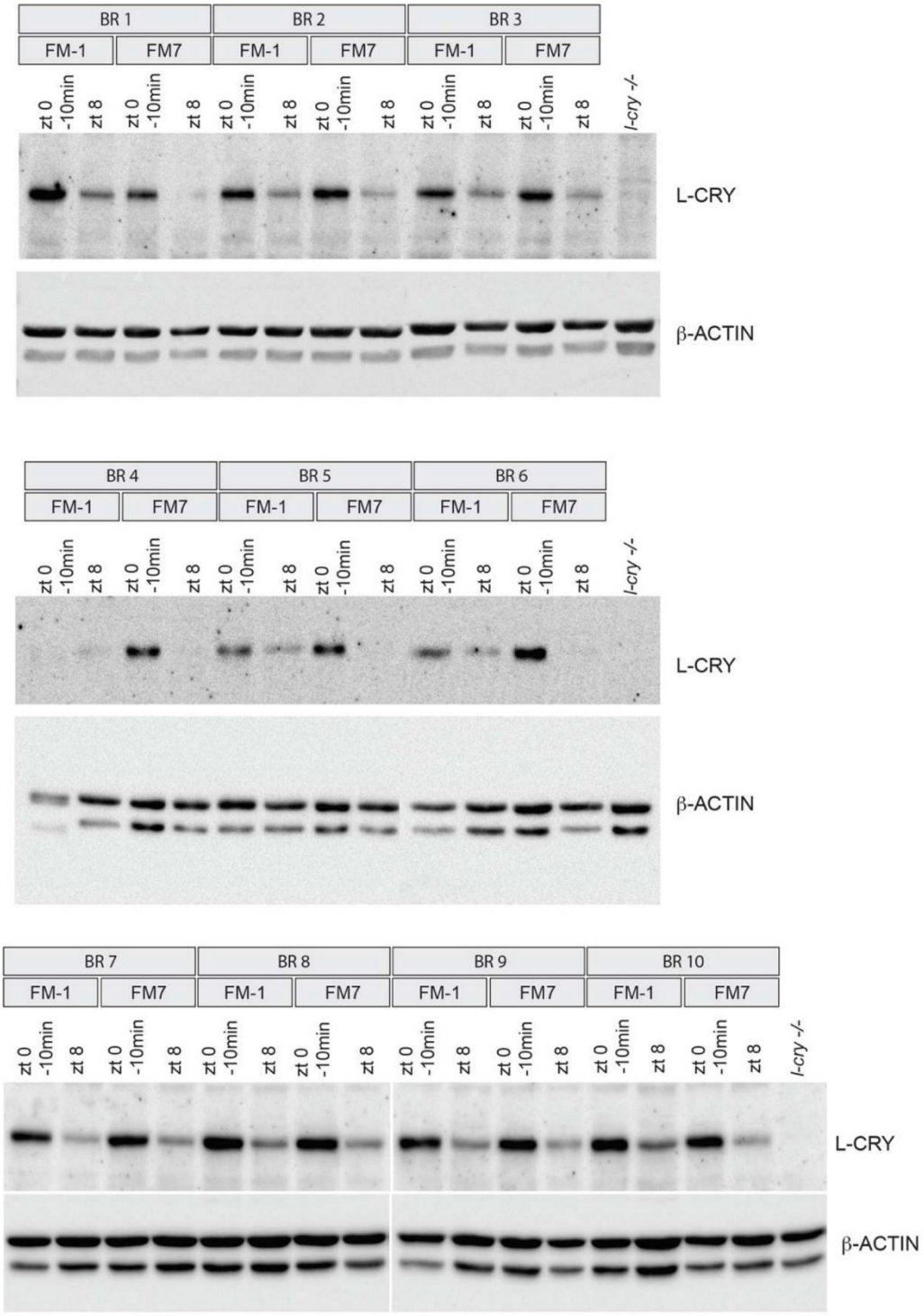

Extended Data Figure 8: Raw images of all Western blots quantified in Fig. 3b. BR: biological replicate.

Supplementary Table

Supplementary Table 1. Raw data obtained from scoring L-Cry subcellular localization signal (see EDF4d-f) using 40x confocal microscopy images like shown in the example in EDF4a'-c''. (Excel table)

6. Article 3: Differential Impacts of the Head on *Platynereis dumerilii* Peripheral Circadian Rhythms

Status: published article

Frontiers in Physiology 10:900 (2018), doi: 10.3389/fphys.2019.00900

Authors:

Enrique Arboleda, **Martin Zurl**, Monika Waldherr and Kristin Tessmar-Raible

Outline:

To address how the central circadian oscillator in the head of *Platynereis* impacts on peripheral circadian rhythms, my colleagues and I tested circadian clock gene oscillations in trunks of intact and head amputated worms under light/dark cycles and under constant darkness. To further assess the role of the central oscillator for peripheral circadian rhythms we assessed two outputs of the circadian clock – circadian locomotor activity and circadian regulation of chromatophore size – in intact and head amputated worms. The results presented in this paper address aim 4 of my thesis.

Contributions:

I performed and analyzed locomotor activity experiments (Fig. 6) and measured light spectra and intensities used in experiments. Together with M.W. I performed and analyzed the qPCRs for headless worms under DD1. Furthermore, I commented and reviewed the manuscript.

frontiers in Physiology

ORIGINAL RESEARCH
published: 11 July 2019
doi: 10.3389/fphys.2019.00900

Differential Impacts of the Head on *Platynereis dumerilii* Peripheral Circadian Rhythms

Enrique Arboleda[1†], *Martin Zurl*[1,2], *Monika Waldherr*[1,2] *and Kristin Tessmar-Raible*[1,2*]

[1] *Max F. Perutz Laboratories, Vienna BioCenter, University of Vienna, Vienna, Austria,* [2] *Research Platform "Rhythms of Life", Vienna BioCenter, University of Vienna, Vienna, Austria*

OPEN ACCESS

Edited by:
Nicholas Simon Foulkes, Karlsruhe Institute of Technology (KIT), Germany

Reviewed by:
Henrik Oster, Universität zu Lübeck, Germany
Charalambos P. Kyriacou, University of Leicester, United Kingdom

***Correspondence:**
Kristin Tessmar-Raible
kristin.tessmar@mfpl.ac.at

†Present address:
Enrique Arboleda, Institut de Génomique Fonctionnelle de Lyon (IGFL), École Normale Supérieure de Lyon, Lyon, France

Specialty section:
This article was submitted to Chronobiology, a section of the journal Frontiers in Physiology

Received: *10 April 2019*
Accepted: *27 June 2019*
Published: *11 July 2019*

Citation:
Arboleda E, Zurl M, Waldherr M and Tessmar-Raible K (2019) Differential Impacts of the Head on Platynereis dumerilii Peripheral Circadian Rhythms. Front. Physiol. 10:900. doi: 10.3389/fphys.2019.00900

The marine bristle worm *Platynereis dumerilii* is a useful functional model system for the study of the circadian clock and its interplay with others, e.g., circalunar clocks. The focus has so far been on the worm's head. However, behavioral and physiological cycles in other animals typically arise from the coordination of circadian clocks located in the brain and in peripheral tissues. Here, we focus on peripheral circadian rhythms and clocks, revisit and expand classical circadian work on the worm's chromatophores, investigate locomotion as read-out and include molecular analyses. We establish that different pieces of the trunk exhibit synchronized, robust oscillations of core circadian clock genes. These circadian core clock transcripts are under strong control of the light-dark cycle, quickly losing synchronized oscillation under constant darkness, irrespective of the absence or presence of heads. Different wavelengths are differently effective in controlling the peripheral molecular synchronization. We have previously shown that locomotor activity is under circadian clock control. Here, we show that upon decapitation worms exhibit strongly reduced activity levels. While still following the light-dark cycle, locomotor rhythmicity under constant darkness is less clear. We also observe the rhythmicity of pigments in the worm's individual chromatophores, confirming their circadian pattern. These size changes continue under constant darkness, but cannot be re-entrained by light upon decapitation. Our works thus provides the first basic characterization of the peripheral circadian clock of *P. dumerilii*. In the absence of the head, light is essential as a major synchronization cue for peripheral molecular and locomotor circadian rhythms, while circadian changes in chromatophore size can continue for several days in the absence of light/dark changes and the head. Thus, in Platynereis the dependence on the head depends on the type of peripheral rhythm studied. These data show that peripheral circadian rhythms and clocks should also be considered in "non-conventional" molecular model systems, i.e., outside *Drosophila melanogaster*, *Danio rerio*, and *Mus musculus,* and build a basic foundation for future investigations of interactions of clocks with different period lengths in marine organisms.

Keywords: marine, annelid, daily, rhythm, clock, chromatophores, transcription, locomotion

INTRODUCTION

Extensive research focusing on drosophilids and mice showed that the daily behavioral, physiological and metabolic cycles in animals arise from coordination of central circadian clocks located in the brain and peripheral clocks present in multiple tissues (Richards and Gumz, 2012; Mure et al., 2018; Pilorz et al., 2018). In Drosophila, several peripheral tissues and appendages (e.g., Malpighian tubules, fat bodies, and antennae) have autonomous peripheral clocks that are directly entrained by environmental cycles independent of the central clock, while others, such as oenocytes, are regulated by the circadian clock located in the brain (Tomioka et al., 2012; Ito and Tomioka, 2016). The mammalian circadian system is highly hierarchically organized. The master central clock in the suprachiasmatic nucleus (SCN) of the brain (often referred to as a "conductor") synchronizes internal clock timing to the environmental solar day by passing the information to the peripheral clocks via endocrine and systemic cues (Mohawk et al., 2012; Partch et al., 2014). These peripheral clocks also have self-sustained circadian oscillators, with the master clock coordinating their phase to prevent desynchronization among peripheral tissues, rather than acting as a pacemaker responsible for the periodicity of the cycling itself (Yoo et al., 2004). Besides being phase-controlled by the "SCN conductor," several mammalian peripheral clocks (e.g., in liver and kidney) have been shown to directly respond to non-photic entrainment cues, like food or exercise (Tahara and Shibata, 2018).

For marine organisms, biorhythms of various period lengths, including circadian and circalunar, have been described across phyla, e.g., as changes in activity levels, coloration and reproductive cycles (reviewed in Tessmar-Raible et al., 2011; Last and Hendrick, 2014; Bulla et al., 2017; Raible et al., 2017). Where studied in detail, like in the marine bristle worm *Platynereis dumerilii* and the marine midge *Clunio marinus*, the light of sun and moon are known to serve as major entrainment cues (Hauenschild, 1960; Zantke et al., 2013; Kaiser et al., 2016). Over recent years, marine rhythms and their possible underlying clockworks have been receiving increasing attention, as the interplay of clocks and rhythms of different organisms is a crucial aspect for ecology (Schwartz et al., 2017).

Molecular data on rhythms and clocks in marine invertebrates have become increasingly available over the last decade, now including the bivalves *Mytilus californianus* (Connor and Gracey, 2011) and *Crassostrea gigas* (Perrigault and Tran, 2017), the sea slugs *Hermissenda crassicornis*, *Melibe leonina*, and *Tritonia diomedea* (Cook et al., 2018; Duback et al., 2018), the isopod *Eurydice pulchra* (Wilcockson et al., 2011; Zhang et al., 2013; O'Neill et al., 2015), the amphipod *Talitrus saltator* (Hoelters et al., 2016), the lobsters *Nephrops norvegicus* (Sbragaglia et al., 2015) and *Homarus americanus* (Christie et al., 2018), the mangrove cricket *Apteronemobius asahinai* (Takekata et al., 2012), the copepods *Calanus finmarchicus* (Häfker et al., 2017), and *Tigriopus californicus* (Nesbit and Christie, 2014), the Antarctic krill *Euphausia superba* (Mazzotta et al., 2010; Teschke et al., 2011; Pittà et al., 2013; Biscontin et al., 2017), the Northern krill *Meganyctiphanes norvegica* (Christie et al., 2018), the marine midge *C. marinus* (Kaiser and Heckel, 2012; Kaiser et al., 2016), and the marine polychaete *P. dumerilii* (Zantke et al., 2013; Schenk et al., 2019). On the marine vertebrate side, especially teleost fish species have been investigated (Park et al., 2007; Sánchez et al., 2010; Hur et al., 2011; Watanabe et al., 2012; Vera et al., 2013; Rhee et al., 2014; Toda et al., 2014; Mogi et al., 2015; Okano et al., 2017).

While most of the above mentioned species are difficult to maintain in the laboratory and to investigate at the level of molecular genetics, *P. dumerilii* is a particularly well-established laboratory model (Fischer and Dorresteijn, 2004; Fischer et al., 2010) for marine chronobiological research. It possesses interacting circadian and circalunar clocks, and complementing the molecular work, a detailed analysis of its circadian locomotor activities has been described for adult stages (Hauenschild, 1960; Zantke et al., 2013, 2014). Evidence of circadian activity also exists for young larval stages within the first days of their development (Tosches et al., 2014). Similar to the isopod *E. pulchra* (Wilcockson et al., 2011; Zhang et al., 2013), *P. dumerilii* also exhibits a circadian rhythm in its body pigmentation (Fischer, 1965; Röseler, 1969, 1970). This rhythm in pigment cell extension versus contraction was described as a segment-autonomous process (Fischer, 1965; Röseler, 1969, 1970), indicating the presence of autonomous peripheral circadian oscillators.

As *P. dumerilii* beheaded individuals survive well for up to 2 weeks (Hofmann, 1976), this feature can be used to study living animals in the absence of its circadian brain clocks. Moreover, *P. dumerilii* has primitive morphological and genetic features, and is hence viewed as evolutionarily slowly evolving (Tessmar-Raible and Arendt, 2003), a feature which is particularly interesting for understanding the ancestral features of different clocks and rhythms, as well as in the light of the-certainly debated- hypothesis that vertebrates originated from a polychaete-like animal (Last and Hendrick, 2014).

The work presented here is the first detailed characterization of several *P. dumerilii* peripheral circadian rhythms and clocks, covering analyses of transcript level changes of core circadian clock genes, as well as body pigmentation and locomotor activity.

MATERIALS AND METHODS

Animal Cultures

Animals were maintained under controlled temperature and on 16:8 h light-dark (LD) or dark-dark (DD) cycles as previously described (Schenk et al., 2019). Sampling points are presented either as zeitgeber time (ZT) for LD conditions or circadian time (CT) for constant darkness (DD). ZT0 is defined as the time of light ON, CT0 defined as the time the light would go ON under DD conditions. All animal work was conducted according to Austrian and European guidelines for animal research.

Worm Decapitation

Animals were anesthetized by adding a few drops of 1 M $MgCl_2$ in the seawater until they stopped moving. They were carefully placed on a microscope slide under a binocular dissecting

microscope, decapitated, and transferred to fresh seawater again. Decapitation was done with sterile surgical blades cutting on the first segments below the pharyngeal region in order to collect only the posterior part of the body (i.e., the trunk). They were consistently performed between ZT 13.5 and ZT14. For re-entrainment, ZT refers to the actual ZT of the new LD regime. For head samples, the region containing the pharynx and the posterior end of the head was removed (see Zantke et al., 2013).

Constant Darkness (DD) Condition

Groups of animals used for DD experiments were collected between ZT 13.5 and ZT14 on individual plastic cups with seawater, wrapped in aluminum paper and placed inside a custom-made dark box in a temperature-controlled environment. After the proper acclimation time (1–5 days depending on the experiment) a plastic cup was taken out at a given CT and animals were used for RNA extraction/RT-qPCR or pigmentation quantification. This method ensured the avoidance of risking a premature exposure to light to the remaining samples in the dark box. Further animal handling (e.g., for decapitation or chromatophore visualization) was done under dim light and as fast as possible.

Circadian Re-entrainment Under White, Blue, and Red Light Conditions

When testing for circadian re-entrainment (i.e., an inverted light cycle) under white, blue, or red light, animals were exposed to the new conditions for 7 days before sampling. Light spectra and intensities of white, blue, and red LEDs (ProfiLuxSimu-L from GHL advanced technology gmbh, Germany) used for circadian re-entrainment were measured using an ILT950 spectrometer (International Light Technologies Inc., Peabody, United States). Special care was taken to account for the standard conditions, where the worms were housed, i.e., 22 cm away from light source and with a transparent plastic lid positioned between the spectrometer and the light source. Measured light intensities for white, red, and blue lights were 8.2×10^{13} photons/cm^2/s, 3.8×10^{13} photons/cm^2/s, and 2.4×10^{13} photons/cm^2/s, respectively (for spectra, see **Supplementary Figure 1**).

Total RNA Extraction and RT-qPCR

Total RNA was extracted from heads or trunks (i.e., decapitated animals) using the RNeasy Mini Kit (QIAGEN). In the case of heads, each biological replica consisted of 4–5 heads (to obtain sufficient amounts of RNA), while for trunks each replica consisted of a single decapitated animal. Reverse transcription was carried out using 0.4 μg of total RNA as template (QuantiTect Reverse Transcription kit, QIAGEN). RT-qPCR analyses were performed using a Step-One-Plus cycler. The expression of each test gene was normalized by the amount of the internal control gene cdc5. The relative expression was calculated using the formula $1/2^{\Delta Ct}$. Primers and PCR program used are listed in Zantke et al. (2013).

Chromatophore Size

Three consecutive segments located toward the middle of the body were selected on each animal to evaluate changes in chromatophore size. In order to precisely re-identify the same segments over the course of the experiments, animals were anesthetized with $MgCl_2$ and a parapodium, two segments away from the region of interest, was removed with a sterile surgical blade. When required, one animal at a time was placed on a glass cover without water and extended carefully. An epifluorescence stereoscope (Zeiss Lumar) with a 488 nm laser and a FITC filter was used to take pictures making sure to always use the same magnification across animals and sampling points. Animals were placed again in seawater until the next sampling point. Image analysis was done using Adobe Photoshop. On fluorescent images, the RGB channels red and blue were lowered to zero, and the three segments of interest were extracted by erasing the unwanted area (chromatophores on each segment have a specific pattern, which makes their visual identification easier). A new layer was generated by using the magic wand tool to single out the bright green chromatophores from the background fluorescence. Using the image's histogram, the number of colored pixels was used as a proxy of chromatophore size. Animals had between 20 and 40 chromatophores along the three segments, but no effort was done to quantify size of individual chromatophores. Instead, the sum of all the chromatophores of interest were used as chromatophore size value at each time point. Absolute pixel number was expressed as a percentage of the maximum value for each animal across all time points of the experiment [i.e., $x_i/(\text{Max}\{x_i,\ldots,x_j\}*100)$]. Average among biological replica and SEM were further calculated.

Locomotor Activity Assay

Immature worms of comparable size were starved for 3 days before the start of the assay. After decapitation, worms were placed in individual hemispherical concave wells (diameter = 35 mm, depth = 15 mm) of a custom-made 36-well clear plastic plate [as described in Ayers et al. (2018)]. Intact worms were also treated with $MgCl_2$ for 5 min prior to locomotor recording to ensure proper comparisons to decapitated worms. Video recording of worm's behavior over several days was accomplished as described previously (Zantke et al., 2013), using an infrared (λ = 990 nm) LED array (Roschwege GmbH) illuminating the behavioral chamber and an infrared high-pass filter restricting the video camera. Worms were recorded over 4 LD cycles (16 h light/8 h darkness), followed by 3 days under constant darkness. White light was generated by custom made LEDs (Marine Breeding Systems, St. Gallen, Switzerland) with the intensity set to $5{,}2 \times 10^{14}$ photons/cm^2/s at the place were worms were housed (for light spectrum see **Supplementary Figure 1**). Trajectories of locomotor activity of individual worms were deduced from the video recordings by an automated tracking software developed by LoopBio gmbh[1] (Vinoth Babu Veedin Rajan et al., unpublished). Locomotor activity trajectories reflect the distance moved of each worm's center point across 6 min time bins. Activity data was plotted as double-plotted actograms

[1] www.loopbio.com

using the ActogramJ plugin for Fiji (Schmid et al., 2011). For primary data see **Supplementary Data 2**.

Statistical Analyses

The main statistical analyses were performed using either the data analysis plug-in in Microsoft Excel using an alpha value of 0.05 (molecular and chromatophore data) or GraphPad Prism (locomotor activity data). For changes in chromatophore size, each two-sample two-tailed student's *t*-test was preceded by an *F*-test to check if the variances of the two groups were equal or not. In the cases were the same animals were used over time (i.e., repeated measures), a paired two-tailed Student's *t*-test was used. To test if transcriptional changes in gene expression over time oscillated to a statistically significant difference (i.e., the curve was not statistically linear), fold change data was analyzed for each sampling point using single factor ANOVA. In order to ease the logistic process of analyzing a considerable amount of data, RNA samples and chromatophore size images were not analyzed blindly but chronologically as experiments were being performed. Two-way ANOVA and *post hoc* tests were performed in R v3.5.1 (R Core Team, 2018) with the package emmeans. All data sets were checked if the assumption of homogeneity of variances and normality were met. In the case of repeated measures ANOVA, GraphPad Prism software was used; sphericity was not assumed and the method of Greenhouse and Geisser was used to adjust the results (see **Supplementary Data 1** for details on two-way ANOVA analyses). Statistical differences in locomotor activity across treatments were estimated using repeated measures ANOVA (GraphPad Prism) followed by Sidak's multiple comparison test. To identify the free-running period length of intact worms under DD conditions Lomb-Scargle periodogram analysis was done using the ActogramJ plugin for Fiji (Schmid et al., 2011).

Availability of Data and Material

All sequence resources referred to here were already published previously and submitted to public databases. All other data that support the findings of this study are available from the corresponding author upon reasonable request.

RESULTS

Platynereis dumerilii Peripheral Circadian Clock Gene Transcripts Quickly Desynchronize Under Complete Darkness

As a starting point, we aimed to test for the presence of peripheral clocks in the body of *P. dumerilii* adults. Based on the previously described and tested molecular components of the core circadian oscillator in *P. dumerilii* heads (Zantke et al., 2013), we analyzed the daily transcriptional fluctuation of *bmal*, *period* and *tr-cry* as representative components of the circadian clock by RT-qPCR (**Figure 1**). Daily fluctuation of *bmal, period*, *tr-cry*, *timeless*, *clock*, and *pdp1* transcripts in the trunk are overall similar to those in the head [**Figures 1A,B**, for *timeless*, *clock,* and *pdp1*, see **Supplementary Figures 2A–C**, compare also with (Zantke et al., 2013)], although overall relative mRNA levels were always significantly higher in heads than in trunks. In the case of *period*, there was also a significant difference in overall transcript levels between trunks under LD and DD conditions, with higher levels at LD (pairwise comparisons of estimated marginal means, Tukey adjusted with alpha = 0.05) (see **Supplementary Data 1** referring to **Figure 1**). Results were similar irrespective of the segment positions used for analyses, i.e., whole trunk (**Figure 1**), last 5–7 segments of the body or the adjacent 5–7 segments toward the anterior part of the animal (**Supplementary Figures 2D–F**) produced consistent results. *Pdu-tr-cry* appears to be the gene that deviates most in this comparison. We attribute this difference to a higher variability of the transcript level synchronization in the trunk given that in most cases it corresponds to the oscillations observed in the head. Alternatively, the presence of the head leads to a shift in the *tr-cry* curve maxima, as the curves for *tr-cry* consistently differ when the head is present (compare **Figures 1A,B**, **2A,B**, **3C** and **Supplementary Figure 2F**, and see also Zantke et al., 2013 for heads, Tosches et al., 2014 for whole larvae). A two-way ANOVA on ZT and condition (i.e., LD Heads and LD Trunks) was carried out to further analyze *tr-cry* transcript changes. There was a statistically significant effect of ZT, condition and, most importantly, interaction between the ZT and the condition on relative mRNA levels [$F(5,95) = 5.3837$, $p = 0.0002$]. A *post hoc* pairwise Tukey analysis for the interaction shows that the low relative mRNA levels at ZT5 on trunks under LD conditions is the main difference between these two conditions (see **Supplementary Data 1**).

We next tested if the peripheral circadian clock transcript oscillations would continue synchronously under constant darkness for 3 days. All tested transcripts dampened strongly, with *tr-cry* still exhibiting weak significant changes across CT (**Figure 1C**).

Light Signals Are Sufficient to Maintain Circadian Clock Transcripts in the Trunk, Independent of the Head

To analyze if the peripheral circadian clock transcript changes in the worm's body were dependent on the circadian clock in its head, we took advantage of the fact that bodies of decapitated animals survive in seawater for about 2 weeks (Hofmann, 1976). Adult animals were decapitated and placed under standard LD cycles before RNA extraction. Relative transcript levels of *bmal*, *period*, and *tr-cry* exhibited overall similar levels and continued a clear diel cycling of expression for at least 3 days in trunks of decapitated animals (**Figure 2A**), indicating that the peripheral circadian clock gene expression continues to synchronously run even in the absence of the brain circadian clock. We then tested core circadian clock transcript changes in trunks of decapitated animals under constant darkness. On the first day of DD (DD1) trunks continue to show a significant oscillation over time in all three genes (**Figure 2B**). However, after 3 days in complete darkness (DD3), relative mRNA levels dampen and no significant changes were detectable for any of the three genes (**Figure 2C**). We also tested for overall

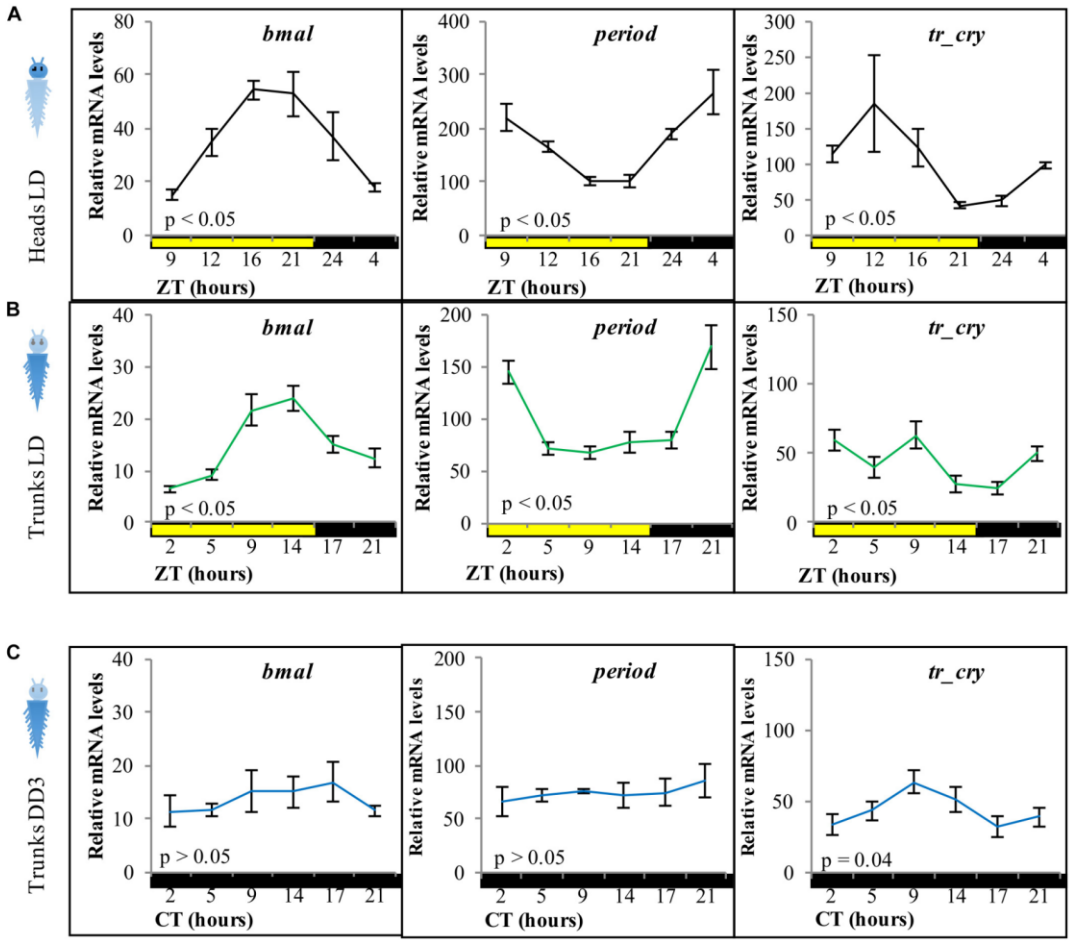

FIGURE 1 | Relative transcript levels of *bmal, period*, and *tr-cry* in panel **(A)** heads under LD conditions, **(B)** trunks under LD conditions, and **(C)** trunks in DD conditions for 3 days on intact animals (i.e., not decapitated). ZT, zeitgeber time; CT, circadian time. *p*-Value estimated on a single factor ANOVA with $n = 6$, 15, and 11 for panels **(A–C)**, respectively (alpha = 0.05). Error bars denote SEM.

relative mRNA levels of expression of each gene under each condition (pairwise comparisons of estimated marginal means, Tukey adjusted with alpha = 0.05, see **Supplementary Data 1** for **Figure 2**). In the trunk *bmal* overall levels were higher in LD than in DD1 and DD3 conditions (which in turn were statistically similar among them), while overall *period* levels were higher in DD1 compared to DD3 and LD conditions (*statistically similar among them*). For *tr-cry*, although LD is also clearly still higher, differences in overall levels on all three conditions are statistically significant (see **Supplementary Data 1** referring to **Figure 2**). These differences possibly reflect differences in the transcriptional activation and repression during the different light conditions, e.g., it is noteworthy that under DD1 levels of the transcriptional suppressor *per* get significantly higher, while the transcript levels of the corresponding "downstream" transcriptional activator *bmal* are lowered under DD1, as would be expected if more *per* is present and translated to protein.

By placing decapitated animals on an inverted light cycle, we next tested for the capacity of peripheral clocks to be re-synchronized by light, again using the transcript oscillations of *bmal*, *per*, and *tr-cry* as readout. Cycling of *bmal* and *per* was re-entrained to the inverted cycle when exposed to white, red or blue light (**Figures 3A,B**, for spectra and intensity see **Supplementary Figure 1**). *tr-cry* transcript oscillations differed from this, in that white and blue light could re-entrain its peripheral oscillations as in the case of *bmal* and *per*, whereas red light did not (**Figure 3C**). To better understand these findings, a two-way ANOVA to simultaneously examine the effect of light treatment (i.e., light color = wavelength) and ZT was performed for each gene (see **Supplementary Data 1**). In the case of *bmal*, ZT [$F(5,146) = 12.6907$, $p = 3.0399e^{-10}$] had a significant effect; with ZT5 and ZT21 having the same levels of expression. A similar result was found for *per*, but with the important addition of a significant interaction between ZT and the light condition ($F(10,144) = 2.7811$, $p = 0.0036$), indicating that the relationship

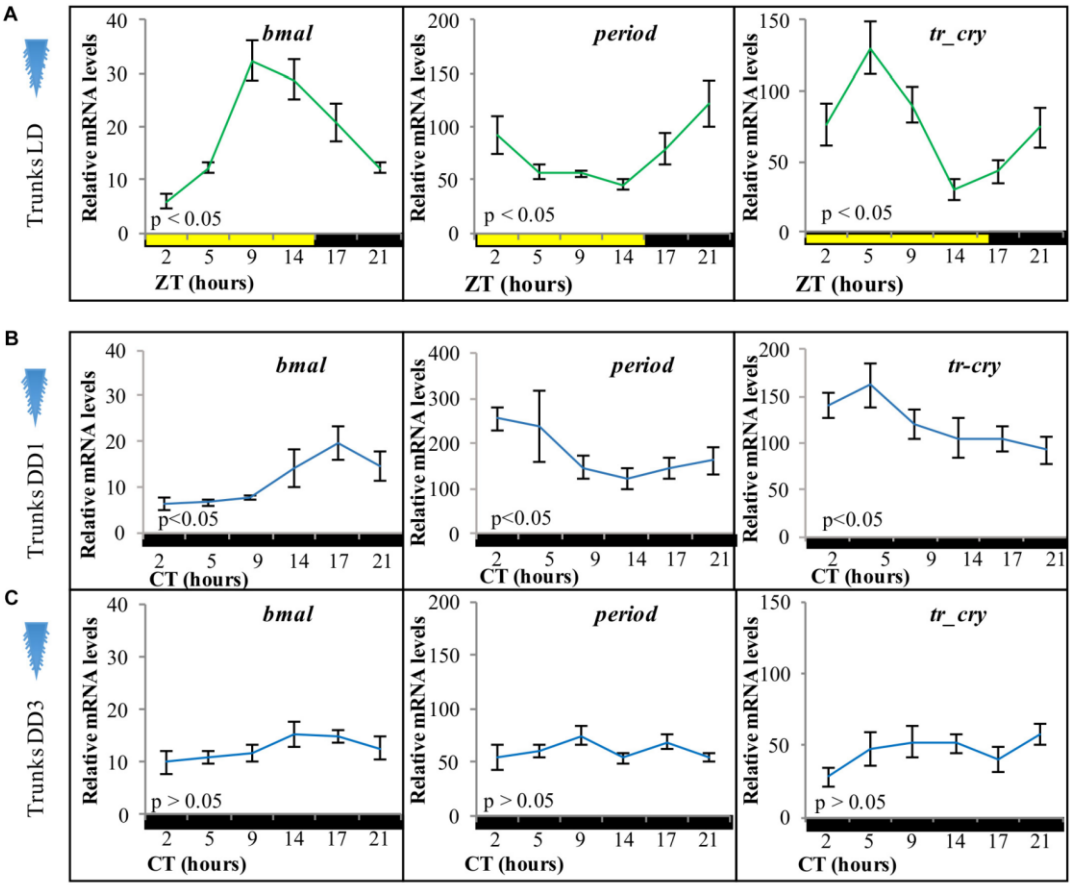

FIGURE 2 | Relative transcript levels of **(A)** *bmal*, **(B)** *period*, and **(C)** *tr-cry* in trunks of decapitated animals placed under **(A)** LD, **(B)** DD conditions for 1 day, and **(C)** DD conditions for 3 days. ZT, zeitgeber time; CT, circadian time. *p*-Value estimated on a single factor ANOVA with $n = 6$ on each condition (alpha = 0.05). Error bars denote SEM.

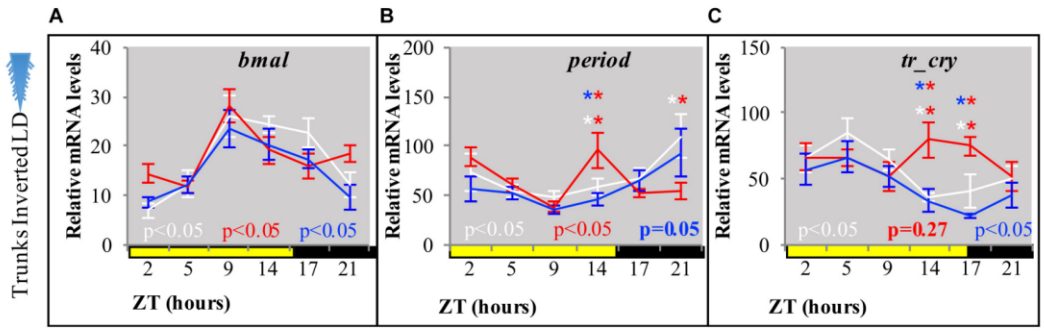

FIGURE 3 | Relative transcript levels of **(A)** *bmal*, **(B)** *period*, and **(C)** *tr-cry* in trunks of decapitated animals placed under inverted LD conditions for 7 days with either white, blue, or red "light color" (for light spectra and intensity see **Supplementary Figure 1**). ZT, zeitgeber time. CT, circadian time. *p*-Value estimated on a single factor ANOVA with (alpha = 0.05). Error bars: SEM. Asterisks: ZTs, where statistically significant differences between light treatments were found after a two-way ANOVA and *post hoc* pairwise comparisons of estimated marginal means, Tukey adjusted with alpha = 0.05 (see also **Supplementary Data 1**).

of ZT and relative mRNA levels is dependent on the type of light. A *post hoc* pairwise Tukey analysis for the interaction indicates that such dependence is due to a specific variation on relative mRNA levels of *per* on tails under red light at ZT14 and ZT21. In the case of *tr-cry*, the situation is more complex. The analysis shows an effect of ZT, Light and a significant interaction between

the two [$F(10,144) = 2.1109$, $p = 0.0271$] on relative mRNA levels. The *post hoc* pairwise analysis of light treatments (i.e., colors) over each ZT shows statistical differences for red light at ZT14 and ZT21, with significantly higher relative mRNA values compared to white or blue light at the same ZTs (**Supplementary Data 1** referring to **Figure 3**). These punctual higher relative mRNA levels are the clearest evidence for the mentioned lack of re-entrainment of *tr-cry* peripheral oscillations by red light. Overall, these results demonstrate that circadian clock transcripts in peripheral tissues can directly respond to changes in the light cycle, independently of the head.

Chromatophore Size Follows a Circadian Pattern and Free-Runs Under Constant Darkness

In order to assess how our findings on core circadian clock transcripts oscillations might relate to physiology and behavior, we investigated possible outputs of peripheral circadian clocks, starting with changes in chromatophore size in the trunk. Chromatophores are located along the dorsal part of the segmented body of *P. dumerilii*. Based on light microscopy analyses it had previously been shown that the worm's chromatophores exhibit a segment-autonomous, diel contraction-expansion rhythm with increasing size during the day and decreasing size at night (Fischer, 1965; Röseler, 1969, 1970).

We first aimed at identifying a possibility to automatize the recording of chromatophore changes. We found that chromatophores exhibit a well-detectable autofluorescence under 488 nm light (**Figures 4A,B**), which can be used for automatic detection by any image software. In order to characterize the pattern of contraction/expansion of the chromatophores, animals were photographed every 3 h over the course of 24 h using a fluorescence microscope. We found a clear circadian pattern with higher chromatophore expansion between ZT2 and ZT11 (**Figure 4C**), and a sharp drop on chromatophore size from ZT11 to ZT14, before lights go off and the subjective night period starts, already suggestive of an autonomous clock-driven process and not a direct light response, again consistent with previous observations (Hempelmann, 1939; Fischer, 1965).

We next focused on sampling points corresponding to ZT/CT2 and ZT/CT14, during which a ∼60% drop in chromatophore size was evident (**Figures 4C**, **5A,B**), and used these two time points as a reference for the study of circadian cycling of pigmentation over multiple days. Chromatophores expansion/contraction continued to cycle in animals placed under constant darkness for five consecutive days (**Figure 5C**).

For evidence that the light used for measuring chromophore size is not causing re-entrainment in this case, see below.

Circadian Pattern of Chromatophore Size Free-Runs, but Cannot Be Re-entrained by Light in Decapitated Animals

In order to assess if the regulation of the cycling on chromatophore size is governed by peripheral clocks, decapitated animals were used. The same animals were photographed at ZT2 and ZT14 prior to decapitation as a starting reference point. Following decapitation, worms were placed in constant darkness for 4 days, and subsequently exposed again to a normal LD cycle for additional 3 days. Chromatophores sizes were registered along the experiment from day 0 to day 4, and again on day 7 to test for possible re-entrainment. Upon decapitation, animals under DD conditions initially continue to exhibit clear rhythms of chromatophore size changes (**Figure 5D**, for individual replicas see **Supplementary Figure 3**). Starting with the second day in DD, the rhythm will, however, start to dampen and become statistically non-significant by day 4 (**Figure 5D**). Subsequent exposure to a normal LD cycle did not lead to a re-synchronization of the chromatophore rhythm (**Figure 5D**). Consistently, cycling of chromatophore size does not get re-entrained on decapitated animals under an inverted LD cycle applied for 5 days (**Figure 5E**). A two-way repeated measurement ANOVA and *post hoc* pairwise analyses, confirmed a significant interaction between CT (i.e., time of subjective day) and the different days in DD [$F(3,15) = 13.34$, $p = 0.0050$], indicating that the difference between CT2 and CT14 gets significantly smaller over time from DD1 to DD4 (see **Supplementary Data 1** referring to **Figure 3**).

In order to rule out that we may have missed phase-shifts on decapitated animals due to the exposure to the 488 nm light during the measurement procedure (due to too low sampling frequency), we also performed a more densely spaced 24 h sampling on day 5 in LD (post decapitation). This experiment confirmed our interpretation of a dampening of the chromatophore size rhythm and inability to re-entrain in the absence of the head (**Figure 5F**). All together, these results suggest a circadian pattern of chromatophore size governed by a peripheral clock, which, however, requires the head to maintain extended synchronization and for re-entrainment by light.

Circadian Locomotor Activity Follows the Light-Dark Cycle, but Does Not Free-Run Under Constant Darkness in Decapitated Worms

We next turned to locomotor activity as a read-out for circadian clock activity. We have previously shown that *P. dumerilii* during new moon (circalunar phase of its circalunar clock) exhibits nocturnal circadian locomotor activity, which free-runs under constant darkness for at least 3 days (Zantke et al., 2013, 2014). We meanwhile established an automated worm locomotor behavioral tracking system, which measures worm activity as distance moved of the worm's center point within 6 min time bins [Ayers et al., 2018, LoopBio (see footnote 1), Vinoth Babu Veedin Rajan *unpublished*]. It should be noted that this new type of analysis measures relative distance moved, compared to the binary (movement: yes or no) manual scoring done by Zantke et al. (2013). Intact worms showed a significant circadian rhythmic locomotor activity under LD and DD conditions (**Figures 6A,B**, for individual actograms see **Supplementary Figure 4**). In contrast decapitated worms exhibit an overall severe reduction in movement and rhythmicity (**Figures 6C,D**, for individual actograms, see **Supplementary Figures 5, 6** and

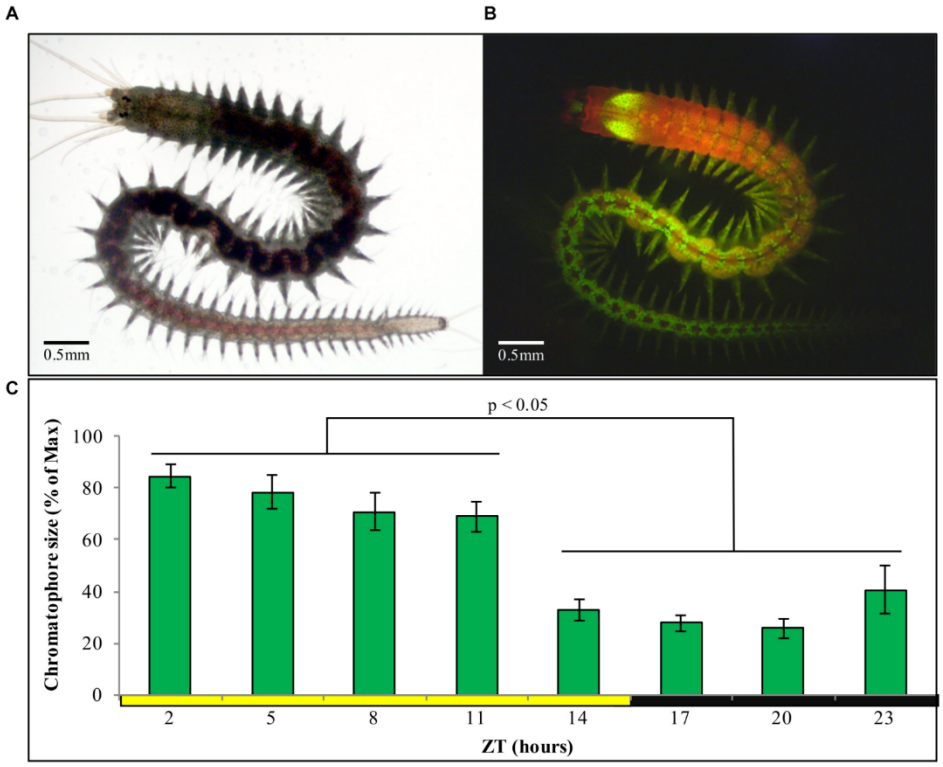

FIGURE 4 | (A) Sexually immature *P. dumerilii* adult under standard light microscopy. **(B)** Same individual as in panel **(A)**, now autofluorescent under 488 nm light and a FITC filter, with chromatophores clearly visible as bright green circles (prominent green autofluorescence of the jaws can also be see in the anterior end). **(C)** Average chromatophore size based on autofluorescence (see materials and methods) of the same group of individuals followed over a 24 h period (n = 15) under standard LD conditions. Pairwise Student's t-tests (preceded by F-tests) were performed comparing each of the ZT h. Individual averages from ZT2 to ZT5 and ZT14 to ZT23 were statistically similar within them but not between them in all permutations possible (alpha = 0.05). Error bars denote SEM.

Supplementary Movies 1–6. Please note that the maximal values of the *Y*-axis for decapitated animals is 5–10 smaller than for non-decapitated controls in order to visibly display movement). Overall, these data suggest that lack of signals from the head lead to a general suppression of movement and lack of circadian information or synchronization signals for the locomotor output. Headless worms are not generally paralyzed, as they can show spontaneous bursts of movement (**Supplementary Figures 5, 6** and **Supplementary Movies 1–6**) and- depending on their stage at decapitation- can proceed to maturation and the associated behavioral changes (Hauenschild, 1966). Similar to the rhythmic transcript oscillations of the core circadian clock genes in the trunk, acute light functions as a synchronization cue to the periphery of headless worms, but without head or light stimuli a circadian locomotor pattern cannot be maintained by the trunk alone in the majority of the worms.

DISCUSSION

Molecular Peripheral Clock

Here, we examine peripheral circadian clock transcript changes and diel rhythms in chromatophore size and locomotor behavior in *P. dumerilii* in the absence and presence of its head. An endogenous circadian rhythm driving body pigmentation change in *P. dumerilii* had been previously proposed based on photographic recordings of isolated groups of body segments during the middle of the day and the night (Röseler, 1969, 1970). With the exception of gills in oysters (Payton et al., 2017), there is no information on fluctuation of circadian clock genes on peripheral tissues or appendages in marine organisms. We document the expression of core circadian clock genes in the periphery of *P. dumerilii*, arguing in favor of a functional circadian peripheral clock and opening an avenue to study the molecular mechanisms of peripheral clocks in marine invertebrates. We show that light/dark cycles can (at least in part) substitute for the head as major synchronizer for continuous peripheral core circadian clock transcript oscillations. We confirm previous work on chromatophore rhythms, which – in contrast to locomotion and transcript oscillations- exhibit free-running rhythms in trunks of headless worms.

As previously reported for the central clock (Zantke et al., 2013), *period* and *bmal* transcripts cycle in antiphase from each other, while *tr-cry* transcripts are neither directly in-phase nor in anti-phase with any of them. Our results on trunks show that cycling of *bmal* and *period* continues under LD conditions,

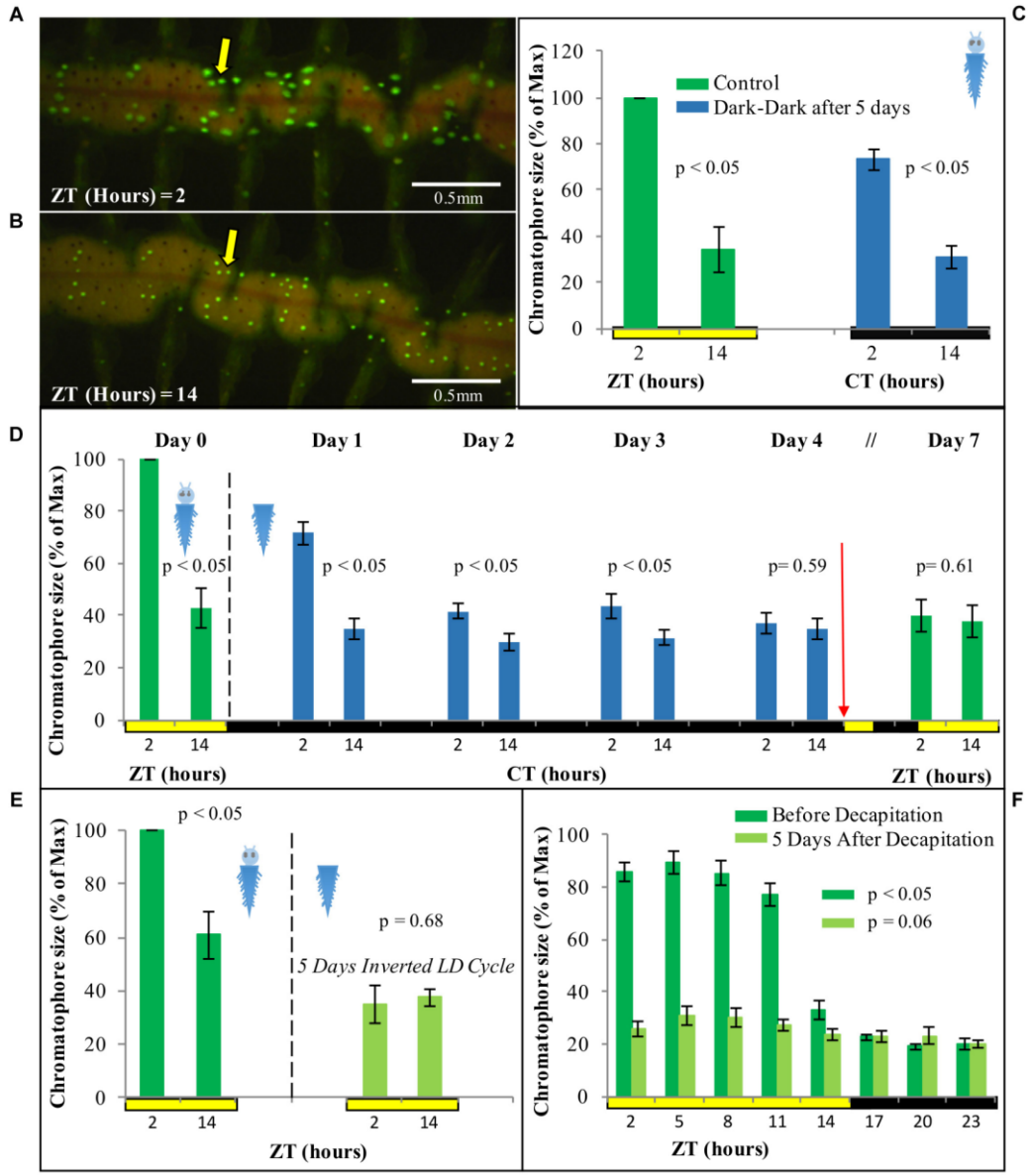

FIGURE 5 | Fluorescent microscopy images of chromatophore size difference between **(A)** ZT2 and **(B)** ZT14 under standard LD conditions. **(C)** Average chromatophore size at ZT/CT 2 and ZT/CT 14 before and after 5 days under DD conditions (n = 4). **(D)** Average chromatophore size at ZT/CT 2 and ZT/CT 14 over seven consecutive days. Dashed line indicates decapitation and placement in DD conditions. Red arrow indicates re-placement under LD conditions (n = 6) (see **Supplementary Figure 3** for individual replicas). **(E)** Average chromatophore size at ZT2 and ZT14 of individuals before and 5 days after decapitation and placement on an inverted LD cycle (n = 6). **(F)** Average chromatophore size, over a 24 h period, of individuals before and 5 days after decapitation (n = 10). For panel **(C)** pairwise Student's t-tests (preceded by F-tests) were performed comparing ZT/CT 2 and ZT/CT 14 at each sampling day. For panels **(D,E)**, the pairwise student's t-tests were paired (i.e., repeated sampling). For panel **(F)**, p-Value was estimated on a single factor ANOVA. Error bars denote SEM and alpha = 0.05 in all cases.

but not under DD independently of the head being present or absent, and can be entrained to an inverted LD cycle on decapitated animals. These results suggest that the peripheral clocks are light dependent (through a yet to be identified set of photoreceptors in the trunk) and either stop, or more likely, desynchronize in the different peripheral cells and tissues (at least as fast as 3 days in DD) in the absence of the head. Consistent with endogenous oscillators desynchronizing over time this desynchronization does not happen immediately upon placement in DD conditions (i.e., DD1). A system with peripheral clocks independent from the central circadian clocks in the brain and entrained directly by environmental signals is reminiscent of

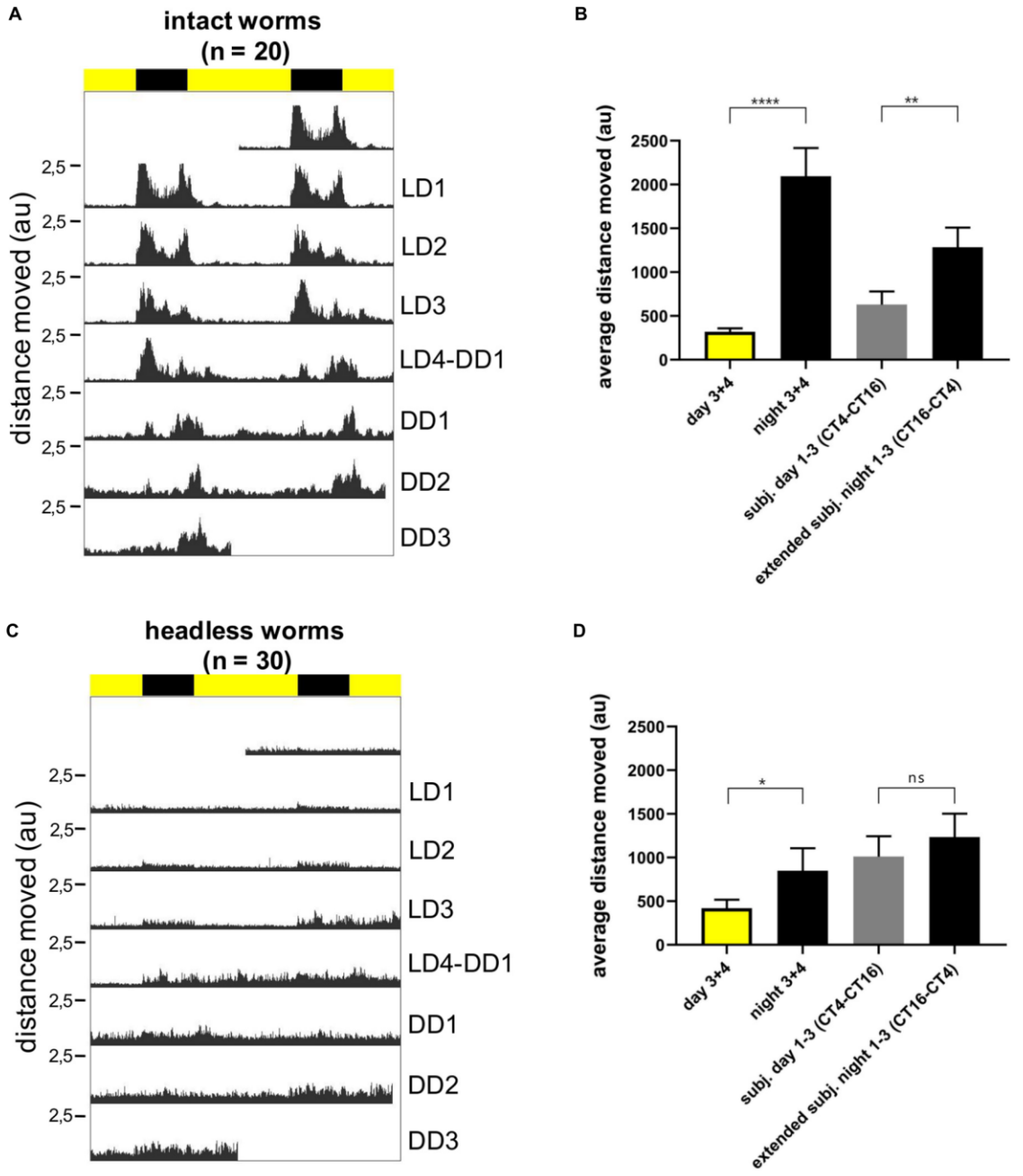

FIGURE 6 | Individual locomotor activity of intact (n = 20) and headless (n = 30) worms under 16 h light and 8 h dark (LD) conditions followed by 3 days of constant darkness (DD). **(A,C)** Average double plotted actograms of intact **(A)** and headless **(C)** worms. Black bar indicates night hours whereas yellow bar indicates day hours during LD conditions. Decapitation of headless worms was performed at ZT14 1 day before recording (=LD0). **(B,D)** Average distance moved of intact **(B)** and headless worms **(D)** during day and nighttime, as well as during different time periods of constant darkness, i.e., CT4-CT16 for subjective day, and CT16-CT4 for subjective night. The subjective night period was extended to CT4 because under DD conditions activity levels cycle with a ca. 25 h ± 0.22 period (mean ± SEM, see **Supplementary Figure 4B**), and therefore activity during DD1-3 subjective night moves into the early phase of the subjective day. For day and night time activity, data from LD3 and LD4 were pooled, since during the first 2 days after head removal worms hardly moved and we did not want to bias our results by a potential post-surgery effect. Bars indicate mean ± SEM. p-Values were calculated using repeated measures ANOVA followed by Sidak's multiple comparison test with $^{****}p < 0.0001$, $^{**}p < 0.01$, and $^{*}p < 0.05$; au, arbitrary unit.

Drosophila melanogaster (Tomioka et al., 2012). In that sense the peripheral clock in *P. dumerilii* resembles that of insects, and light reception in the trunk likely occurs via Cryptochromes and/or Opsins. Candidates include Go-Opsin1 and rOpsin1 (Backfisch et al., 2013; Ayers et al., 2018).

Light exhibits different effects on the different readouts. In the cases of transcript oscillations and locomotor activity the head is not required for its impact, suggesting that peripheral photoreceptors mediate this signal. Interestingly, different wavelengths appear to have differential peripheral effects on transcript oscillations (red light being able to re-entrain *per* and *bmal* trunk oscillations, but not *tr-cry*), which already indicates the involvement of more than one photoreceptor. It will be interesting for future studies to understand why *tr-cry* transcripts behave differently from *bmal* and *per* transcripts under different light conditions. These differences could be the result of *tr-cry* only being expressed in a subset of tissues/cell types that do not desynchronize as quickly.

As in the case of insects (Tomioka et al., 2012) and mammals (Reppert and Weaver, 2002), questions regarding how peripheral clocks are entrained and the actual mechanisms that peripheral clock use to drive transcriptional changes on various tissues are still questions to be answered in *P. dumerilii*, as is the case for the specific functions of the peripheral clocks.

It should be noted that our experiments were performed on the complete trunk (or at least several segments), which also leaves open questions regarding the peripheral circadian cycling and their synchronizations in specific segmentally repeated organs and tissues.

Chromatophore Size and the Peripheral Clock

Daily changes in chromatophore size on *P. dumerilii* can be easily used as a visual read out of the circadian clock, adding up to its locomotor activity, circalunar spawning, and clock-related genes as means to study chronobiology in this model system.

Remarkably, the first studies on the cyclic changes of body pigmentation in *P. dumerilii* date back to Hempelmann (1939). Based on this and further classical work, these changes in body pigmentation were already attributed to an endogenous circadian rhythm present in each segment of the worm's body (Fischer, 1965; Röseler, 1969, 1970), pointing at the existence of peripheral circadian clocks long before their molecular mechanism had been unraveled and circadian peripheral oscillations were proven to exist in the peripheral tissues in mammals (Tosini and Menaker, 1996; Balsalobre et al., 1998; Schibler et al., 2003; Dibner et al., 2010). Our analyses support the classical studies on Platynereis, in that chromatophore size in the body of *P. dumerilii* is higher during day time, with a major drop before the night begins; which argues in favor of a clock-driven manifestation and not a direct light response. The average magnitude of this change corresponds with previous quantitative reports by Fischer (1965). We report that individuals placed in DD for 5 days still exhibit a significant daily difference on chromatophore size, although its maximum value decreases by 25% compared to the initial LD conditions. It has been reported that such cycling starts to fade on individual chromatophores after 7 days in DD (Fischer, 1965), but we did not test for the long term stability of the cycle for individual chromatophores. Noticeably, a similar circadian cycling of chromatophore size on DD and inverted LD cycles has been shown for the marine isopod *E. pulchra* (Zhang et al., 2013), posing the questions if this regulation is similar.

Changes in chromatophore size with a circadian cycling is commonly seen in crustaceans (Fingerman, 1955; Fingerman and Yamamoto, 1967; Fingerman et al., 1969; Zhang et al., 2013). There is usually an increase in size during the day thought to be related to UV protection (Darnell, 2012), but an inverted pattern of bigger chromatophore size during the night, to possibly enable individuals to camouflage with the substrate, can also be found (Stevens et al., 2013). The fact that *P. dumerilii* is mostly active during the night (Zantke et al., 2013), when pigmentation is lower, does not argue in favor of a camouflage role; especially since pigmentation does not respond to changes in background brightness (Fischer, 1965). The most parsimonious option is therefore, a role of pigmentation in protecting the animal from UV light. It should be noted, however, that it has also been often proposed, but not tested, that circadian changes in pigmentation might be a mechanism related to energy saving (Stevens, 2016).

Remarkably, in our hands the re-entrainment of chromatophore rhythms by light requires the presence of the head. This might be either because the required photoreceptor(s) are located in the head or because hormonal feedback signals, such as *Pdu*-PDF (pigment dispersing factor) (Shahidi et al., 2015), are required for the synchronization process. It is likely that pigmentation in *P. dumerilii* is controlled by a hormonal process, as in some crustaceans (Fingerman and Yamamoto, 1967; Fingerman et al., 1969; Nery et al., 1999), which in turn is governed by the central clock. The hormonal nature of the cycling on chromatophore size has been further supported by the immediate reaction of chromatophores, present on isolated skin tissue, when coelomic fluid from *P. dumerilii* during a given time point (e.g., day or night) is added (Röseler, 1970).

Finally, while we overall confirm previous work on the chromatophore rhythms in the trunk of *P. dumerilii*, there is one clear difference between our findings and that of Röseler (1970). Her work shows that chromatophore rhythms can still be re-entrained by white light even in the absence of the prostomium (head), whereas in our hands decapitated animals do not re-entrain their chromatophore rhythm in response to white light. We identified two main reasons that might explain this discrepancy. The materials and methods of her paper do not state the light intensity and spectrum. It is thus possible that this strongly deviates from our conditions. The other difference is the extent of head removal. In our study we removed the head including the jaw piece, whereas Röseler (1970) specifies prostomium-removal, which implies that her worms still possessed the jaw and the surrounding tissue. This region possesses multiple neurons and neurosecretory cells, which could be important for proper re-entrainment. Further work will certainly help to disentangle these differences.

CONCLUSION

We find that the overall circadian clock transcript oscillations of the trunk are under strong control of the LD cycle and do not show synchronized oscillation under constant darkness, irrespective of the absence or presence of heads. In the absence of heads, locomotor activity is also strongly coordinated by the LD cycle and significantly reduced. In contrast, circadian changes of body pigmentation in the trunk free-run over several days in constant darkness, even in the absence of the head. Jointly these data indicate that autonomous peripheral clocks exist in the trunk of the bristle worm, coordinating for instance pigmentation. However, the synchronization of rhythmic circadian oscillations in other peripheral tissues and their respective output are more strongly coordinated by light than by the circadian oscillator positioned in the head of the worm. Our data build a basis for future analyses of the multiple clocks of the bristle worm, but also suggest that peripheral clocks should be taken into consideration when studying other organisms with circadian and non-circadian oscillators.

DATA AVAILABILITY

All datasets generated for this study are included in the manuscript and/or the **Supplementary Files**.

ETHICS STATEMENT

All animal work was conducted according to the Austrian and European guidelines for animal research. Please note that our work is performed on invertebrates, which according to these guidelines do not require special animal experimental permissions or committees.

AUTHOR CONTRIBUTIONS

EA and KT-R designed the study and wrote the manuscript. MZ reviewed and commented on the manuscript, and contributed to locomotor activity experiments and measurement of light spectra and intensities. MW and MZ performed the qPCRs for headless worms DD1. EA performed all other experiments. EA, MW, KT-R, and MZ did the data analysis, interpretation, and discussion.

FUNDING

KT-R received funding for this research from the European Research Council under the European Community's Seventh Framework Programme (FP7/2007–2013) ERC Grant Agreement 337011, the research platform "Rhythms of Life" of the University of Vienna, the Austrian Science Fund (FWF, http://www.fwf.ac.at/en/): START award (#AY0041321) and research project grant (#P28970). MZ has in part been financially supported by an FWF grant to the F. Raible lab (#I2972). None of the funding bodies was involved in the design of the study, collection, analysis, and interpretation of data or in writing the manuscript. This manuscript has been released as a preprint: Arboleda et al., 2019. https://doi.org/10.1101/593772 (Arboleda et al., 2019).

ACKNOWLEDGMENTS

We thank the members of the Tessmar-Raible and Raible groups for their discussions, especially Juliane Zantke, Vinoth Babu Veedin Rajan, Birgit Pöhn, and Max Hofbauer for sharing details on the automated locomotor behavioral tracking prior to publication. Our thanks to Andreij Belokurov and Margaryta Borysova for excellent worm care at the MFPL aquatic facility. Our thanks are also due to Claudia Lohs and Katharina Schipany for excellent technical assistance.

SUPPLEMENTARY MATERIAL

The Supplementary Material for this article can be found online at: https://www.frontiersin.org/articles/10.3389/fphys.2019.00900/full#supplementary-material

REFERENCES

Arboleda, E., Zurl, M., and Tessmar-Raible, K. (2019). Differential impacts of the head on *Platynereis dumerilii* peripheral circadian rhythms. *bioRxiv* 593772. doi: 10.1101/593772

Ayers, T., Tsukamoto, H., Gühmann, M., Veedin Rajan, V. B., and Tessmar-Raible, K. (2018). A Go-type opsin mediates the shadow reflex in the annelid Platynereis dumerilii. *BMC Biol.* 16:41. doi: 10.1186/s12915-018-0505-8

Backfisch, B., Rajan, V. B. V., Fischer, R. M., Lohs, C., Arboleda, E., Tessmar-Raible, K., et al. (2013). Stable transgenesis in the marine annelid Platynereis dumerilii sheds new light on photoreceptor evolution. *PNAS* 110, 193–198. doi: 10.1073/pnas.1209657109

Balsalobre, A., Damiola, F., and Schibler, U. (1998). A serum shock induces circadian gene expression in mammalian tissue culture cells. *Cell* 93, 929–937.

Biscontin, A., Wallach, T., Sales, G., Grudziecki, A., Janke, L., Sartori, E., et al. (2017). Functional characterization of the circadian clock in the Antarctic krill, Euphausia superba. *Sci. Rep.* 7:17742. doi: 10.1038/s41598-017-18009-2

Bulla, M., Oudman, T., Bijleveld, A. I., Piersma, T., and Kyriacou, C. P. (2017). Marine biorhythms: bridging chronobiology and ecology. *Philos. Trans. R. Soc. Lond. B Biol. Sci.* 372, 20160253. doi: 10.1098/rstb.2016.0253

Christie, A. E., Yu, A., Roncalli, V., Pascual, M. G., Cieslak, M. C., Warner, A. N., et al. (2018). Molecular evidence for an intrinsic circadian pacemaker in the cardiac ganglion of the American lobster, Homarus americanus - Is diel cycling of heartbeat frequency controlled by a peripheral clock system? *Mar. Genomics* 41, 19–30. doi: 10.1016/j.margen.2018.07.001

Connor, K. M., and Gracey, A. Y. (2011). Circadian cycles are the dominant transcriptional rhythm in the intertidal mussel *Mytilus californianus*. *Proc. Natl. Acad. Sci. U.S.A.* 108, 16110–16115. doi: 10.1073/pnas.1111076108

Cook, G. M., Gruen, A. E., Morris, J., Pankey, M. S., Senatore, A., Katz, P. S., et al. (2018). Sequences of circadian clock proteins in the nudibranch molluscs *Hermissenda crassicornis*, *Melibe leonina*, and *Tritonia diomedea*. *Biol. Bull.* 234, 207–218. doi: 10.1086/698467

Darnell, M. Z. (2012). Ecological physiology of the circadian pigmentation rhythm in the fiddler crab Uca panacea. *J. Exp. Mar. Biol. Ecol.* 42, 39–47. doi: 10.1016/j.jembe.2012.05.014

Dibner, C., Schibler, U., and Albrecht, U. (2010). The mammalian circadian timing system: organization and coordination of central and peripheral clocks. *Annu. Rev. Physiol.* 72, 517–549. doi: 10.1146/annurev-physiol-021909-135821

Duback, V. E., Sabrina Pankey, M., Thomas, R. I., Huyck, T. L., Mbarani, I. M., Bernier, K. R., et al. (2018). Localization and expression of putative circadian clock transcripts in the brain of the nudibranch Melibe leonina. *Comp. Biochem. Physiol., Part A Mol. Integr. Physiol.* 223, 52–59. doi: 10.1016/j.cbpa.2018.05.002

Fingerman, M. (1955). Persistent daily and tidal rhythms of color change in *Callinectes sapidus*. *Biol. Bull.* 109, 255–264. doi: 10.2307/1538725

Fingerman, M., Rao, K. R., and Ring, G. (1969). Restoration of a rhythm of melanophoric pigment dispersion in eyestalkless fiddler crabs, uca pugilator (Bosc), at a low temperature 1). *Crustaceana* 17, 97–105. doi: 10.1163/156854069X00097

Fingerman, M., and Yamamoto, Y. (1967). Daily rhythm of melanophoric pigment migration in eyestalkless fiddler crabs, uca pugilator (Bosc). *Crustaceana* 12, 303–319. doi: 10.1163/156854067X00279

Fischer, A. (1965). Über die chromatophoren und den farbwechsel bei dem polychäten *Platynereis dumerilii*. *Z. Zellforsch. Mikrosk. Anat.* 65, 290–312. doi: 10.1007/BF00400123

Fischer, A., and Dorresteijn, A. (2004). The polychaete *Platynereis dumerilii* (Annelida): a laboratory animal with spiralian cleavage, lifelong segment proliferation and a mixed benthic/pelagic life cycle. *BioEssays* 26, 314–325. doi: 10.1002/bies.10409

Fischer, A. H., Henrich, T., and Arendt, D. (2010). The normal development of *Platynereis dumerilii* (Nereididae, Annelida). *Front. Zool.* 7:31. doi: 10.1186/1742-9994-7-31

Häfker, N. S., Meyer, B., Last, K. S., Pond, D. W., Hüppe, L., and Teschke, M. (2017). Circadian clock involvement in zooplankton diel vertical migration. *Curr. Biol.* 27, 2194.e–2201.e. doi: 10.1016/j.cub.2017.06.025

Hauenschild, C. (1960). Lunar periodicity. *Cold Spring Harb. Symp. Quant. Biol.* 25, 491–497.

Hauenschild, C. (1966). Der hormonale einfluss des gehirns auf die sexuelle entwicklung bei dem polychaeten *Platynereis dumerilii*. *Gen. Comp. Endocrinol.* 6, 26–73. doi: 10.1016/0016-6480(66)90108-0

Hempelmann, F. (1939). Chromatophoren bei Nereis. *Z. Wiss. Zool. Abt. A* 152, 353–383.

Hoelters, L., O'Grady, J. F., Webster, S. G., and Wilcockson, D. C. (2016). Characterization, localization and temporal expression of crustacean hyperglycemic hormone (CHH) in the behaviorally rhythmic peracarid crustaceans, *Eurydice pulchra* (Leach) and *Talitrus saltator* (Montagu). *Gen. Comp. Endocrinol.* 237, 43–52. doi: 10.1016/j.ygcen.2016.07.024

Hofmann, D. K. (1976). Regeneration and endocrinology in the polychaete *Platynereis dumerilii*: an experimental and structural study. *Wilehm Roux Arch. Dev. Biol.* 180, 47–71. doi: 10.1007/BF00848884

Hur, S.-P., Takeuchi, Y., Esaka, Y., Nina, W., Park, Y.-J., Kang, H.-C., et al. (2011). Diurnal expression patterns of neurohypophysial hormone genes in the brain of the threespot wrasse *Halichoeres trimaculatus*. *Comp. Biochem. Physiol. Part A Mol. Integr. Physiol.* 158, 490–497. doi: 10.1016/j.cbpa.2010.12.011

Ito, C., and Tomioka, K. (2016). Heterogeneity of the peripheral circadian systems in *Drosophila melanogaster*: a review. *Front. Physiol.* 7:8. doi: 10.3389/fphys.2016.00008

Kaiser, T. S., and Heckel, D. G. (2012). Genetic architecture of local adaptation in lunar and diurnal emergence times of the marine midge *Clunio marinus* (Chironomidae, Diptera). *PLoS One* 7:e32092. doi: 10.1371/journal.pone.0032092

Kaiser, T. S., Poehn, B., Szkiba, D., Preussner, M., Sedlazeck, F. J., Zrim, A., et al. (2016). The genomic basis of circadian and circalunar timing adaptations in a midge. *Nature* 540, 69–73. doi: 10.1038/nature20151

Last, K. S., and Hendrick, V. J. (2014). "The clock-work worms: diversity and function of clock expression in marine polychaete worms," in *Annual, Lunar, and Tidal Clocks*, eds H. Numata and B. Helm (Tokyo: Springer), 179–199. doi: 10.1007/978-4-431-55261-1_10

Mazzotta, G. M., De Pittà, C., Benna, C., Tosatto, S. C. E., Lanfranchi, G., Bertolucci, C., et al. (2010). A cry from the krill. *Chronobiol. Int.* 27, 425–445. doi: 10.3109/07420521003697494

Mogi, M., Uji, S., Yokoi, H., and Suzuki, T. (2015). Early development of circadian rhythmicity in the suprachiamatic nuclei and pineal gland of teleost, flounder (*Paralichthys olivaeus*), embryos. *Dev. Growth Differ.* 57, 444–452. doi: 10.1111/dgd.12222

Mohawk, J. A., Green, C. B., and Takahashi, J. S. (2012). Central and peripheral circadian clocks in mammals. *Annu. Rev. Neurosci.* 35, 445–462. doi: 10.1146/annurev-neuro-060909-153128

Mure, L. S., Le, H. D., Benegiamo, G., Chang, M. W., Rios, L., Jillani, N., et al. (2018). Diurnal transcriptome atlas of a primate across major neural and peripheral tissues. *Science* 359:eaao0318. doi: 10.1126/science.aao0318

Nery, L. E., Da Silva, M. A., and Castrucci, A. M. (1999). Possible role of non-classical chromatophorotropins on the regulation of the crustacean erythrophore. *J. Exp. Zool.* 284, 711–716.

Nesbit, K. T., and Christie, A. E. (2014). Identification of the molecular components of a *Tigriopus californicus* (Crustacea, Copepoda) circadian clock. *Comp. Biochem. Physiol. Part D Genom. Proteom.* 12, 16–44. doi: 10.1016/j.cbd.2014.09.002

Okano, K., Ozawa, S., Sato, H., Kodachi, S., Ito, M., Miyadai, T., et al. (2017). Light- and circadian-controlled genes respond to a broad light spectrum in Puffer Fish-derived Fugu eye cells. *Sci. Rep.* 7:46150. doi: 10.1038/srep46150

O'Neill, J. S., Lee, K. D., Zhang, L., Feeney, K., Webster, S. G., Blades, M. J., et al. (2015). Metabolic molecular markers of the tidal clock in the marine crustacean *Eurydice pulchra*. *Curr. Biol.* 25, R326–R327. doi: 10.1016/j.cub.2015.02.052

Park, J.-G., Park, Y.-J., Sugama, N., Kim, S.-J., and Takemura, A. (2007). Molecular cloning and daily variations of the Period gene in a reef fish *Siganus guttatus*. *J. Comp. Physiol. A Neuroethol. Sens. Neural. Behav. Physiol.* 193, 403–411. doi: 10.1007/s00359-006-0194-6

Partch, C. L., Green, C. B., and Takahashi, J. S. (2014). Molecular architecture of the mammalian circadian clock. *Trends Cell Biol.* 24, 90–99. doi: 10.1016/j.tcb.2013.07.002

Payton, L., Perrigault, M., Hoede, C., Massabuau, J.-C., Sow, M., Huvet, A., et al. (2017). Remodeling of the cycling transcriptome of the oyster *Crassostrea gigas* by the harmful algae *Alexandrium minutum*. *Sci. Rep.* 7:3480. doi: 10.1038/s41598-017-03797-4

Perrigault, M., and Tran, D. (2017). Identification of the molecular clockwork of the oyster *Crassostrea gigas*. *PLoS One* 12:e0169790. doi: 10.1371/journal.pone.0169790

Pilorz, V., Helfrich-Förster, C., and Oster, H. (2018). The role of the circadian clock system in physiology. *Pflugers Arch. Eur. J. Physiol.* 470, 227–239. doi: 10.1007/s00424-017-2103-y

Pittà, C. D., Biscontin, A., Albiero, A., Sales, G., Millino, C., Mazzotta, G. M., et al. (2013). The antarctic krill euphausia superba shows diurnal cycles of transcription under natural conditions. *PLoS One* 8:e68652. doi: 10.1371/journal.pone.0068652

R Core Team (2018). *R: A Language and Environment for Statistical Computing*. Available at: www.R-project.org (accessed June 15, 2019).

Raible, F., Takekata, H., and Tessmar-Raible, K. (2017). An overview of monthly rhythms and clocks. *Front. Neurol.* 8:189. doi: 10.3389/fneur.2017.00189

Reppert, S. M., and Weaver, D. R. (2002). Coordination of circadian timing in mammals. *Nature* 418, 935–941. doi: 10.1038/nature00965

Rhee, J.-S., Kim, B.-M., Lee, B.-Y., Hwang, U.-K., Lee, Y. S., and Lee, J.-S. (2014). Cloning of circadian rhythmic pathway genes and perturbation of oscillation patterns in endocrine disrupting chemicals (EDCs)-exposed mangrove killifish *Kryptolebias marmoratus*. *Comp. Biochem. Physiol. C Toxicol. Pharmacol.* 164, 11–20. doi: 10.1016/j.cbpc.2014.04.001

Richards, J., and Gumz, M. L. (2012). Advances in understanding the peripheral circadian clocks. *FASEB J.* 26, 3602–3613. doi: 10.1096/fj.12-203554

Röseler, I. (1969). Untersuchungen über den physiologischen Farbwechsel bei dem polychaeten *Platynereis dumerilii*. *Zool Anz. Suppl-Bd Verh Zool. Ges.* 33, 267–273.

Röseler, I. (1970). Die Rhythmik der chromatophoren des Polychaeten *Platynereis dumerilii*. *Zeitschrift für vergleichende Physiologie* 70, 144–174. doi: 10.1007/BF00297714

Sánchez, J. A., Madrid, J. A., and Sánchez-Vázquez, F. J. (2010). Molecular cloning, tissue distribution, and daily rhythms of expression of per1 gene in European sea bass (*Dicentrarchus labrax*). *Chronobiol. Int.* 27, 19–33. doi: 10.3109/07420520903398633

Sbragaglia, V., Lamanna, F., Mat, A. M., Rotllant, G., Joly, S., Ketmaier, V., et al. (2015). Identification, characterization, and diel pattern of expression of

canonical clock genes in *Nephrops norvegicus* (Crustacea: Decapoda) Eyestalk. *PLoS One* 10:e0141893. doi: 10.1371/journal.pone.0141893

Schenk, S., Bannister, S. C., Sedlazeck, F. J., Anrather, D., Minh, B. Q., Bileck, A., et al. (2019). Combined transcriptome and proteome profiling reveals specific molecular brain signatures for sex, maturation and circalunar clock phase. *eLife* 8:e41556. doi: 10.7554/eLife.41556

Schibler, U., Ripperger, J., and Brown, S. A. (2003). Peripheral circadian oscillators in mammals: time and food. *J. Biol. Rhythms* 18, 250–260. doi: 10.1177/0748730403018003007

Schmid, B., Helfrich-Förster, C., and Yoshii, T. (2011). A new imageJ plug-in "ActogramJ" for chronobiological analyses. *J. Biol. Rhythms* 26, 464–467. doi: 10.1177/0748730411414264

Schwartz, W. J., Helm, B., and Gerkema, M. P. (2017). Wild clocks: preface and glossary. *Philos. Trans. R. Soc. B Biol. Sci.* 372, 20170211. doi: 10.1098/rstb.2017.0211

Shahidi, R., Williams, E. A., Conzelmann, M., Asadulina, A., Verasztó, C., Jasek, S., et al. (2015). A serial multiplex immunogold labeling method for identifying peptidergic neurons in connectomes. *eLife* 4:e11147. doi: 10.7554/eLife.11147

Stevens, M. (2016). Color change, phenotypic plasticity, and camouflage. *Front. Ecol. Evol.* 4:51. doi: 10.3389/fevo.2016.00051

Stevens, M., Rong, C. P., and Todd, P. A. (2013). Colour change and camouflage in the horned ghost crab *Ocypode ceratophthalmus*. *Biol. J. Linn. Soc.* 109, 257–270. doi: 10.1111/bij.12039

Tahara, Y., and Shibata, S. (2018). Entrainment of the mouse circadian clock: effects of stress, exercise, and nutrition. *Free Radic. Biol. Med.* 119, 129–138. doi: 10.1016/j.freeradbiomed.2017.12.026

Takekata, H., Matsuura, Y., Goto, S. G., Satoh, A., and Numata, H. (2012). RNAi of the circadian clock gene period disrupts the circadian rhythm but not the circatidal rhythm in the mangrove cricket. *Biol. Lett.* 8, 488–491. doi: 10.1098/rsbl.2012.0079

Teschke, M., Wendt, S., Kawaguchi, S., Kramer, A., and Meyer, B. (2011). A circadian clock in Antarctic krill: an endogenous timing system governs metabolic output rhythms in the euphausid species *Euphausia superba*. *PLoS One* 6:e26090. doi: 10.1371/journal.pone.0026090

Tessmar-Raible, K., and Arendt, D. (2003). Emerging systems: between vertebrates and arthropods, the Lophotrochozoa. *Curr. Opin. Genet. Dev.* 13, 331–340. doi: 10.1016/S0959-437X(03)00086-8

Tessmar-Raible, K., Raible, F., and Arboleda, E. (2011). Another place, another timer: marine species and the rhythms of life. *Bioessays* 33, 165–172. doi: 10.1002/bies.201000096

Toda, R., Okano, K., Takeuchi, Y., Yamauchi, C., Fukushiro, M., Takemura, A., et al. (2014). Hypothalamic expression and moonlight-independent changes of Cry3 and Per4 implicate their roles in lunar clock oscillators of the lunar-responsive Goldlined spinefoot. *PLoS One* 9:e109119. doi: 10.1371/journal.pone.0109119

Tomioka, K., Uryu, O., Kamae, Y., Umezaki, Y., and Yoshii, T. (2012). Peripheral circadian rhythms and their regulatory mechanism in insects and some other arthropods: a review. *J. Comp. Physiol. B Biochem. Syst. Environ. Physiol.* 182, 729–740. doi: 10.1007/s00360-012-0651-1

Tosches, M. A., Bucher, D., Vopalensky, P., and Arendt, D. (2014). Melatonin signaling controls circadian swimming behavior in marine zooplankton. *Cell* 159, 46–57. doi: 10.1016/j.cell.2014.07.042

Tosini, G., and Menaker, M. (1996). Circadian rhythms in cultured mammalian retina. *Science* 272, 419–421.

Vera, L. M., Negrini, P., Zagatti, C., Frigato, E., Sánchez-Vázquez, F. J., and Bertolucci, C. (2013). Light and feeding entrainment of the molecular circadian clock in a marine teleost (*Sparus aurata*). *Chronobiol. Int.* 30, 649–661. doi: 10.3109/07420528.2013.775143

Watanabe, N., Itoh, K., Mogi, M., Fujinami, Y., Shimizu, D., Hashimoto, H., et al. (2012). Circadian pacemaker in the suprachiasmatic nuclei of teleost fish revealed by rhythmic period2 expression. *Gen. Comp. Endocrinol.* 178, 400–407. doi: 10.1016/j.ygcen.2012.06.012

Wilcockson, D. C., Zhang, L., Hastings, M. H., Kyriacou, C. P., and Webster, S. G. (2011). A novel form of pigment-dispersing hormone in the central nervous system of the intertidal marine isopod, *Eurydice pulchra* (leach). *J. Comp. Neurol.* 519, 562–575. doi: 10.1002/cne.22533

Yoo, S.-H., Yamazaki, S., Lowrey, P. L., Shimomura, K., Ko, C. H., Buhr, E. D., et al. (2004). PERIOD2::LUCIFERASE real-time reporting of circadian dynamics reveals persistent circadian oscillations in mouse peripheral tissues. *Proc. Natl. Acad. Sci. U.S.A.* 101, 5339–5346. doi: 10.1073/pnas.0308709101

Zantke, J., Ishikawa-Fujiwara, T., Arboleda, E., Lohs, C., Schipany, K., Hallay, N., et al. (2013). Circadian and circalunar clock interactions in a marine annelid. *Cell Rep.* 5, 99–113. doi: 10.1016/j.celrep.2013.08.031

Zantke, J., Oberlerchner, H., and Tessmar-Raible, K. (2014). "Circadian and circalunar clock interactions and the impact of light in *Platynereis dumerilii*," in *Annual, Lunar, and Tidal Clocks: Patterns and Mechanisms of Nature's Enigmatic Rhythms*, eds H. Numata and B. Helm (Tokyo: Springer), 143–162. doi: 10.1007/978-4-431-55261-1_8

Zhang, L., Hastings, M. H., Green, E. W., Tauber, E., Sladek, M., Webster, S. G., et al. (2013). Dissociation of circadian and circatidal timekeeping in the marine crustacean *Eurydice pulchra*. *Curr. Biol.* 23, 1863–1873. doi: 10.1016/j.cub.2013.08.038

Conflict of Interest Statement: The authors declare that the research was conducted in the absence of any commercial or financial relationships that could be construed as a potential conflict of interest.

7. Discussion

My work advances our understanding of molecular clocks and their modulation by light in various ways: Firstly, I showed that naturalistic moonlight has a potent effect on circadian timing in *Platynereis*, establishing this species as a potent model organism to study effects of moonlight on circadian timing (discussed in 7.1). Secondly, my work contributes to the understanding of how moonlight and sunlight are discriminated for clock entrainment in *Platynereis* and *Drosophila* (discussed in 7.2-7.5). Finally, my work also contributes to a better understanding of the entrainment of peripheral circadian rhythms in *Platynereis* (discussed in 7.6).

7.1. *Platynereis* as a novel model to study circadian effects of moonlight

The first aim of this thesis was to test if *Platynereis dumerilii* could be used as a model species to study the effects of moonlight on circadian timing. In article #1, I addressed this question by using an automated locomotor tracking system to assess the timing of swarming onset under light regimes that mimic the intensity and spectrum of sun and moonlight measured at the natural habitat of *Platynereis*. I could show that in addition to sunlight, moonlight affects the timing of swarming onset by shortening the period length of a plastic circadian/circalunidian clock. This allows the worms to anticipate - dependent on moon phase - during which hours of the night moonlight is present, and time swarming onset to the dark hours of the respective night. In nature this is likely beneficial to avoid predators that hunt during moonlight.

While effects of moonlight on circadian behaviour have been reported for several species in field studies (as described in section 3.6), these studies fall short in providing mechanistic insights on how moonlight affects circadian behaviour. The establishment of a behavioural assay to study this phenomenon under laboratory conditions in a genetically accessible model system is an important step towards unraveling the biological mechanisms that underlie moonlight perception for circadian timing.
In *Drosophila* modest moonlight effects on the endogenous circadian clock have been reported as well (Bachleitner et al., 2007) but then could not be seen under natural conditions (Vanin et al., 2012), likely because of the low nighttime temperatures under natural conditions. In contrast, we believe that in *Platynereis* the effects of artificial

moonlight on circadian timing observed in the lab are also relevant under natural conditions for two reasons: (i) experimental temperature conditions mimic those experienced in the field (constant ~20 °C) and (ii) moonlight spectra in this study were adapted to moonlight measurements performed at the natural habitat.

When assessing potential effects of moonlight in established model species such as rodents and *Drosophila*, animals have so far been only subjected to continuous moonlight during the whole night, instead of providing moonlight only during certain hours of the night, as it would be the case for most nights in the natural environment. Separating the night in a moonlit and a dark portion allows to address if a species has a preference for either condition and if it can be classified as lunarphilic or lunarphobic. Subjecting a nocturnal species such as mice or hamsters to continuous moonlight during the whole night might fall short in revealing an impact of moonlight on circadian behaviour in a natural context, where they in fact would have the opportunity to restrict foraging behaviour to either the dark or moonlit portion of the night.
To mimic natural conditions even more closely, future studies could also mimic the changes in light intensity that correlate with the position of sun and moon above the horizon. Implementing this aspect also in the swarming assay would give more accurate insights into when swarming onset is actually initiated relative to the time of moonrise in nature.

7.2. Decoding sunlight vs moonlight for clock mediated timing

A second aspect in which my work advances our understanding of light entrainment of biological clocks under naturalistic conditions is the aspect of how moonlight and sunlight are discriminated for clock entrainment. This is relevant not only for *Platynereis* but for the entire animal kingdom, as the circadian system of many animals is in principle sensitive to light levels of moonlight intensity (reviewed in section 3.6 and 3.7). Also in animals in which moonlight might not play a role for circadian timing under field conditions, the circadian system needs to discriminate moonlight from sunlight to prevent a disturbance of the circadian system by moonlight. Similarly, for species that possess a moonlight entrained monthly clock such as several marine species (reviewed in section 3.5), discriminating sunlight from moonlight for this timing system is equally important.

In article #1 and #2 we present data that suggest that in *Drosophila* and *Platynereis* a light-sensitive cryptochrome is required to discriminate between sun and moonlight valence for clock entrainment. We found that flies and worms that lack cryptochrome exhibit an increased circadian behavioural response to a moonlight stimulus given during the night (article #1, Fig. 2D,F,G and Fig. 4A-C). Furthermore, in flies dCry prevents internal desynchronization of molecular circadian clock gene oscillations among subgroups of circadian clock neurons under moonlight exposure (article #1, Fig. 4D-H). At a first glance it seems paradoxical that taking a light receptor away leads to an increased and aberrant response to a light stimulus. However, it is consistent with a role of cryptochrome in decoding sun versus moonlight valence as flies and worms that lack cryptochrome cannot adequately adapt to a naturalistic light regime that involves both sun and moonlight.

I propose that the common key feature of the two light-responsive cryptochromes of *Platynereis* (L-Cry) and *Drosophila* (dCry) that enable them to discriminate sun- from moonlight lies in a biophysically defined light intensity threshold: light intensities above this threshold activate a cryptochrome mediated signaling pathway that encodes sunlight, while light below this threshold activates a signaling pathway that involves cryptochrome and other photoreceptors and that encodes moonlight. We provide three lines of evidence, which include biophysical, behavioural and biochemical data, that are consistent with this model.

Firstly, we found that on a biophysical level, sunlight fully photoreduces L-Cry´s cofactor flavin adenine dinucleotide (FAD) within minutes, while prolonged moonlight exposure (>3h) leads to a distinct moonlight state of L-Cry, which is characterized by partial photoreduction of FAD and photoreduction kinetics that are distinct from the sunlight state (article #2, Fig. 1). Similarly, dCry bound FAD gets fully photoreduced by naturalistic sunlight, however it does not get photoreduced by naturalistic moonlight, at least not under the tested in vitro conditions (article #1, Fig. 5).

Secondly, on a behavioural level, we provide evidence that L-Cry mediates distinct circadian responses to naturalistic sun and moonlight, consistent with the existence of two distinct L-Cry dependent signaling pathways that encode moon and sunlight. Specifically, we show that constant sunlight leads to an L-Cry-dependent arrest of the circadian clock, while constant moonlight leads to an L-Cry-dependent period shortening of the circadian clock (article #1, Fig. 2B, C). Similarly, it has been shown in *Drosophila* that

dCry disrupts circadian behaviour under bright light (Emery et al., 2000), while under dim light in the range of moonlight intensity dCry mediates a period lengthening of the circadian clock (Yoshii et al., 2004).

Thirdly, on a biochemical level, we show that naturalistic sunlight but not moonlight leads to degradation of L-Cry (article #1, Fig. 3), suggesting that L-Cry engages via two distinct signaling modes in a sunlight and a moonlight signaling pathway. Furthermore, L-Cry seems to signal in different cellular compartments during naturalistic sunlight and moonlight conditions: while upon sunlight stimulation L-Cry localizes to the cytosol (article #2, Fig. 3), and subsequently gets degraded (article #1, Fig. 3), under moonlight conditions L-Cry is almost exclusively localized to the nucleus (article #1 Fig. 3 and article #2 Fig. 3). These observations are consistent with the existence of a canonical *Drosophila*-like Cry-signaling pathway in *Platynereis* that is active under sunlight but not moonlight. In *Drosophila* this pathway involves a light-dependent binding of Cry to Tim and the subsequent degradation of both proteins, thereby resetting the circadian clock (reviewed in section 3.3).

The fact that moonlight, in contrast to sunlight, does not reduce protein levels of L-Cry and the different subcellular localizations of L-Cry under sun- and moonlight conditions suggest that the L-Cry mediated behavioural effects of moonlight are mediated independently of the putative canonical L-Cry signaling pathway. Similarly, in *Drosophila* it has been reported that dim light pulses of long duration do not lead to a degradation of dCry, while at the same time the authors show that dCry is involved in entraining circadian behavioural rhythms to these dim light pulses (Vinayak et al., 2013), suggesting that a non-canonical dCry signaling pathway exists that is involved in the adjustment of the circadian clock to dim light.

In summary, albeit dim light of moonlight intensity does not seem to trigger degradation of dCry nor L-Cry, both cryptochromes seem to be involved in circadian dim light/moonlight perception through a non-canonical signaling pathway. The exact mechanism of this cryptochrome-dependent moonlight signaling pathway still needs to be elucidated, and might differ in *Drosophila* and *Platynereis*, as dCry in contrast to L-Cry did not respond to prolonged naturalistic moonlight in vitro (article 1, Fig. 5). This suggest that dCry either acts downstream of a more sensitive light receptor, or that dCry in vivo is more light sensitive than in our in vitro assay. However, a function of dCry downstream of a moonlight photoreceptor might well be possible, as it has been shown that (i) dCry can

act as a transcriptional repressor in the photoreceptors of the eye (Collins et al., 2006), and (ii) rhodopsins expressed in the eyes are required for the circadian perception of artificial moonlight given during the night (Schlichting et al., 2014).
In *Platynereis*, the aforementioned identification of a distinct moonlight state of L-Cry after prolonged moonlight exposure (>3h) in vitro (article #2, Fig1) would be consistent with a direct moonlight activation of L-Cry that elicits a yet unknown downstream signaling pathway. However, L-Cry might in addition also act downstream of faster-acting moonlight sensors, especially considering that during a waning moon light regime the latency of L-Cry activation by moonlight would be too slow to accurately track the time of moonrise.

The remarkable light sensitivity of r-opsin1 signaling as revealed in a cell-culture based system (article #1, Fig. 6A), along with the finding that *r-opsin1* mutants show an impaired response in shifting their timing of swarming onset in response to a waning moonlight stimulus (article #1, Fig. 6B, C), suggests that ropsin1 signaling is activated at moonlight intensity and adjusts the phase of the clock to naturalistic nocturnal moonlight. Moonlight detection by eye rhabdomeric opsins has also been reported for *Drosophila*, although there the shift in locomotor activity seems to be mainly induced by light masking (Kempinger et al., 2009), while the effect of moonlight on the endogenous clock itself under a combined sun/moonlight regime is rather small (Bachleitner et al., 2007; Kempinger et al., 2009; Schlichting et al., 2014).

The exact signaling pathway on how r-opsin1 and L-Cry adjust the circadian clock to moonlight still needs to be discovered. One candidate hormone that might be involved in this moonlight signaling pathway is the neuropeptide pigment dispersing factor (PDF). In *Drosophila* PDF is thought to mediate light input from the visual system to the circadian clock (reviewed in Schlichting, 2020). Furthermore, it has been shown that *pdf* knock-out flies in contrast to wildtypes cannot shift their evening activity peak into the night in response to an artificial moonlight stimulus provided during the night (Helfrich-Förster, 2009). Therefore, it would be interesting to test if in *Platynereis* the impaired response of *r-opsin1* mutants to a waning full moon regime is mediated by PDF.

7.3. Three distinct cellular states might encode sunlight, moonlight and darkness

The existence of two light signaling pathways with different light sensitivities that both entrain the clock poses a potential mechanism on how animals can discriminate moonlight from sunlight for clock entrainment. Based on our data I propose a model of 3 different cellular states that could encode sunlight, moonlight or darkness conditions both in *Drosophila* and in *Platynereis*: Under sunlight conditions cryptochrome gets fully photoreduced and binds cytosolic Tim which leads to a constant degradation of both Tim and Cry, resetting the clock. Under moonlight conditions the canonical Cry pathway is not activated and Cry accumulates in the nucleus. There it either is directly activated by prolonged moonlight exposure to signal in a non-canonical fashion and/or acts downstream of rhodopsin signaling to modulate the period of the clock. Under darkness Cry also accumulates in the nucleus but is not photoactivated directly nor indirectly. If and how rhodopsin and cryptochrome signaling interact to eventually impact on circadian clock gene cycling still needs to be elucidated. The fact that in *Drosophila* and *Platynereis* Cry is not only expressed in inner brain neurons that express circadian clock genes, but also in the photoreceptors of the eyes (article #1, 3G and Yoshii et al., 2008), would be consistent with the idea that rhodopsins and cryptochrome might act together even within the same cell to encode moonlight, sunlight or darkness.

7.4. Stabilizing the circadian clock against a disturbance by moonlight - implications from *Drosophila*

The mechanism on how dCry prevents internal circadian desynchronization under artificial full moon conditions among the different circadian clock neuron clusters that control morning and evening activity (article #1, Fig. 4) could be solely explained by dCry´s function to synchronize clock neurons to sunlight, irrespective of its function in dim light sensing. This is because dCry is expressed both in morning and evening cells (Benito et al., 2008; Yoshii et al., 2008). So although moonlight during the night slightly desynchronizes circadian clock gene oscillations in morning and evening oscillators cells (Bachleitner et al., 2007), dCry would resynchronize the molecular circadian clock gene oscillations in both morning and evening cells with each other as soon as the sun rises through the canonical cryptochrome signaling pathway. In contrast, mutant flies that lack dCry rely solely on rhodopsin signaling, which may delay circadian clock gene oscillations

in evening cells compared to morning cells during moonlit nights, and there is no dCry to resynchronize these oscillations again during the day. In other words, abolishing the main sunlight signaling pathway might unmask the internal desynchronization effects mediated by the very light-sensitive visual signaling pathway. This model could explain why we observed a delayed evening activity of *Drosophila cry* mutants compared to wildtypes under artificial full moon conditions. Furthermore, it would be consistent with studies that showed that *Drosophila melanogaster cry* mutants show an increased ability to delay their evening activity peak to the evenings of long photoperiods (Kistenpfennig et al., 2018; Menegazzi et al., 2017; Rieger et al., 2003), indicating that dCry prevents morning and evening oscillators to drift apart under such artificially long photoperiods which this *Drosophila* species would not experience in its natural habitat.

It will be interesting to test if similar systems designed to discriminate moonlight from sunlight exist also in mammals, including humans and if impairing the "sunlight signaling" pathway would make individuals more susceptible to circadian effects of moonlight or photoperiod. Interestingly, in humans, a specific missense mutation (P10L) in melanopsin, which – such as insect Cry - is regarded as the main circadian sunlight photoreceptor, is associated with seasonal defective disorder (Roecklein et al., 2009) and an increased effect of photoperiod on sleep onset (Roecklein et al., 2012). One possible explanation for this paradoxical gain of function effect might be explained by a stronger influence of rod and cone photoreception on circadian timing once melanopsin signaling is impaired. As human sleep onset has also been shown to be affected by the moon cycle (Cajochen et al., 2013; Casiraghi et al., 2021) and in light of the increased response to moonlight in *Drosophila cry* mutants (#article 1, Fig. 4), it would be interesting to test if the P10L melanopsin variant would make humans more susceptible to the effect of moonlight on sleep onset.

7.5. Aschoff´s rule revisited: considering circadian responses to moonlight

When making predictions on how the circadian system of a species responds to constant light, biologists have primarily taken into consideration if an animal is nocturnal or diurnal. It has been proposed that diurnal animals shorten their circadian period under constant dim and bright light while nocturnal animals would lengthen it. This prediction

has been referred to as Aschoff´s first rule and is based on observations in some diurnal (lizards, starlings, finches) and nocturnal (mice) vertebrates (Pittendrigh, 1960). However, a follow-up article that reviewed many more species found that there are several exceptions to this rule including some diurnal mammals (e.g. some squirrel species) and most diurnal insects (Aschoff, 1979). Most tested diurnal insects (such as *Drosophila* and several ground beetle species) were found to increase their period length under constant light irrespective if they show nocturnal or diurnal activity profiles. *Platynereis* also breaks Aschoff´s rule, as it is a nocturnal species and decreases its circadian period length under constant artificial moonlight. Functionally, this feature of the clock likely allows *Platynereis* to advance the clock during the nights following a full moon to time swarming onset to the beginning of the night where no moonlight is present. Therefore, it might be useful also for other species to consider if and how they react to moonlight in their native environment to better understand the functional significance of certain circadian clock properties.

7.6. First insights into the entrainment of peripheral circadian rhythms in *Platynereis*

In article #3 we aimed at a first characterization of the entrainment and maintenance of circadian rhythms in peripheral tissues. We found that circadian chromatophore size regulation is maintained under constant darkness in animals without a head (Fig. 5D), indicating the existence of a self-maintained circadian clock in the trunk that can function independently of the head. However, we found that overall circadian clock gene oscillations across the whole trunk are not maintained in a synchronized fashion after 3 days in constant darkness, while they cycle in a synchronized fashion under LD cycles (Fig. 1). Interestingly, this synchrony under LD cycles does not require the head (Fig. 3), indicating that photoreceptors present in the trunk can synchronize circadian clock gene oscillations throughout the trunk. This indicates that like in *Drosophila*, peripheral tissues are intrinsically photosensitive and do not necessarily rely on the central clock to entrain their molecular circadian rhythms. However, one limitation of this study is that we only looked at circadian clock gene oscillations in the trunk as a whole, thereby losing spatial resolution. To understand which circadian processes in the trunk are under the control of

the central circadian oscillator and which are entrained by local photoreceptors, will require an approach that targets specific tissues or organs.

One of these candidate photoreceptors that might synchronize peripheral circadian clock gene oscillations to the LD cycle is r-opsin1, as it is expressed in the parapodia of the worms trunk (Backfisch et al., 2013). It would be interesting to test if r-opsin1 mediated moonlight signaling is also relevant in the trunk or if peripheral circadian clock gene oscillations are exclusively entrained by sunlight. As circadian chromatophore size regulation is thought to have mainly evolved to protect the organism from damaging UV light during the day (Miner et al., 2000), it would make little sense from this perspective if circadian chromophore size regulation would be sensitive to moonlight. If chromophore size regulation was indeed moonlight insensitive, it might also be controlled by a circadian clock that runs with a period length closer to the 24h solar day rather than the 24.8h lunar day. Interestingly, we found that if worms are kept for 5 days in constant darkness, chromatophores were smaller at CT14 compared to CT2 (article #3, Fig. 5b), similar as under a LD light regime. This would not be possible if the clock was running with an endogenous ~25h rhythmicity (like the clock that controls swarming onset) as this would delay the chromatophore cycle on day 5 under DD by about 5 hours and hence chromatophores should be larger at CT14 compared to CT2 (article #3, compare Fig. 5B and 5F).
Although further experiments would be needed to test this hypothesis, following up on this avenue might yield interesting conceptual questions about the coexistence of circadian and circalunidian timers in *Platynereis*, such as the possibility that monthly rhythms might arise from an overlay of a 24h and a 24.8h timer (Soong & Chang, 2012; Zantke et al., 2013). Interestingly, the coexistence of a circadian (~24h) timer that controls chromatophore size and an independent circatidal (~12.4h) timer that controls locomotor activity has been shown to exist in the intertidal crab Eurydice pulchra (Zhang et al., 2013).

7.7. Conclusions

In this thesis I uncovered a surprisingly strong influence of naturalistic moonlight on the circadian timing of reproductive behaviour in *Platynereis dumerilii*. By mimicking waning

and waxing moonlight regimes, I could show that swarming onset is timed to the portion of the night where no moonlight is present. This timing is not an immediate response to moonlight but mediated by a moonlight-sensitive plastic circadian clock, which shortens its period length under moonlight exposure. This discovery allowed us to investigate how moonlight is perceived and how it is discriminated from sunlight for circadian timing. We find that naturalistic sunlight and naturalistic moonlight are likely perceived through distinct signaling pathways. The sunlight signaling pathway is associated with a translocation of nuclear L-Cry into the cytosol and its subsequent degradation, while the moonlight signaling pathway requires both r-opsin1 and L-Cry signaling and is associated with a distinct L-Cry state, where FAD bound L-Cry gets partially photoreduced but L-Cry is neither translocated to the cytoplasm nor is it degraded (for summary model see article #1, Fig. 7). The function of a light-sensitive cryptochrome to distinguish moonlight from sunlight seems to extend to insects, as we find that *Drosophila* Cry shields the fly clock from a disturbance by moonlight.

This work bears potential relevance for the scientific community that goes beyond the chronobiology of *Platynereis* and *Drosophila*. Firstly, it suggests that distinct light input pathways to the circadian clock may have evolved in part also to discriminate lunar from solar light illumination. Secondly, our findings emphasize that under naturalistic conditions circadian systems with high light sensitivity need to adapt to different moon phases. The discovery that a waning moonlight regime has such a pronounced effect on circadian timing of swarming onset in *Platynereis* might hint at an important yet overlooked effect of moonlight on circadian timing also in other species. Importantly, the few studies that investigated circadian effects of moonlight under laboratory conditions (mainly in mice, hamsters and *Drosophila*) only used light regimes with continuous nocturnal moonlight, rather than waning or waxing moonlight regimes. Using these latter light regimes might be better suited to assess circadian effects of moonlight, since they allow animals to restrict their activity either to times of darkness, moonlight or sunlight. To solve global conservation challenges, it is important to know how widespread the effect of moonlight on circadian timing is, as anthropogenic light pollution can easily interfere with these fundamental timing mechanisms, which are relevant for species survival (Ayalon et al., 2020).

8. Technical contribution – Article 4: A versatile depigmentation, clearing, and labeling method for exploring nervous system diversity

Status: published article
Science Advances Vol. 6, no. 22, eaba03656 (2020), doi: 10.1126/sciadv.aba0365

Authors:
Marko Pende, Karim Vadiwala, Hannah Schmidbaur, Alexander W. Stockinger,
Prayag Murawala, Saiedeh Saghafi, Marcus P. S. Dekens, Klaus Becker,
Roger Revilla-i-Domingo, Sofia-Christina Papadopoulos, **Martin Zurl**, Pawel Pasierbek,
Oleg Simakov, Elly M. Tanaka, Florian Raible, Hans-Ulrich Dodt

Outline:
Whole-body imaging of fluorescently labeled proteins or nucleic acids requires protocols that make tissues transparent. A particular challenge is to clear pigmented tissue, like eyes or chromatophores, in order to image molecules within or below these structures. Here, we develop a depigmentation and clearing protocol that is applicable to a variety of model species ranging from annelids and squids to axolotls and zebrafish. We show that this protocol is compatible with a wide range of downstream labeling and imaging techniques that include immunohistochemistry, RNA in situ hybridization, EdU labeling of proliferative cells and imaging of endogenous fluorescence.

Contributions:
I discovered Vasotocin-positive cell bodies below the eyes of *Platynereis dumerilii* and performed and analyzed anti-Vasotocin immunostainings shown in Figure 2G.

NEUROSCIENCE

A versatile depigmentation, clearing, and labeling method for exploring nervous system diversity

Marko Pende[1,2*†], Karim Vadiwala[3†], Hannah Schmidbaur[4], Alexander W. Stockinger[3], Prayag Murawala[5‡], Saiedeh Saghafi[1], Marcus P. S. Dekens[3], Klaus Becker[1,2], Roger Revilla-i-Domingo[3], Sofia-Christina Papadopoulos[1], Martin Zurl[3], Pawel Pasierbek[6], Oleg Simakov[4], Elly M. Tanaka[5], Florian Raible[3*], Hans-Ulrich Dodt[1,2]

Tissue clearing combined with deep imaging has emerged as a powerful alternative to classical histological techniques. Whereas current techniques have been optimized for imaging selected nonpigmented organs such as the mammalian brain, natural pigmentation remains challenging for most other biological specimens of larger volume. We have developed a fast DEpigmEntation-Plus-Clearing method (DEEP-Clear) that is easily incorporated in existing workflows and combines whole system labeling with a spectrum of detection techniques, ranging from immunohistochemistry to RNA in situ hybridization, labeling of proliferative cells (EdU labeling) and visualization of transgenic markers. With light-sheet imaging of whole animals and detailed confocal studies on pigmented organs, we provide unprecedented insight into eyes, whole nervous systems, and subcellular structures in animal models ranging from worms and squids to axolotls and zebrafish. DEEP-Clear thus paves the way for the exploration of species-rich clades and developmental stages that are largely inaccessible by regular imaging approaches.

INTRODUCTION

The focus on a handful of well-established "molecular model species" has been instrumental to drive biological discovery and technological development for the past decades. However, it is increasingly recognized that these model species only cover a limited spectrum of ecological diversity, calling for a more systematic effort in establishing novel model systems (*1*–*4*). Advances in the establishment of versatile technologies are keys in this effort. This is exemplified by the progress in RNA sequencing technology or the advent of precise genome editing methodology, tools that have begun to pave the way for systematic research into less conventional models (*5*–*12*).

In contrast to sequencing or genome editing technologies, other methodologies are still far more restricted in their applicability and use, resulting in substantial limitations concerning the exploration of less established biological models. One critical area is the imaging of cells or molecules in the context of their natural tissue environment and the imaging of complete tissues and organisms. This often involves sectioning and reconstruction, resource-intensive processes that are particularly challenging in cases similar to the nervous system, where dissected nerves and individual neuronal projections are notoriously difficult to reconstruct. Whereas advanced microscope setups provide superior resolution in thin samples, deep imaging of nervous systems, other tissues, or whole organisms therefore remains a key challenge outside few well-established model systems. Major reasons for this are the scattering of light caused by the differences in the refractive indices (RIs) of biological molecules (e.g., water versus lipid versus protein) and the absorption of light by natural pigments (*13*).

Driven by research on the mammalian brain, various methods have been established to resolve the heterogeneity in RIs in unpigmented samples. This includes the removal of lipids from lipid-rich tissues such as the central nervous system and the use of media that are able to match RIs. Strategies to match the RI and/or to remove lipids have been broadly classified in two categories: those relying primarily on organic solvents, such as the benzyl alcohol with benzyl benzoate (BABB) (*14*), Three-dimensional imaging of solvent-cleared organs (3DISCO) and immunolabeling-enabled three-dimensional imaging of solvent-cleared organs (iDISCO) (*15*–*17*), ultimate DISCO (uDISCO) (*18*), stabilised DISCO (sDISCO) (*19*), polyethylene glycol (PEG)-associated solvent system (PEGASOS) (*20*) or 2nd generation ethyl cinnamate-based clearing (2ECi) (*21*) protocols; and those primarily relying on hydrophilic reagents and detergents, including the ClearT (*22*), Rapid clearing method based on Triethanolamine and Formamide (RTF) (*23*), Clear, unobstructed brain imaging cocktails and computational analysis (CUBIC) (*24*–*27*), Scale (*28*, *29*) or SeeDB (*30*, *31*) methods, and variants of the clear lipid-exchanged anatomically rigid imaging/immunostaining-compatible tissue hydrogel (CLARITY) (*32*, *33*) approach [reviewed in (*13*, *34*)].

While each of these techniques offers unique advantages, they are not easily applicable to many species of ecological or evolutionary interest that exhibit pigmentation. Although several existing clearing protocols decolorize heme, the blood pigment, they have not been optimized for removal of other body pigments. Animals produce a variety of additional pigments through conserved biochemical pathways. Several of these pigments are characterized by poor solubility: Melanin, a tyrosine-derived ultraviolet protectant, is very poorly soluble in both lipid- and water-based solvents [reviewed in (*35*)] yet serves as a prominent pigment of the vertebrate retinal pigment epithelium (RPE), a cell layer acting to diminish photo-oxidative

[1]Department for Bioelectronics, FKE, Vienna University of Technology, Gußhausstraße 25-25A, building CH, 1040 Vienna, Austria. [2]Section for Bioelectronics, Center for Brain Research, Medical University of Vienna, Spitalgasse 4, 1090 Vienna, Austria. [3]Max Perutz Labs and Research Platform "Rhythms of Life", University of Vienna, Vienna BioCenter, Dr. Bohr-Gasse 9/4, 1030 Vienna, Austria. [4]Department of Neuroscience and Development, University of Vienna, Althanstraße 14, 1090 Vienna, Austria. [5]Research Institute of Molecular Pathology (IMP), Vienna BioCenter, Campus-Vienna-Biocenter 1, 1030 Vienna, Austria. [6]Institute of Molecular Biotechnology of the Austrian Academy of Sciences (IMBA), Vienna BioCenter, Dr. Bohr-Gasse 3, 1030 Vienna, Austria.
*Corresponding author. Email: marko.pende@tuwien.ac.at (M.P.); florian.raible@univie.ac.at (F.R.)
†These authors contributed equally to this work.
‡Present address: Mount Desert Island Biological Laboratory, Bar Harbor, ME 04609, USA.

stress and absorb scattered light. Likewise, ommochromes are a class of pigments derived from tryptophan catabolism that are particularly abundant in invertebrate species. They are tricyclic compounds consisting of phenoxazone or phenothiazine subunits and are for instance responsible for yellow, red, brownish, or black pigmentation of insect eyes, cephalopod body pigmentation, or integuments (*36*). Another class of abundant and poorly soluble pigments are pterins, cyclic compounds biochemically derived from guanosine triphosphate; pterins are cofactors of the enzymatic biosynthesis of ommochromes and thus often found in combination with those pigments, e.g., in invertebrate eyes (*35*). Whereas natural albinism, the application of pathway inhibitors, or the selection for single or combined mutants in the respective pigment pathways provides advantages for clearing and deep imaging, these are not broadly applicable approaches for many species of interest. Despite some recent efforts, such as the combination of decalcification and bleaching to adapt a CUBIC protocol for use in pigmented crustaceans (*37*) or the mouse eye–specific EyeCi protocol (*38*), the variety of body and eye pigments found in animals therefore remains a central challenge for the broad use of clearing and deep imaging. Further, it also remains unclear if any attempt to combine depigmentation and clearing would preserve other biomolecules for single or multiple imaging approaches.

Here, we provide a novel, fast, and simple method that combines depigmentation with tissue clearing in samples from five different species representing four distinct animal clades (annelids, molluscs, bony fishes, and tetrapods) and sizes up to several centimeters in length. This method, which we term DEpigmEntation-Plus-Clearing (DEEP-Clear), combines advantages of methods previously categorized in either organic solvent– or hydrophilic reagent–based clearing approaches, allowing for complete whole-body clearing and RI matching of fixed specimens within less than a day. DEEP-Clear efficiently removes naturally occurring pigments including pterins, ommochromes, heme, carotenoids, and melanin. DEEP-Clear is compatible with immunohistochemical (IHC) analysis in specimens fixed with either paraformaldehyde (PFA) or Bouin's fixative, thus allowing the visualization of a broad range of epitopes. Moreover, it allows the visualization of 5-ethynyl-2′-deoxyuridine (EdU)–labeled chromatin of proliferative cells and is compatible with transgenically expressed fluorophores. Last, DEEP-Clear retains compatibility with whole-mount fluorescence RNA in situ hybridization (RNA-FISH), a technique that has been left out of the focus of most existing clearing methods (*34*). DEEP-Clear permits deep imaging of labeled structures across scales, ranging from whole-body imaging using advanced light-sheet microscopy to detailed high-resolution investigation using confocal microscopy. Thus, DEEP-Clear is a highly versatile tool that will make depigmentation, tissue clearing, labeling, and imaging applicable to a broad spectrum of animal model systems and experimental approaches.

RESULTS

DEEP-Clear enables combined depigmentation and clearing across four animal clades

Pende and coworkers (*39*) have recently developed a CUBIC-based approach (FlyClear) that not only renders different tissues transparent but also causes depigmentation of eyes in *Drosophila melanogaster* while preserving endogenous transgenic green fluorescent protein (GFP) and mCherry signal. Given that *D. melanogaster* eyes contain both ommochromes and pterins (*35*), we hypothesized that this protocol could serve as a suitable basis for developing a depigmentation and tissue clearing approach of broader applicability to other animal model organisms and possibly also be compatible with other detection methods. We decided to focus our work on representatives of four distinct noninsect animal clades:

1) The marine bristle worm *Platynereis dumerilii* as a representative of annelids (adult samples, around 15 mm in length).

2) The Hawaiian bobtail squid *Euprymna scolopes* and the longfin inshore squid *Doryteuthis pealeii*, two cephalopod molluscs (hatchling stage, 3 mm in length).

3) The zebrafish *Danio rerio* as a representative for bony fishes (from larva to juvenile stages of around 12 mm in length).

4) The axolotl *Ambystoma mexicanum* as a reference species for tetrapods (juvenile samples, up to 35 mm in length).

Both annelids and molluscs are key groups in the large lophotrochozoan superphylum, while bony fishes and tetrapods are the most species-rich groups of deuterostomes. Our choice of models therefore covers a substantial spectrum of ecologically relevant noninsect animal diversity. Moreover, the selected species and developmental stages also provide exemplary access to interesting neurobiological aspects (such as central nervous system regeneration, cranial nerve complexity, or different types of visual organs) that strongly benefit from a method providing depigmentation, clearing, active labeling, and whole-body imaging.

In a systematic set of experiments, we gradually modified the FlyClear protocol and chemistry to achieve decolorization of different kinds of pigments and tissue clearing in all of these species, resulting in a revised DEEP-Clear protocol adaptable for each of the investigated samples (Fig. 1A). Key steps in this process were (i) the combination of FlyClear's Solution-1, a hyperhydration-based solution containing an aminoalcohol *N*,*N*,*N*′,*N*′-Tetrakis(2-hydroxyethyl) ethylenediamine (THEED), detergent (Triton X-100), and urea with acetone (an organic solvent) resulting in increased depigmentation speed, thereby reducing possible damage by extended exposure; (ii) the inclusion of a peroxide-bleaching step for melanin-containing samples; and (iii) the variation of urea content and pH in Solution-1 to reduce swelling effects or tissue damage encountered in the squid and zebrafish models. Together, all postfixation clearing steps can be performed within 24 hours or less for each of the samples (Fig. 1A), making DEEP-Clear easy to incorporate into existing workflows. As illustrated in Fig. 1 (B and C), the application of the organic solvent step substantially reduced depigmentation time in the two tested invertebrate models and had synergistic effects on pigment removal (Fig. 1D), allowing us to generate depigmented, transparent samples for each of the species (Fig. 1E).

With respect to the different pigment types, DEEP-Clear treatment in annelids depigmented the adult eyes that have previously been characterized to contain pterins (fig. S1A) (*40*), along with the additional red pigments in the body erythrophores (fig. S1, A and B) and the heme-based blood pigments (fig. S1B) (*41*). We noted that the treatment also destains the chlorophyll of the consumed spinach in the worm gut (fig. S1C). Furthermore, DEEP-Clear removes ommochrome-based pigments in squid (fig. S1D). As exemplified for the zebrafish fin (Fig. 1D), treatment solely with acetone at room temperature causes depigmentation of xanthophores that carry pteridines and carotenoid pigments but does not remove the characteristic black melanin pigments present in melanophores (Fig. 1D). Moreover, melanin in the analyzed vertebrate eyes and body tissues could not be fully solubilized by individual treatment with Solution-1,

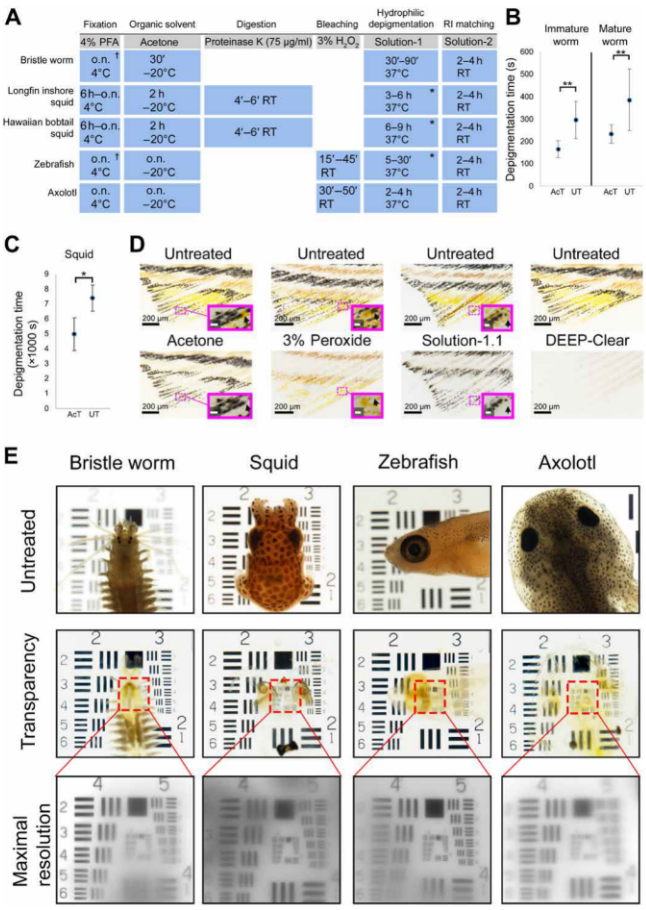

Fig. 1. A rapid method combining depigmentation with tissue clearing in representatives of four distinct and species-rich animal clades. (**A**) Main steps of the DEEP-Clear protocol, including incubation times for the five main model systems presented in this study. (**B**) Systematic advancement of eye depigmentation speed by acetone pretreatment in immature and mature worms. Quantified comparisons between acetone-treated (AcT) and untreated (UT) head halves incubated with Solution-1. All values are mean ± SD; statistical significance was determined by a Wilcoxon test, yielding *P* values of $P = 0.00166$ (immature worms) and $P = 0.00192$ (mature worms). (**C**) Systematic advancement of eye depigmentation speed by acetone pretreatment in squid. Quantification of depigmentation time in acetone-treated and untreated squid halves upon incubation with Solution- 1.1. Values are mean ± SD; statistical significance was determined by a Wilcoxon test ($P = 0.01285$). (**D**) Differential and synergistic impact of acetone, peroxide, and Solution-1.1 on zebrafish fin pigments. Panels show fins of untreated (top) and treated (bottom) zebrafish fins. Insets: Magnification of dashed area and impact of different treatments on respective pigments (black arrows). Xanthophore containing pteridine and carotenoid pigments (yellow and orange) and melanophore containing melanin pigment (black). Rightmost panels show the overall impact of the full DEEP-Clear protocol. (**E**) Wide-field images of specimens placed on top of a USAF 1951 chart. Uncleared samples in PBS (top panels), same samples after depigmentation and refractive index (RI) matching in Solution-2 (middle panels), and higher magnification of red rectangular areas indicating the highest level of transparency reached after RI matching (bottom panels). Scale bars in the insets of (D), 20 µm. In (A), dagger indicates the possibility of fixation with Bouin's solution; asterisks indicate the use of Solution-1.1 incubation instead of Solution-1. o.n., overnight; RT, room temperature; h, hour; ', minutes. In (B) and (C), $*P < 0.05$ and $**P < 0.01$. Photo credit: Marko Pende, Medical University of Vienna.

even with increased pH (13) and extended incubation times. In axolotl eye and body tissues, melanin was merely reduced (fig. S1E), whereas in zebrafish, this prolonged Solution-1 treatment led to severe tissue damage, requiring a change to the urea-reduced Solution-1.1 for subsequent experiments in zebrafish. The difficulty of solubilizing melanin is a known shortcoming of current clearing approaches (*13*, *27*) and prompted us to include the pretreatment step with 3% hydrogen peroxide to achieve full depigmentation of melanin-containing samples (Fig. 1A). Pretreatment solely with hydrogen peroxide efficiently bleached melanin, but not the xanthophore pigments of pteridine and carotenoid nature in zebrafish fins (Fig. 1D), and also diminished pigmentation in the axolotl eye (fig. S1F). By contrast, combining this peroxide treatment with the established acetone and Solution-1(.1) treatment, as well as appropriate RI matching, preserved sample morphology and yielded the highest levels of tissue transparency as assessed on a 1951 United States Air Force resolution test chart (USAF chart) (Fig. 1E and fig. S1G). As the use of peroxide damages signal from transgenic fluorophores, strategies to relabel these fluorophores are presented in a later section. For RI matching, we used Solution-2 containing meglumine diatrizoate; for larger specimens including lipid-rich tissues, this solution was further modified by supplementing with *N*′-methylnicotinamide and antipyrine (referred to as Solution-2.2), in line with published strategies to raise RI without causing tissue deformation (*27*).

Together, these results establish that DEEP-Clear is able to efficiently reduce poorly soluble pigments even in large specimens that would otherwise be impossible to use for deep imaging. A qualitative survey of five published methods, applied to specimens of all four clades (fig. S2A), and a systematic quantification of light transmittance through the eyes of cleared and noncleared samples (fig. S2B) provide experimental support for the notion that DEEP-Clear can tackle a spectrum of pigments for which existing methods are not optimized.

Preservation of fine structures across scales and visualization of transgenic signals

We next investigated (i) whether endogenous structures and molecules were preserved in acetone pretreated samples, (ii) whether they could be relabeled in cases where a peroxide bleaching step was included, and (iii) whether fine tissue structures remained intact.

While extended acetone treatment is considered to denature fluorescent proteins, we noted that acetone-treated transgenic zebrafish and mice (fig. S3, A to C) retained their respective fluorescent protein fluorescence: We detect similar or slightly reduced fluorescent signal intensity yields by comparing untreated samples with samples exposed to acetone overnight at −20°C for *brn3c::mGFP* and *HuC::Gal4; UAS::syp-GFP* zebrafish and Thy1-YFP-H mice (fig. S3, A to C). In DEEP-Clear–treated pMos{rops::egfp}^{vbci2} adult worms (Fig. 2A), we could visualize the projection path of enhanced GFP–positive (EGFP$^+$) eye photoreceptor cells (Fig. 2B). Similarly, light-sheet microscopy on complete worms was able to resolve both cell bodies and individual projections of the peripheral EGFP$^+$ cells from individual parapodia onto and along the fibers of the ventral nerve cord of the trunk (Fig. 2, C and D) (*42*). As signal stability is a relevant aspect both for imaging and sample archiving, we also used DEEP-Clear–treated worm specimens to assess whether EGFP signal could be effectively preserved on a long-term basis. These analyses revealed that, even after several weeks, EGFP$^+$ structures could clearly be distinguished from autofluorescence, exhibiting only limited decay when compared to the first day of recording (fig. S4, A to D). Although pigmentation

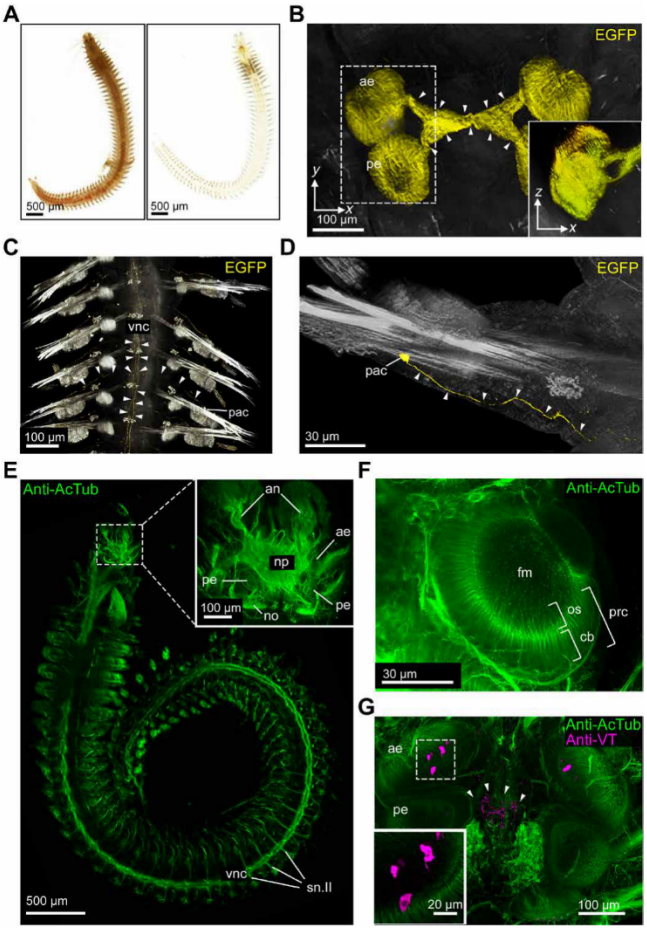

Fig. 2. Global and focused insight into the adult annelid nervous system. (**A**) Comparison of uncleared (left) and DEEP-Clear processed (right) bristle worm specimens. (**B**) Imaging of EGFP signal in photoreceptors of DEEP-Clear–processed pMos{rops::egfp}^{vbci2} animals by light-sheet microscopy. Arrowheads indicate projections from the eyes into the central-brain neuropil. Inset shows the *XZ* projection of the boxed area. (**C** and **D**) EGFP$^+$ parapodial cell bodies and their projections (arrowheads) into and along the ventral nerve cord as visualized by light-sheet microscopy. (**E** to **G**) Anti-acetylated alpha-tubulin (anti-AcTub) immunolabeling revealing the annelid nervous system, visualized either by light-sheet microscopy [(E) whole animal, including the stereotypical trunk nervous system; inset showing major structures of the brain] or confocal microscopy [(F) anterior eye, with photoreceptor cells exhibiting segmentation into outer segments protruding into the central filling mass and basal cell bodies; (G) brain, with the inset showing a magnification of the boxed region of the anterior eye]. The specimen in (G) shows a colabeling by anti-Vasotocin (anti-VT) immunohistochemistry, and arrowheads indicate VT$^+$ puncta (putative dense core vesicles) in deep neurite projections. Corresponding VT$^+$ cell bodies can be seen in close proximity to the anterior eyes. an, antennal nerve; cb, cell body; fm, filling mass; no, nuchal organ; np, neuropil; os, outer segment; pac, parapodial receptor cells; ae, anterior eye; pe, posterior eye; prc, eye photoreceptor cell; sn.II, segmental nerve II; vnc, ventral nerve cord.

is no relevant challenge in analyzing mammalian brain samples, we used hemispheres of a Thy1-YFP-H transgenic mouse brain to assess imaging of a large specimen. In this experiment, DEEP-Clear treatment allowed for imaging fluorescent cell bodies across close to 6000 µm of depth, comparable to the established CUBIC approach (fig. S5, A to E) (*26*). To investigate whether the use of peroxide in the context of melanized sample processing was compatible with signal relabeling, we performed anti-GFP stainings in respective DEEP-Clear–processed *brn3c::mGFP* zebrafish samples of different developmental stages [6, 10, 17, and 23 days post fertilization (dpf); fig. S6, A to D]. Anti-GFP immunohistochemistry allowed us to visualize the characteristic projections of retinal ganglion cells to the optic tectum (fig. S6, B to D) (*43*). To address whether finer, subcellular structures would be preserved if a peroxide treatment step was included in the DEEP-Clear procedure, we used *HuC::Gal4; UAS::syp-GFP* specimens that express a GFP fusion protein of the presynaptic vesicle marker synaptophysin (*44*). Consistent with previous work on the presence of this marker in arborizations of neurons during tectal development (*44*, *45*), our analyses revealed a dense mesh of punctate structures in the tectum of 3 dpf larvae (fig. S6E). Similar puncta were also found in the mid-hindbrain region and the adjacent cerebellum (fig. S6F).

Systemic and focal analyses of postlarval invertebrate nervous systems

As endogenously expressed fluorophores are restricted to more established laboratory models, we performed a series of additional experiments to assess whether DEEP-Clear was also compatible with various immunohistochemically labeled epitopes. We focused most of our analyses on the nervous system of the respective species because the complexity of the nervous system presents a particular challenge to classical, section-based labeling efforts, as neural projections extending over different sections are very difficult to reconstruct. Moreover, the nervous system is of special relevance for evolutionary and comparative analyses.

For exploring the compatibility of DEEP-Clear with IHC analyses, we took advantage of antibodies that recognize conserved or specific epitopes. Across all species, we used a monoclonal antibody directed against acetylated alpha-tubulin that has been widely used to visualize animal nervous systems (*46*–*51*). In the axolotl, we also used the TuJ1 antibody that is directed against a neuron-specific beta III tubulin isoform (TUBB3) (*52*–*54*). We complemented these overall neuroanatomical analyses by performing immunohistochemistry against more specifically expressed epitopes. When required, we used a modified solution for RI matching (Solution-2.1) in which we included four parts of Solution-2 and one part of VECTASHIELD or embedded the samples in pure VECTASHIELD for preventing fluorophore bleaching. For analyzing global neuroanatomy, we used light-sheet microscopy, complementing these analyses with confocal analyses to study cellular or subcellular details.

In Solution-1–treated adult *P. dumerilii* specimens immunostained with anti-acetylated tubulin antibody, light-sheet microscopy revealed uniform labeling of both cephalic and noncephalic parts of the central nervous system, as well as the diagnostic segmental nerves of the annelid peripheral nervous system (Fig. 2E and movies S1 and S2) (*55*). Closer inspection of the cephalic region yielded detailed insight into brain structures and a high-resolution view of the adult eye cups (Fig. 2F). The fine structure of the eye that we obtained by confocal microscopy of complete heads matches well with the models previously obtained by laborious analyses of tissue sections by light and electron microscopy (*56*, *57*). We further performed immunostaining with an antibody directed against a *P. dumerilii* neuropeptide, Vasotocin (VT). In mature adult worms, detection of this antibody consistently labeled punctate structures in a meshwork of neurites reaching deep into the median brain, which prior work has

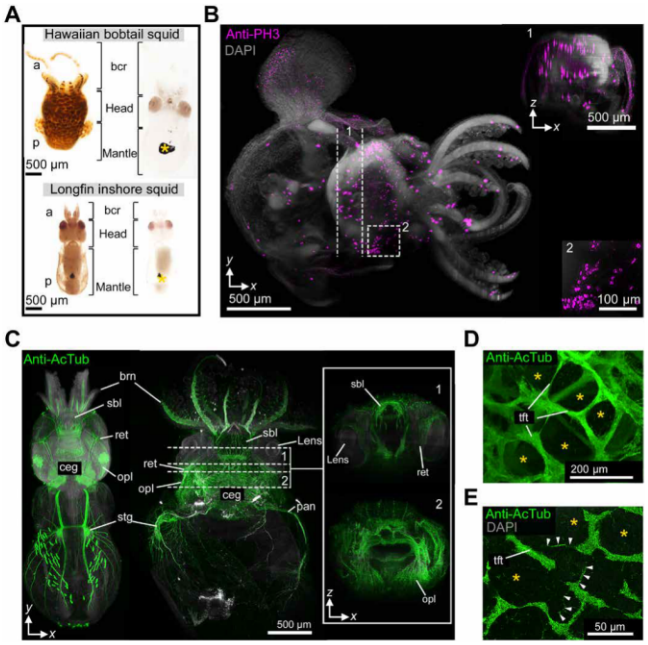

Fig. 3. Insight into the nervous system structures in whole-mount specimens of squid hatchlings. (**A**) Comparison of uncleared (left) and DEEP-Clear–processed (right) squid hatchlings (anterior up), documenting the removal of eye and body pigments (asterisk indicates remaining ink sac melanin). (**B**) Light-sheet acquisition of anti–phosphohistone H3 immunolabeling (bobtail squid, dorsal view, anterior to the right; dashed lines and box demarcate the area of the *XZ* slice shown in inset 1 and the enlargement in inset 2). DAPI, 4′,6-diamidino-2-phenylindole. (**C** to **E**) Visualization of the nervous system using anti-AcTub labeling. (C) Light-sheet acquisition (dorsal views, anterior up) in longfin inshore squid (left) and the Hawaiian bobtail squid (right). Inset shows two *XZ* projections of the respective areas (1 and 2) dashed in the *XY* view. (D and E) Confocal views of the deep medulla of the bobtail squid optic lobe, revealing the diagnostic structure of thick fiber tracts embracing perikarya (asterisks) and fine transversal fibers (arrowheads) of the Hawaiian bobtail squid. a, anterior; bcr, brachial crown; brn, brachial nerves; ceg, cerebral ganglion; opl, optic lobe; p, posterior; pan, pallial nerve; ret., retina; sbl, superior buccal lobe; stg, stellate ganglion; tft, thick fiber tract.

established as the release site of the animal infracerebral gland, where neurohormones are likely emitted into the circulating system (*58*). We also detected respective VT^+ cell bodies in direct proximity to the ventral face of the anterior eye cups, an area that is difficult to image without DEEP-Clear procedure due to massive amount of shielding eye pigments (Fig. 2G).

We next investigated squid hatchlings that had been depigmented and cleared using Solution 1.1 (Fig. 3A), immunolabeled, and lastly matched to an RI of 1.45 with antifade-mounting medium (VECTASHIELD). Despite the size of the specimens (around 3 mm × 1 mm × 1 mm), light-sheet analysis revealed a deep antibody staining of the mitotic cell marker phosphorylated histone H3 (PH3) (Fig. 3B) (*59*). These analyses revealed, among other domains, mitotic cell clusters usually masked by pigments (Fig. 3B, insets 1 and 2, and movie S3). Furthermore, we could visualize and compare, in undissected specimens, characteristic regions of the complete longfin inshore and the Hawaiian bobtail squid nervous system (Fig. 3C; fig. S7, A to C; and movies S4 and S5) (*55*). As for octopods, the sepiolid optic lobes are known to have an elaborate structure, with the deep medulla exhibiting large aggregates of perikarya interrupted by thicker fiber tracts. Owing to the strong pigmentation of the mantle, this elaborate, tree-like tissue structure has previously mainly been analyzed by histological analysis of serial sections (*55*, *60*, *61*). First accounts of its formation during *E. scolopes* or *Sepia pharaonis* development, respectively, have thus been provided using x-ray micro–computed tomography (micro-CT) or magnetic resonance imaging (MRI) (*62*, *63*). Our squid specimens not only revealed individual projections of sensory cells in the retina (fig. S7, B and C) but also allowed us to record high-resolution image stacks reaching deep into the optic lobe. These recordings provided direct insight into the architecture of the optic lobe, including the meshwork of fiber tracts in the deep medulla (Fig. 3, D and E, and movie S6). Moreover, they revealed individual, fine fibers branching between these tracts (arrowheads in Fig. 3E) that are likely part of the tangential arborization of higher-order processing neurons identified in cephalopod squid and octopus lobe sections (*60*, *61*). Together, these results corroborate the versatility of the DEEP-Clear approach and its suitability to provide global and local insight into invertebrate nervous systems using light microscopy at unprecedented level.

Whole-mount deep-tissue labeling and imaging in postlarval vertebrates

For our further experiments in zebrafish, we deliberately used larger specimens of around 12 mm × 1 mm × 1 mm (3 to 5 weeks of age), which are characterized by strong body pigmentation, and exhibit a strongly melanized RPE. Specimens were depigmented and cleared as established above (Figs. 1, A and D and 4A). Even in anti-acetylated alpha-tubulin–stained specimens of around 6 and 12 mm in length, light-sheet analysis revealed labeling of both the central and peripheral nervous systems (Fig. 4, B and C, and movie S7). While the neuroanatomy of the adult zebrafish brain has already been characterized in detail using techniques such as histology (*64*) and super-resolution track density imaging (*65*), the characterization of eyes and cranial nerves has mainly been restricted to larval and early postlarval stages (*51*, *66*–*68*). As illustrated by a lateral view of the labeled juvenile head (Fig. 4B, inset, and movie S8), both eyes and cranial nerve branches, including the anterior lateral line system, can be well resolved in the DEEP-Clear–treated juveniles (Fig. 4B, inset), extending the stages accessible to these investigations. Likewise, we resolved the star-like arrangement of individual bundles of retinal ganglion cells whose projections exit the optic disk to form the optic nerve (Fig. 4B, inset). DEEP-Clear thus provides in-depth insight into retinal structures at stages that are traditionally hard to access by light microscopy due to the shielding effect of the RPE. As for bristle worms and squid, we also used DEEP-Clear in combination with additional antisera. Using an anti-serotonin antibody, we could visualize serotonergic cells in the retina, spinal cord, and raphe areas (Fig. 4C and movie S9). Likewise, anti–phosphohistone H3 immunolabeling revealed a number of putative mitotic cells across the juvenile head (Fig. 4D and movie S10).

Similar to zebrafish, analyses of the neuroanatomy of the axolotl have mainly been restricted to tissue sections (*52*) (https://msu.edu/course/zol/402/atlas/). After subjecting cleared juvenile specimens (Fig. 5A) to anti-TUBB3 immunohistochemistry, even large axolotl specimens (25 mm in length) allowed light-sheet visualization of deep tissue–labeled neurons (Fig. 5B and movie S11). This allowed us to acquire complete views of the axolotl nervous system (Fig. 5B), distinguish major regions of the axolotl brain and cranial nerves

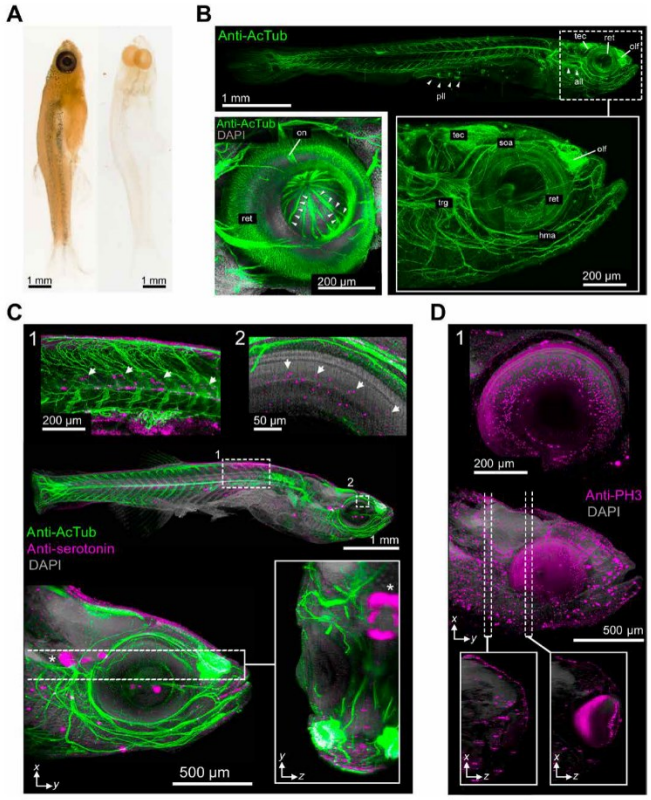

Fig. 4. DEEP-Clear–enabled analysis of the eyes and cranial nervous system of postlarval zebrafish. (**A**) Comparison of uncleared (left) and DEEP-Clear–processed (right) zebrafish juveniles. (**B** and **C**) Visualization of the nervous system using anti-AcTub immunohistochemistry (lateral views, anterior to right). (B) Light-sheet acquisition of central and peripheral nervous system (arrowheads indicating lateral line), with the right inset showing a close-up of the head. Left inset: confocal view of retina and bundles of retinal ganglion cells (arrowheads) exiting through the optic disk to form the optic nerve. (C) Light-sheet acquisition of a specimen colabeled by anti-serotonin immunohistochemistry. Magnifications in the top insets show serotonergic cells in (1) the spinal cord and (2) in the eye. The lower image shows a sagittal view of the head and a corresponding *YZ* slice (inset), with an asterisk close to serotonergic cells of the raphe area. (**D**) Sagittal view of a light-sheet–acquired juvenile head showing $PH3^+$ cells. Lower insets show *XZ* projections of the indicated areas, revealing PH3-labeled cells deep in the brain, inset (1) provides an enlarged view of the right eye. All, anterior lateral line; hma, hyomandibular arch; soa, supraorbital arch; tec, tectum; trg, trigeminal ganglion; olf, olfactory epithelium; on, optic nerve; pll, posterior lateral line. Photo credit: Marko Pende, Medical University of Vienna.

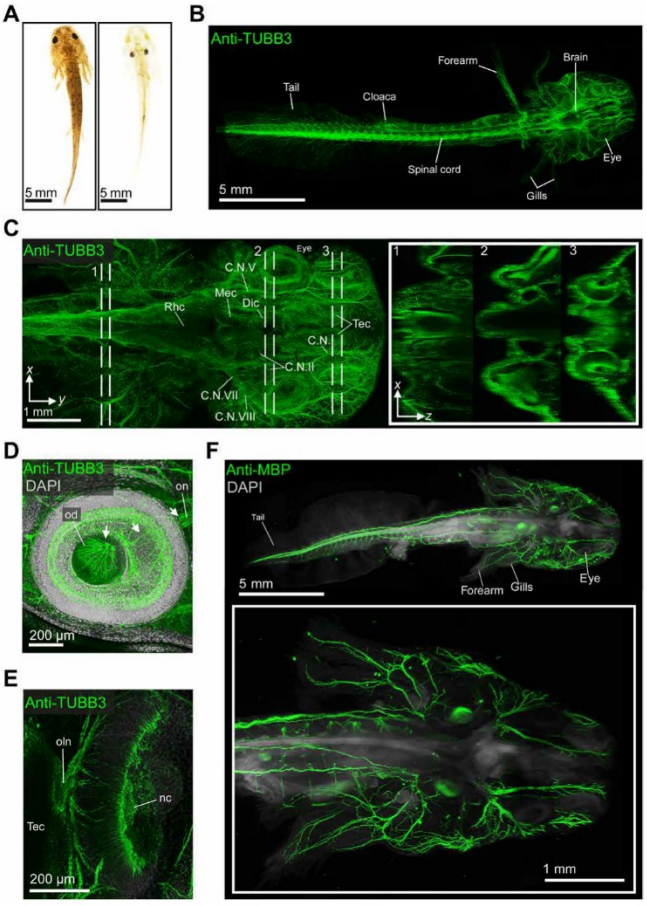

Fig. 5. Whole-body immunolabeling of the juvenile axolotl nervous system. (**A**) Comparison of uncleared (left) and DEEP-Clear–processed (right) axolotl juveniles (around 3 months of age). (**B** to **E**) DEEP-Clear–processed juveniles stained by anti–beta III tubulin (anti-TUBB3) to mark the nervous system. (B) Overview of the juvenile anatomy and nervous system in a DEEP-Clear–processed specimen imaged with light-sheet microscopy. (C) Close-up of the head region, revealing the major brain neuroanatomy and branches of the cranial nerves. The inset shows three *XZ* projections taken at the indicated positions. (D) Focus on the eye region of a specimen revealing the projection of retinal ganglion cells (arrows) through the optic disk to form the optic nerve. (E) Axolotl nose showing innervation of the olfactory nerve. (**F**) Labeling of central and peripheral nervous system using anti-MBP antibody and 4′,6-diamidino-2-phenylindole. Inset shows higher magnification of peripheral nerves. nc, nasal cavity; oln, olfactory nerve; od, optic disk; Rhc, rhombencephalon; Mec, mesencephalon; Dic, diencephalon; C.N., cranial nerve. Photo credit: Marko Pende, Medical University of Vienna

(Fig. 5C), and visualize the exiting of neurons through the optic disk, as in zebrafish (Fig. 5D), or the olfactory system (Fig. 5E and movie S12).

To further assess immunolabeling efficiency of large heterogeneous tissue, as well as preservation and accessibility of different cellular compartments, we performed analogous immunostainings with antibodies against the (i) intracellular membrane-associated myelin basic protein (MBP; Fig. 5F), (ii) acetylated tubulin (fig. S8A), (iii) myosin heavy chain (fig. S8B and movies S13 and S14), (iv) phosphorylated histone H3 (PH3; fig. S8C), and (v) the transcription factors sex-determining region Y-related high-mobility group box 9 (SOX9; fig. S8D) and paired-related homeobox protein 1 (PRRX1) (fig. S8, E and F). In all cases, our results were in line with the expected patterns. Anti-MBP immunohistochemistry highlighted presumptive oligodendrocytes and Schwann cells throughout the specimen and the spinal cord (Fig. 5F) (*51*). Similar to anti-TUBB3 (Fig. 5, B to E), anti-acetylated tubulin immunohistochemistry highlighted the overall neuroanatomy, along with additional small structures in the gills (fig. S8A) that likely reflect ciliated cells found to cover the external gills of amphibians (*69*). The transcription factors PRRX1 and SOX9 that we investigated in the context of the growing limb showed nuclear expression in the connective tissue and chondrocytes, respectively, in agreement with previous data (*70*–*72*), while anti-myosin heavy chain immunohistochemistry highlighted

skeletal musculature across the specimen. Together, these results provided direct evidence that DEEP-Clear processing is compatible with the labeling and imaging of epitopes across tissues and subcellular compartments, providing a versatile tool for future studies.

Compatibility with multiple active labeling approaches (IHC, RNA-FISH, and EdU)

In a last set of experiments, we assessed the compatibility of DEEP-Clear with two additional active labeling techniques: picolyl azide–based click chemistry and RNA in situ hybridization. For these experiments, we focused on the adult eyes of *P. dumerilii*, each of which has an everted, cup-shaped retina. A dense layer of pigments separates the outer segments of the photoreceptors from their basal parts. Like the retina of lower vertebrates (fishes and amphibians), the eye of *P. dumerilii* is known to grow continuously during the animal's lifetime, but the details of this growth have not been experimentally assessed yet. We therefore incubated adult animals for 24 hours in seawater supplemented with EdU, a thymidine analog labeling S phase nuclei, and then subjected them to DEEP-Clear. We combined the detection of EdU with in situ hybridization for *r-opsin1* expression, detected using a fluorescent tyramide–based amplification strategy (*73*). A part of these analyses was performed in the background of the aforementioned pMos{rops::egfp}^{vbci2} strain, allowing us to use EGFP as an independent marker. Cell proliferation was not only consistently detected in the medial brain (asterisks in Fig. 6, A to C) but also revealed within the eye cup (arrows in Fig. 6, D and E). In all tested immature animals and a subset of metamorphosing specimens, EdU-labeled cells were found in the area closest to the pupil, which is normally inaccessible to light microscopy. Our finding is consistent with the hypothesis that the worm retina extends by apposition of new photoreceptor cells along its marginal zone (*57*), similar to the ciliary marginal zone in teleosts (*74*).

The detection of *r-opsin1* transcripts in photoreceptors suggested that DEEP-Clear–processed specimens could be used to explore the expression of additional genes within eye photoreceptor cells, while that was previously impeded by the strong pigmentation of the eyes. We therefore performed analogous RNA in situ hybridizations with riboprobes against *gq*, a gene encoding a Gq alpha subunit that we previously found to be correlated with *r-opsin1*$^{+}$ cells in the trunk (*42*), and *tmdc/c2433*, a gene encoding an uncharacterized putative transmembrane protein that we recently identified as a candidate for the EGFP cell-specific transcriptome. Fluorescent detection of riboprobes, followed by DEEP-Clear processing, revealed that *gq*, as well as the previously unknown transcript *tmdc/c2433*, was clearly localized to the four adult eyes of the worm, similar to *r-opsin1* transcripts (Fig. 6F). This result confirms *gq* and *tmdc/c2433* as parts of the eye photoreceptor signature and provides proof of concept for the compatibility of DEEP-Clear with systematic in situ hybridization assays. We independently confirmed this compatibility also in the zebrafish using a riboprobe directed against a melanopsin gene (*opn4.1*) expressed in the 6 dpf larval eye. Our results in the fish reproduce the previously reported expression of this gene in horizontal and some photoreceptor cells (*75*, *76*) using the tyramide signal amplification (TSA)/Cy3 detection method bypassing the need to perform stainings on tissue sections (fig. S9). Together, these results support that DEEP-Clear can be readily combined with RNA in situ hybridization and thus a technique that is broadly used not only in standard developmental model species but also typically by researchers exploring new and unconventional models.

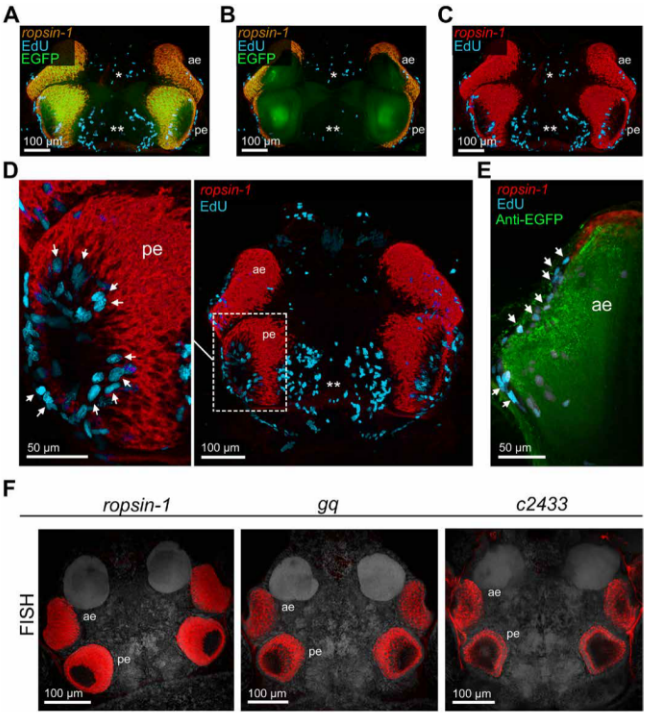

Fig. 6. Retinal growth patterns and molecular signatures of annelid eye photoreceptors. (**A** to **C**) Codetection of incorporated EdU (magenta), riboprobes against *ropsin-1* (overlay with EGFP is yellow, and pure signal is red), and EGFP (green) in premature pMos{rops::egfp}^{vbci2} bristle worms. Single and double asterisks indicate regions of cell proliferation in the anterior and posterior ganglionic region, respectively. (**D** and **E**) Similar codetection of EdU (magenta), *ropsin-1* (red), and EGFP epitopes (green), including close-ups of the posterior (D, left) and anterior (E) eye region. Arrows point to the proliferative cells in either eye. (**F**) Fluorescent detection of riboprobes against *ropsin-1* (left), *gq* (middle), and *tmdc/c2433* (right) in comparative RNA whole-mount hybridizations, revealing expression of all three genes in eye photoreceptors of the worm head. All dorsal views, anterior to the top. ae, anterior eye; pe, posterior eye.

DISCUSSION

DEEP-Clear provides a novel, tailored clearing method that harnesses different strategies to remove distinct classes of poorly soluble pigments—including pterins, heme, ommochromes, carotenoids, and melanin—that are abundant in many animal tissues and across phyla. It effectively combines elements and reagents from protocols that have previously been categorized as either organic solvent– or hydrophilic reagent–based approaches (*13*, *33*). This combination has synergistic effects, both by advancing depigmentation speed and removing pigments of different nature, thus shortening the overall time required for all clearing steps of DEEP-Clear in the targeted species to few hours, even for specimens that measure several centimeters in length. This synergy likely reduces the risks posed by extensive detergent, urea (*32*), and peroxide exposure. A possible limitation of the applicability of DEEP-Clear is thick bone structures, for which dehydration-based whole mouse clearing approaches offer solutions (*18*, *20*). However, these techniques tend to compromise tissue morphology through unavoidable anisotropic shrinkage.

A second aspect that makes DEEP-Clear attractive for a broad use is its applicability to reference species of four distinct, species-rich animal clades. The removal of poorly soluble pigments eliminates a long-standing obstacle for the use of clearing, labeling, and

imaging approaches outside the context of lowly pigmented structures like mouse brains, where clearing approaches have been most regularly used. The removal of melanin required peroxide treatment, generally known to cause tissue damage and loss of endogenous fluorophore signal. However, the short peroxide incubation times, which are facilitated by the aforementioned synergistic effects of the other clearing chemicals, as well as the possibility of relabeling bleached fluorescent proteins by IHC, represent suitable solutions. Therefore, DEEP-Clear provides imaging access to diverse tissues and organs that are shielded by natural pigmentation. Our work exemplifies this most directly for the analysis of visual systems across all investigated clades. These usually require researchers to label and image individual tissue sections, followed by reconstruction of their three-dimensional (3D) structures. DEEP-Clear bypasses the need for this time-consuming process by providing direct whole-mount access to these structures that favors easier analysis and higher throughput. Whereas we focused our analysis on nervous system aspects, DEEP-Clear also paves the way for other levels of analysis in the presented clades, such as bacterial symbiosis and bioluminescence, a fundamental postlarval event in squids (*77*, *78*).

A third feature that makes DEEP-Clear attractive as a versatile toolbox is its compatibility with a panel of active molecular labeling techniques. Whereas fluorescent reporters (detected either directly or using IHC relabeling in peroxide-treated samples) require the ability of prior genetic manipulation, the compatibility of DEEP-Clear with immunohistochemistry provides direct benefits for the exploration of a broad panel of target organisms. Provided that suitable immunolabeling conditions are established, DEEP-Clear processing, combined with immunohistochemistry, can reveal structural features ranging from the tissue level (e.g., the architecture of the cephalopod optic lobe) down to subcellular structures such as presynaptic vesicles. Although tissue clearing relies on delipidation, we find membrane-associated epitopes such as MBP or synaptophysin EGFP to remain detectable, likely due to initial cross-linking. The possibility to label and image specific molecular features throughout a specimen distinguishes DEEP-Clear from label-free techniques such as x-ray micro-CT and MRI that have been used for imaging the nervous system of different cephalopod species (*62*, *63*) and the adult zebrafish brain (*65*).

Compatibility with the detection of RNAs in intact tissues has been rather neglected in the development of current clearing protocols (*34*), with the exception of the 2ECi protocol (*21*), and the CLARITY (*32*) and SWITCH (*79*) methods. Unlike immunohistochemistry, which requires the availability of high-affinity antibodies for any given target, suitable riboprobes for in situ hybridization can be generated at low costs and for any gene identified in the respective species. DEEP-Clear will thus be applicable to explore gene expression patterns in new model systems and validate cellular fingerprints obtained by single-cell transcriptomics. The additional compatibility of DEEP-Clear with the detection of proliferative cells (EdU and picolyl azide–based click chemistry) opens possibilities for studying regeneration and development, an area that is directly relevant for three of the investigated model species (*21*, *71*, *80*, *81*).

Last, beyond providing optical access to specific tissues and organs, DEEP-Clear also generates substantial potential for whole-animal analyses, provided that fixation conditions retain tissue integrity and that deep penetrance of labels is not prevented (e.g., by titration of antibodies by abundant epitopes at the periphery of specimens). In our experiments, we could observe deep immunolabeling even in large specimens for epitopes of different protein classes, for different subcellular localization (nuclear, membrane-associated, and cytoplasmic), for two major fixation techniques (Bouin's fixative and PFA), and throughout different body structures. On the acquisition side, the removal of diverse pigments and the high level of overall transparency make DEEP-Clear–processed specimens compatible with advanced light-sheet microscopy. This imaging technique allowed us to capture 3D images of specimens with a thickness of close to 6000 μm and a length of several centimeters, pushing the size limits imposed by regular confocal analysis. Likewise, it offers substantially faster acquisition times and lower data amounts, by passing, or at least strongly limiting, the need to stitch many different acquisitions as they would be generated using separate confocal datasets from different parts of large specimens. Taken together, the speed and broad compatibility of DEEP-Clear remove existing restrictions in the use of tissue clearing and imaging approaches beyond more selective contexts and thereby provides a powerful tool for the exploration of novel model systems across scales.

MATERIALS AND METHODS

Animals

Mouse (Mus musculus)

Thy1-YFP-H mice (*82*) were bred and kept at the animal care center of the Medical University, Vienna. All experiments and animal handling were carried out in compliance with Austrian ethical guidelines.

Bristle worm (P. dumerilii)

Wild-type and pMos{rops::egfp}^{vbci2} worms were raised at temperatures between 18° and 20°C and kept in a 16:8-hour light-dark (LD) cycle. Animals were anesthetized using 7.5% $MgCl_2$ (50%) (Roth, A537.1) and artificial seawater (50%) before fixation. All experiments and animal handling were carried out in compliance with Austrian ethical guidelines.

Hawaiian bobtail squid (E. scolopes) and longfin inshore squid (Doryteuthis pealeii)

Squid eggs were obtained from cultures from S. Nyholm (Department of Molecular and Cell Biology, University of Connecticut, Storrs, USA) and J. Foster (University of Florida, Space Life Science Lab, Merritt Island, USA). The Marine Biological Laboratory's Cephalopod Breeding Initiative (Woods Hole, Massachusetts, USA, affiliated to University of Chicago) provided laboratory-reared specimens that were fixed on site. Egg clutches were shipped in well-oxygenated water to Vienna Schönbrunn Zoo. Eggs were kept in 26° to 27°C warm tanks at 12:12-hour LD cycles at the aquarium facility of the zoo. Live animals were maintained in accordance with the European general guidelines for cephalopod care and welfare (*83*).

Zebrafish (D. rerio)

Wild-type, *brn3c:mGFP*, and *HuC::Gal4; UAS::syp-GFP* fish were raised at 28°C and kept in a 16:8- or 14:10-hour LD cycle. All experiments and animal handling were carried out as per the local Austrian and European ethical guidelines (approved animal protocols GZ: 342445/2016/12 and GZ: BMWFW-66.006/0012-WF/II/3b/2014). Animals were anesthetized using 0.2 to 0.3% tricaine (abcr GmbH, AB142950) before fixation.

Axolotl (A. mexicanum)

Axolotls were raised at 20°C and kept in a 12:12-hour LD cycle. Husbandry followed established standards (*84*). Animals were anesthetized in 0.03% benzocaine (Sigma-Aldrich, E1501) before sacrifice. All experiments and animal handling were carried out as

per the local Austrian and European ethical guidelines (approved animal protocol GZ: 9418/2017/12).

Solutions

Marine phosphate-buffered saline (PBS) consists of 50 mM sodium phosphate buffer with 0.5 M NaCl diluted in dH_2O (pH 7.4). Solution-1 consists of 8 to 10% (v/v) THEED (Sigma-Aldrich, 87600-100ML), 5% (v/v) Triton X-100 (Roth, 3051.2), and 25% (w/v) urea (Roth, X999.2) in dH_2O, e.g., 4 to 5 ml of THEED, 2.5 ml of Triton X-100, and 12.5 g of urea filled up to 50 ml with dH_2O. Solution-1.1 consists of 8 to 10% (v/v) THEED (Sigma-Aldrich, 87600-100ML), 5% (v/v) Triton X-100 (Roth, 3051.2), and 5% (w/v) urea (Roth, X999.2) in dH_2O. For Solution-2, a 50% (w/w) meglumine diatrizoate (Sigma-Aldrich, M5266) solution in PBS (pH 9 to 9.3; e.g., 10 g of meglumine diatrizoate added to 10 ml of PBS) was adjusted to an RI of 1.45 by further adding of meglumine diatrizoate. Solution-2.1 was prepared by mixing four parts of Solution-2 with one part of VECTASHIELD (Vector laboratories, H-1000). For Solution-2.2, 11 g of meglumine diatrizoate was added to 9 ml of PBS (pH 9 to 9.3) supplemented with 2 g of antipyrine (Sigma-Aldrich, A5882-100G) and 0.8 g of *N′*-methylnicotinamide (Santa Cruz Biotechnology, sc-295821A), with an RI adjusted to 1.48.

DEEP-Clear protocol and its combination with other techniques

Details on cloning, the detailed DEEP-Clear protocol in different clades, the combination of DEEP-Clear with immunostaining, and the combination of DEEP-Clear with RNA in situ hybridization and EdU labeling are listed in Supplementary Material and Methods.

Assessing the effect of solutions and comparison with established methods

For details on the assessment of the impact of acetone and for comparison with established techniques, see Supplementary Material and Methods.

Imaging and image processing

For details on light-sheet microscopy, fluorescence stereomicroscopy, laser-scanning confocal and two-photon microscopy, and image processing, see Supplementary Material and Methods.

Qualitative and quantitative assessments and statistical analyses

For quantification of the impact of acetone on depigmentation speed, the quantification of fluorescence signal stability, the qualitative and quantitative assessment of transparency, assessment of contrast, and quantification of signal transmission, see Supplementary Material and Methods.

SUPPLEMENTARY MATERIALS

Supplementary material for this article is available at http://advances.sciencemag.org/cgi/content/full/6/22/eaba0365/DC1

View/request a protocol for this paper from *Bio-protocol*.

REFERENCES AND NOTES

1. J. Bolker, Model organisms: There's more to life than rats and flies. *Nature* **491**, 31–33 (2012).
2. E. A. Brenowitz, H. H. Zakon, Emerging from the bottleneck: Benefits of the comparative approach to modern neuroscience. *Trends Neurosci.* **38**, 273–278 (2015).
3. K. Tessmar-Raible, D. Arendt, New animal models for evolution and development. *Genome Biol.* **6**, 303 (2005).
4. G. Warren, In praise of other model organisms. *J. Cell Biol.* **208**, 387–389 (2015).
5. K. Achim, J.-B. Pettit, L. R. Saraiva, D. Gavriouchkina, T. Larsson, D. Arendt, J. C. Marioni, High-throughput spatial mapping of single-cell RNA-seq data to tissue of origin. *Nat. Biotechnol.* **33**, 503–509 (2015).
6. C. B. Albertin, O. Simakov, T. Mitros, Z. Y. Wang, J. R. Pungor, E. Edsinger-Gonzales, S. Brenner, C. W. Ragsdale, D. S. Rokhsar, The octopus genome and the evolution of cephalopod neural and morphological novelties. *Nature* **524**, 220–224 (2015).
7. C. E. Cook, J. Chenevert, T. A. Larsson, D. Arendt, E. Houliston, P. Lénárt, Old knowledge and new technologies allow rapid development of model organisms. *Mol. Biol. Cell* **27**, 882–887 (2016).
8. N. Liscovitch-Brauer, S. Alon, H. T. Porath, B. Elstein, R. Unger, T. Ziv, A. Admon, E. Y. Levanon, J. J. C. Rosenthal, E. Eisenberg, Trade-off between transcriptome plasticity and genome evolution in cephalopods. *Cell* **169**, 191–202.e11 (2017).
9. L. L. Moroz, A. B. Kohn, Single-neuron transcriptome and methylome sequencing for epigenomic analysis of aging. *Methods Mol. Biol.* **1048**, 323–352 (2013).
10. K. Belhaj, A. Chaparro-Garcia, S. Kamoun, N. J. Patron, V. Nekrasov, Editing plant genomes with CRISPR/Cas9. *Curr. Opin. Biotechnol.* **32**, 76–84 (2015).
11. A. F. Gilles, M. Averof, Functional genetics for all: Engineered nucleases, CRISPR and the gene editing revolution. *EvoDevo* **5**, 43 (2014).
12. J. D. Sander, J. K. Joung, CRISPR-Cas systems for editing, regulating and targeting genomes. *Nat. Biotechnol.* **32**, 347–355 (2014).
13. K. Tainaka, A. Kuno, S. I. Kubota, T. Murakami, H. R. Ueda, Chemical principles in tissue clearing and staining protocols for whole-body cell profiling. *Annu. Rev. Cell Dev. Biol.* **32**, 713–741 (2016).
14. H.-U. Dodt, U. Leischner, A. Schierloh, N. Jährling, C. P. Mauch, K. Deininger, J. M. Deussing, M. Eder, W. Zieglgänsberger, K. Becker, Ultramicroscopy: Three-dimensional visualization of neuronal networks in the whole mouse brain. *Nat. Methods* **4**, 331–336 (2007).
15. K. Becker, N. Jährling, S. Saghafi, R. Weiler, H. U. Dodt, Chemical clearing and dehydration of GFP expressing mouse brains. *PLOS ONE* **7**, e33916 (2012).
16. A. Ertürk, K. Becker, N. Jährling, C. P. Mauch, C. D. Hojer, J. G. Egen, F. Hellal, F. Bradke, M. Sheng, H.-U. Dodt, Three-dimensional imaging of solvent-cleared organs using 3DISCO. *Nat. Protoc.* **7**, 1983–1995 (2012).
17. N. Renier, Z. Wu, D. J. Simon, J. Yang, P. Ariel, M. Tessier-Lavigne, iDISCO: A simple, rapid method to immunolabel large tissue samples for volume imaging. *Cell* **159**, 896–910 (2014).
18. C. Pan, R. Cai, F. P. Quacquarelli, A. Ghasemigharagoz, A. Lourbopoulos, P. Matryba, N. Plesnila, M. Dichgans, F. Hellal, A. Ertürk, Shrinkage-mediated imaging of entire organs and organisms using uDISCO. *Nat. Methods* **13**, 859–867 (2016).
19. C. Hahn, K. Becker, S. Saghafi, M. Pende, A. Avdibašić, M. Foroughipour, D. E. Heinz, C. T. Wotjak, H.-U. Dodt, High-resolution imaging of fluorescent whole mouse brains using stabilised organic media (sDISCO). *J. Biophotonics* **12**, e201800368 (2019).
20. D. Jing, S. Zhang, W. Luo, X. Gao, Y. Men, C. Ma, X. Liu, Y. Yi, A. Bugde, B. O. Zhou, Z. Zhao, Q. Yuan, J. Q. Feng, L. Gao, W.-P. Ge, H. Zhao, Tissue clearing of both hard and soft tissue organs with the PEGASOS method. *Cell Res.* **28**, 803–818 (2018).
21. W. Masselink, D. Reumann, P. Murawala, P. Pasierbek, Y. Taniguchi, F. Bonnay, K. Meixner, J. A. Knoblich, E. M. Tanaka, Broad applicability of a streamlined ethyl cinnamate-based clearing procedure. *Development* **146**, dev166884 (2019).
22. T. Kuwajima, A. A. Sitko, P. Bhansali, C. Jurgens, W. Guido, C. Mason, *Clear*^{T}: a detergent- and solvent-free clearing method for neuronal and non-neuronal tissue. *Development* **140**, 1364–1368 (2013).
23. T. Yu, J. Zhu, Y. Li, Y. Ma, J. Wang, X. Cheng, S. Jin, Q. Sun, X. Li, H. Gong, Q. Luo, F. Xu, S. Zhao, D. Zhu, RTF: A rapid and versatile tissue optical clearing method. *Sci. Rep.* **8**, 1964 (2018).
24. T. C. Murakami, T. Mano, S. Saikawa, S. A. Horiguchi, D. Shigeta, K. Baba, H. Sekiya, Y. Shimizu, K. F. Tanaka, H. Kiyonari, M. Iino, H. Mochizuki, K. Tainaka, H. R. Ueda, A three-dimensional single-cell-resolution whole-brain atlas using CUBIC-X expansion microscopy and tissue clearing. *Nat. Neurosci.* **21**, 625–637 (2018).
25. E. A. Susaki, K. Tainaka, D. Perrin, F. Kishino, T. Tawara, T. M. Watanabe, C. Yokoyama, H. Onoe, M. Eguchi, S. Yamaguchi, T. Abe, H. Kiyonari, Y. Shimizu, A. Miyawaki, H. Yokota, H. R. Ueda, Whole-brain imaging with single-cell resolution using chemical cocktails and computational analysis. *Cell* **157**, 726–739 (2014).
26. E. A. Susaki, K. Tainaka, D. Perrin, H. Yukinaga, A. Kuno, H. R. Ueda, Advanced CUBIC protocols for whole-brain and whole-body clearing and imaging. *Nat. Protoc.* **10**, 1709–1727 (2015).
27. K. Tainaka, T. C. Murakami, E. A. Susaki, C. Shimizu, R. Saito, K. Takahashi, A. Hayashi-Takagi, H. Sekiya, Y. Arima, S. Nojima, M. Ikemura, T. Ushiku, Y. Shimizu, M. Murakami, K. F. Tanaka, M. Iino, H. Kasai, T. Sasaoka, K. Kobayashi, K. Miyazono, E. Morii, T. Isa, M. Fukayama, A. Kakita, H. R. Ueda, Chemical landscape for tissue clearing based on hydrophilic reagents. *Cell Rep.* **24**, 2196–2210.e9 (2018).

28. H. Hama, H. Kurokawa, H. Kawano, R. Ando, T. Shimogori, H. Noda, K. Fukami, A. Sakaue-Sawano, A. Miyawaki, Scale: A chemical approach for fluorescence imaging and reconstruction of transparent mouse brain. *Nat. Neurosci.* **14**, 1481–1488 (2011).
29. H. Hama, H. Hioki, K. Namiki, T. Hoshida, H. Kurokawa, F. Ishidate, T. Kaneko, T. Akagi, T. Saito, T. Saido, A. Miyawaki, ScaleS: An optical clearing palette for biological imaging. *Nat. Neurosci.* **18**, 1518–1529 (2015).
30. M.-T. Ke, S. Fujimoto, T. Imai, SeeDB: A simple and morphology-preserving optical clearing agent for neuronal circuit reconstruction. *Nat. Neurosci.* **16**, 1154–1161 (2013).
31. M.-T. Ke, Y. Nakai, S. Fujimoto, R. Takayama, S. Yoshida, T. S. Kitajima, M. Sato, T. Imai, Super-resolution mapping of neuronal circuitry with an index-optimized clearing agent. *Cell Rep.* **14**, 2718–2732 (2016).
32. K. Chung, J. Wallace, S.-Y. Kim, S. Kalyanasundaram, A. S. Andalman, T. J. Davidson, J. J. Mirzabekov, K. A. Zalocusky, J. Mattis, A. K. Denisin, S. Pak, H. Bernstein, C. Ramakrishnan, L. Grosenick, V. Gradinaru, K. Deisseroth, Structural and molecular interrogation of intact biological systems. *Nature* **497**, 332–337 (2013).
33. B. Yang, J. B. Treweek, R. P. Kulkarni, B. E. Deverman, C.-K. Chen, E. Lubeck, S. Shah, L. Cai, V. Gradinaru, Single-cell phenotyping within transparent intact tissue through whole-body clearing. *Cell* **158**, 945–958 (2014).
34. R. J. Vigouroux, M. Belle, A. Chédotal, Neuroscience in the third dimension: Shedding new light on the brain with tissue clearing. *Mol. Brain* **10**, 33 (2017).
35. G. Shamim, S. K. Ranjan, D. M. Pandey, R. Ramani, Biochemistry and biosynthesis of insect pigments. *Eur. J. Entomol.* **111**, 149–164 (2014).
36. F. Figon, J. Casas, Ommochromes in invertebrates: Biochemistry and cell biology. *Biol. Rev. Camb. Philos. Soc.* **94**, 156–183 (2018).
37. A. Konno, S. Okazaki, Aqueous-based tissue clearing in crustaceans. *Zool. Lett.* **4**, 13 (2018).
38. Y. Henning, C. Osadnik, E. P. Malkemper, EyeCi: Optical clearing and imaging of immunolabeled mouse eyes using light-sheet fluorescence microscopy. *Exp. Eye Res.* **180**, 137–145 (2019).
39. M. Pende, K. Becker, M. Wanis, S. Saghafi, R. Kaur, C. Hahn, N. Pende, M. Foroughipour, T. Hummel, H.-U. Dodt, High-resolution ultramicroscopy of the developing and adult nervous system in optically cleared *Drosophila melanogaster*. *Nat. Commun.* **9**, 4731 (2018).
40. M. Viscontini, W. Hummel, A. Fischer, Pigmente von Nereiden (*Annelida*, Polychaeten). 1., Vorläufige Mitteilung. Isolierung von Pterindimeren aus den Augen von *Platynereis dumerilii* (*Audouin & Milne Edwards*) 1833. *Helvetica Chimica Acta* **53**, 1207–1209 (1970).
41. C. Hauenschild, A. Fischer, *Großes Zoologisches Praktikum* (Gustav Fischer, 1969).
42. B. Backfisch, V. B. Veedin Rajan, R. M. Fischer, C. Lohs, E. Arboleda, K. Tessmar-Raible, F. Raible, Stable transgenesis in the marine annelid *Platynereis dumerilii* sheds new light on photoreceptor evolution. *Proc. Natl. Acad. Sci. U.S.A.* **110**, 193–198 (2013).
43. T. Xiao, T. Roeser, W. Staub, H. Baier, A GFP-based genetic screen reveals mutations that disrupt the architecture of the zebrafish retinotectal projection. *Development* **132**, 2955–2967 (2005).
44. C. M. Niell, M. P. Meyer, S. J. Smith, In vivo imaging of synapse formation on a growing dendritic arbor. *Nat. Neurosci.* **7**, 254–260 (2004).
45. M. P. Meyer, S. J. Smith, Evidence from in vivo imaging that synaptogenesis guides the growth and branching of axonal arbors by two distinct mechanisms. *J. Neurosci.* **26**, 3604–3614 (2006).
46. D. Arendt, K. Tessmar, M.-I. Medeiros de Campos-Baptista, A. Dorresteijn, J. Wittbrodt, Development of pigment-cup eyes in the polychaete *Platynereis dumerilii* and evolutionary conservation of larval eyes in Bilateria. *Development* **129**, 1143–1154 (2002).
47. G. Piperno, M. T. Fuller, Monoclonal antibodies specific for an acetylated form of alpha-tubulin recognize the antigen in cilia and flagella from a variety of organisms. *J. Cell Biol.* **101**, 2085–2094 (1985).
48. S. Shigeno, M. Yamamoto, Organization of the nervous system in the pygmy cuttlefish, *Idiosepius paradoxus* Ortmann (Idiosepiidae, Cephalopoda). *J. Morphol.* **254**, 65–80 (2002).
49. R. T. Williams, J. W. Bridges, Fluorescence of solutions: A review. *J. Clin. Pathol.* **17**, 371–394 (1964).
50. L. Bally-Cuif, P. Vernier, in *Fish Physiology*, S. F. Perry, M. Ekker, A. P. Farrell, C. J. Brauner, Eds. (Academic Press, 2010), vol. 29, pp. 25–80.
51. C. Brösamle, M. E. Halpern, Nogo–Nogo receptor signalling in PNS axon outgrowth and pathfinding. *Mol. Cell. Neurosci.* **40**, 401–409 (2009).
52. R. Amamoto, V. G. L. Huerta, E. Takahashi, G. Dai, A. K. Grant, Z. Fu, P. Arlotta, Adult axolotls can regenerate original neuronal diversity in response to brain injury. *eLife* **5**, e13998 (2016).
53. M. K. Lee, J. B. Tuttle, L. I. Rebhun, D. W. Cleveland, A. Frankfurter, The expression and posttranslational modification of a neuron-specific beta-tubulin isotype during chick embryogenesis. *Cell Motil. Cytoskeleton* **17**, 118–132 (1990).
54. L. McHedlishvili, H. H. Epperlein, A. Telzerow, E. M. Tanaka, A clonal analysis of neural progenitors during axolotl spinal cord regeneration reveals evidence for both spatially restricted and multipotent progenitors. *Development* **134**, 2083–2093 (2007).
55. T. Bullock, G. A. Horridge, *Structure and Function in the Nervous Systems of Invertebrates* (San Francisco, Freeman, 1965).
56. A. Fischer, On the structure and light-dark adaptation of eyes of the polychaete *Platynereis dumerilii*. *Z. Zellforsch. Mikrosk. Anat* **61**, 338–353 (1963).
57. A. Fischer, J. Brökelmann, The eye of *Platynereis dumerilii* (Polychaeta): its fine structure in ontogenetic and adaptive change. *Z. Zellforsch. Mikrosk. Anat.* **71**, 217–244 (1966).
58. D. K. Hofmann, Regeneration and endocrinology in the polychaete *Platynereis dumerilii*: An experimental and structural study. *Wilhelm Roux. Arch. Dev. Biol.* **180**, 47–71 (1976).
59. D. Verduzco, J. F. Amatruda, Analysis of cell proliferation, senescence, and cell death in zebrafish embryos. *Methods Cell Biol.* **101**, 19–38 (2011).
60. J. Z. Young, Regularities in the retina and optic lobes of octopus in relation to form discrimination. *Nature* **186**, 836–839 (1960).
61. J. Z. Young, The central nervous system of *Loligo*. I. The optic lobe. *Philos. Trans. R. Soc. B* **267**, 263–302 (1974).
62. A. Kerbl, S. Handschuh, M.-T. Nödl, B. Metscher, M. Walzl, A. Wanninger, Micro-CT in cephalopod research: Investigating the internal anatomy of a sepiolid squid using a non-destructive technique with special focus on the ganglionic system. *J. Exp. Mar. Biol. Ecol.* **447**, 140–148 (2013).
63. Y.-C. Liu, T.-H. Liu, C.-H. Su, C.-C. Chiao, Neural organization of the optic lobe changes steadily from late embryonic stage to adulthood in cuttlefish *Sepia pharaonis*. *Front. Physiol.* **8**, 538 (2017).
64. M. F. Wullimann, B. Rupp, H. Reichert, *Neuroanatomy of the Zebrafish Brain* (Birkhäuser, 1996).
65. J. F. P. Ullmann, F. Calamante, S. P. Collin, D. C. Reutens, N. D. Kurniawan, Enhanced characterization of the zebrafish brain as revealed by super-resolution track-density imaging. *Brain Struct. Funct.* **220**, 457–468 (2015).
66. S.-i. Higashijima, Y. Hotta, H. Okamoto, Visualization of cranial motor neurons in live transgenic zebrafish expressing green fluorescent protein under the control of the *islet*-1 promoter/enhancer. *J. Neurosci.* **20**, 206–218 (2000).
67. J. Icha, C. Kunath, M. Rocha-Martins, C. Norden, Independent modes of ganglion cell translocation ensure correct lamination of the zebrafish retina. *J. Cell Biol.* **215**, 259–275 (2016).
68. Y. Wan, A. D. Almeida, S. Rulands, N. Chalour, L. Muresan, Y. Wu, B. D. Simons, J. He, W. A. Harris, The ciliary marginal zone of the zebrafish retina: Clonal and time-lapse analysis of a continuously growing tissue. *Development* **143**, 1099–1107 (2016).
69. M. Nokhbatolfoghahai, J. R. Downie, The external gills of anuran amphibians: Comparative morphology and ultrastructure. *J. Morphol.* **269**, 1197–1213 (2008).
70. J. D. Currie, A. Kawaguchi, R. M. Traspas, M. Schuez, O. Chara, E. M. Tanaka, Live imaging of axolotl digit regeneration reveals spatiotemporal choreography of diverse connective tissue progenitor pools. *Dev. Cell* **39**, 411–423 (2016).
71. T. Gerber, P. Murawala, D. Knapp, W. Masselink, M. Schuez, S. Hermann, M. Gac-Santel, S. Nowoshilow, J. Kageyama, S. Khattak, J. D. Currie, J. Gray Camp, E. M. Tanaka, B. Treutlein, Single-cell analysis uncovers convergence of cell identities during axolotl limb regeneration. *Science* **362**, eaaq0681 (2018).
72. E. Nacu, E. Gromberg, C. R. Oliveira, D. Drechsel, E. M. Tanaka, FGF8 and SHH substitute for anterior-posterior tissue interactions to induce limb regeneration. *Nature* **533**, 407–410 (2016).
73. K. Tessmar-Raible, P. R. H. Steinmetz, H. Snyman, M. Hassel, D. Arendt, Fluorescent two-color whole mount in situ hybridization in *Platynereis dumerilii* (Polychaeta, Annelida), an emerging marine molecular model for evolution and development. *BioTechniques* **39**, 460–464 (2005).
74. P. R. Johns, Growth of the adult goldfish eye. III. Source of the new retinal cells. *J. Comp. Neurol.* **176**, 343–357 (1977).
75. W. I. Davies, L. Zheng, S. Hughes, T. Katherine Tamai, M. Turton, S. Halford, R. G. Foster, D. Whitmore, M. W. Hankins, Functional diversity of melanopsins and their global expression in the teleost retina. *Cell. Mol. Life Sci.* **68**, 4115–4132 (2011).
76. V. Matos-Cruz, J. Blasic, B. Nickle, P. R. Robinson, S. Hattar, M. E. Halpern, Unexpected diversity and photoperiod dependence of the zebrafish melanopsin system. *PLOS ONE* **6**, e25111 (2011).
77. M. McFall-Ngai, Hawaiian bobtail squid. *Curr. Biol.* **18**, R1043–R1044 (2008).
78. S. V. Nyholm, M. J. McFall-Ngai, The winnowing: Establishing the squid-*vibrio* symbiosis. *Nat. Rev. Microbiol.* **2**, 632–642 (2004).
79. E. Murray, J. H. Cho, D. Goodwin, T. Ku, J. Swaney, S.-Y. Kim, H. Choi, Y.-G. Park, J.-Y. Park, A. Hubbert, M. McCue, S. Vassallo, N. Bakh, M. P. Frosch, V. J. Wedeen, H. S. Seung, K. Chung, Scalable proteomic imaging for high-dimensional profiling of intact systems. *Cell.* **163**, 1500–1514 (2015).

80. C.-H. Chen, K. D. Poss, Regeneration genetics. *Annu. Rev. Genet.* **51**, 63–82 (2017).
81. E. Gazave, J. Béhague, L. Laplane, A. Guillou, L. Préau, A. Demilly, G. Balavoine, M. Vervoort, Posterior elongation in the annelid *Platynereis dumerilii* involves stem cells molecularly related to primordial germ cells. *Dev. Biol.* **382**, 246–267 (2013).
82. G. Feng, R. H. Mellor, M. Bernstein, C. Keller-Peck, Q. T. Nguyen, M. Wallace, J. M. Nerbonne, J. W. Lichtman, J. R. Sanes, Imaging neuronal subsets in transgenic mice expressing multiple spectral variants of GFP. *Neuron* **28**, 41–51 (2000).
83. G. Fiorito, A. Affuso, J. Basil, A. Cole, P. de Girolamo, L. D'Angelo, L. Dickel, C. Gestal, F. Grasso, M. Kuba, F. Mark, D. Melillo, D. Osorio, K. Perkins, G. Ponte, N. Shashar, D. Smith, J. Smith, P. L. R. Andrews, Guidelines for the care and welfare of cephalopods in research –A consensus based on an initiative by CephRes, FELASA and the Boyd Group, FELASA and the Boyd Group. *Lab. Anim.* **49**, 1–90 (2015).
84. S. Khattak, P. Murawala, H. Andreas, V. Kappert, M. Schuez, T. Sandoval-Guzmán, K. Crawford, E. M. Tanaka, Optimized axolotl (*Ambystoma mexicanum*) husbandry, breeding, metamorphosis, transgenesis and tamoxifen-mediated recombination. *Nat. Protoc.* **9**, 529–540 (2014).
85. K. Becker, S. Saghafi, M. Pende, I. Sabdyusheva-Litschauer, C. M. Hahn, M. Foroughipour, N. Jährling, H.-U. Dodt, Deconvolution of light sheet microscopy recordings. *Sci. Rep.* **9**, 17625 (2019).
86. I. Costantini, J.-P. Ghobril, A. P. Di Giovanna, A. L. A. Mascaro, L. Silvestri, M. C. Müllenbroich, L. Onofri, V. Conti, F. Vanzi, L. Sacconi, R. Guerrini, H. Markram, G. Iannello, F. S. Pavone, A versatile clearing agent for multi-modal brain imaging. *Sci. Rep.* **5**, 9808 (2015).

Acknowledgments: We would like to acknowledge the following colleagues for providing help, input, or reagents: S. Nyholm (Department of Molecular and Cell Biology, University of Connecticut, Storrs, USA); J. Foster (University of Florida, Space Life Science Lab, Merritt Island, USA); The Marine Biological Laboratory's Cephalopod Breeding Initiative (Woods Hole, Massachusetts, USA; affiliated to University of Chicago); A. Weissenbacher (Tiergarten Schönbrunn, Vienna); M. Wullimann (LMU, Munich); W. Haubensak, D. Keays, G. Nordmann, S. Nimpf, E. P. Malkemper, L. Landler, T. Hochstoeger, A. Pauli, K. Panser, and members of Elly Tanaka laboratory [Research Institute of Molecular Pathology (IMP), Vienna], T. Lendl and K. Aumayr (IMP/IMBA/GMI Biooptics Facility); J. Knoblich, D. Reumann, S. Bian, F. Bonnay, J. Sidhaye, O. Wueseke, J. Penninger, M. Orthofer, and M. Onji (Institute of Molecular Biotechnology/IMBA, Vienna); M. Borysova and A. Belokurov (Max Perutz Laboratories, Vienna); Max Perutz Laboratories Central Facility Biooptics-Light Microscopy (Vienna); K. Elsayad, L. Zhang, A. Kavirayani, and T. Engelmaier [Vienna BioCenter Core Facilities (VBCF), Vienna]; and Y. Albert Pan (Virginia Tech Carilion, Roanoke). We also acknowledge members of the Raible and Tessmar-Raible laboratories, as well as two anonymous reviewers, for detailed and constructive feedback that helped to improve this study. **Funding:** The study was funded by the Austrian Science Fund (FWF; projects P30035, P28970, P23102, P30686, I2972, F78, and M1674). The Advanced Microscopy Facility of the Vienna Biocenter Core Facilities (VBCF) acknowledges support from the City of Vienna and the Austrian Ministry of Science (Vision 2020). **Author contributions:** M.P. conceived parts of the study, developed DEEP-Clear protocols, performed light-sheet imaging and parts of confocal imaging, tested compatibility with endogenous fluorescence, and wrote parts of the manuscript. K.V. conceived parts of the study; tested compatibility of DEEP-Clear with immunolabeling, in situ hybridization, EdU labeling approaches; did parts of confocal imaging; and wrote parts of the manuscript. M.P. and K.V. performed the principal experiments for the study. H.S. contributed to the experiments in the Hawaiian bobtail squid and wrote parts of the manuscript. A.W.S. performed experiments to detect the proliferative compartment in the bristle worm eyes. P.M. characterized antibodies for axolotl tissues, contributed to the interpretation of experiments in axolotl, and wrote parts of the manuscript. S.S. was responsible for ultramicroscope and objective design. M.P.S.D. performed fluorescent in situ hybridization in zebrafish. K.B. developed imaging processing tools and performed statistics. R.R.-i-D. contributed to the identification of the eye photoreceptor signature genes. S.-C.P. assisted with DEEP-Clear experiments. P.P. assisted with confocal imaging and image processing. M.Z. performed and analyzed anti-VT immunostainings. O.S. contributed to the analysis of Hawaiian bobtail squid experiments. E.M.T. contributed to the analysis of axolotl experiments. F.R. conceived parts of the study, supervised the study, analyzed results, and wrote parts of the manuscript. H.-U.D. supervised parts of the study and provided light-sheet infrastructure and DEEP-Clear reagents. All authors read and approved the manuscript. **Competing interests:** The authors declare that they have no competing interests. **Data and materials availability:** All data needed to evaluate the conclusions in the paper are present in the paper and/or the Supplementary Materials. Raw microscopy datasets are available from the corresponding authors upon request. The sequence of *P. dumerilii tmdc/c2433* has been submitted to GenBank (MK330892).

Submitted 30 October 2019
Accepted 27 March 2020
Published 29 May 2020
10.1126/sciadv.aba0365

Citation: M. Pende, K. Vadiwala, H. Schmidbaur, A. W. Stockinger, P. Murawala, S. Saghafi, M. P. S. Dekens, K. Becker, R. Revilla-i-Domingo, S.-C. Papadopoulos, M. Zurl, P. Pasierbek, O. Simakov, E. M. Tanaka, F. Raible, H.-U. Dodt, A versatile depigmentation, clearing, and labeling method for exploring nervous system diversity. *Sci. Adv.* **6**, eaba0365 (2020).

9. References

Altimus, C. M., Güler, A. D., Alam, N. M., Arman, A. C., Prusky, G. T., Sampath, A. P., & Hattar, S. (2010). Rod photoreceptors drive circadian photoentrainment across a wide range of light intensities. *Nature Neuroscience*, *13*(9), 1107–1112.

Aschoff, J. (1979). Circadian Rhythms: Influences of Internal and External Factors on the Period Measured in Constant Conditions. *Zeitschrift Für Tierpsychologie*, *49*, 225–249.

Ayalon, I., Rosenberg, Y., Benichou, J. I. C., Campos, C. L. D., Sayco, S. L. G., Nada, M. A. L., Baquiran, J. I. P., Ligson, C. A., Avisar, D., Conaco, C., Kuechly, H. U., Kyba, C. C. M., Cabaitan, P. C., & Levy, O. (2020). Coral Gametogenesis Collapse under Artificial Light Pollution. *Current Biology*, *31*, 1–7.

Babcock, R. C., Bull, G. D., Harrison, P. L., Heyward, A. J., Oliver, J. K., Wallace, C. C., & Willis, B. L. (1986). Synchronous spawnings of 105 scleractinian coral species on the Great Barrier Reef. *Marine Biology*, *90*(3), 379–394.

Bachleitner, W., Kempinger, L., Wülbeck, C., Rieger, D., & Helfrich-Förster, C. (2007). Moonlight shifts the endogenous clock of Drosophila melanogaster. *Proceedings of the National Academy of Sciences*, *104*(9), 3538–3543.

Backfisch, B., Veedin Rajan, V. B., Fischer, R. M., Lohs, C., Arboleda, E., Tessmar-Raible, K., & Raible, F. (2013). Stable transgenesis in the marine annelid Platynereis dumerilii sheds new light on photoreceptor evolution. *Proceedings of the National Academy of Sciences of the United States of America*, *110*(1), 193–198.

Benito, J., Houl, J. H., Roman, G. W., & Hardin, P. E. (2008). The blue-light photoreceptor CRYPTOCHROME is expressed in a subset of circadian oscillator neurons in the Drosophila CNS. *Journal of Biological Rhythms*, *23*(4), 296–307.

Berndt, A., Kottke, T., Breitkreuz, H., Dvorsky, R., Hennig, S., Alexander, M., & Wolf, E. (2007). A novel photoreaction mechanism for the circadian blue light photoreceptor Drosophila cryptochrome. *Journal of Biological Chemistry*, *282*(17), 13011–13021.

Boch, C. A., Ananthasubramaniam, B., Sweeney, A. M., Doyle, F. J., & Morse, D. E. (2011). Effects of light dynamics on coral spawning synchrony. *Biological Bulletin*, *220*(3), 161–173.

Botts, R. T., Eppert, A. A., Wiegman, T. J., Blankenship, S. R., Rodriguez, A., Wagner, A. P., Ullrich, S. E., Allen, G. R., Garley, W. M., Asselin, E. M., & Mooring, M. S. (2020). *Does*

Moonlight Increase Predation Risk for Elusive Mammals in Costa Rica ?

Brown, D. R. (1952). *Natural illumination charts. Research and Development Project NS 714-100*. Department of the Navy, Bureau of Ships, Washington, D.C.

Cajochen, C., Altanay-Ekici, S., Münch, M., Frey, S., Knoblauch, V., & Wirz-Justice, A. (2013). Evidence that the lunar cycle influences human sleep. *Current Biology*, *23*(15), 1485–1488.

Casiraghi, L., Spiousas, I., Dunster, G. P., Mcglothlen, K., Fernández-duque, E., Valeggia, C., & Iglesia, H. O. De. (2021). *Moonstruck sleep : Synchronization of human sleep with the moon cycle under field conditions*. *7*, 1–9.

Ciocca, M., & Wang, J. (2013). By the light of the silvery Moon: Fact and fiction. *Physics Education*, *48*(3), 360–367.

Collins, B., Mazzoni, E. O., Stanewsky, R., & Blau, J. (2006). Drosophila CRYPTOCHROME is a circadian transcriptional repressor. *Current Biology*, *16*(5), 441–449.

Damiola, F., Le Minli, N., Preitner, N., Kornmann, B., Fleury-Olela, F., & Schibler, U. (2000). Restricted feeding uncouples circadian oscillators in peripheral tissues from the central pacemaker in the suprachiasmatic nucleus. *Genes and Development*, *14*(23), 2950–2961.

Emery, P., Stanewsky, R., Hall, J. C., & Rosbash, M. (2000). Drosophila cryptochromes: A unique circadian-rhythm photoreceptor. *Nature*, *404*(March), 456–457.

Erkert, H. G. (2008). Diurnality and nocturnality in nonhuman primates: Comparative chronobiological studies in laboratory and nature. *Biological Rhythm Research*, *39*(3), 229–267.

Erkert, H. G., & Gröber, J. (1986). Direct Modulation of Activity and Body Temperature of Owl Monkeys (Aotus lemurinus griseimembra) by Low Light Intensities. *Folia Primatologica*, *47*(4), 171–188.

Erkert, H. G., & Thiemann, A. (1983). Dark switch in the entrainment of circadian activity rhythms in night monkeys, Aotus trivirgatus Humboldt. *Comparative Biochemistry and Physiology*, *74A*(2), 307–310.

Evans, J. A., Elliott, J. A., & Gorman, M. R. (2007). Circadian effects of light no brighter than moonlight. *Journal of Biological Rhythms*, *22*(4), 356–367.

Evans, J., Elliott, J., & Gorman, M. (2009). Dim nighttime illumination accelerates adjustment to timezone travel in an animal model. *Current Biology*, *19*(4), 156–157.

Fage, L., & Legendre, R. (1923). Les danses nuptiales de quelques Néréidiens. *Comptes*

Rendus Acad. Sci. Paris, *177*, 982–985.

Fernández-Duque, E., de la Iglesia, H., & Erkert, H. G. (2010). Moonstruck primates: Owl monkeys (Aotus) need moonlight for nocturnal activity in their natural environment. *PLoS ONE*, *5*(9), 1–6.

Foster, R. G., Hughes, S., & Peirson, S. N. (2020). Circadian Photoentrainment in Mice and Humans. *Biology*, *9*(180).

Franke, H. (1985). On a clocklike mechanism timing lunar-rhythmic reproduction in Typosyllis prolifera (Polychaeta). *Journal Of Comparative Physiology A Neuroethology Sensory Neural And Behavioral Physiology*, *156*, 553–561.

Fukunaga, K., Yamashina, F., Takeuchi, Y., Yamauchi, C., & Takemura, A. (2020). Moonlight is a key entrainer of lunar clock in the brain of the tropical grouper with full moon preference. *BMC Zoology*, *5*(1), 1–13.

Fukushiro, M., Takeuchi, T., Takeuchi, Y., Hur, S. P., Sugama, N., Takemura, A., Kubo, Y., Okano, K., & Okano, T. (2011). Lunar phase-dependent expression of cryptochrome and a photoperiodic mechanism for lunar phase-recognition in a reef fish, goldlined spinefoot. *PLoS ONE*, *6*(12).

Fullston, T., Palmer, N. O., Owens, J. a, Mitchell, M., Bakos, H. W., & Lane, M. (2012). Diet-induced paternal obesity in the absence of diabetes diminishes the reproductive health of two subsequent generations of mice. *Human Reproduction (Oxford, England)*, *27*(5), 1391–1400.

Gerrish, G. A., Morin, J. G., Rivers, T. J., & Patrawala, Z. (2009). *Darkness as an ecological resource : the role of light in partitioning the nocturnal niche*. *160*, 525–536.

Giangrande, A. (1988). *Polychaete zonation and its relation to algal distribution down avertical cliff in the western Mediterranean (Italy): a structuralanalysis. Journal of experimental marine biology and ecology, 120(3): 263-276. 120*(1964), 263–276.

Giangrande, A., Delos, A. L., Musco, L., Licciano, M., & Pierri, C. (2003). Polychaete assemblages of rocky shore along the South Adriatic coast (Mediterranean Sea). *Marine Biology*, *143*, 1109–1116.

Giebultowicz, J. M., & Hege, D. M. (1997). Circadian clock in Malpighian tubules. *Nature*, *386*, 664.

Giebultowicz, J. M., Stanewsky, R., Hall, J. C., & Hege, D. M. (2000). Transplanted Drosophila excretory tubules maintain circadian clock cycling out of phase with the host. *Current Biology*, *10*(2), 107–110.

Gliwicz, Z. M. (1986). A Lunar Cycle in Zooplankton. *Ecology*, *67*(4), 883–897.

Harrison, R. L., Babcock, R. C., Bull, G. D., Oliver, J. K., Wallace, C. C., & Willis, B. L. (1984). Mass spawning in tropical reef corals. *Science*, *223*(4641), 1186–1189.

Hartmann-Schroeder, G. (1996). *Annelida, Borstenwuermer, Polychaeta: Die Tierwelt Deutschlands, Teil 58*.

Hauenschild, C. (1960). Lunar Periodicity. *Cold Spring Harbor Symposia on Quantitative Biology*, *25*(0), 491–497.

Helfrich-Förster, C. (2009). Does the morning and evening oscillator model fit better for flies or mice? *Journal of Biological Rhythms*, *24*(4), 259–270.

Hernández-León, S., Almeida, C., Yebra, L., & Arístegui, J. (2002). Lunar cycle of zooplankton biomass in subtropical waters: Biogeochemical implications. *Journal of Plankton Research*, *24*(9), 935–939.

Hirsh, J., Riemensperger, T., Coulom, H., Iché, M., Coupar, J., & Birman, S. (2010). Roles of Dopamine in Circadian Rhythmicity and Extreme Light Sensitivity of Circadian Entrainment. *Current Biology*, *20*(3), 209–214.

Hoang, N., Schleicher, E., Kacprzak, S., Bouly, J. P., Picot, M., Wu, W., Berndt, A., Wolf, E., Bittl, R., & Ahmad, M. (2008). Human and Drosophila cryptochromes are light activated by flavin photoreduction in living cells. *PLoS Biology*, *6*(7), 1559–1569.

Hsiao, S. M. (1996). Semilunar follicular cycle of an intertidal fish: the Fundulus model. *Biology of Reproduction*, *54*(4), 809–818.

Huck, M., Juárez, C. P., & Fernández-Duque, E. (2017). Relationship between moonlight and nightly activity patterns of the ocelot (Leopardus pardalis) and some of its prey species in Formosa, Northern Argentina. *Mammalian Biology*, *82*, 57–64.

Ivanchenko, M., Stanewsky, R., & Giebultowicz, J. M. (2001). Circadian photoreception in Drosophila: Functions of cryptochrome in peripheral and central clocks. *Journal of Biological Rhythms*, *16*(3), 205–215.

Jacobs, R. P. W. M. ., & Pierson, E. S. (1979). *Zostera marina spathes as a habitat for Platynereis dumerilii (Audouin and Milne-Edwards, 1834)*. *6*, 403–406.

John, W., Lindsay, A., & David, W. (2012). *Fear of the dark or dinner by moonlight ? Reduced temporal partitioning among Africa ' s large carnivores*. *93*, 2590–2599.

Kaniewska, P., Alon, S., Karako-Lampert, S., Hoegh-Guldberg, O., Levy, O., Alon, S., Vigneault, F., Eminaga, S., Christodoulou, D., Seidman, J., Church, G., Eisenberg, E., Babcock, R., Bull, G., Harrison, P., Heyward, A., Oliver, J., Wallace, C., Willis, B., …

Oshlack, A. (2015). Signaling cascades and the importance of moonlight in coral broadcast mass spawning. *ELife*, *4*, 1506–1511.

Kempinger, L., Dittmann, R., Rieger, D., & Helfrich-Förster, C. (2009). The nocturnal activity of fruit flies exposed to artificial moonlight is partly caused by direct light effects on the activity level that bypass the endogenous clock. *Chronobiology International*, *26*(2), 151–166.

King, A. N., & Sehgal, A. (2020). Molecular and circuit mechanisms mediating circadian clock output in the Drosophila brain. *European Journal of Neuroscience*, *51*(1), 268–281.

Kistenpfennig, C., Nakayama, M., Nihara, R., Tomioka, K., Helfrich-förster, C., & Yoshii, T. (2018). A Tug-of-War between Cryptochrome and the Visual System Allows the Adaptation of Evening Activity to Long Photoperiods in Drosophila melanogaster. *Journal of Biological Rhythms*, *33*(1), 24–34.

Konopka, R. J., & Benzer, S. (1971). Clock mutants of Drosophila melanogaster. *Proceedings of the National Academy of Sciences of the United States of America*, *68*(9), 2112–2116.

Konopka, R. J., Pittendrigh, C., & Orr, D. (1989). Reciprocal behaviour associated with altered homeostasis and photosensitivity of Drosophila clock mutants. *Journal of Neurogenetics*, *6*, 1–10.

Korringa, P. (1947). Relations between the Moon and Periodicity in the Breeding of Marine Animals. *Ecological Monographs*, *17*, 347–381.

Krisciunas, K. (1991). A MODEL OF THE BRIGHTNESS OF MOONLIGHT. *The Astronomical Society of the Pacific*, *103*, 1033–1039.

Kronfeld-Schor, N., Dominoni, D., de la Iglesia, H., Levy, O., Herzog, E. D., Dayan, T., & Helfrich-Forster, C. (2013). Chronobiology by moonlight. *Proceedings of the Royal Society B: Biological Sciences*, *280*(1765), 20123088–20123088.

Kyba, C. C. M., Mohar, A., & Posch, T. (2017). How bright is moonlight? *Astronomy and Geophysics*, *58*(1), 1.31-1.32.

Lachaise, D., & Silvain, J. (2004). *How two Afrotropical endemics made two cosmopolitan human commensals : the Drosophila melanogaster – D . simulans palaeogeographic riddle*. 17–39.

Lall, G. S., Revell, V. L., Momiji, H., Al Enezi, J., Altimus, C. M., Güler, A. D., Aguilar, C., Cameron, M. A., Allender, S., Hankins, M. W., & Lucas, R. J. (2010). Distinct

contributions of rod, cone, and melanopsin photoreceptors to encoding irradiance. *Neuron*, *66*(3), 417–428.

Last, K. S., Hobbs, L., Berge, J., Brierley, A. S., & Cottier, F. (2016). Moonlight Drives Ocean-Scale Mass Vertical Migration of Zooplankton during the Arctic Winter. *Current Biology*, *26*(2), 244–251.

Lee, S. K., Sonoda, T., & Schmidt, T. M. (2019). M1 Intrinsically Photosensitive Retinal Ganglion Cells Integrate Rod and Melanopsin Inputs to Signal in Low Light. *Cell Reports*, *29*(11), 3349-3355.e2.

Levy, O., Appelbaum, L., Leggat, W., Gothlif, Y., Hayward, D. C., Miller, D. J., & Hoegh-Guldberg, O. (2007). Light-Responsive Cryptochromes from a Simple Multicellular Animal, the Coral Acropora millepora. *Science (New York, N.Y.)*, *318*(5849), 467–470.

Lockard, R. B., & Owings, D. H. (1974). Seasonal Variation in Moonlight Avoidance by Bannertail Kangaroo Rats. *Journal of Mammalogy*, *55*(1), 189–193.

Longcore, T., Rich, C., & DelBusso, L. (2017). Artificial Night Lighting and Protected Lands Ecological Effects and Management Approaches. *Natural Resource Report NPS/NRSS/NSNS/NRR*, *1493*.

Lucas, R. J., Lall, G. S., Allen, A. E., & Brown, T. M. (2012). How rod, cone, and melanopsin photoreceptors come together to enlighten the mammalian circadian clock. In *Progress in Brain Research* (1st ed., Vol. 199). Elsevier B.V.

Menegazzi, P., Dalla Benetta, E., Beauchamp, M., Schlichting, M., Steffan-Dewenter, I., & Helfrich-Förster, C. (2017). Adaptation of Circadian Neuronal Network to Photoperiod in High-Latitude European Drosophilids. *Current Biology*, *27*(6), 833–839.

Miner, B. G., Morgan, S. G., & Hoffman, J. R. (2000). Postlarval chromatophores as an adaptation to ultraviolet radiation. *Journal of Experimental Marine Biology and Ecology*, *249*(2), 235–248.

Mourier, J., Maynard, J., Parravicini, V., Ballesta, L., Clua, E., Domeier, M. L., Mourier, J., Maynard, J., Parravicini, V., Ballesta, L., Clua, E., & Domeier, M. L. (2016). Extreme Inverted Trophic Pyramid of Reef Sharks Supported by Spawning Groupers. *Current Biology*, *26*(15), 2011–2016.

Naylor, E. (2010). Chronobiology of marine organisms. In *Chronobiology of Marine Organisms*. Cambridge University Press.

Neumann, D. (1988). Temperature compensation of circasemilunar timing in the

intertidal insect Clunio. *Journal of Comparative Physiology A*, *163*(5), 671–676.

Ogueta, M., Hardie, R. C., & Stanewsky, R. (2018). Non-canonical Phototransduction Mediates Synchronization of the Drosophila melanogaster Circadian Clock and Retinal Light Responses. *Current Biology*, *28*(11), 1725-1735.e3.

Ozturk, N., Selby, C. P., Annayev, Y., Zhong, D., & Sancar, A. (2011). Reaction mechanism of Drosophila cryptochrome. *Proceedings of the National Academy of Sciences of the United States of America*, *108*(2), 516–521.

Patke, A., Young, M. W., & Axelrod, S. (2020). Molecular mechanisms and physiological importance of circadian rhythms. *Nature Reviews Molecular Cell Biology*, *21*(2), 67–84.

Peschel, N., Chen, K. F., Szabo, G., & Stanewsky, R. (2009). Light-Dependent Interactions between the Drosophila Circadian Clock Factors Cryptochrome, Jetlag, and Timeless. *Current Biology*, *19*(3), 241–247.

Pittendrigh, C. S. (1960). Circadian rhythms and the circadian organization of living systems. *Cold Spring Harbor Symposia on Quantitative Biology*, *25*, 159–184.

Plautz, J. D., Kaneko, M., Hall, J. C., & Kay, S. A. (1997). Independent photoreceptive circadian clocks throughout Drosophila. *Science*, *278*(5343), 1632–1635.

Prugh, L. R., & Golden, C. D. (2014). *Does moonlight increase predation risk ? Meta-analysis reveals divergent responses of nocturnal mammals to lunar cycles*. 504–514.

Ranzi, S. (1931). Ricerche sulla biologia sessuale degli Annelidi. *Pubblicazione Del Stazione Zoologie de Napoli*, *11*, 271–292.

Rieger, D., Stanewsky, R., & Helfrich-Förster, C. (2003). Cryptochrome, compound eyes, Hofbauer-Buchner eyelets, and ocelli play different roles in the entrainment and masking pathway of the locomotor activity rhythm in the fruit fly Drosophila melanogaster. *Journal of Biological Rhythms*, *18*(5), 377–391.

Roecklein, K. A., Rohan, K. J., Duncan, W. C., Rollag, M. D., Rosenthal, N. E., Lipsky, R. H., & Provencio, I. (2009). A missense variant (P10L) of the melanopsin (Opn4) gene is associated with Seasonal Affective Disorder. *Journal of Affective Disorders*, *114*(1–3), 279–285.

Roecklein, K. A., Wong, P. M., Franzen, P. L., Hasler, B. P., Wood-Vasey, W. M., Nimgaonkar, V. L., Miller, M. A., Kepreos, K. M., Ferrell, R. E., & Manuck, S. B. (2012). Melanopsin gene variations interact with season to predict sleep onset and chronotype. *Chronobiology International*, *29*(8), 1036–1047.

Rumanova, V. S., Okuliarova, M., & Zeman, M. (2020). Differential effects of constant light and dim light at night on the circadian control of metabolism and behavior. *International Journal of Molecular Sciences*, *21*(5478), 1–20.

Saigusa, M. (1980). Entrainment of a Semilunar Rhythm by a Simulated Moonlight Cycle in the Terrestrial Crab , Sesarma haematocheir. *Oecologia*, *46*(1), 38–44.

Schlichting, M. (2020). Entrainment of the Drosophila clock by the visual system. *Neuroscience Insights*, *15*, 1–6.

Schlichting, M., Grebler, R., Peschel, N., Yoshii, T., & Helfrich-Förster, C. (2014). Moonlight detection by drosophila's endogenous clock depends on multiple photopigments in the compound eyes. *Journal of Biological Rhythms*, *29*(2), 75–86.

Schlichting, M., Weidner, P., Diaz, M., Menegazzi, P., Dalla Benetta, E., Helfrich-Förster, C., & Rosbash, M. (2019). Light-Mediated Circuit Switching in the Drosophila Neuronal Clock Network. *Current Biology*, *29*(19), 3266-3276.e3.

Selcho, M., Millán, C., Palacios-Muñoz, A., Ruf, F., Ubillo, L., Chen, J., Bergmann, G., Ito, C., Silva, V., Wegener, C., & Ewer, J. (2017). Central and peripheral clocks are coupled by a neuropeptide pathway in Drosophila. *Nature Communications*, *8*(May).

Smith, M., Croy, I., & Persson Waye, K. (2014). Human sleep and cortical reactivity are influenced by lunar phase. *Current Biology*, *24*(12), 551–552.

Soong, K., & Chang, Y. H. (2012). Counting circadian cycles to determine the period of a circasemilunar rhythm in a marine insect. *Chronobiology International*, *29*(10), 1329–1335.

Stanewsky, R., Kaneko, M., Emery, P., Beretta, B., Wager-Smith, K., Kay, S. A., Rosbash, M., & Hall, J. C. (1998). The cry(b) mutation identifies cryptochrome as a circadian photoreceptor in Drosophila. *Cell*, *95*(5), 681–692.

Stokkan, K. A., Yamazaki, S., Tei, H., Sakaki, Y., & Menaker, M. (2001). Entrainment of the circadian clock in the liver by feeding. *Science*, *291*(5503), 490–493.

Takeuchi, Y., Kabutomori, R., Yamauchi, C., Miyagi, H., Takemura, A., Okano, K., & Okano, T. (2018). Moonlight controls lunar-phase-dependency and regular oscillation of clock gene expressions in a lunar-synchronized spawner fish, Goldlined spinefoot. *Scientific Reports*, *8*(1), 1–12.

Tessmar-Raible, K., Raible, F., & Arboleda, E. (2011). Another place, another timer: Marine species and the rhythms of life. *BioEssays : News and Reviews in Molecular, Cellular and Developmental Biology*, *33*(3), 165–172.

Vanin, S., Bhutani, S., Montelli, S., Menegazzi, P., Green, E. W., Pegoraro, M., Sandrelli, F., Costa, R., & Kyriacou, C. P. (2012). Unexpected features of Drosophila circadian behavioural rhythms under natural conditions. *Nature*, *484*(7394), 371–375.

Vinayak, P., Coupar, J., Hughes, S. E., Fozdar, P., Kilby, J., Garren, E., Yoshii, T., & Hirsh, J. (2013). Exquisite Light Sensitivity of Drosophila melanogaster Cryptochrome. *PLoS Genetics*, *9*(7), 1–10.

Whitmore, D., Foulkes, N. S., & Sassone-Corsi, P. (2000). Light acts directly on organs and cells in culture to set the vertebrate circadian clock. *Nature*, *404*(6773), 87–91.

Whitmore, D., Foulkes, N. S., Strähle, U., & Sassone-Corsi, P. (1998). Zebrafish Clock rhythmic expression reveals independent peripheral circadian oscillators. *Nature Neuroscience*, *1*(8), 701–707.

Yoshii, T., Funada, Y., Ibuki-Ishibashi, T., Matsumoto, A., Tanimura, T., & Tomioka, K. (2004). Drosophila cry(b) mutation reveals two circadian clocks that drive locomotor rhythm and have different responsiveness to light. *Journal of Insect Physiology*, *50*(6), 479–488.

Yoshii, T., Todo, T., Wülbeck, C., Stanewsky, R., & Helfrich-Förster, C. (2008). Cryptochrome is present in the compound eyes and a subset of Drosophila's clock neurons. *Journal of Comparative Neurology*, *508*(6), 952–966.

Zantke, J., Bannister, S., Rajan, V. B. V., Raible, F., & Tessmar-Raible, K. (2014). Genetic and genomic tools for the marine annelid Platynereis dumerilii. *Genetics*, *197*(1), 19–31.

Zantke, J., Ishikawa-Fujiwara, T., Arboleda, E., Lohs, C., Schipany, K., Hallay, N., Straw, A. D., Todo, T., & Tessmar-Raible, K. (2013). Circadian and Circalunar Clock Interactions in a Marine Annelid. *Cell Reports*, *5*(1), 99–113.

Zhang, L., Hastings, M. H., Green, E. W., Tauber, E., Sladek, M., Webster, S. G., Kyriacou, C. P., & Wilcockson, D. C. (2013). Dissociation of circadian and circatidal timekeeping in the marine crustacean eurydice pulchra. *Current Biology*, *23*(19), 1863–1873.